Fundamentals of Concentration-encoded Molecular Communication

by

Mohammad Upal Mahfuz

Thesis submitted to the
Faculty of Graduate and Postdoctoral Studies
in partial fulfillment of the requirements
for the Doctorate in Philosophy degree in Electrical Engineering

School of Electrical Engineering and Computer Science
Faculty of Engineering
University of Ottawa

Abstract

Molecular communication (MC) is a new bio-inspired communication paradigm towards realizing the communication and networking at the nanoscale to microscale dimensions among a vast number of engineered natural and/or artificial nanomachines communicating with each other to form a nanonetwork. In this thesis, we investigate a concentration-encoded molecular communication (CEMC) system where the transmitting nanomachine (TN) and the receiving nanomachine (RN) communicate with a single type of information molecules by modulating the transmission rate of information molecules at the TN. The information molecules undergo ideal (i.e. free) diffusion in three dimensions and become available to the RN that observes the concentration of the received molecules at its receptors and thus decodes the message. Our research shows that it is possible to realize complex modulation methods, combat the intersymbol interference (ISI), determine the effective communication ranges based on available signal concentration, develop signal detection schemes, and apply simple channel codes in a CEMC system. It has been found that the performance of the CEMC system is influenced by communication ranges, transmission data rates, ISI, and detection schemes. It is possible to sense the concentration signal intensity and develop optimum receiver structures that can detect the transmitted symbols at the RN. It is also possible to develop optimum signal detection schemes based on the interactions between the information molecules and the receptors using stochastic chemical kinetics (SCK) of the reaction events. Applying simple channel codes at the TN shows that it is possible to increase effective communication range in the CEMC system, however, this increases the complexity of the RN in implementing the detection circuitry. Finally, potential applications of CEMC would be in materializing CEMC-based molecular nanonetworks for emerging areas, e.g. in cancer detection and treatment, targeted drug delivery, and environmental protection and pollution control.

Acknowledgements

First of all, I would like to thank the almighty Allah for giving me the opportunity to complete this thesis work.

I would like to express my deepest thanks and gratitude to my supervisors, Professor Dimitrios Makrakis and Professor Hussein T. Mouftah for accepting me as a Ph.D. student and for their guidance and advice all through my Ph.D. studies. By closely working with them I have learnt many things from them in the last few years, which, I strongly believe, will help me in my future career. Thank you! I would like to thank the Natural Sciences and Engineering Research Council of Canada (NSERC) for the financial support in the form of PGS-D scholarship during the years 2010-2013 and the University of Ottawa for the Excellence Award and the Admisssions Scholarship during the years 2009-2014. I also thankfully acknowledge the financial support received from the WiSense project.

I would also like to thank Professor Karin Hinzer at the University of Ottawa and Professor Steven McGarry at Carleton University for providing me with valuable feedbacks during my Ph.D. thesis proposal and final examinations. I also thank Professor Karin Hinzer at the University of Ottawa and Professor Ashraf Matrawy at Carleton University for being in my Ph.D. comprehensive examination committee. I would also like to thank Professor Andrew Eckford at York University and Professor Voicu Groza at the University of Ottawa for providing me with their valuable comments during my thesis examination.

I am also thankful to all my colleagues at the University of Ottawa for all their helps and supports that made my study at the University of Ottawa a success. My special thanks go to Dr. Muhammad Jahangir Hossain Sarker and Dr. Binod Vaidya at the University of Ottawa for all their advice and discussions. I am also thankful to my colleague Joel Sandé for all the interesting discussions.

Finally, I am very much thankful to my family: my father Mohammad Mahfuzul Huq and my mother Selina Khatun, without whose love, inspiration, patience, and support I wouldn't have come this far in my life, my special thanks to my mother for her passion to send me to St. Gregory's High School for my childhood education, my brothers Raihan Mahfuz Huq and Rachaen Mahfuz Huq for their love and understanding, and last but not least, my wife Suraiya Akter for standing beside me with all the love, care, patience, and

sacrifices during my course of studies, our daughter Liana Ushnata Mahfuz, and our son Raif Mohammad Mahfuz, for their love and patience. I have been very much thankful to the almighty Allah for giving me a wonderful family.

To my parents Mohammad Mahfuzul Huq and Selina Khatun and my wife Suraiya Akter, without whose love and sacrifice I would not have come this far.

Table of Contents

List of Tables

List of Figures

Nomenclature

AHL	Acyl homoserine lactone
ASK	Amplitude-shift keying
ATP	Adenosine triphosphate
B_{Sys}	Bit rate of system
BM	Branch metric
BE	Block encoder
BER	Bit error rate
BSC	Binary symmetric channel
bps	Bits per second
CC	Convolutional code
CCK	Classical chemical kinetics
cdf	Cumulative distribution function
CDMA	Code division multiple access
CE	Convolutional encoder
CEMC	Concentration-encoded molecular communication
CI	Confidence interval
CIR	Channel impulse response
CLT	Central limit theorem
CME	Chemical master equation
CNT	Carbon nanotube
CTRW	Continuous-time random walk
DNA	Deoxyribonucleic acid
ED	Strength (or energy)-based detection
EM	Electro-magnetic
FC	Full complexity
FFPE	Fractional Fokker-Planck equation
FPT	First passage time
FSO	Free-space optical
FSK	Frequency-shift keying
FT	Fixed threshold
IM	Impulse modulation
ISI	Intersymbol interference
ITER	Interference energy to total available energy ratio
M-AM	Multilevel amplitude modulation
MAP	Maximum a posteriori probability
MC	Molecular communication
MEMS	Micro electro mechanical system
ML	Maximum likelihood
MM	Molecular motor
MoSK	Molecule-shift keying
M-PAM	Multilevel pulse amplitude modulation
MRBP	Molecule-receptor binding process
MRI	Magnetic resonance imaging

MS	Mean square
NEMS	Nano electro mechanical system
NoC	Network on chip
NPC	Nuclear pore complex
OOK	On-off keying
PAM	Pulse amplitude modulation
pdf	Probability density function
PM	Path metric
RC	Reduced complexity
RF	Radio frequency
RIS	Received information sequence
RMS or rms	Root mean square
RN	Receiving nanomachine
RNA	Ribonucleic acid
ROC	Receiver operating characteristics
RRE	Reaction rate equations
SCK	Stochastic chemical kinetics
SD	Sampling-based detection
SIR	Signal to interference strength (i.e. energy) ratio
TIS	Transmitted information sequence
TN	Transmitting nanomachine
VAI	Vibrio fischeri Auto-Inducer
VRV	Virtual receive volume
WPF	Weak peak filtering
VT	Variable threshold

List of Symbols

A_{in}	Input amplitude at steady state
A_{out}	Output amplitude at steady state
a_{SCK}	Propensity function
A_{α}, $A_{\tilde{\mu}}$	Coefficients related to $w_T(t)$ and $\lambda_{\text{AD}}(X)$ distributions respectively
AL	Steady state amplitude loss
AL_{ini}	Initial amplitude loss
$a_{\text{SD}}, a_{\text{ED}}$	Coefficients of the square of the observation variable in the expression of test statistic
$B_i(t), B_j(t)$	The *i*-th and *j*-th paths based on random walk motion of a molecule
$\mathbf{b}$	Bit vector $\mathbf{b} = [b_0, b_1, b_2, ..., b_{(N_b-1)}]$
$b_{\text{SD}}, b_{\text{ED}}$	Coefficients of the observation variable in the expression of test statistic
c	Initial amplitude loss indicator quantity
$\vec{c}_C$	Encoded bit sequence
$\text{cdf}(\cdot)$	Cumulative distribution function of the quantity in the parentheses
D	Diffusion constant
d	Steady state amplitude loss indicator quantity
d_{dim}	Dimension of the propagation system
d_{H}	Hamming distance
$E(\cdot)$	Expected value of the quantity in the parentheses
E_S	The received desired signal strength
E_U	The received total (i.e. desired and interference) signal strength
E_I	The received interference signal strength
F_0	Strength of the impulse function
$F_{\alpha}(r,t)$	Probability of getting a molecule in a three-dimensional space at a distance r from the TN at time t, where the molecule experiences pure subdiffusion in three-dimensional unbounded propagation medium
f	Transmission data rate
$f_{\text{Bit-0}}, f_{\text{Bit-1}}$	Modulation frequencies for bits 0 and 1 respectively
f_{sin}	Frequency of sinusoidal transmission
$G(\vec{r},t)$	Mean CIR at position $\vec{r}$ and time t
$G_{RN}(r,t)$	Mean number of the available molecules in the volume VRV
GM	Code generator matrix
$g(r,t)$	The energy-normalized CIR of the CEMC channel
gm_i^j	Code generator matrix elements, i and j are integers.
H	Fox H function
I_{Area-i}	*i*-th interference area

$I_{(r,f)}$	The received interference signal strength ratio for a single pulse transmission
i	Index of a quantity
$\hat{i}, \hat{j}, \hat{k}$	Unit vectors along *X*, *Y*, *Z* axes respectively
$i_{\text{approx}}(t)$	Approximate interference signal intensity available at the RN at time *t*
J_x, J_y, J_z	Net flux of molecules in *X*, *Y*, and *Z* directions respectively
K	An arbitrary constant denoting the number of random realizations
K_{ch}	Number of random channel realizations considered
K_{SCK}	Random variable denoting the number of reactions in an interval
$K_{\alpha}^{\bar{\mu}}$	Generalized diffusion constant in anomalous diffusion
k_C	Message length
k_D	The Boltzman constant
(k,u)	Fourier-Laplace space parameters
lim	Limit operator
L_g	Level gap, i.e. the difference in $U(r,t)$ when a bit switches either from 0 to 1 or from 1 to 0.
ℓ	Conditional probability
M	Number of amplitude levels (alphabet size)
M_u	Alphabet size of the uncoded system
M_{RN}	Remory size of the RN
$\vec{m}_C$	binary information sequence
N	Number of observations in respective cases
N_b	Number of bits in the sequence
N_{samp}	Number of samples per symbol
$N_{n_{\text{SCK}},j,j\neq 0}$	Number of undesired (i.e. ISI-causing) reactions during an interval
$N_{s_{\text{SCK}}}$	Number of desired reactions during an interval
N_{sym}	Number of symbols
N_Z	Length of $\vec{z}_C$
n	Index of observation
n_C	Codeword length
n_{jump} , k_{jump}	Number of jumps or steps taken by a molecule
$n_s(t)$	Diffusion noise intensity
$n_{\text{ED}}^{\text{Noise}}$	Diffusion noise strength quantity
$n_{\text{ISI}}(t)$	ISI-producing noise intensity caused by the residual molecules
$n_{\text{SCK},j}$	Symbol-wise probabilities
P_D	Probability of detection
P_{FA}	Probability of false alarm
$p_{L,}p_R$	Probability that a molecule will take the next step to the left or to the right respectively

$p(\vec{r},t)$	The probability of finding a single molecule at a distance $\vec{r}=\hat{i}\cdot x_r+\hat{j}\cdot y_r+\hat{k}\cdot z_r$ at time t
p_X	Cross over probability
$p_{\tilde{\upsilon}}(t)$	The $\tilde{\upsilon}$-th realization of the energy-normalized CIR
Q_0, Q_1	Number of molecules released by the TN
$Q(t)$	Transmission rate of the molecules at the TN as a function of time
Q_{average}	Average value of sinusoidal transmission rate
Q_{amp}	Amplitude of sinusoidal transmission rate
Q_{avg}	Pulse amplitude (constant) in pulse-based transmission rate
Q_{b_j}	Number of transmitted molecules
$Q_{b_j^M}$	Number of transmitted molecules in M-ary system
$R_{\mu}^{(i)}, i=\{0,1\}$	Mean strength ratio of ISI-producing molecules to desired signal molecules at a specific hypothesis
$R_{\sigma}^{(i)}, i=\{0,1\}$	Standard deviation strength ratio of ISI-producing molecules to desired signal molecules at a specific hypothesis
$\vec{r}$	The vector indicating the location of the RN in three dimensions
SIR	Signal to interference strength ratio
$\widetilde{SIR}_{(r,f)}$	Approximate signal to interference strength ratio
$S_{(r,f)}$	The desired signal strength ratio for a single pulse transmission
$S_{\text{sym (AD)}}$	Probability of getting one molecule available at the RN during the current symbol duration T_{sym}
$s(t)$	Mean number of molecules available at the reception volume of the RN at time t
$s_{\text{approx}}(t)$	Approximate desired signal intensity available at the RN at time t
$s_{b_j}(r,t)$	Mean number of the available molecules in the volume VRV in response to Q_{b_j}
s_{SCK}	Symbol-wise probabilities
s_{ED}	Mean signal strength
$T(\bullet), T_k, T', T'', T_1$	Test statistic
T_b	Duration of a bit in binary CEMC system
T_{Ch}	Characteristic time
T_{obs}	Observation time
T_p	Pulse-width in a pulse-based CEMC system
T_{sym}	Symbol duration
T_T	Absolute temperature
t	Time variable
t_{int}	Integer denoting an instant of time
t_s	Sampling time interval

$t_{50\%}$, $t_{90\%}$	Times to achieve 50% and 90% of the molecules being available at the RN respectively
U	Number of molecules available at the location of the RN
V	CE memory length
VRV	The reception volume of the RN
var	Variance operator
$\pm v_x$	Velocity of a molecule
w_C, w_{C1}	Percentage of the total number of molecules "received" during the symbol duration
$w_T(t)$	Waiting time distribution
$w_i[n], i = \{0,1\}$	Normal distributed random variable with zero-mean and non-unity variance
X, Y, Z	Positions at the Cartesian (X, Y, Z) coordinate system
$X(t_i)$	Displacement at time t_i
x, x_{ED}	Standard normal variable $\mathcal{N}(0,1)$
x_r, y_r, z_r	Position of the RN in Cartesian coordinate system
$y(t)$	Output signal intensity of the CEMC channel with the diffusion noise only
y_{ED}	Signal strength affected by diffusion noise
$z(t)$	Output signal intensity of the CEMC channel with the diffusion noise and intersymbol interference
$\vec{z}_C$	Detected sequence of samples
z_{ED}	Observation variable in strength-based detection
z_{SCK}	Observation variable in strength-based detection in SCK approach
α	Anomalous subdiffusion exponent
ς	Variable of integration
θ	Phase angle of sinusoidal transmission
δ_X	Length of a single step
$\delta(t)$	Dirac delta function
∇^2	Laplacian operator
τ	Time taken by a molecule to make a single step
$\tau_{\text{D (RMS)}}$	RMS delay spread
τ_{E} , $\overline{\tau}_{\text{E}}$	Delay and mean excess delay respectively
τ_{ini}	Initial phase error (s)
τ_{ss}	Steady state phase error (s)
$\mathcal{N}(\mu_X, \sigma_X^2)$	The pdf of a Gaussian (normal) distributed random variable with mean μ_X and variance σ_X^2
$\mu_{\text{ISI}}, \sigma_{\text{ISI}}^2$	Mean and variance of ISI quantities
μ_s, σ_s^2	Mean signal and variance of diffusion noise respectively
$\mu_{\text{ISI (ED)}}$	Mean value of strength of ISI-producing molecules
$\tilde{\mu}$	Anomalous diffusion exponent related to position
$\sigma_{\text{ISI (ED)}}^2$	Variance of strength of ISI-producing molecules

$\sigma^2_{S(ED)}$	Variance of diffusion noise strength
η_{fluid}	Viscosity of the fluid
ρ_{mole}	Radius of the information molecules
$\gamma, \gamma_i, \gamma_{ED}, \gamma'_{ED}$	Threshold for comparsion
$\phi_{\tilde{C}}$	Characteristic function of any quantity $\tilde{C}$
χ^2_i	Chi-square pdf with *i* degrees of freedom
$\mathcal{Q}$	Right-tail probability
ξ	Ratio of amplitude levels
$\Lambda^{(0)}$	Mean signal strength to diffusion noise strength standard deviation ratio
λ_{SCK}	Rate of Poisson's random variable
λ_C	Sequence number
$\lambda_{AD}(X)$	Jump length distribution
η_{SCK}	Specific probability rate constant for molecular reaction between an information molecule and a receptor
ρ_{SCK}	Distinct molecule and receptor pairs available in the VRV
$\Re$	Concentration of receptors on the surface of the RN
υ	Constraint length
$\varnothing_A$	Constant that depends on the amplitude of the pulse transmission
Ω_S	State in Trellis
$\Im$	Fourier Transform
$\psi(X,t)$	Joint distribution of jump length and waiting time
${}_0\mathcal{L}_t^{1-\alpha}$	Rieman-Liouville operator
$\mathcal{T}$	Time constant in anomalous diffusion process
$\Gamma(.)$	Gamma function
$\tilde{\upsilon}$	Index of realization of the signal
$\Pi(t)$	Rectangular pulse signal of unit amplitude
$\sum^2$	Jump length variance
$\mathbb{L}$	Laplace Transform operator

Chapter 1: Introduction

1.1 Background: Nanoscale Communication and Networks

Nanotechnology is rapidly changing today's world in almost all areas, ranging from natural and health sciences, through biotechnology and molecular systems biology, to communication engineering. The idea of nanotechnology was first introduced by the Nobel laureate scientist Richard P. Feynman in his 1959 talk entitled "*There is plenty of room at the bottom*" when he also mentioned about some of the possible ways that would help achieve the goal of nanotechnology [FEY-60]. Many technological fields, especially those in science and engineering, are experiencing a significant revolution by virtue of the possibility of manipulating matter at the nanometre scale [ALF-06]. As nanotechnology is progressing the development of the nanomachines is also offering promising techniques in the area of nanomanufacturing. Developments in the area of nanobiotechnology, in particular, are paving the way to building nanoscale devices, e.g. nanomachines, by applying the principles of nanomanufacturing [LIU-12] [BHA-05]. For example, a molecular motor (MM) made by dynein[1] [BUS-10], p. 33, which performs a power stroke[2], is an excellent example of a nanomachine. It is well-accepted that nanoscale devices like nanomachines have a huge potential in nanomedicine (e.g. cancer biology [ALB-08], p. 1205, [FRE-05] [RAV-09] [FRI-06]) along with many other benefits in several other fields as mentioned in Chapter 2.

A nanomachine can be viewed as a machine at the nanoscale dimensions e.g. a molecular motor [FRE-05] [AKY-08]. Alternatively, a nanomachine can also be considered as a collection of several other nanomachines working cooperatively e.g. a biological cell. Please note that in some of the available literature nanomachines are sometimes named as *nanorobots;* both terms refer to the same entity. It is well-reported that nanomachines of the size of a bacterium, approximately 1 μm [ALB-08], p.16, have the ability to sense and actuate in the microscopic environment and thus could provide novel capabilities that can be

[1] A microtubule motor protein that walks along the microtubule [ALB-08], p. 711.

[2] The phase of the complete MM cycle when the MM is attached with the molecular track [BUS-10], p. 33.

leveraged in many applications [CAV-06]. On another note, unlike silicon-based devices, devices based on biological materials and mechanisms show unique characteristics, e.g. biocompatibility, the ability of being self-organized, and the ability of being used in a massively parallel manner, and offer functional complexity (suitable for better design and engineering of a nano-to-micro system), all of which are important for a new communication paradigm to exist towards the next generation of information technology [NAK-10c].

Why communication at the nanoscale?

Firstly, although individual nanomachines are capable of performing simple tasks [AKY-08], interconnections of nanomachines are needed to perform complex tasks that cannot otherwise be done by a single nanomachine [ALF-06]. For a nanonetwork to be formed nanoscale communication must be realized among nanomachines forming the nanonetwork [AKY-08]. As a result, thoughts on nanomachine communication and networking have started to come into play [AKY-10] [BUS-09] [PAR-09] [MAL-12].

Another reason for nanoscale communication is that as the component size goes down to the nanoscale we still need to communicate with components at that tiny size in order to build nano-micro systems. Although existing communication techniques in chip components involve metallic wired and radio frequency (RF) wireless interconnects [CHA-01], it is not clear whether information transmission among communicating nanomachines would be using the same principles [ALF-06]. Wired and wireless communication techniques will probably not hold for a long time to interconnect chip components and so new nanoscale communication techniques need to be sought.

Since the research field of *nanoscale communication and networks* itself is very new, the amount of knowledge available in this field is also somewhat limited. Several new applications of nanoscale communication systems will require new forms of wireless channels at the nanoscale. For example, by virtue of the nanoscale communication techniques it would be possible to send information to or receive information from many biological cells within the body, which would allow the body to detect and cure [AKY-08] certain deadly diseases in an easier way compared to today's medical treatments. Communication between a pair of nanomachines is fundamental to realizing a *nanoscale*

communication network composed of a vast number of nanomachines. Networking among a vast number of communicating nanomachines with current techniques involves communication mechanisms exceeding nanoscale dimensions because of the limitations of the present day downscaling technologies [BUS-09]. As a result, it goes without saying that both, *nanoscale communication* and *nanoscale communication networks* require a new communication paradigm in order to be realized successfully.

Three approaches of the new communication paradigm are currently under consideration: "dry" techniques [LAC-09] using non-biological nanostructures such as carbon nanotubes (CNT) [BUS-10], p. 93, "wet" techniques [LAC-09] using biological approaches such as molecular communication (MC) [NAK-11a], p. 49, and techniques using a quantum mechanical approach [BUS-09].

Dry techniques refer to all nanoscale communication techniques that are based on structures of carbon, silicon, and inorganic materials. Despite the progress of nanoscale device technologies, nanoscale communication techniques based on conventional electromagnetic (EM) communication systems suffer from the limitations in terms of transceiver size and complexity [JOR-11] and extremely high frequency [AKY-10], which generates a motivation towards investigations into novel materials based on *graphene*, e.g. graphene nanoribbons (GNR) and carbon nanotube (CNT). Graphene is a mono-atomic layer of hexagonal carbon atoms that can be rolled, forming a single-wall CNT [BHU-04], p. 41. Since the wave velocity in GNR and CNT can be up to one hundred times lower than the speed of light in vacuum, the operating frequency in GNR-based and CNT-based nanoantennas can also be up to two orders of magnitude lower than that in non-carbon nanoantennas [AKY-10]. As a result, a significant amount of research is motivated towards the characterization and modeling of graphene-based EM transceivers in the terahertz (THz) band in the range from 100 GHz to 10 THz [JOR-11]. In addition, in order to realize *small-scale networking* [BUS-09], quantum phenomena could also be considered. For instance, it is reported that a quantum wireless network based on quantum routing mechanism can be constructed [CHE-05].

1.2 Overview of Molecular Communication

MC has already been materialized in naturally occurring biological systems [ALB-08] quite extensively. It is known that MC is used for the intra-cellular, inter-cellular, inter-organ, and inter-species communications [NAK-10a]. In addition, MC has recently been used extensively as one of the key technologies in synthetic biology and bio-NEMS/MEMS fields of research [NAK-12]. With MC being the most biologically suitable communication paradigm, we focus our research on the MC-based approach. MC is a bio-inspired communication paradigm that uses molecules in order to communicate information between the transmitting nanomachine (TN) and receiving nanomachine (RN) [MOR-10]. MC between nanomachines can be realized based on molecular motor-based microtubule networks [MOO-08] [MOO-06] [MOO-09] [SCH-03] and diffusion-based propagation of molecules [BER-93] [BOS-63] [URS-11].

Based on several characteristics of the molecules, there are several possible technologies to encode information using MC. For example, in *concentration-encoding,* information can be encoded in concentration of transmitted molecules [MAH-10b] where a binary "1" and "0" are represented by sending higher and lower number of molecules by the TN respectively. In *time-encoding*, the information bits are encoded in the release time of molecules at the TN [SRI-12]. In *molecular encoding*, the binary bits are encoded in the different types of molecules by the TN [MOO-09a]. In addition to these common techniques, information bits can also be encoded in the molecule transmission order e.g. in [ATA-12].

In this thesis, we have investigated into the possibilities of **concentration-encoded molecular communication (CEMC)** system where the TN uses only a single type of information molecules and information symbols are encoded into the number of transmitted molecules by the TN. For example, in case of M-ary signaling in CEMC, the M different symbols are represented by using the one of the M different numbers of transmitted molecules (of the same type) by the TN. The RN observes the received concentration of the molecules at its location and thus decodes the information accordingly.

1.3 CEMC Challenges

MC and nanonetworks are very recent fields of research in the area of communication systems and networking, thus the volume of existing research in this area is limited. This provides new technical challenges and the opportunity for significant new research contributions, which, however, needs to be performed following an interdisciplinary research perspective. While it is very promising that nanomachines will possibly be built in the near future [OZI-05], existing knowledge on nanomachine communication and networking still do not provide a clear understanding of how the nanomachines will actually communicate [AKY-10a]. At the present time nanomachine communication is experiencing several key challenges that need to be overcome first before any development is made on the system design. Below we categorize the challenges of CEMC in two main sections: first, the challenges related to the architecture of the communication system, and second, the challenges related to signal characteristics.

CEMC signal experiences a concentration attenuation and temporal spreading as a function of both communication range, i.e. the TN-RN distance, and transmission data rate [MAH-10a]. In addition, the CEMC signal is also influenced by the *diffusion constant* of the information molecules in the propagation medium and the properties of the propagation medium. However, when the effects of information molecules and propagation medium are assumed negligible, the performance factors of a CEMC system are confined to the effects of the communication range and the transmission data rate requirement of the CEMC system.

Attenuation loss and temporal spreading have several impacts that give rise to a number of challenges in CEMC. For example, the effective communication range between the TN and the RN is reduced compared to that for ensuring a reliable communication link between the TN and the RN, which gives rise to the fact that **improving the communication range** is a big challenge in CEMC. In addition, MC is a very slow (nm to μm/s) communication technique compared to EM communication [NAK-11a]. As a result, it is always desired that a new technique be developed, which would increase the communication speed between nanomachines when CEMC is used. Thus, **improving the communication speed** is another big challenge in CEMC. Apart from these, one significant impact of concentration attenuation and temporal spreading is that the CEMC becomes unreliable [THO-04] due to

occurrence of severe intersymbol interference (ISI) [MAH-10b]. Therefore, **combating the ISI** is what is highly desired. Regarding the CEMC system's performance, several things are still unknown. For example, propagation channel needs to be understood thoroughly in order to understand the communication mechanism between nanomachines. Several encoding-decoding techniques and their processing efficiency are still unknown. Especially, in the bio-hybrid design of the CEMC system, communication signal processing would be at the cell level, which raises a challenge of whether the proposed modulation and demodulation techniques are biologically suitable or not.

1.4 Motivation

The lack of sufficient knowledge on concentration-based encoding in MC is the principal motivation of this research. Since MC itself is a new communication paradigm, the telecommunications research community lacks proper knowledge of the CEMC system in the aspects of nanonetworks. Therefore, this thesis makes an effort to provide an in-depth description and analysis of the CEMC system between a pair of nanomachines, which is fundamental to the realization of molecular nanonetworks, especially from the view point of identifying the CEMC channel and performance evaluation based on suitable modulation and detection schemes. Although the present day research technologies still need some time to manufacture a fully functional nanomachine, we strongly believe that research investigations focusing on communication aspects of CEMC need to be conducted in parallel from a sufficiently early time in order to get the fullest benefit from these research investigations.

In CEMC, the molecules transmitted by the TN undergo random walk-based diffusion mechanism and reach the RN in a probabilistic manner and, therefore, not all of the molecules transmitted reach the RN located at a given distance from the TN at a given time [BER-93] [BOS-63]. This phenomenon is governed by the diffusion of molecules in a propagation medium, and as a result, gives concentration attenuation [MAH-10a] of molecular signal. Although the diffusion mechanism has been known for more than a hundred years [PHI-06] [ROB-23], the concept of using diffusion as a communication technique is relatively new [AKY-08] [HIY-05] [SUD-05] [NAK-05] [MOO-07]. The work in [HIY-05] identified the research challenges in MC, which include encoding and decoding

of the information (i.e. signal) on to information molecules, propagation of molecules in a controlled way for conveying information, and information transmission and reception system design for carrier information molecules. However, the work did not consider analyzing the MC channel from channel impulse response (CIR) perspective. In the discussions of encoding and decoding of information in MC [HIY-05], several possible techniques to encode information in MC have been mentioned, e.g. using the three-dimensional structure, polarity, motion, and magnetization of the information molecules. However, the work in [HIY-05] did not include the possibility of using concentration-based information encoding-decoding in diffusion-based MC, which could be a new research area as shown in our work. Intracellular calcium concentration ($[Ca^{+2}]$) can be used to encode information by modulating its frequency, amplitude, and duration [PRA-00].

The works reported in [ATA-07], [ATA-08], and [ATA-08a] considered molecule-receptor binding process (MRBP), as shown in [KRI-02], [ROS-00], in order to compute the capacity of a CEMC channel; however, without considering the diffusion-based propagation effects of information molecules. The studies reported in [KRI-02] and [ROS-00] considered all the molecules be present at the receptors of the RN and did not consider the effects of diffusion process in the propagation medium.

The diffusion-based MC system has been recently modeled by several researchers. In [MAH-10a], it is reported that, when the TN and the RN are located at a fixed distance, the input-output concentration characteristics can be established for the very fundamental ideal (i.e. free) diffusion-based [BER-93] CEMC channel, such that any output concentration can be obtained by convolving the input signal (i.e. transmission rate of molecules) with the impulse response of the CEMC channel. In addition, it was observed in [MAH-10a] that the impulse response of the CEMC channel is a function of both communication range (i.e. the distance between the TN and the RN) and time. Another work reported in [PIE-10] proposed an end-to-end channel model for diffusion-based MC system including the channel effects, where the authors investigated the end-to-end system on the basis of signal transmitter, propagation, and receiver modules. However, the model presented in [PIE-10] did not consider the noise effects of the diffusion-based propagation, which have been described in [PIE-11] with the concepts of "*particle-sampling*" and "*particle-counting*" noises. On an additional note, an analysis of the reception noise due to MRBP in a

diffusion-based MC system has been given in [PIE-11b]. Researchers have mentioned that molecules can accumulate in the RN and thus can cause "noise" in the communication process [MOO-09a].

In CEMC, we explore the probability of getting a molecule at the location of the RN at any time instant, which constitutes the average concentration of available molecules at the location of the RN, when a large number of molecules are sent by the TN. The concentration of molecules at the RN is a random variable with a signal-dependent mean and variance [MAH-13]. In addition, the channel capacity using the deterministic diffusion-based CEMC channel has been investigated by modeling the MRBP as a *propensity function*[3]-based approach, which finally comes up to a Gaussian approximation to the number of reactions during a given interval of time, e.g. a symbol time interval [ATA-10].

Since MC is a new nanomachine communication paradigm, the proposed channel models in [MAH-10a] and [PIE-10] have motivated the recent research on efficient modulation and coding techniques that would be well-suited for the CEMC channel. Many of the conventional digital communication results do not hold for the CEMC system and a thorough revision of the classical communication theories and techniques needs to be done in the aspect of MC [JOR-10] [PIE-10]. For example, CEMC is a slow process compared to EM wave communications. The amplitude of concentration bears the information signal of the system. ISI degrades the performance of a CEMC system, especially at high transmission rates. In some aspects MC is similar to intensity modulated optical signaling [PAR-97] and in similarity with the free-space optical (FSO) communication that propagates through atmosphere [ALE-97], the CEMC channel [MAH-10a] experiences time-varying signal fading due to random walk motion of the molecules themselves and turbulence experienced by the propagation channel. Both of these effects contribute to the ISI effects that this thesis has focused on. This gave us the impetus to propose sampling-based detection (SD) and strength (i.e. energy)-based detection (ED) schemes for the CEMC system, both based upon the intensity of the received molecular concentration [MAH-11]. CEMC signal detection schemes have been investigated in detail in later chapters of this

[3] Propensity function indicates the probability of a reaction event between an information molecule and a receptor [GIL-00].

thesis. Although it is still not clear to the research community whether conventional signal processing techniques of traditional communication systems would be suitable for the CEMC system, the receiver processing of molecular signals is an extremely new area of research at the present time.

To the best of our knowledge, some recent research works investigated the diffusion of molecules from the CIR perspectives and found its spatial-dependence and temporal-dependence characteristics [MAH-10a] [PIE-10] [GAR-11]. The CEMC channel between a pair of nanomachines in a fluidic medium can be expressed as its CIR that depends on the communication range and time. In this thesis, we investigate several aspects of the CEMC system in detail. Since *ideal* diffusion [BER-93], p. 6, is the most general, widely-used, and a simple diffusion-based propagation in MC technique [MOO-12b] [MOO-11a], in this thesis we focus on the ideal (i.e. free) diffusion-based CEMC system. Spatiotemporal characterization of the impulse response of the CEMC channel [MAH-10] [MAH-10a] [MAH-10b] is important in the sense that the impulse response is the basis of almost all advanced communication signal processing in CEMC. On another note, since CEMC is a slow process, techniques need to be investigated such that data rate can be increased in CEMC, which gives us the motivation to search for the multilevel modulations in the case of CEMC system [MAH-10b] [MAH-11a].

Our research has provided promising results and has been published in a number of papers. The list of the papers published, accepted, and submitted for publication is provided in a separate section in this chapter.

1.5 Objectives

Having reviewed the available literature on CEMC system this dissertation attempts to focus on the overall description of the CEMC channel and evaluate its performance. Understanding CEMC thoroughly would be helpful in realizing MC-based nanonetworks and their related applications. The principal objective of this thesis is to develop an overall framework of an *ideal diffusion*-based CEMC system that uses a single type of information molecules to communicate information between a pair of nanomachines. More importantly, an investigation into the diffusion dynamics of the CEMC channel would constitute another major objective of this research.

1.6 Thesis Contributions

The objectives mentioned above have been addressed throughout this thesis. The main contributions and achievements that have been made in this thesis are as follows:

1) We have made a thorough investigation into spatiotemporal distribution of signal intensity and strength in CEMC. In addition, we have shown that simple modulation techniques, e.g. amplitude-based modulation schemes, namely, impulse modulation (IM), pulse amplitude modulation (PAM), and frequency-based modulation schemes, namely, frequency-shift keying (FSK), can be successfully applied to CEMC. We have shown that both binary and M-ary modulation techniques can be possible in CEMC. More importantly, based on signal intensity and strength, by addressing the issue of ISI and signal distortion, we have determined the effective communication ranges for short-range, medium-range, and long-range CEMC in commonly seen biologically suitable propagation media, namely, air, water, and blood plasma. This would provide insight in the design of effective communication links in CEMC-based nanonetworks. Chapter 3 provides the details in this regard.

2) We have proposed two novel detection techniques, namely, sampling-based detection (SD) and strength (or energy)-based detection (ED) techniques, for CEMC. In SD, the RN detects the transmitted symbol by sampling the available signal intensity at one or more temporal instants, while in ED, it accumulates the number of molecules that become available at the RN in order to detect the transmitted symbol. We have developed and analyzed the optimum receivers in detail for SD and ED in CEMC. These two detection techniques have been presented in Chapters 4 and 5 respectively.

3) We have also introduced the optimum strength-based receiver based on stochastic chemical kinetics (SCK) of the reaction events between information molecules and receptors. We have presented the receiver model in detail for pulse-transmitted OOK CEMC system. We have also proposed a variable threshold-based detection scheme and shown that it outperforms the fixed threshold-based detection scheme by providing an improvement in the effective communication ranges. Chapter 6 provides the details in this regard.

4) For the first time ever in the domain of CEMC, we have introduced the application of convolutional coding techniques in pulse-transmitted CEMC and shown that convolutional codes can provide a significant amount of gain in the signal to interference strength ratio

(SIR) at the RN and thus help increase the effective communication range in CEMC. Chapter 7 provides the details in this regard.

5) For the first time ever in the domain of CEMC, using fractional diffusion approach we have presented an investigative analysis to study the effects of subdiffusion (anomalous diffusion) on CEMC. Results show that, unlike normal diffusion, the CIR in subdiffusion has distinctive time-dispersive properties that should be taken into consideration when designing a CEMC system based on subdiffusion. Chapter 8 provides the details in this regard.

1.7 Thesis Outline

Chapter 1 presents the motivation, major objectives, and contributions of this thesis. The general background and the importance of this research are presented in Chapter 1 in order to bring the current research topic into proper significance. Chapter 1 also provides a list of publications produced from the contributions of this thesis study. Chapter 2 provides a general discussion of the state-of-the-art of the CEMC system. Having provided a brief introduction to the nanomachines and the communication techniques to realize communication between nanomachines, Chapter 2 sheds light on the general ideas of the CEMC system. Chapter 3 describes the characteristics of CEMC channel. Two novel detection techniques, namely, the sampling-based and the strength-based detection techniques, have been presented in detail in Chapters 4 and 5 respectively. Chapter 6 presents the strength-based detection model based on SCK. Chapter 7 introduces the applications of channel codes in CEMC. Chapter 8 presents the subdiffusive CEMC system. Finally, Chapter 9 concludes this thesis with directions to future research. All the programming works related to this thesis have been performed with MATLAB® software.

1.8 List of Publications

As direct outcomes of this research the list below shows the contributions that have already been published, accepted, under revision, and submitted for publication.

1.8.1 Peer-reviewed Journal Papers

[J1] M.U. Mahfuz, D. Makrakis, and H.T. Mouftah, “A Comprehensive Analysis of Strength-Based Optimum Signal Detection in Concentration-Encoded Molecular

Communication with Spike Transmission," revised version submitted to *IEEE Transactions on Nanobioscience*, September, 2014.

[J2] M.U. Mahfuz, D. Makrakis, and H.T. Mouftah, "A Comprehensive Study of Sampling-Based Optimum Signal Detection in Concentration-Encoded Molecular Communication," *IEEE Transactions on Nanobioscience*, Vol. 13, Issue 3, September, 2014, pp. 208-222, DOI: 10.1109/TNB.2014.2341693.

[J3] M.U. Mahfuz, D. Makrakis, and H.T. Mouftah, "Strength-Based Optimum Signal Detection in Concentration-Encoded Pulse-Transmitted OOK Molecular Communication with Stochastic Ligand-Receptor Binding," *Simulation Modelling Practice and Theory*, Vol. 42, Special Issue: Molecular Communications, March 2014, pp. 189-209, Elsevier, DOI: http://dx.doi.org/10.1016/j.simpat.2013.11.005.

[J4] M.U. Mahfuz, D. Makrakis, and H.T. Mouftah, "Performance Analysis of Convolutional Coding Techniques in Diffusion Based Concentration Encoded PAM Molecular Communication Systems," *BioNanoScience*, Vol. 3(3), 2013, pp. 270-284, Springer, DOI: 10.1007/s12668-013-0086-5.

[J5] M.U. Mahfuz, D. Makrakis, and H.T. Mouftah "On the characterization of binary concentration-encoded molecular communication in nanonetworks," *Nano Communication Networks*, Vol. 1 (2010), pp. 289-300, Elsevier.

1.8.2 Peer-reviewed Book Chapters

[BC1] M.U. Mahfuz, D. Makrakis, and H.T. Mouftah, "Concentration-Encoded Molecular Communication in Nanonetworks. Part 1: Fundamentals, Issues, and Challenges," to appear in *Modeling, Methodologies and Tools for Molecular and Nano-scale Communications*, Eds. Junichi Suzuki, Tadashi Nakano, and Michael J. Moore, Springer, 2014.

[BC2] M.U. Mahfuz, D. Makrakis, and H.T. Mouftah, "Concentration-Encoded Molecular Communication in Nanonetworks. Part 2: Performance Evaluation," to appear in *Modeling, Methodologies and Tools for Molecular and Nano-scale Communications*, Eds. Junichi Suzuki, Tadashi Nakano, and Michael J. Moore, Springer, 2014.

1.8.3 Peer-reviewed Conference Papers

[C1] M.U. Mahfuz, D. Makrakis, and H. Mouftah, "An Investigative Analysis on Concentration-Encoded Subdiffusive Molecular Communication in Nanonetworks," in *Proc. 14th IEEE International Conference on Nanotechnology (IEEE-NANO 2014)*, 18-21 August, 2014, Toronto, Canada, pp. 244-249.

[C2] M.U. Mahfuz, D. Makrakis, and H.T. Mouftah, "A Generalized Strength-Based Signal Detection Model for Concentration-Encoded Molecular Communication," in *Proc. 8th International Conference on Body Area Networks (BodyNets 2013)*, Track: Nano-scale Communications and Networking, 30 Sept.-02 Oct. 2013, Boston, MA, USA, pp. 461-467, DOI: 10.4108/icst.bodynets.2013.253560. **(Recipient of BODYNETS-2013 Student Participation Grant)**

[C3] M.U. Mahfuz, D. Makrakis, and H.T. Mouftah, "Sampling Based Optimum Signal Detection in Concentration-Encoded Molecular Communication Receiver Architecture and Performance," in *Proc. 6th International Conference on Bio-inspired Systems and Signal Processing (BIOSIGNALS-2013)*, Barcelona, Spain, 11-14 February, 2013, pp. 372-376.

[C4] M.U. Mahfuz, D. Makrakis, and H.T. Mouftah, "Concentration Encoded Molecular Communication: Prospects and Challenges Towards Nanoscale Networks," in *Proc. International Conference on Engineering, Research, Innovation and Education (ICERIE-2013)*, Sylhet, Bangladesh, 11-13 January, 2013, pp. 508-513.

[C5] M.U. Mahfuz, D. Makrakis, and H.T. Mouftah, "Strength Based Receiver Architecture and Communication Range and Rate Dependent Signal Detection Characteristics of Concentration Encoded Molecular Communication," in *Proc. Seventh International Conference on Broadband and Wireless Computing, Communication and Applications (BWCCA-2012)*, Victoria, Canada, 12-14 November, 2012, pp. 28-35.

[C6] M.U. Mahfuz, D. Makrakis, and H.T. Mouftah, "Transient Characterization of Concentration-Encoded Molecular Communication with Sinusoidal Stimulation," in *Proc. 4th IEEE International Symposium on Applied Sciences in Biomedical and Communication Technologies (ISABEL-2011)*, Barcelona, Spain, 26-29 October, 2011.

[C7] M.U. Mahfuz, D. Makrakis, and H.T. Mouftah, "A Comprehensive Study of Concentration-Encoded Unicast Molecular Communication with Binary Pulse

Transmission," in *Proc. 11th IEEE International Conference on Nanotechnology (IEEE NANO-2011)*, Oregon, USA, 15-18 August, 2011, pp. 227-232.

[C8] M.U. Mahfuz, D. Makrakis, and H. Mouftah, "On the Characteristics of Concentration-Encoded Multi-Level Amplitude Modulated Unicast Molecular Communication," in *Proc. 24th IEEE Canadian Conference on Electrical and Computer Engineering (IEEE CCECE-2011)*, Niagara Falls, ON, 8-11 May, 2011, pp. 312-316.

[C9] M.U. Mahfuz, D. Makrakis, and H. Mouftah, "Characterization of Intersymbol Interference in Concentration-Encoded Unicast Molecular Communication," in *Proc. 24th IEEE Canadian Conference on Electrical and Computer Engineering (IEEE CCECE-2011)*, Niagara Falls, ON, 8-11 May, 2011, pp. 164-168.

[C10] M.U. Mahfuz, D. Makrakis, and H. Mouftah, "On the Detection of Binary Concentration-Encoded Unicast Molecular Communication in Nanonetworks," in *Proc. 4th International Conference on Bio-inspired Systems and Signal Processing (BIOSIGNALS-2011)*, Rome, Italy, 26-29 January, 2011, pp. 446-449.

[C11] M.U. Mahfuz, D. Makrakis, and H. Mouftah, "Spatiotemporal Distribution and Modulation Schemes for Concentration-Encoded Medium-To-Long Range Molecular Communication," in *Proc. 25th IEEE Biennial Symposium on Communications*, Kingston, Canada, 12-14 May, 2010, pp. 100-105.

[C12] M.U. Mahfuz, D. Makrakis, and H. Mouftah, "Characterization of Molecular Communication Channel for Nanoscale Networks," in *Proc. 3rd International Conference on Bio-inspired Systems and Signal Processing (BIOSIGNALS-2010)*, Valencia, Spain, 20-23 January, 2010, pp. 327-332.

1.8.4 Poster Presentations

[P1] M.U. Mahfuz, D. Makrakis, and H. Mouftah, "An Investigative Analysis on Concentration-Encoded Subdiffusive Molecular Communication in Nanonetworks," presented at *WiSense Workshop* 2014, University of Ottawa, 28 August, 2014 **(Recipient of the 2nd place of Best Poster Award)**.

[P2] M.U. Mahfuz, D. Makrakis, and H. Mouftah, "Signal Detection in Concentration-Encoded Molecular Communication," in *Proc. 5th Annual WiSense Workshop*, University of Ottawa, Ontario, Canada, 29-30 August, 2013.

[P3] M.U. Mahfuz, D. Makrakis, and H. Mouftah, "Communication at the Nanoscale: Prospects and Challenges of Concentration-Encoded Molecular Communication," in *Proc. 4th Annual WiSense Workshop*, University of Ottawa, Ontario, Canada, 08 September, 2012 **(Honourable Mention Poster Award)**.

[P4] M.U. Mahfuz, D. Makrakis and H.T. Mouftah, "A Comprehensive Study of Concentration-Encoded Unicast Molecular Communication with Binary Pulse Transmission", presented at *3rd Annual WiSense Workshop*, University of Ottawa, Ontario, September, 2011.

[P5] M.U. Mahfuz, D. Makrakis and H.T. Mouftah, "Spatiotemporal Distribution and Modulation Schemes for Medium-to-Long Range Molecular Communication", presented at *2nd Annual WiSense Workshop*, Queen's University, Kingston, May 2010 **(Second Best Poster Award)**.

Chapter 2: State of the Art

2.1 Introduction

In this chapter, a survey of the related previous works done in the field of CEMC has been presented. The literature review focuses on five main areas of the surveyed topic. CEMC particularly involves MC that, in general, requires interdisciplinary knowledge from several technical fields of study ranging from material science through biophysics and computer science to electrical engineering, communication systems, and computer networks. Therefore, first, we present a general and historical perspective of the topic. We then present related works on CEMC as well as the theories involved. Literature reviews on limitations as well as application areas of CEMC and molecular nanonetworks have been presented next. While this chapter provides a general overview of the related works done in this research, the following chapters present the related work in a fashion more relevant to the contents of the corresponding chapters.

2.2 General and Historical Perspective

The random walk motion of a particle, for example, a molecule, suspended in a fluid medium e.g. air, water, or blood plasma, is due to the billions of collisions of the particular molecule with the molecules of the surrounding environment within a very small time period, where these collision events take place at the time scale of picoseconds [HÖF-13]. Although the ideas of continuous-time and discrete-time random walk are the same, they are mainly distinguished by the very nature of the step size the particle takes between any two states, and the corresponding time the particle remains in the previous state before it jumps into the next step [MET-00]. The history of random walk motion of particle is quite old. Random walk was first observed in 1827 by Scottish botanist Robert Brown (1773–1858) who first observed with the microscope that the pollen particles appeared to be jiggling at high speed while being suspended in water medium. However, it was not until 1905 that such motion observed by Robert Brown was explained by Albert Einstein such that it was due to the extremely large number of collisions among particles [EIN-05]. For example, due

to collisions a small particle named *lysozyme*[4] [ALB-08], p. 6, can take 10^{12} steps in one second [BER-93]. Random walk motion of particles is also known as the *Brownian motion* of particles. As an emerging communication paradigm, MC is being considered as a new physical layer (PHY) option for communicating nanomachines [NAK-13] [NAK-12] [AKY-08]. Random walk of molecules is the main underlying communication principle of diffusion-based CEMC.

2.2.1 Nanotechnology, Nanomachines and Nanonetworks

Among the many areas of technology in recent times nanotechnology has brought about a remarkable progress in research in the field of communication systems and engineering. Nanotechnology has enabled the existence of communication systems and networks at the nanoscale. The word "nanotechnology" refers to creating and manipulating the matter at the scale of an atom i.e. at the nanometre scale. On 29 December 1959 the Nobel laureate scientist Dr. Richard Feynman (1918-1988) delivered a talk entitled "*There's Plenty of Room at the Bottom An Invitation to Enter a New Field of Physics*" where he first mentioned that in the near future devices would be miniaturized down to atomic scale [FEY-60]. In addition, he pointed out proposals of how to possibly accomplish the miniaturization and prepare devices at the atomic scale. Fifteen years later, in 1974 the term "nanotechnology" was first defined by Japanese scientist Norio Taniguchi [TAN-74] to describe the control of materials at the nanometre scale as "*Nano-technology mainly consists of the processing of, separation, consolidation, and deformation of materials by one atom or one molecule.*" Since then the idea of nanotechnology is still new in our society. Nanoscale refers to the dimension in the range from 1 nm (nanometre)[5] to 100 nm [FRE-05] [AKY-08] [XIA-03]. When size goes down to the nanoscale, physical, chemical, electrical, magnetic, optical, and mechanical properties of materials change and novel properties arise in the matter [MEY-06], which can be beneficial to communication engineering if harnessed properly. An example of the novel characteristics that arises at the nanoscale is the melting

[4] Lysozyme is a kind of enzyme [ALB-08].

[5] 1 nm is equal to 10^{-9} (i.e. billionth) of a metre. It is approximately 1/80,000 of the typical diameter of a human hair, or 10 times the diameter of a hydrogen atom [LAC-09].

point of a particle of 5 nm size that may deviate "as much as couple of hundreds of degrees" as compared to the bulk melting point [MEY-06]. Another example would be a silicon nanowire of 5 nm diameter whose band gap may increase from 1.1 eV to approximately 3 eV [MEY-06].

Nanoscale devices have at least one dimension in the range from 1 nm to 100 nm [XIA-03]. According to available literature, the dimension of 100 nm is important in the sense that under this limit new material properties arise due to the laws of quantum physics [LAC-09]. In this chapter, we are particularly interested to see how nanotechnology can benefit communication engineering discipline.

Nanoscale communication is targeted for nanomachines that can communicate among themselves in order to form "*nanonetworks*" and/or initiate certain functions [AKY-08]. A nanomachine is an artificial or naturally (e.g. biologically) occurring entity of nano- to micro-scale dimensions that is capable of performing some simple tasks. A nanomachine can be considered as the most basic functional unit at the dimensions equivalent to the atomic and molecular scales. Examples of the tasks that a nanomachine is capable of are simple molecular computations, sensing and detection of molecules, generation of motion, and performing chemical reactions. In the area of molecular nanotechnology, most molecular biological systems are themselves nanomachines, examples of which include molecular motors, namely, *kinesin*, *dynein*, and *myosin* that convert chemical energy in the form of ATP hydrolysis to mechanical work and thus generate motion [BUS-10], p. 33. While man-made nanomachines are yet to be manufactured, natural biological nanomachines are already available in nature and are able to be engineered to perform tasks in a controlled manner [NAK-11a]. The engineered nanomachines are discussed in Section 2.2.5. In its structure a nanomachine is assumed to have an arranged set of molecules that are able to perform one or more of the tasks mentioned above. In addition, it is also assumed that a nanomachine is a building block of more complex systems, e.g. nano-robots (a.k.a. nanobots), nano-processors, nano-memories, or nano-clocks [AKY-08].

A large number of nanomachines can collaborate with one another and thereby perform comparatively complex tasks in a distributed manner, which would otherwise not be possible by a single nanomachine. The resulting interconnection of a number of nanomachines is known as *nanonetworks* [AKY-08]. Collaboration and coordination among

nanomachines necessarily require a nanomachine to communicate with other nanomachines, which is the main research topic of *nanoscale communication networks.* In available literature, "*nanoscale communication networks*" and "*nanonetworks*" are both equally found to mean a collection of large number of nanomachines working collaboratively. In this research work, we use the same trend and, therefore, when we use the terms *nanoscale communication networks* and *nanonetworks* they both mean the same. As a result, this allows us to use the terms alternatively. Nanonetworks would be able to enhance the functionality of a single nanomachine in several ways, a few of which are mentioned below [AKY-08].

Complex tasks— A single nanomachine, e.g. a biological cell or a chemical sensor, is unable to do complex tasks by itself. However, communication in terms of exchanging information and commands among networked nanomachines would surely allow them to perform complex tasks in a collective manner. Examples of such collaborated tasks are targeted drug delivery in the body to treat diseases.

Enhanced workspace— The workspace of a single nanomachine is extremely limited. Since nanonetworks will have a large number of interconnected nanomachines in collaboration, the workspace of the nanonetworks will be increased. Examples include nanonetworks in the environmental protection, monitoring, and control. Human body is another example of nanonetworks where a large number of nanomachines work cooperatively in order to accomplish certain tasks.

Controlled behaviour— Nanonetworks will have a huge number of nanomachines interconnected with each other. Since nanomachines are of extremely small size and in some applications they are assumed to be deployed over a wide range of areas ranging from a few metres to kilometres, controlling a specific nanomachine is very challenging. However, the formed nanonetworks would allow the member nanomachines to interact with each other as needed.

Network of nanomachines— Since a bio-nanonetwork, formed of a large number of member nanomachines, is focused on one task, several such nanomachines can work together collaboratively, performing identical or complementary tasks. For instance, human body tissues and organs work cooperatively to eliminate toxic materials and support regulating mechanisms, e.g. in controlling the metabolism diseases like diabetes.

2.2.2 Approaches to Development of Nanomachines

At the present time three approaches to nanomachine development, namely, *top-down approach*, *bottom-up approach*, and *bio-hybrid approach*, have been considered as the most likely for use to the artificial nanomachine development [AKY-08]. The *top-down approach* is based on the downscaling the micro-scale components with the help of available manufacturing techniques, for instance, electron beam lithography [TSE-03], micro-contact printing [WIL-96]. Examples of nanomachines built by using this principle are the nano-electromechanical systems (NEMS) components [AKY-08] [MEY-06]. Top-down approach requires a very sophisticated processing of materials at the nanoscale and thus experiences a high cost in the manufacturing process when the component size approaches the nanoscale dimensions [QIN-12]. For example, the cost of photolithography equipment advanced with nanofabrication capability can be as high as $50 million [QIN-12]. In addition, when size goes down to nanoscale the atoms or molecules tend to stick together due to the Van Der Waals attraction force [BHU-04], p. 550. Recent developments of nanomachines by following the top-down approach [QIN-12] [YUN-07] [AKY-08] are still in the early stage of research and development.

The *bottom-up approach* to developing nanomachines is based on using molecules as the building block to develop the nanomachines. Recently, a number of nanomachines, e.g. molecular differential gears and pumps, have been designed theoretically by using this approach [AKY-08]. Although the manufacturing technique, called *molecular manufacturing*, using controlled arrangements of molecules is yet to become reality, there is a good hope that molecular manufacturing techniques would become matured in the next few decades and thus the development of nanomachines with the *bottom-up approach* would become reasonably possible. And, in addition, it is expected that the bottom-up approach will have certain advantages over the top-down approach [OZI-05].

Finally, the bio-hybrid approach to developing nanomachines is based on the inspiration that several nanoscale components present in the biological cells can be considered as nanomachines and thus be used and even engineered as nanomachines to perform desired functions in a controlled manner. An example of the bio-hybrid approach to developing nanomachines is an engineered biological cell that has a nucleus (nano-processing unit), endoplasmic reticulum (nano-storage unit), gap junctions (biological transceivers), receptors

(nano-sensors), flagellum (nano-actuators), mitochondrion (nano-power unit), and vacuoles (nano-energy scavenger) [AKY-08]. The bio-hybrid approach also encourages us to use these nanomachines in the biological cell as models to develop new nanomachines and/or use them as building blocks in order to develop more complex systems known as nano-robots.

2.2.3 Expected Features and Functionalities of a Nanomachine

Although natural nanomachines are already there in nature, artificial man-made nanomachines are yet to be manufactured. However, the expected features and functionalities of nanomachines are given in the following. Nanomachines are expected to be *self-contented* meaning that they should have a set of instructions to realize the intended task. The set of instructions could either be embedded on their own molecular structure, or stored in another storage from where the nanomachines would be able to read the instructions when required [AKY-08]. *Self-assembly* would allow the nanomachines to be assembled from several parts without external intervention. *Self-replication* allows a nanomachine to make a copy of it by using the external elements. *Locomotion* enables a nanomachine to move from one place to another. *Communication* allows nanomachines to create more complex structures by communicating, cooperating, and collaborating with other nanomachines. Communication among nanomachines also enables decentralization and distributed intelligence, a.k.a. *swarm intelligence* [LAC-09]. While all of the desired features mentioned above can be obtained from the natural nanomachines, e.g. a biological cell, there can be additional features, e.g. *multi-tasking* and *multi-interfacing*, that can also be considered as expected features of a nanomachine. *Multi-tasking* allows a cell to perform multiple tasks, e.g. taking nutrients from the environment, running chemical processes etc., at the same time. *Multi-interfacing* allows a cell to communicate with several other entities using different communication methods. For example, a cell can simultaneously communicate with *molecule-receptor binding process* (MRBP), *gap junctions*, and *molecular motors*. Therefore, it is expected that a nanomachine should also be able to achieve multi-interfacing ability.

2.2.4 Architecture of a Nanomachine

Referring back to the expected features of a nanomachine, in order to realize a nanomachine, the generalized architecture of a nanomachine that is somewhat complete in its functionalities should have the following functional units: *control unit* that executes the instructions stored in the instruction storage and that is equivalent to the nucleus of a biological cell [ALB-08], *communication unit* that communicates with other nanomachines by sending and receiving messages and is equivalent to the gap junctions and molecule receptors in a biological cell [BUS-10], p. 49, [FRE-99], p. 84, *reproduction unit* that generates a replica of itself and is equivalent to the deoxyribonucleic acid (DNA) sequence in a biological cell, *power unit* that powers all the individual components of the nanomachine and is equivalent to the mitochondrion in a biological cell, *sensor and actuator units* that interface the nanomachine with the external environment and are equivalent to the molecule receptors and flagella respectively in a biological cell [AKY-08] [LAC-09]. It is hoped that in the near future completely synthetic nanomachines [OZI-05] would become a reality, achieve the expected features of a nanomachine in general, and thus be able to perform the required tasks of a TN and an RN.

2.2.5 Engineered Natural and Synthetic Nanomachines

The TN and the RN need communication functionality in its structure in order to realize a communication system working. These functionalities include synthesizing, storing, and releasing information molecules [NAK-11a]. This sub-section describes how natural nanomachines can be engineered to perform the desired tasks. It also introduces how artificial nanomachine (and cell-like) structures can be built based upon biologically-friendly materials and techniques. One of the existing techniques to develop synthetic nanomachines is to modify and add communication and logic functionalities in the existing biological nanomachines through genetic engineering [NAK-11a]; p. 66; [NAK-11], [MOO-07]; p. 1042. For example, it is found that sender nanomachines can be engineered to synthesize and release information molecules, e.g. acyl homoserine lactone (AHL) molecules, by using the specific metabolic pathways and those receiver nanomachines can be engineered to react to a specific concentration level of information molecules and thus react accordingly by synthesizing reporter proteins [NAK-11a].

The information molecules transmitted by the TN can diffuse freely in the propagation environment and thus reach the RNs and make the communication possible between them. By using the principles of synthetic biology, more specifically, genetic engineering, it is possible to develop *logic functions, toggle switches,* and *oscillators* by using a biological nanomachine, e.g. a biological cell [NAK-11a]. It is also possible to build artificial cell-like structures, by using biological materials e.g. lipid bilayer similar to a cell membrane structure, that can enclose some fundamental components of the artificial cell [NAK-11a]. When a lipid bilayer membrane forms a cell-like structure it is then possible to add functional protein inside the vesicles created by the lipid bilayer. Research shows that such a cell-like structure is capable of replicating itself and producing sender and receiver functionalities [NAK-11a].

2.3 Communication at the Nanoscale

Nanonetworks basically refer to the two branches of research on the communication technologies at the nanoscale: first, *dry techniques* that involve nanostructures, modified materials, and interconnected devices derived from the downscaling of the existing micro-scale technologies, and second, *wet techniques* that are derived from the communication mechanisms and components mainly inspired from the biological systems and materials. While both dry and wet techniques represent communication mechanism at the nanoscale, communication takes place in different forms in both of these techniques. This section represents a brief overview of the different techniques and components of communication at the nanoscale.

2.3.1 Dry and Wet Techniques

Dry techniques refer to the communication techniques that are derived from nanoscale techniques that deal with the fabrication of the carbon, silicon, and other inorganic materials and their involvement with communication at the nanoscale. As mentioned earlier, dry techniques offer communication solutions by downscaling the currently available micro-scale technologies and are meant for the building of the devices at the nanoscale. Examples of dry techniques of nanoscale communication include nanowired communication [LAC-

09], carbon nanotube (CNT)-based communication [BUS-10], p. 93, nanophotonic communication [LAC-09], and free space wireless optical communication [HRA-05].

Wet techniques deal with the study of natural and engineered biological systems as well as the artificial structures based on bio-materials, and use the inspiration from those already existing systems to design a nanoscale communication system capable of offering a basis for realizing nanonetworks. Biological systems mostly operate in the aqueous environment and hence the name of these "wet" communication techniques [ALF-06]. MC is a very well-known example of wet techniques, and a new paradigm for communication at the nanoscale. MC is being considered as a new physical layer option for communication and networking among a huge number of natural and man-made nanomachines [NAK-13] [AKY-08] [PAR-09] [NAK-12] [MAH-10b] [MOR-07a] [MOO-07]. In addition, the noticeable feature of MC is that MC is a truly interdisciplinary field of research that spans physics, nanotechnology, chemistry, biotechnology, and communication technologies. MC, as a wet communication technique, would be a main focus of this research study.

2.3.2 Nanomachine Communication

Although a single nanomachine is of very limited capabilities and can handle forces of the order of pico-Newtons (pN), a huge number of nanomachines would form a nanonetwork in order to handle big tasks that require forces of the order of Newtons (N). The analysis of a single communication link between a pair of nanomachines is important in the sense that it is fundamental to the understanding of the communication system in nanonetworks. In nature, it is found that two biological cells can communicate in the concentration-dependent manner using information molecules [NAK-11a]. When communication at the nanoscale is investigated, available literature suggests that there can be four possible ways of communication, namely, *nano-mechanical*, *nano-acoustic*, *nano-electromagnetic* (EM), and *molecular communication* (MC). In nano-mechanical communication, the TN and the RN are in direct contact with each other and the information is communicated by means of the movements of the nano-mechanical contacts (hinges) between them [FRE-99], p. 183. In nano-acoustic communication, the information is communicated by means of an encoding technique that relies on the variations of the pressure waves [FRE-99], p. 177. EM-based nanoscale communication technique relies on the modulation of EM waves transmitted by

and received from nanomachines [AKY-10c]. Finally, MC technique uses molecules as the messages in order to encode the information from the TN destined to the RN. In MC paradigm, the TN transmits information molecules in order to communicate information to the RN [NAK-12] [HIY-05] [SUD-05].

MC-based techniques for communicating nanomachines offer the following two main benefits over other communication techniques at the nanoscale: first, in nano-mechanical communication the TN and the RN would need to be in direct contact with each other, which may not always be possible for a pair of communicating nanomachines; MC-based techniques relax this restriction. Second, because of the size and operating principles of acoustic transducers and RF transceivers, it is reported that their respective implementations in integrated circuits at nanoscale and molecular scale are not feasible [AKY-08]. While the (bio-inspired) MC transceivers are basically nanomachines that can transmit and receive molecules and many of these nanomachines already exist in the nature, thus the ability to materialize them is already proven. Therefore, of the four communication techniques mentioned above, in the available literature, the MC technique is thought to be the most biologically suitable technique [AKY-08] for communication among nano- to micro-scale biological nanomachines and so the MC technique has been considered in this research.

2.3.3 MC and CEMC

If we look back into the history of MC we see that the field of MC was pioneered by Suda and colleagues who performed some preliminary works back in 2005 on establishing the idea of nanoscale communication networks in the design of bionanomachines [HIY-05] [SUD-05] [NAK-05] [MOR-06]. Later on, the research was carried forward by the same research group during the year 2006 [MOO-06] [MOR-06] [MOO-06a] [SAS-06] [NAK-06] [MOR-06a]. In the year 2007, MC research was published by several research groups, for instance, by Suda and colleagues [NAK-07] [MOR-07a] [MOR-07] [MOO-07] [MOO-07a], Eckford and colleagues [ECK-07] [ECK-07a], Akan and colleagues [ATA-07], and Walsh and colleagues [WAL-07]. In the years 2008-2012, a high surge of research results started to come into existence, in which several research groups in the world published their research results and promoted the research of nanoscale communication in general. Among those are the ones led by Akyildiz and colleagues [AKY-08] [AKY-10] [JOR-11] [AKY-

10a] [JOR-12] [AKY-11] [JOR-11a] [KUR-11] [PIE-11] [PIE-11a] [AKY-10c] [JOR-10] who proposed the idea of *nanonetworks* [AKY-08] [AKY-10a], Nakano and colleagues [NAK-11a] [NAK-10a] [NAK-11c] [NAK-12] [NAK-12a] [NAK-12b] [OKA-12] [MOO-11a] [NAK-11] [NAK-11b] [NAK-10] [NAK-10b] and Mahfuz and colleagues [MAH-10] [MAH-10a] [MAH-10b] [MAH-11] [MAH-11a] [MAH-11b] [MAH-11c] [MAH-12a].

A generic MC system consists of a TN, an RN, and a propagation medium between them. The propagation medium is also known as the "channel" [MAH-10a]. Figure 2.1 shows a typical diffusion-based MC channel between a TN and an RN. As shown in Fig. 2.1, the TN is located at the origin (0,0,0). In MC, information may be encoded onto several characteristics of the information molecules, for instance, type of the information molecules used i.e. *distinct molecules* [ECK-07], internal structure of the information molecules i.e. *molecular-encoding* [LAC-09], or the concentration of information molecules i.e. *concentration-encoding* [MAH-10b], [MAH-11]. *Concentration-encoding* enables information to be encoded in the amplitude of the transmission rate of the molecules by the TN, and correspondingly, by decoding the encoded information by observing the number of information molecules received by the RN per unit volume of the solvent molecules used. Concentration-encoding is relatively simple because it does not require altering the internal structure of the information molecules, nor does it require sending distinct molecules for information communication. That has given us the impetus to concentrate on the CEMC system in this research. In this thesis, we focus on concentration-encoding and investigate into various characteristics of a CEMC system between a pair of nanomachines in a fluidic medium.

The molecules released by the TN undergo ideal (i.e. free) diffusion in three dimensions in the propagation medium, while being governed by random walk-based diffusion mechanism. The molecules probabilistically reach the RN located at a distance r from the TN. As shown in Fig. 2.1, the TN transmits information molecules at a given (predefined) rate. Examples of information molecules include proteins and ions that contain information to be transmitted [BUS-10] [SMI-00]. Examples of the propagation media include water, blood plasma, and air [LAC-09]. Like TN, RN is a nanomachine that can receive the information molecules at its receptor sensors. Propagation of molecules can take place with either active transportation (e.g. molecular motors) [MOR-07a] [FAR-11] or passive

transportation known as *diffusion* [BER-93], p. 5, [BOS-63]. In diffusion, the information molecules propagate spontaneously in the surrounding environment due to thermal effects. In this research, as shown in Fig. 2.2, we consider a diffusion-based propagation channel for CEMC purposes between a pair of nanomachines.

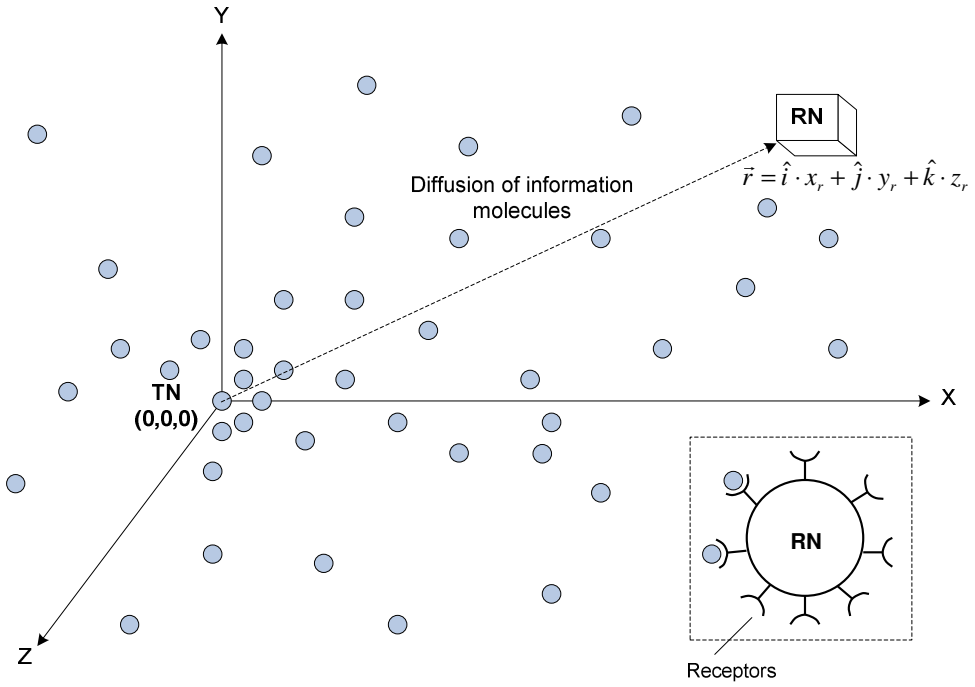

Figure 2.1 Ideal (i.e. free) diffusion of information molecules in three dimensions in the unbounded propagation medium. The RN is shown to be in the centre of a small virtual receive volume (VRV) [ATA-10]. The receptors of the RN shown in inset bind with a single type of molecules.

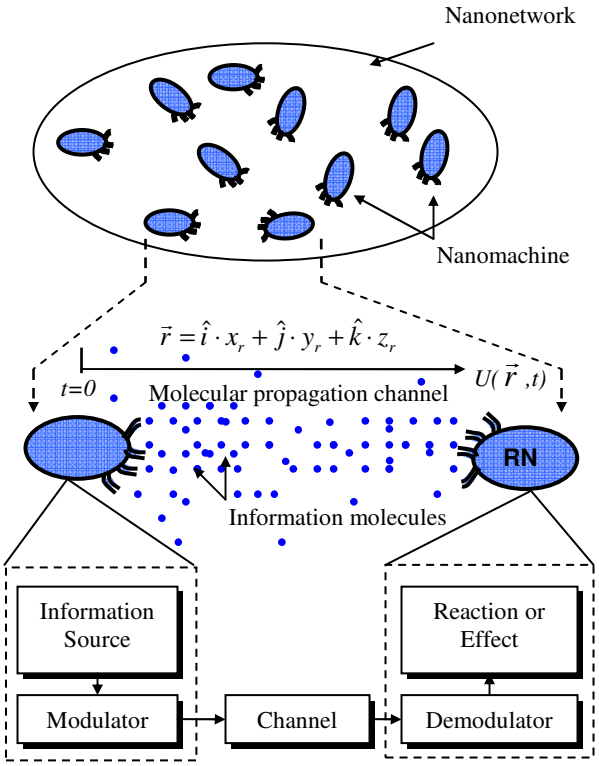

Figure 2.2 A general view of a nanonetwork (top) and a single MC channel between a TN and an RN (bottom). The five components of MC system are also shown.

2.3.4 MC Phases

A TN communicates with an RN by means of five-phase communication mechanism. The first phase is "*encoding*" with which the TN translates the information into the information molecules such that it becomes possible for RN to detect the information.

In the second phase of MC, the TN transmits the encoded information molecules in the propagation medium, the communication phase being known as the "*sending*" phase.

The transmitted molecules propagate in the environment and the phase of communication is known as the "*propagation*" phase. In passive transportation, the information molecules thus sent by the TN diffuse passively in the environment due to Brownian motion without using chemical energy. Diffusion of information molecules depends on the size and molecular weight of the molecules, structural characteristics of the propagation medium, e.g. viscosity, flow of the medium, pressure, dispersion, and absolute temperature [BUS-10], p. 234, [LAC-09]. However, in this study in order to investigate into

the characteristics of CEMC system only, we have not considered the variations of these factors over the observation time; rather we have considered commonly used values for these factors where necessary.

Next, in the "*receiving*" phase the information encoded in the molecules is detected by the RN. Available information molecules, i.e. the output of diffusion-based CEMC channel, are received by the RN according to the MRBP based on the affinity of the information molecules to the receptors of the RN. In this research, we concentrate on the channel only, and we consider both the available number of molecules at the output of the diffusion-based CEMC channel without considering the MRBP, and the number of reactions between information molecules and the receptors based on SCK [GIL-00].

Finally, in the "*decoding/reaction effect*" phase, the detected information is decoded and the RN generates appropriate biochemical reaction effects depending on the decoded information. As shown in Fig. 2.1, the RN has a number of receptors on its surface. All the receptors are identical such that they bind with the same type of information molecules used in the CEMC system. For example, the circular shaped information molecules as shown in Fig. 2.1 bind with the semi-circular receptors as shown in the inset.

2.4 Diffusion-Based Propagation of Molecules

2.4.1 Macroscopic Theory of Diffusion

The propagation of information molecules can be explained with two main theories, namely, the *macroscopic theory* and the *microscopic theory* of diffusion [BER-93], p. 5. Due to the probabilistic nature of the number of the molecules available at the RN, the *macroscopic theory* of diffusion [BER-93], p. 16, explains the available *mean* number of molecules at the RN by providing the average value of the amplitude of concentration signal that is present at the location of the RN. When diffusion is explained in terms of the macroscopic theory, it is assumed that there exist a large number of information molecules in the system and the diffusion process is explained in terms of the average number of the molecules in the system. From the macroscopic theory point of view, diffusion of molecules in the fluidic medium can be explained by the Fick's first and second laws of diffusion [BER-93] [CRA-75]. Fick's laws of diffusion are the differential equations that describe the non-uniform distribution of molecules in the fluidic medium in spatial and temporal domain.

Fick's first law states that net flux J_x of molecules at position X is proportional to the slope of the concentration function U at X, the constant of proportionality being equal to $-D$, where D is the diffusion constant of the information molecules in the medium, and can be expressed as the following.

$$J_x = -D\frac{\partial U}{\partial X} \tag{2.1}$$

There will not be any particle flux (i.e. $J_x = 0$) if the molecules are uniformly distributed over space, and correspondingly, the distribution of molecules will not change over time if $J_x = 0$.

Fick's second law follows from his first law and represents the time rate of change of the concentration of the information molecules at a location provided that the *total number of information molecules is conserved*, i.e. the information molecules are neither created nor destroyed by the system. Fick's second law of diffusion can be expressed as below.

$$\frac{\partial U}{\partial t} = -\frac{\partial J_x}{\partial X} \quad \Rightarrow \quad \frac{\partial U}{\partial t} = D\frac{\partial^2 U}{\partial X^2}. \tag{2.2}$$

Fick's second law of diffusion states the time rate of change of concentration of information molecules at X and t, which is proportional to the curvature of the concentration function at X and t, the constant of proportionality being equal to D. If the slope of concentration $\partial U/\partial X$ is constant, i.e. $\frac{\partial^2 U}{\partial X^2} = 0$, then the concentration is stationary, i.e. $\frac{\partial U}{\partial t} = 0$.

In the three dimensional case, the information molecules propagate independently in three dimensions and so the diffusion equation can be written in three dimensions as the following,

$$\frac{\partial U(X,Y,Z,t)}{\partial t} = D\nabla^2 U(X,Y,Z,t) \quad \Rightarrow \quad \frac{\partial U}{\partial t} = D\nabla^2 U. \tag{2.3}$$

when written in short by not writing the functional dependence of (X,Y,Z,t), where ∇^2 is the three-dimensional Laplacian operator denoted as $\nabla^2 = \frac{\partial^2}{\partial X^2} + \frac{\partial^2}{\partial Y^2} + \frac{\partial^2}{\partial Z^2}$, and

$\vec{r} = \hat{i} \cdot x_r + \hat{j} \cdot y_r + \hat{k} \cdot z_r$ is the vector representing the distance between the TN and the RN in the three dimensional space using Cartesian coordinates.

Solution of Fick's Second law in Three Dimensions

Let us first consider that the information molecules are released by the TN in an impulsive manner, i.e. Q_0 molecules are released at the location of the TN $(0,0,0)$ at time $t = 0$, meaning that the solution of the mean number of information molecules that become available at the location of the RN for an instantaneous point source in an unbounded infinite reception volume can be obtained as the following, where $\vec{r} = \hat{i} \cdot x_r + \hat{j} \cdot y_r + \hat{k} \cdot z_r$, so $r^2 = {x_r}^2 + {y_r}^2 + {z_r}^2$, and radial symmetry is assumed [BER-93].

$$U(r,t) = \frac{Q_0}{(4\pi Dt)^{\frac{3}{2}}} \exp \frac{-r^2}{4Dt} \tag{2.4}$$

The concentration of available molecules in molecules per unit volume depends on the location of the RN and the time elapsed after the release of the molecules. For the sake of simplicity, the available concentration $U(r,t)$ of molecules at the location of RN can also be termed as the "*signal intensity*" and any integral of $U(r,t)$ can be termed as the "*signal strength*" [MAH-11]. The significance of Eq. (2.4) is that it indicates the CIR of the CEMC channel [MAH-10a].

In this research, when considering diffusion in homogenous medium, we have considered that D does not vary over time and space and that the chosen value of D of small information molecules in water medium is 10^{-6} cm^2/second. The values of D based on other types of information molecules and/or propagation media can also be found in several text books, e.g. [ALB-08], p. 1318, [FRE-99], p. 73. Understanding the solution to the diffusion equation in three-dimensional space, we can say that the quantity $U(r,t)$ indicates the available information molecules at the location of the RN.

The propagation of information molecules is affected by the noise generated from and within the propagation environment itself. Examples of such noise generating sources are thermal energy, electric fields, magnetic fields, EM waves, e.g. energy of a photon absorbed by the solvent and solute molecules, and also the molecules that do not take part in MC, as

well as other nanomachines that are idle in the system [MOO-07]. The quantity $U(r,t)$ denotes the mean number of molecules that are available per unit volume of the solvent molecules at the RN and ready to be received by the RN. As shown in Fig. 2.1, the RN is assumed to be located at the centre of a small virtual receive volume (VRV) [ATA-10], i.e. the total sensing volume of the RN. Thus the total number of molecules in VRV available for reception, where VRV has a unit volume [ATA-14], e.g. 1 μm^3, i.e. the typical volume of a bionanomachine (a bacterium) [NAK-13], would represent the amplitude $s(t)$ of the available molecular concentration signal intensity at the RN [MAH-11] and can be expressed as below.

$$s(t) = \iiint_{\text{VRV}} U(x_r, y_r, z_r, t)\, dXdYdZ \tag{2.5}$$

$$\Rightarrow s(t) = \iiint_{\text{VRV}} \frac{Q_0}{(4\pi Dt)^{\frac{3}{2}}} \exp \frac{-\left(x_r^{\,2} + y_r^{\,2} + z_r^{\,2}\right)}{4Dt}\, dXdYdZ$$

2.4.2 Microscopic Theory of Diffusion

The *microscopic theory* of diffusion explains propagation of a single molecule from the TN to the RN. Correspondingly, the probability of getting the emitted molecule at the RN is investigated. The term "microscopic" refers to the single molecule involved. In the following, the propagation of a single molecule emitted by the TN has been reviewed from the viewpoint of two basic principles: first, with the understanding of the Wiener process, and second, with the application of the binomial theorem. However, it can be seen that both principles provide the same expression of the "*probability of having a single molecule at the location of the RN,*" which, therefore, proves the correctness of both approaches, especially in the calculation of the additive diffusion noise in the concentration signal available for reception at the RN.

To understand diffusion of a molecule, the one-dimensional example as shown in Fig. 2.3 can be a good example. The steps taken by the molecule at each step is δ_X. The time the molecule remains in one state before it moves to the next state is τ. We consider an ensemble of Q_0 molecules present in the system. From the one-dimensional propagation

model shown in Fig. 2.3, it can be derived [BER-93] that if the molecule is at $X_i(t)$ at time t then at $(t+\tau)$ the position of the molecule will be

$$X_i(t+\tau) = X_i(t) + \sqrt{2D\tau}\,\mathcal{N}(0,1). \tag{2.6}$$

Similarly, the displacements in the Y and Z dimensions can be found as follows.

$$\begin{aligned} Y_i(t+\tau) &= Y_i(t) + \sqrt{2D\tau}\,\mathcal{N}(0,1) \\ Z_i(t+\tau) &= Z_i(t) + \sqrt{2D\tau}\,\mathcal{N}(0,1) \end{aligned} \tag{2.7}$$

The diffusion constant D, in cm^2/second unit, can also be defined as $D = k_D T_T / 6\pi\eta_{\text{fluid}}\rho_{\text{mole}}$, where k_D is the Boltzman constant, T_T is the absolute temperature, η_{fluid} is the viscosity of the fluid, and ρ_{mole} is the radius of the information molecules [FRE-99], p. 72.

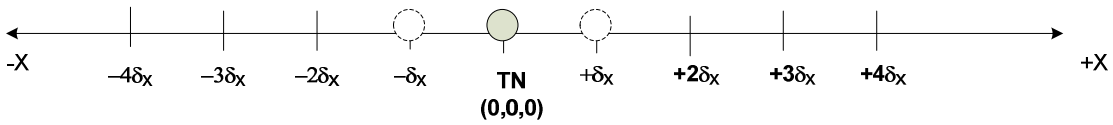

Figure 2.3 Molecules released at TN execute one-dimensional random walk. The molecule released at TN $(0,0,0)$ at $t=0$ has equal probability of taking the step to the right or to the left and move to $X=+\delta_X$ or $X=-\delta_X$ respectively at $t=\tau$. The similar phenomenon takes place after every step, thus completing an unbiased random walk in one dimension.

Explanation with Wiener Process

In the three-dimensional random-walk model considered in this work, a molecule starts its journey at time $t=0$ at (0,0,0), i.e. at the location of the TN. Each molecule moves to the right or to the left in exactly every τ seconds with a velocity of $\pm v_x$ a distance $\pm v_x\tau$. Although the parameters τ and δ_X depend on several factors, e.g. the size of the molecules, the size of the solvent (liquid) molecules, the structure of the liquid, and the absolute temperature, in normal diffusion-based MC system for the sake of simplicity we tend to consider τ and δ_X as constants and that probabilities of a molecule going to the left (p_L) and to the right (p_R) are equal, i.e. $p_L = p_R = 0.5$. Each step is memory-less, meaning that

the molecule jumps randomly to right or left forgetting what direction it went to in its last leg. Successive steps taken by the molecules are independent and the random walk is unbiased. Each molecule moves independently of all other molecules without interacting with other molecules, which is a reasonably realistic assumption when the solution is dilute [BER-93], p. 7. The propagation medium is assumed to be homogenous for the information molecules. The diffusion constant is assumed to remain unchanged in the entire duration of the observation time.

Each of the Q_0 molecules can be considered separately in the three-dimensional unbounded propagation environment. The molecule diffuses in three dimensions as per ideal diffusion in the propagation medium. The ideal (i.e. free) diffusion of a molecule can be explained as Wiener process [DUR-10], ch. 8, whereby the displacement of each molecule in the infinitesimal time τ (i.e after completing one jump) can be modeled by a Gaussian random variable with a variance of $2D\tau$. Since each jump of each molecule is a random process, the position of the molecule after time t can be thought of as a Wiener process after n_{jump} jumps where $t = n_{\text{jump}}\tau$. Considering each of the transmitted molecules separately, the probability density function (pdf) of a single molecule being available at the RN at the three-dimensional space $\left(X(t), Y(t), Z(t)\right)$ is a three-dimensional *normal* distribution with mean located at $(0,0,0)$, i.e. the location of the TN, and variance $2Dt$ in each dimension. This can be expressed as below. Diffusion mechanism being statistically independent in each of the three dimensions [BER-93], p. 11, this yields the probability of getting a molecule at the RN as the following, where $r^2 = x_r{}^2 + y_r{}^2 + z_r{}^2$.

$$P_{XYZ} = \frac{1}{\left(4\pi Dt\right)^{3/2}} \exp\frac{-r^2}{4Dt} \tag{2.8}$$

Explanation with Binomial Distribution

Availability of a molecule at the RN can also be explained using the binomial distribution. As mentioned before, the molecule steps to the right with a probability p_R and to the left with a probability p_L, where $p_L = 1 - p_R$. The probability that a molecule steps exactly k_{jump} times to the right in n_{jump} steps can be given by the binomial distribution [BER-93]. For

$p_R = p_L = 1/2$, mean displacement of a molecule after n_{jump} steps $\left\langle X(n_{\text{jump}}) \right\rangle = 0$ and the corresponding mean square displacement $\left\langle X^2(n_{\text{jump}}) \right\rangle = n_{\text{jump}} \delta_X{}^2$ [BER-93]. An information molecule steps an enormous number of times every second. As result, the values of both n_{jump} and $n_{\text{jump}} p_R$ (i.e. the number of steps taken to the right) are finite and large numbers. Correspondingly, when $n_{\text{jump}} \to \infty$, $n_{\text{jump}} p_R \to \infty$ is valid and under these conditions in a three-dimensional unbounded propagation environment, the binomial distribution can be approximated to normal distribution [BER-93], p. 121, as shown below.

$$p(\vec{r}, t) = \frac{1}{(4\pi D t)^{3/2}} \exp\left(-\frac{r^2}{4Dt} \right) \tag{2.9}$$

This is the probability of finding one molecule at a distance r where $r^2 = x_r{}^2 + y_r{}^2 + z_r{}^2$, and at time t, assuming spherical symmetry [BER-93], p. 21. The variance of this distribution in each dimension is $2Dt$.

2.5 CEMC Limitations

2.5.1 Speed of Communication

Unlike EM wave-based communication where the EM wave propagates at the speed of light (3×10^8 m/s), CEMC is extremely slow, providing the low speed in MC approximately in the range from nm/s to μm/s [NAK-11a]. In the case of diffusion-based CEMC, the molecules propagate by means of thermal excitation without expending any chemical energy. As a result, due to the random walk motion the molecules face an enormous number of collisions in the path and the effective communication range becomes less. In the case of molecular motor-based communication, the molecules (payloads) are carried by the molecular motors, e.g. kinesin, dynein, and myosin, over the molecular rails, e.g. microtubule networks, by converting the chemical energy into mechanical work [BUS-10], p. 33. The speed of movement of the molecular motor over microtubule networks is also very slow, which results in the low speed of the payload transfer in MC with the active transport. Yet both diffusion-based passive transport and molecular motor-based active transport mechanisms of MC provide unique ways to communicate at the nanoscale, which would probably not be easy by using other schemes of communication at the nanoscale. As an example of MC, a

macro-molecule, e.g. a functional protein, has a complex chemical structure that represents some specific biological functions, e.g. catalysis of a chemical reaction [NAK-11a]. Therefore, even if the speed is low MC provides a promising way of communication at the nanoscale.

2.5.2 Communication Ranges

The communication range is another important issue that limits the effectiveness of the CEMC. Unlike EM wave-based communication where the transmitter and the receiver can be as long as hundreds of kilometres away but still communicating reliably enough, the TN and the RN in CEMC should be in the range from nm to μm apart in order to make the communication reliable [MAH-10b]. Effective communication range is short because the concentration of molecules experiences attenuation and temporal spreading [MAH-10a] that make the available concentration of molecules very low in amplitude and distorted in nature when the RN is located far from the TN. It has been found that the closer the TN and the RN are the better the CEMC between them becomes.

2.5.3 Noise and Interference

As mentioned earlier, the molecular propagation is affected by the noise and the interference mainly because of the diffusion-based propagation of molecules in the propagation medium, the temporal spreading the signal experiences, and the undesired effects the signal receives from the surrounding environment itself. The first two cases produce ISI while the last one produces undesired molecules and undesired molecular reactions that create noise in the desired signal. In addition, the characteristics of the propagation medium and that of the information molecules also contribute to the noise effects that the signal experiences in the CEMC channel. For example, in the case of inhomogeneous medium the propagation effects may not be like those in the homogenous medium [VAN-05]. Interactions between information molecules and receptors can also create noise effects in the signal [THO-04].

2.6 Approaching CEMC Challenges

Given the technical challenges involving MC and nanonetworks, some recent research works that have been performed in this field towards addressing these challenges are briefly mentioned in this section. Recent research shows that MC techniques offer a high potential

in realizing nanonetworks. EM-based nanonetworks are the counterpart of MC-based nanonetworks [JOR-11] [AKY-10]. Network architecture and communication challenges of a generalized EM-based nanonetwork and its roles towards "*the Internet of nano-things*" have been presented in [AKY-10]. Given the fact that molecules travel probabilistically from TN to RN, the impulse response of the MC channel needs to be understood properly. MC receiver performance and channel characteristics must be investigated in detail before analysing any complex signaling technique and/or testing new algorithms. Temporal spreading causes ISI that influences the correct detection of the transmitted symbol and, therefore, ISI must be taken care of properly. Early results of CIR stemmed from the diffusion theory in the fluidic medium [MAH-10a] has found that molecular concentration experiences attenuation that is equivalent to path loss in traditional wireless communication. Concentration attenuation and temporal spreading of the CIR creates the ISI, which makes communication unreliable. When system architecture is concerned, it is known recently that the existence of chemically powered "*dream nanomachines*" is in the not-too-distant future [OZI-05]. The prospect of artificial bionanomachines created by integrating biomolecules with man-made nanostructure is very promising [NAK-11a] [MOR-10]. An example of a hybrid bio-nano-chemo-mechanical rotary device is the one assembled from ATP synthase and nickel propeller [OZI-05]. Weak MC signals can be amplified by using relay channels as shown in recent works [NAK-10a] [NAK-11c] where in the former [NAK-10a] the authors developed an information theoretic approach in the design and analysis of a molecular relay channel.

In order to address the mentioned challenges, recent research started with a basic distinction between *dry* and *wet* nanotechnologies [GUL-10]. Dry and wet nanotechnologies have been mentioned in Section 2.3.1. In the framework of wet technologies, the behaviour of the materials change drastically [ALF-06] and it may not be suitable to use EM wave-based techniques in the wet nanotechnology setting; rather it is a better idea to draw the inspiration from biology in order to design communication system and signaling [ALF-06]. Bio-inspired MC-based communication is, therefore, still quite unexplored compared to the matured traditional communication systems at the macro-scale.

MC-based technologies are very useful in the design of nano-chips because of its high energy efficiency compared to its conventional counterpart based on electrical signaling

[ALF-06]. In addition, wet technologies possess resilience to failures [ALF-06], which makes it very attractive as a communication technology in aqueous medium. Diffusion of molecules can avoid necessary wiring in electronics when they can be used to connect nanomachines. Therefore, it is anticipated that the wet technologies would possibly be very useful in the future networks-on-chip (NoC) as well [ALF-06].

2.6.1 Engineered and Artificial Nanomachines

By virtue of recently achieved developments on the area of nanomachines and MC, it is now possible to engineer nanomachines to do required and controlled tasks, e.g. to achieve synchronization between the TN and the RN [MOO-07] [MOO-11], control the release rate of molecules such that concentration-based modulation schemes become possible [NAK-11a] [SCH-93]. It is also possible to develop logic gates by using Belousov-Zhabotinsky (BZ) reactions [MOO-07], realize impulsive passive transportation and intercellular passive transportation [MOO-07], and produce some required functionalities in biological cells by applying genetic engineering [NAK-11a]. DNA logic gates can also be built by using the pieces of single- and double-stranded DNA [KRO-11]. Several other circuits can also be built by using molecular technology, e.g. the largest molecular circuit that has been built is composed of 74 different DNA molecules and can compute the square root operation of any number up to 15 and round the answer to the nearest integer [KRO-11].

The principles of nano-mechatronics need to be explored in view of the nanomachines and it is hoped that such bionanomachines will play a very constructive role in the field of nanomedicine and molecular biomedical engineering in the future [LIU-12]. On another note, the research on artificial nanomachines [OZI-05] using biological materials has also achieved a noticeable development. For example, biological cell-like structures by using lipid bilayers [NAK-11a] and “minimalistic” nuclear pore complex (NPC) [JOV-11] by using biological and synthetic components together are now possible. NPC is a large protein complex that crosses the nuclear membrane for allowing the transportation of water-soluble molecules (including ribonucleic acid (RNA) and ribosomes) across this membrane [ALB-08], p. 705. Very recently, a group of scientists at the California Institute of Technology built “the most complex biochemical circuit ever created from scratch” [KRO-11] that would help us understand the biological information processing system and biochemical

pathways in more detail, which would provide more control over the biochemical reactions and possibly biological nanomachines with enhanced capabilities [KRO-11]. When the TN releases a number of information molecules, it is important that the molecules be received in the sequence that they were sent with, else not receiving molecules in-sequence would certainly introduce decoding errors. To ensure in-sequence molecule delivery three classes of approach, namely, sender-oriented, receiver-oriented, and environment-oriented approaches, have been proposed in a recent work [NAK-10b] where the authors modeled the reception noise on the basis of ligand-receptor kinetics and stochastic chemical kinetics.

2.6.2 Engineered CEMC

It is also possible to engineer CEMC and produce controlled propagation, switching, addressing among nanomachines [NAK-11a]. Ideal diffusion-based CEMC is in principle a broadcast communication technique where the information molecules undergo random walk motion. As shown earlier, the RN contains a finite number of receptors on its surface and the receptors are specific and can respond to a single type of information molecules only in a concentration-dependent manner, meaning that the RN responds only when a certain number of information molecules is present in a high enough concentration, e.g. above a threshold value or between a band of concentration levels. This gives a provision that the TN can select an RN by sending the information molecules in an appropriate number such that they can be present at the RN in a desired concentration. By controlling the amount of transmitted molecules the TN can select the desired RN. For example, when a TN wants to communicate with a nearby RN (with a known concentration band on which the RN responds) the TN can adjust the transmitted number of molecules such that the concentration of molecules at the particular RN nearby only reaches a desired threshold concentration and the concentration of information molecules at distant RNs cannot reach the desired concentration and so they cannot respond to the TN's communication. By this the TN can adopt an addressing mechanism in a concentration-dependent manner [NAK-11a]. For instance, it is possible to engineer a bacterium to transmit information molecules called Vibrio fischeri Auto-Inducer (VAI) and the VAI molecules create a concentration gradient in the fluidic medium, the highest of the concentration gradient being located at the location of the TN. Thus it is possible for the TN to communicate selectively with the

desired RN by adjusting the number of transmitted molecules. Some interesting works also include measuring and analyzing distance in MC [MOO-12b], investigating into transmission, propagation, and reception options [MOO-12] as well as multiplexing in MC [MOO-12a].

2.7 Applications of Molecular Nanonetworks and Their Roles to the Emerging Society

Molecular nanonetworks in general have several potential applications that would most likely bring about constructive changes to our emerging society in the next few decades when the research and development in this area will be matured enough to offer many fruitful applications [AKY-08] [NAK-12]. A few of those potential applications have been mentioned in this section.

Biomedical applications are the most important and major application group that would be benefitted by molecular nanonetworks. For example, it is now already known that with the help of nanotechnology and nanoscale communication it is possible to interact with biological cells, tissues, and organs [NAK-11a] [MAH-12]. In addition, molecular nanonetworks offer biocompatibility and biostability. Their principal applications in the biomedical field would be in developing immune system support systems, bio-hybrid implant systems, targeted drug delivery systems, health monitoring systems, and nano-systems modified with genetic engineering [AKY-08]. MC can help fight against cancer by providing new knowledge in its detection and treatment. Drugs may be encapsulated in nanoscale capsules and then propagated in the medium. These nanoscale capsules can bind to specific receptors of the cancerous cells. The nano-capsule is the communication interface and it ensures any drug to reach the correct location. This approach also reduces the amount of drug necessary and so reduces side effects. From another point of view, when a nanomachine can detect some special molecules released from a sick (e.g. cancerous) cell it can announce, through the nanonetworks it belongs to, that there is a sick cell in its vicinity and thereby other nanomachines and/or cells nearby become alerted about that and can turn on their protective measures against that [MAH-12].

In the development of *industrial and consumer products*, nanonetworks can help with the new materials, processes, and novel quality control techniques. For example, advanced food and water quality control techniques could be developed that are capable of detecting

small bacteria and toxic substance in food and water [AKY-08]. In addition, advanced fabrics that contain nanonetworks would be able to provide improved functionalities, e.g. antimicrobial textiles [AKY-08], and could be another application area of the molecular nanonetworks.

Molecular nanonetworks would bring a remarkable progress in the *military* field. For example, molecular nanonetworks could be used in the battlefield in order to monitor battlefield and soldier performance. They could also be used in the detection of harmful chemical and biological agents as part of defense activities [AKY-08].

Finally, molecular nanonetworks would bring several benefits in the environmental applications. One main reason is that they are principally bio-inspired. For example, molecular nanonetworks could be used to help in the bio-degradation processes in garbage-handling [AKY-08]. In nature, it is found that nanoscale communication with pheromones is a means to trigger some of the behavioural processes among species. Thus it may be possible to use molecular nanonetworks to control the presence of animals in particular regions of the environment, thereby helping in the animal and bio-diversity control [AKY-08]. Nanonetworks could also be used to monitor and control air pollution. Nano-filters could provide improved air quality by removing harmful materials from the air [AKY-08].

The role of active transport on chip design— It is possible to have bio-molecular motors working outside the biological cells in favourable aqueous conditions, e.g. with a suitable temperature and pH. This has a potential application in chip design based on bio-materials. It is expected that chips based on bio-materials would have extended capabilities [HIY-09] [HIY-10] over conventional chips manufactured with dry techniques. The first successful demonstration of molecular delivery system for MC with experiment has been performed by NTT DoCoMo [DOC-08].

2.8 Conclusion

This chapter provides a brief state of the art of MC system in general. A brief background on the involvement of nanotechnology into communication system is presented by describing the relationship between nanomachines, nanonetworks, and MC. CEMC system is then described in detail with system components, system processes, and diffusion-based propagation of molecules in fluidic medium. This chapter also explains how engineered

CEMC systems would be developed. Finally, several limitations of CEMC are discussed and benefits of molecular nanonetworks to the emerging society are explained by providing several novel applications to the good of humankind.

Chapter 3: Characteristics of Diffusion-based CEMC

3.1 Introduction

The main focus of this chapter is given to spatiotemporal distribution of signal strength, modulation schemes suitable for short-range, medium-range, and long-range CEMC, transient loss, and detection noise margin in CEMC between two communicating nanomachines in a nanonetwork. Spatiotemporal distribution of a carrier signal in the form of concentration of diffused molecules in the molecular propagation channel and diffusion-dependent communication ranges have been explained for various scenarios. Finally, the performance analysis of modulation schemes has been evaluated in the form of steady state loss of amplitude of the received concentration signals and its dependence to transmitter-receiver distance.

In this chapter, spatial and temporal distributions of concentration signal intensity is discussed with the reference to mean concentration signal intensity discussed in Chapter 2. Two significant open problems in wet techniques are the following: (a) determine and characterize the signal strength of the molecular propagation channel, and (b) find efficient modulation schemes such that RNs can identify the message conveyed by the particular flow of molecules with the highest accuracy possible. As explained in Chapter 2, signal intensity is defined as the concentration of information molecules, emitted by TN, at a certain point in the propagation medium at a certain instant of time. First, we focus on the case of binary CEMC with the information encoded in the amplitude of transmission rate of information molecules. In this chapter, we provide an in-depth analysis of spatial distribution of the signal intensity and signal strength and relate that with range and time for three different types of propagation media, namely, air, water, and blood plasma. We also investigate different modulation approaches and find out how the molecular signal behaves within the channel in the selected propagation media.

The main factors that affect spatiotemporal molecular concentration distribution of received molecules are the distance between RN and TN, diffusion constant, transmission rate, and concentration threshold. The TN-RN distance and transmission data rate affect modulation and detection of concentration signal, and for this reason they will be investigated thoroughly.

Most of our results on characteristics of diffusion-based CEMC system presented in this chapter have been published in [MAH-10], [MAH-10a], [MAH-10b], and [MAH-11].

This chapter is organized as follows: Section 3.2 discusses the related work on this area. Section 3.3 describes the system model. Section 3.4 gives a brief description of the modulation options for CEMC system. Section 3.5 discusses the performance of a CEMC system as described by Fick's laws diffusion dynamics. Finally, Sections 3.6–3.8 describe the performance of the CEMC system under various scenarios. Finally, Section 3.9 concludes the chapter.

3.2 Related Work

Related work on this area includes a physical end-to-end model for molecular communication including transmitter, propagation, and receiver modules that provided numerical results for normalized gain and delay as functions of input frequency and communication range [PIE-10]. An energy model for the communication among nanomachines based on energy budget of transmitter was proposed in [KUR-10]. A design of in-vitro MC technique was reported in [MOO-09a] that evaluated the system by maximizing the probability of information molecules reaching the receiver and the rate of information molecules reaching the receiver. In [ATA-08], using the principles of mass action kinetics a molecule delivery model was introduced and correspondingly an information theoretical approach was developed to derive a closed form expression of capacity of a molecular channel between two nanomachines. The work in [ATA-08] also proposed an "adaptive molecular error compensation scheme" for MC between the nanomachines.

The major attention of the work in [PAR-09] is on long range MC options. Information capacity bounds with distinct and non-distinct particles in Brownian motion have been analyzed theoretically in [ECK-07] and [ECK-07a]. The work in [LAC-09] used "orientating" parameter values for the analyses. By "orientating" it was reported in [LAC-09] that factors e.g. pressure, communication medium, and temperature influence diffusion constant D for each environment, and thus the values of D were chosen in a range of values for a particular medium. For instance, for air, water, and human body (blood plasma) media, the selected values of diffusion constant D are 0.43, 10^{-6}, and 2.2×10^{-7} cm^2/s

respectively. However, an in-depth numerical analysis is necessary before attempting the use of such parameter values in the analyses. This chapter provides an extensive numerical analysis on molecular concentration, modulation, detection loss and its limitations for the three selected propagation media. This knowledge is a must for producing an accurate parameterization process of an end-to-end CEMC system.

3.3 System Model

In order to derive the channel characteristics and diffusion-based noise distribution, we first consider an instantaneous transmission of Q_0 molecules at the location of the TN $(0,0,0)$ at time $t = 0$ as shown in Chapter 2. Instantaneous transmission is important because it would provide the CIR of the CEMC system. When CEMC channel is fully understood, it would be possible to investigate several other transmission and modulation schemes, e.g. PAM, on-off keying (OOK), and FSK [HAY-00], p. 205, 247, 345, in the CEMC channel, in order to show the performance of the CEMC channel when a specific modulation scheme is applied. In this chapter, we also refer to Fig. 2.1 and assume the following in the system.

- **Transmitter:** The TN can precisely control the departure time and the number of molecules. The TN is transparent to the released molecules, meaning that the TN does not affect the movement of the released molecules nor does it react with them. The medium between the TN and the RN is three-dimensional, with the transmitter located at the origin $(0,0,0)$ and the RN at any other location in the three-dimensional space. The location of the RN can be identified by the vector $\vec{r} = \hat{i} \cdot x_r + \hat{j} \cdot y_r + \hat{k} \cdot z_r$ that has the origin as the starting point and the location of the RN as the ending point. Here $\hat{i}, \hat{j}, \text{and } \hat{k}$ denote the unit vectors in $X, Y,$ and Z axes respectively, $r^2 = {x_r}^2 + {y_r}^2 + {z_r}^2$ and r is the Euclidian distance between the TN and the RN. The TN releases a number of molecules of the same type and each of the molecules propagates independently to the RN meaning that for molecules i and j, the paths $B_i(t)$ and $B_j(t)$ to the RN are independent if $i \neq j$. Following the ideal diffusion mechanism based on random walk motion [BER-93], p. 11, the RN decodes the information symbols by measuring the molecular concentration at its receptor's location [MAH-11]. The TN and the RN are synchronized in time [MOO-09a] [MOO-11]. Time-synchronization between the TN and the RN can be achieved by using external signals [MOO-11].

• **Propagation:** The molecules undergo ideal (i.e. free) normal diffusion in the propagation medium in three dimensions. This means that in each dimension in space each of the released molecules has equal probability of taking the next step to the right (forward) or to the left (backward) from its previous position [BER-93], p. 7. In addition, the molecules propagate infinitely even after the first hitting time at the RN. The RN can sense the number of molecules available for reception at the RN and the molecules that reach the RN are not removed from the system [ATA-10]. This ensures free diffusion of molecules according to Fick's laws [BER-93], p. 18, [BOS-63], and the molecules can, therefore, become available to the RN multiple times according to the ideal diffusion phenomenon in three dimensions in an unbounded propagation medium. Unlike the use of the time of arrival of a single molecule at the RN or other encoding schemes, the concentration of available molecules at the location of the RN is used to decode the information symbols.

• **Receiver:** The sensing time of RN is much shorter than the passage time, regardless of whether it is a *first passage time* (FPT) or a higher order passage time. The first passage time of a molecule is the time duration from the release of the molecule at TN to the time instant when the molecule first hits the receptor of the RN [ECK-07a]. Alternatively, FPT can also be termed as the *propagation delay*. Higher order passage times indicate scenarios when the molecule reaches the RN multiple times. The RN contains a number of receptors on its surface with which it senses the intensity of concentration (see Fig. 2.1). Surrounding the RN we assume a small VRV [ATA-10] with the RN located at its centre. Diffused molecules interact with the receptors and may bind with them according to *molecule-receptor binding process* (MRBP) that depends on the affinity of information molecules to the receptors. In general, we consider available molecules at the location of the RN wherever MRBP is not specified.

In addition, regarding the propagation of molecules, in the discrete-time random walk model of ideal diffusion, the step size δ_X and the time τ, i.e. the time the molecule remains in one state before it moves to the next state are constant [BER-93], p. 7, [BOS-63]. Also, in ideal diffusion, the movement of a molecule to a new position is statistically independent of its previous movement. This makes the discrete-time random walk model Markovian. In anomalous diffusion model, δ_X and τ are considered as random variables [MET-00]. Investigative results of CEMC based on anomalous subdiffusion are presented in Chapter 8.

3.3.1 System Components

As shown in Fig. 2.1, a generic CEMC system between a pair of nanomachines consists of a TN, an RN, and a propagation medium between them. The propagation medium can also be thought of as "channel" [MAH-10a] in similarity with the traditional wireless communication systems [RAP-02]. The TN transmits information molecules at a given rate. Examples of information molecules are proteins and ions that contain information to be transmitted. Examples of propagation medium are water (D = 10^{-6} cm^2/s), air (D = 0.43 cm^2/s), and blood plasma (D = 2.2 $\times 10^{-7}$ cm^2/s for simple message and 1 $\times 10^{-9}$ cm^2/s for complex message) [LAC-09]. Both TN and RN are artificial devices or modified biological cells [NAK-11a]. RN can receive information molecules at its receptors.

While in the propagation medium there may exist other molecules that may cause undesired chemical reactions [MOO-07] and thus may create noise in the system, we have not considered such cases in our research and so in the system model presented in this chapter we consider that the propagation medium consists of solvent molecules only through which the information molecules diffuse and ultimately reach the RN probabilistically. It should be noted that information molecules (e.g. protein, ion) are different from solvent molecules (e.g. water, air, blood plasma) and are of larger size than the solvent molecules.

3.3.2 CIR Characteristics: Distance and Temporal Dependence

The idea of CIR of the CEMC channel in nanonetworks came in fact from the well-known time-dependent solution to concentration of diffused substance as governed by the macroscopic theory of diffusion and expressed by Fick's laws [BER-93], p. 18, [BOS-63]. Unlike EM wave-based propagation, molecular propagation should be treated with the particle theory of propagation. For example, the number of molecules available for reception from a point source per unit of volume can be calculated from the solutions to Fick's laws of diffusion as the following [BOS-63].

$$U(r,t) = \frac{Q_0}{(4\pi Dt)^{\frac{3}{2}}} \exp\left(\frac{-r^2}{4Dt}\right) \tag{3.1}$$

Here the symbols have already been explained earlier. The diffusion constant D depends on the medium through which molecules propagate. The average CIR of CEMC

channel and its characteristics can be deduced from Eq. (3.1) [MAH-10a]. In order to determine the CIR, the CEMC channel is excited by an impulsive emission of Q_0 molecules released at time $t = 0$ and the average CIR in response to this can be expressed as Eq. (3.1).

The output concentration signal intensity $U(r,t)$ can also be expressed as the following.

$$U(r,t) = Q_0 \otimes g(r,t) \tag{3.2}$$

Here $g(r,t)$ is the average CIR of CEMC channel and is expressed as

$$g(r,t) = \frac{1}{(4\pi Dt)^{3/2}} \exp\left(\frac{-r^2}{4Dt}\right) \tag{3.3}$$

and the symbol ⊗ indicates convolution operation in time domain.

The impulse response of CEMC channel needs to be investigated in order to find output concentration of molecules at the location of RN. CIR $g(r,t)$ is a function of both time t and TN-RN distance r. Investigating into $g(r,t)$ it is clear that, unlike EM wave-based propagation, modeling CEMC channel cannot be explained in terms of separate distance dependence and temporal dependence. For instance, the exponent part in the expression of $g(r,t)$ is a function of both distance r and time t. In free space, EM waves propagate at the speed of light (3×10^8 m/s). In some cases, wireless channels are realistically assumed to be stationary for short propagation times between sender and receiver. But unlike EM wave propagation, molecular propagation is a very slow process and so spatiotemporal variation of CIR should be investigated in-depth even for short distances [MAH-10]. Spatiotemporal variation rather plays a significant role in terms of the analyses of path-loss and output signal. As mentioned earlier, the concentration of molecules at a distance r and at time t, $U(r,t)$, is the intensity [MAH-11] of molecular concentration signal at RN. Therefore, any integral of $U(r,t)$ over time would indicate the strength (or, alternatively, energy) [MAH-11] of CEMC signal. CIR $g(r,t)$ is normalized to its total energy (i.e. strength) over the entire observation time as $g(r,t) \Big/ \int_0^{T_{obs}} g(r,t)dt$ [MAH-13] [MAH-13d] where, in ideal case of diffusion of molecules, $T_{obs} = \infty$; however, in numerical simulations, T_{obs} = 1–10 hours should be reasonable enough to study the performance of CEMC systems. Figure 3.1 below shows the energy-normalized CIR $g(r,t)$ at TN-RN distances of 800 nm and 100 μm in water medium. As shown in Fig. 3.1, CIR becomes temporally spread when r increases

causing ISI in signal detection. A comparison of the characteristics of CIR of CEMC channel at different TN-RN distances in air medium can be found in [MAH-10a] whereas the performance of CEMC system based on binary pulse transmission scheme in air, water, and blood plasma propagation media can be found in this chapter and has been reported in [MAH-10b]. Figure 3.1 below shows the temporal spreading of CIR as sensed by the RN over a time scale up to 200 s and at communication ranges of 800 nm and 100 μm in water medium. CIR is of significant importance because it indicates the amount of pathloss in the form of concentration loss and its temporal spreading in propagation for different TN-RN distances. The distance-dependence of CIR can be used to investigate into the effects of pathloss and residual molecules during symbol detection process. As shown in Fig. 3.1, the number of molecules available for reception at the RN is reduced as communication range increases.

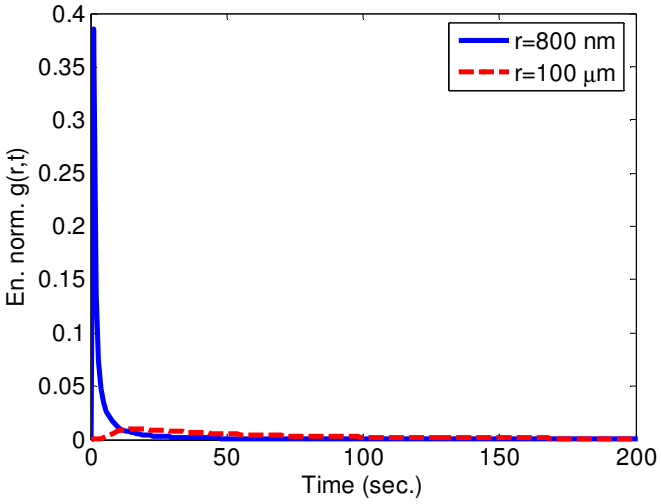

Figure 3.1 The CIR of the CEMC channel sensed by the RN when the propagation medium is water. As shown in Chapter 4, RN is a sampling-based receiver that samples the concentration intensity at regular (uniform) time intervals of 1 s known as the sampling intervals.

3.3.3 Extension to Time-Dependent Transmission

In addition to the instantaneous transmission as mentioned above, time-dependent transmission rate, i.e. when transmission rate of molecules at the TN is a function of time, is quite common in nature [KRI-02] [ROS-00] and so can be used in CEMC [ALB-08], p. 74, [MOO-11a], [MOS-05]. The output of CEMC channel in response to time-dependent transmission signals can be computed by taking time-domain convolution of the

transmission rate with the CIR of CEMC channel. For example, considering spherical symmetry, when $Q(t)$ is the time function of transmission rate of molecules in molecules per second unit, mean available concentration signal intensity at a distance r and time t can be expressed by taking the integral as below [BOS-63].

$$U(r,t) = \int_0^t \frac{Q(\varsigma)}{\{4\pi D(t-\varsigma)\}^{\frac{3}{2}}} e^{\frac{-r^2}{4D(t-\varsigma)}} d\varsigma = Q(t) \otimes g(r,t) \tag{3.4}$$

where $r^2 = x_r^{\,2} + y_r^{\,2} + z_r^{\,2}$ when a Cartesian coordinate system is assumed, ς is the variable of integration, and the other symbols are as described earlier.

3.4 Transmission and Modulation Schemes

In the transmission phase of CEMC, the TN releases molecules in the propagation medium. The transmission rate, or in other words, the concentration of transmitted molecules at the TN can be varied in several ways, based on the characteristic feature of the concentration signal at the TN. In the following, we focus on three commonly used modulation schemes in CEMC.

3.4.1 Impulse Modulation

In impulse modulation (IM), the TN releases all the molecules as an impulsive manner at the beginning of each symbol. Two different schemes, namely, generalized amplitude-shift keying (ASK)-based and OOK-based schemes, can exist in IM. In generalized ASK scheme, as shown in Eq. (3.5), the TN transmits $Q_1\delta(t)$ and $Q_0\delta(t)$ molecules when it wants to send a symbol[6] 1 and 0 respectively [MAH-13], where $Q_1 \gg 1$, $Q_0 \gg 1$, $\delta(t)$ is the Dirac delta function [HAY-02], and $Q_1 > Q_0$ in general. Here $Q(t)$ denotes the signal transmitted by the TN.

$$Q(t) = \begin{cases} Q_1\delta(t) & \text{Bit 1} \\ Q_0\delta(t) & \text{Bit 0} \end{cases} \tag{3.5}$$

[6] In binary scheme, each symbol is represented as a bit (1 or 0), while in M-ary scheme, each symbol composes of $\log_2 M$ bits, where M is the alphabet size [HAY-00].

However, in OOK scheme, as shown in Eq. (3.6), the TN sends Q_1, where $Q_1 \gg 1$, molecules when it wants to send symbol 1 and does not send any molecules at all when it wants to send symbol 0, meaning that the TN remains apparently in "on" and "off" states while transmitting bits 1 and 0 respectively. Figures 3.2(a) and 3.2(b) show ASK and OOK schemes based on IM in CEMC.

$$Q(t) = \begin{cases} Q_1 \delta(t) & \text{Bit 1} \\ 0 & \text{Bit 0} \end{cases} \tag{3.6}$$

3.4.2 Pulse Amplitude Modulation

Pulse-based transmission of molecules in CEMC system is also possible. Unlike impulsive transmission, in pulsed transmission, e.g. in PAM, the TN sends a pulse of molecules with a given pulse-width T_p where $0 < T_p \leq T_{sym}$ and T_{sym} denotes the symbol interval. A given T_{sym} determines the separation between the starts of two consecutive pulses of molecules representing two different symbols 1 and 0, and so, T_{sym} determines the effective data rate f of the CEMC system as $f = 1/T_{sym}$. Like in conventional communication systems, in CEMC it is also desired to have a higher transmission data rate in order to increase the speed of communication, which faces a challenge in providing reliable CEMC with lower BER between nanomachines while minimizing the effects of ISI.

Like in impulsive transmission, it is also possible to have generalized ASK and OOK schemes both based on pulse transmission. In pulse-based ASK scheme, the TN sends pulses of two different amplitudes to represent the symbols 1 and 0. Eq. (3.7) expresses the signal for each symbol when ASK-based transmission is adopted, where $Q_1 \gg 1$, $Q_0 \gg 1$, and $\Pi(t)$ denotes a rectangular pulse with unity amplitude. The amplitude of the pulse $\Pi(t)$ is unity from $t = 0$ to $t = T_p$ and 0 everywhere else.

$$Q(t) = \begin{cases} Q_1 \Pi(t); & \text{Bit 1} \\ Q_0 \Pi(t); & \text{Bit 0} \end{cases} \tag{3.7}$$

OOK scheme is a special case of ASK scheme when $Q_0 = 0$. As shown in Eq. (3.8), in pulse-based OOK, the TN sends a pulse of molecules only to represent symbol 1 and does not send any molecules to represent symbol 0 and, hence, it apparently remains "off" to represent symbol 0. A detailed account of pulse-based modulation schemes in CEMC can be

found in [MAH-11], [MAH-10b], [MAH-11a], [MAH-11d], [MAH-11b]. Figures 3.2(c) and 3.2(d) show pulse-based transmission schemes in CEMC.

$$Q(t) = \begin{cases} Q_1 \Pi(t); & \text{Bit 1} \\ 0; & \text{Bit 0} \end{cases} \tag{3.8}$$

3.4.3 Multilevel PAM

By varying the number of molecules transmitted by the TN, it is possible to design a multilevel PAM (M-PAM) scheme based on generalized ASK. In M-PAM, the TN transmits each symbol by using one of the M different transmitted numbers of molecules, meaning that each symbol can be represented by $\log_2 M$ bits being transmitted [MAH-11a]. It is possible to implement M-PAM based on both IM and PAM schemes. Transmitted signals in M-PAM can be expressed as shown in Eq. (3.9) below.

$$Q(t) = Q_m \Pi(t), \text{ where } m = \{1, 2, 3, ..., M\} \text{ and } Q_m \gg 1. \tag{3.9}$$

3.4.4 Sinusoidal Transmission Scheme

While IM, PAM, and M-PAM modulation schemes are all based upon varying the amplitudes of the transmitted number of molecules in impulse-based and pulse-based transmissions, it is also possible to vary the rate of change of the sinusoidal variation of molecular transmission rate, thereby making it possible to design FSK modulation in CEMC [MAH-10]. As shown in Fig. 3.3, transmitted signals in sinusoidal-based transmission can be expressed as below.

$$Q(t) = Q_{\text{average}} + Q_{\text{amp}} \sin(2\pi f_{\text{sin}} t) \tag{3.10}$$

Here Q_{average}, Q_{amp}, and f_{sin} denote the average, the amplitude, and the frequency of sinusoidal transmission of molecules respectively at the TN. Since concentration of molecules can never be a negative number, in Eq. (3.10), $Q_{\text{average}} \geq Q_{\text{amp}}$. In Eq. (3.10), different information symbols can be encoded by varying either of Q_{average}, Q_{amp}, and f_{sin}, or any combination of these quantities. Based on sinusoidal signaling, varying amplitudes Q_{average} and/or Q_{amp} would give multilevel amplitude modulation (M-AM), while varying f_{sin} would give FSK scheme [MAH-10b] [MAH-11c].

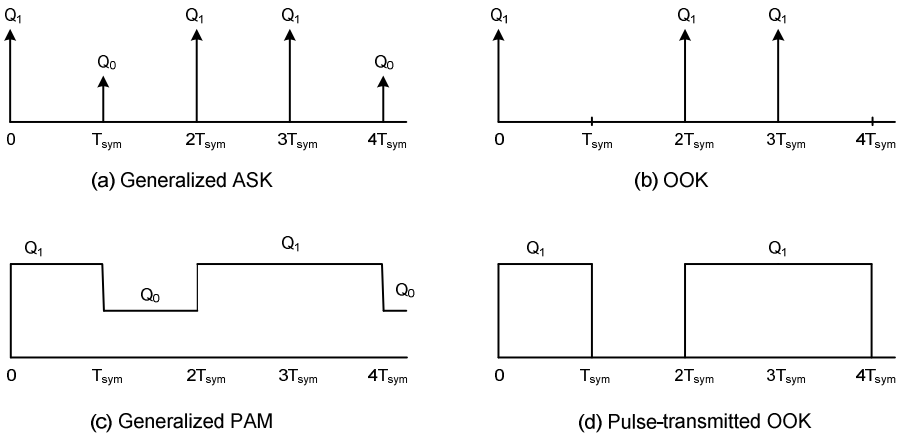

Figure 3.2 Generalized ASK and OOK transmission schemes: IM in (a) and (b), PAM in (c) and (d). For PAM, $T_p = T_{sym}$ is assumed.

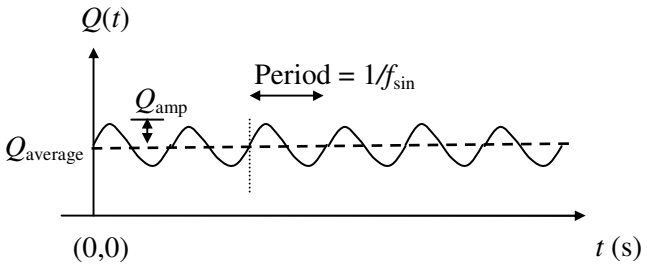

Figure 3.3 Continuous transmission with sinusoidal variation where f_{sin} is the frequency of sinusoidal variation.

3.5 Fick's Laws Diffusion Dynamics

In CEMC, amplitude and frequency (i.e. the rate of change of amplitude) of the concentration signal are two important characteristics of the transmitted signal that can be varied in order to materialize various modulation schemes as shown in Section 3.4. As shown earlier, in IM and PAM, information symbols are represented by the number of transmitted molecules at the beginning of symbol interval by following impulsive and pulsed transmissions respectively. In order to represent different symbols, FSK-modulated signaling in CEMC relies on varying the frequency of amplitude variation of information

molecules at the TN. In this section, based on Fick's laws of diffusion, we focus on mean concentration of molecules at the location of RN.

3.5.1 Fick's Laws Concentration Channel

Fick's laws of diffusion have been widely known for a long time [EIN-05] [PHI-06] and express the mean concentration of information molecules that become available at RN through propagation by means of Brownian motion [BOS-63]. In ideal diffusion, it is assumed that the total number of molecules is conserved, i.e. no molecules are created or destroyed, which provides us with the probability of having a molecule available at the RN as shown in Section 3.3.2. Several works that focus on the concentration channel based on Fick's laws are reported in [MAH-10a], [MAH-10b], and [SHA-12].

3.6 Pulse-based CEMC Model

3.6.1 Single Pulse Transmission

In pulse-transmitted CEMC system, in order to understand the performance of transmitting a bit sequence completely, it is necessary to first understand the performance of transmitting a single pulse in CEMC channel. Figure 3.4 shows output signals at various communication ranges when a single pulse with pulse width 50 s is transmitted by the TN. As shown in Fig. 3.4, when communication range increases, signal gets temporally spread and thereby causes increased level of ISI at the current symbol.

The performance of a pulse transmission can be explained on the basis of *desired signal strength ratio* $S_{(r,f)}$ and *interference strength ratio* $I_{(r,f)}$ expressed as shown in Eq. (3.11), where E_S, E_U, and E_I are *received desired signal strength*, *received total signal (i.e. desired and interference signals) strength*, and *received interference signal strength* respectively [MAH-11].

$$S_{(r,f)} = \frac{E_S}{E_U} = \frac{\int_0^{T_{\text{sym}}} U(r,t)dt}{\int_0^{T_{\text{obs}}} U(r,t)dt} \quad \text{and} \tag{3.11}$$

$$I_{(r,f)} = \frac{E_I}{E_U} = \frac{\int_{T_{\text{sym}}}^{T_{\text{obs}}} U(r,t)dt}{\int_0^{T_{obs}} U(r,t)dt} = \frac{(E_U - E_S)}{E_U} = 1 - S_{(r,f)}$$

Here E_S, E_U, and E_I can be found by taking integrals of the ouput signal $U(r,t)$ over $(0,T_{\text{sym}})$, $(0,T_{\text{obs}})$, and $(T_{\text{sym}},T_{\text{obs}})$ intervals respectively, as shown in Eq. (3.11), where T_{sym} and T_{obs} denote symbol duration and observation time respectively.

In case of single pulse transmission, Fig. 3.5 shows the strength ratio quantities at various communication ranges. When r increases beyond 10 μm, $S_{(r,f)}$ decreases, meaning that the effective desired signal strength decreases. Since at any r and f, $S_{(r,f)} + I_{(r,f)} = 1$, when $S_{(r,f)}$ decreases, $I_{(r,f)}$ increases and vice versa. A decrease in $S_{(r,f)}$ indicates that more of the output signal strength would be interfering with the detection of the current symbol, and hence an increased level of ISI at the RN.

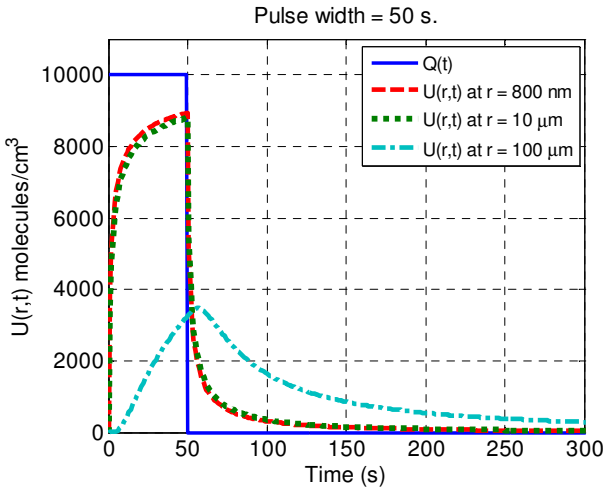

Figure 3.4 Available concentration signal intensity at the RN in response to a pulse transmission of pulse width of 50 s, i.e. data rate f = 0.02 bits per second (bps), in water medium [MAH-12a].

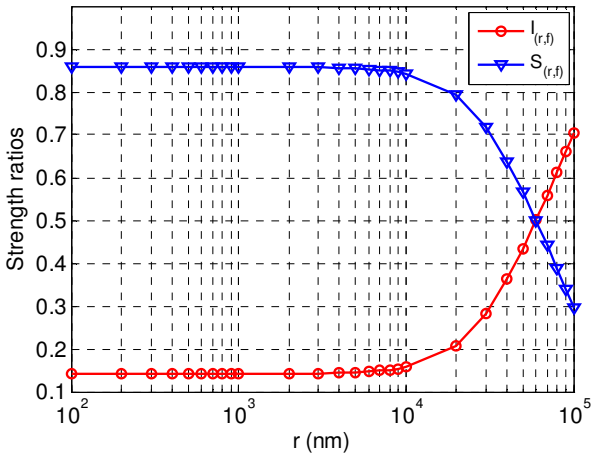

Figure 3.5 Strength ratios at various r when pulse width is 100 s and observation time is 10000 s.

3.6.2 Bit Sequence Transmission

While the performance of a single pulse transmission provides us with the concepts of desired signal strength and interference signal strength in case of single pulse only, a similar approach can be adopted in pulse-transmitted CEMC scheme in order to send a sequence of bits in the propagation medium. Performance metrics in case of pulse-transmitted OOK-modulated scheme for transmitting a random sequence of bits have been provided in detail in [MAH-11]. As shown in Fig. 3.2(d), a TN releases molecules at a fixed rate of Q_1 molecules per second during the entire symbol duration T_{sym} when it wants to send a bit 1 and does not transmit any molecule at all when it wants to send bit 0. Therefore, the entire observation time can be given as $T_{\text{obs}} = N_b T_{\text{sym}}$ where N_b is the total number of bits in the bit sequence to be transmitted. In case of transmitting a random sequence of bits based on OOK modulation, the signal strengths E_S and E_I can be expressed as the following [MAH-11].

$$E_S = \int_0^{T_{obs}} s_{\text{approx}}(t)\,dt \quad \text{and} \quad E_I = \int_0^{T_{obs}} i_{\text{approx}}(t)\,dt \tag{3.12}$$

Here the signal quantities $s_{\text{approx}}(t)$ and $i_{\text{approx}}(t)$ in Eq. (3.12) can be expressed as follows and incorporate the effects of residual molecules originating from the previous symbols that contribute to desired signal strength at the current symbol [MAH-11].

$$s_{\text{approx}}(t) = \begin{cases} U(r,t) & \text{when } U(r,t) \le Q(t) \\ Q(t) & \text{else.} \end{cases} \tag{3.13}$$

$$i_{\text{approx}}(t) = \begin{cases} U(r,t) - Q(t) & \text{when } U(r,t) > Q(t) \\ 0 & \text{else} \end{cases}$$

The strength quantities E_S and E_I are very useful in the sense that they can provide us with the techniques to determine effective communication ranges in CEMC [MAH-10b]. It should be noted here that E_S and E_I provide approximate values of the signal and the interference strengths only respectively, and therefore, do not provide accurate estimates of the same [MAH-13d]. Based on Eq. (3.12), in pulse-transmitted OOK scheme, the corresponding strength ratios for transmitting a random sequence of bits can be found as $S_{(r,f)} = E_S / E_U$ and $I_{(r,f)} = E_I / E_U$ respectively, where E_U is as described in Eq. (3.11). For transmitting a random sequence of bits, as shown in Fig. 3.6(b), due to the effects of ISI-producing molecules, $S_{(r,f)}$ increases when compared to the same quantity as shown in Fig. 3.5 in case of a single pulse transmission. Although analyzing a random sequence of bits based on the above metrics is not exact, it provides promising results on the effective communication ranges for CEMC systems [MAH-10b].

Effective communication ranges for pulse-transmitted CEMC system have been categorized among short, medium, and long ranges in three different types of communication environment, e.g. in air, water, and blood plasma, as reported in [MAH-10] and [MAH-10b]. Determining effective communication ranges are important when a nanonetwork of a large number of nanomachines is to be materialized. For example, by computing average concentration of molecules at the RN as found using Fick's laws for pulse-transmitted CEMC, effective communication ranges in water medium can be found as < 800 nm for short-range, 800 nm up to 10 μm for medium-range, and > 10 μm for long range [MAH-10b]. Similar short, medium, and long ranges in air can be found as $r < 0.5$ mm, 0.5 mm $\le r \le 1$ cm, and $r > 1$ cm respectively [MAH-10b]. Similarly, short, medium, and long ranges in blood plasma can be found as $r < 400$ nm, 400 nm $\le r \le 5$ μm, and $r > 5$ μm respectively [MAH-10b]. The diffusion constants of information molecules in air, water, and blood plasma media, as considered in the determination of effective communication ranges, are 0.43 cm^2/s, 10^{-6} cm^2/s, and 2.2×10^{-7} cm^2/s respectively [LAC-09] [MAH-10b]. Apart from this, as discussed in the previous chapter, increasing effective communication

range is desired in CEMC. For example, it is shown in [MAH-13d] that convolutional coding techniques can be applied to pulse-transmitted CEMC systems in order to increase effective communication range, details of which are presented in Chapter 7.

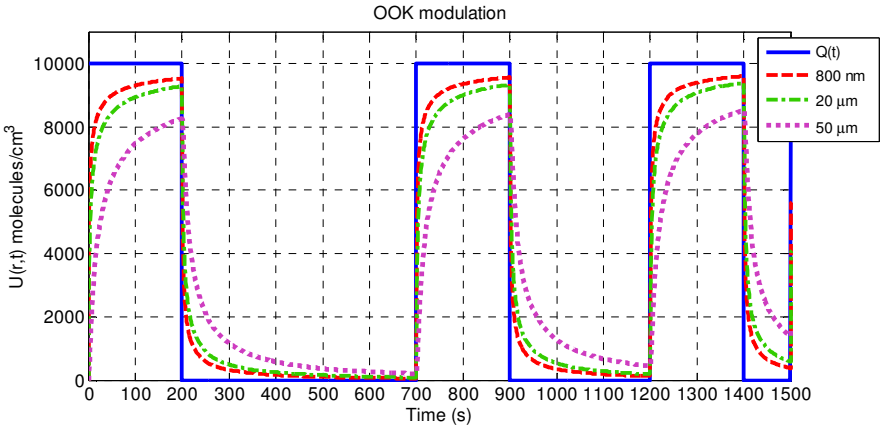

(a) First 15 bits {110000011000110} of a random sequence of bits with pulse-based OOK modulation where $T_{sym} = 100$ s.

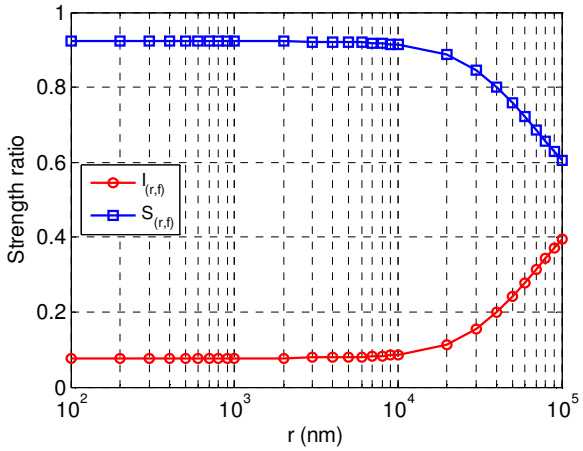

(b) Strength ratios when a random sequence of bits with $T_{sym} = 100$ s is transmitted by the TN.

Figure 3.6 Transmission of a random sequence of bits in Fick's laws CEMC channel.

3.7 Sinusoidal-based CEMC Model

Apart from using pulse-transmitted signaling scheme, it is also possible to use a sinusoidal-based signaling scheme in CEMC [MAH-11c]. Sinusoidal transmission rates can be expressed as shown in Section 3.4. The sinusoidal transmission rate as shown in Eq. (3.10) can also be expressed as the following [MAH-11c].

$$Q'(t) = \begin{cases} 1 + Q'_{amp} \sin(2\pi f_{sin} t) & \text{for } t \geq 0 \\ 0 & \text{for } t < 0 \end{cases} \quad (3.14)$$

Here $Q'(t)$ and Q'_{amp} indicate transmission rate and amplitude of sinusoidal variation respectively, both normalized to $Q_{average}$, which results in unitless quantities $Q'(t)$ and Q'_{amp} expressed as $Q'(t) = Q(t)/Q_{average}$ and $Q'_{amp} = Q_{amp}/Q_{average}$ respectively. Correspondingly, $U'(r,t)$ denotes signal intensity in response to $Q'(t)$, meaning that $U'(r,t)$ is equal to $U(r,t)$ normalized to $Q_{average}$. The zero initial phase assumption in Eq. (3.10) allows us to investigate into phase errors in sinusoidal-based signaling in CEMC. Figure 3.7 shows the variation of signal intensity in response to a sinusoidal transmission rate.

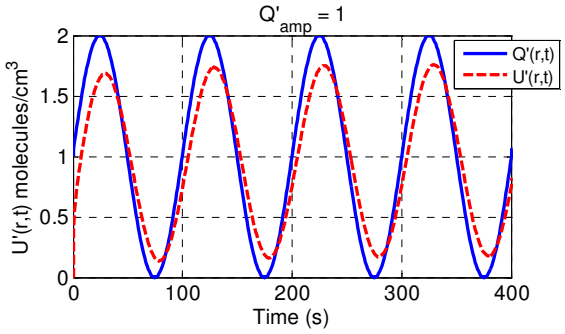

(a)

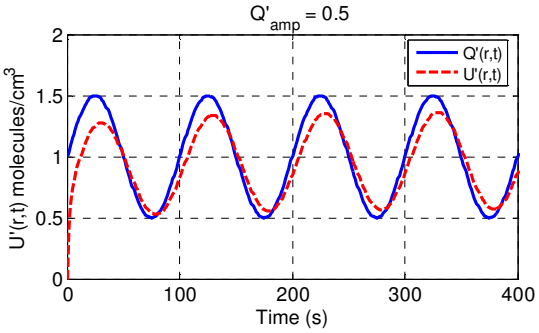

(b)

Figure 3.7 Output signal intensity $U'(r,t)$ in response to $Q'(t)$ with f_{sin} = 0.01 Hz, θ = 0 radian, and r = 1 μm, and (a) Q'_{amp} = 1 and (b) Q'_{amp} = 0.5.

Initial and steady-state phase errors, initial and steady-state amplitude losses, and detection noise margin have been explained in detail in our earlier work reported in [MAH-11c] using eye diagram [LEE-94] representations as shown in Fig. 3.8. Results show that

even with zero initial phase $U'(r,t)$ suffers from phase errors and amplitude loss that vary over communication ranges and transmission data rates. Transients of phase errors for a given TN-RN pair would also cause problem in the detection of FSK-modulated signals. Fig. 3.8(a) and 3.8(b) respectively show the eye diagram representations of input $Q'(t)$ and output $U'(r,t)$ signals at the RN. As shown in Fig. 3.8(b), τ_{ini} and τ_{ss} denote initial and steady state phase errors respectively at the RN. In addition, initial and steady state amplitude losses, denoted as AL_{ini} and AL respectively, at the RN can be found as below, where the quantities c and d can be found as shown in Fig. 3.8(b).

$$AL_{ini} = \frac{Q'_{amp}}{c} \quad \text{and} \quad AL = \frac{Q'_{amp}}{d} \tag{3.15}$$

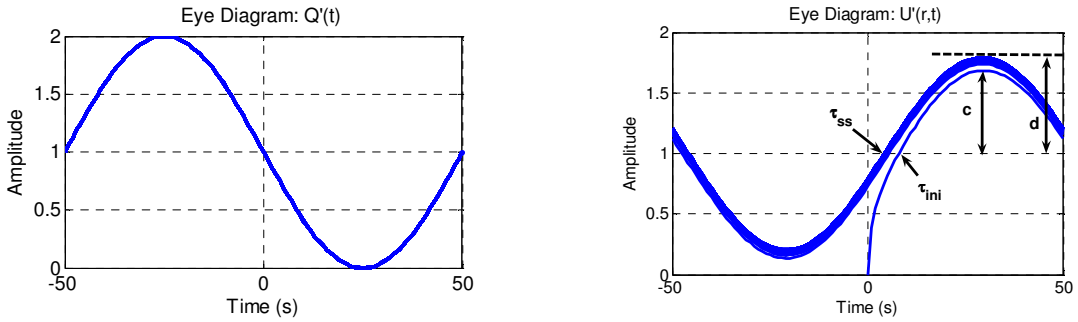

(a) $Q'(t)$ (b) $U'(r,t)$

Figure 3.8 Representation of input and output signals at r = 1 μm using eye diagrams when $Q_{average}$ = Q_{amp} (i.e. Q'_{amp} = 1).

Sinusoidal-based signaling can be used in implementing FSK-modulated CEMC. As shown in Fig. 3.9, a higher frequency sinusoidal signal representing symbol 1 would experience more amplitude loss at the RN, which would most likely be creating a problem in the detection of output frequency at the RN. In addition to amplitude loss, higher frequency components also experience higher phase errors at the RN, which in turn may cause problems in detecting FSK-modulated signals.

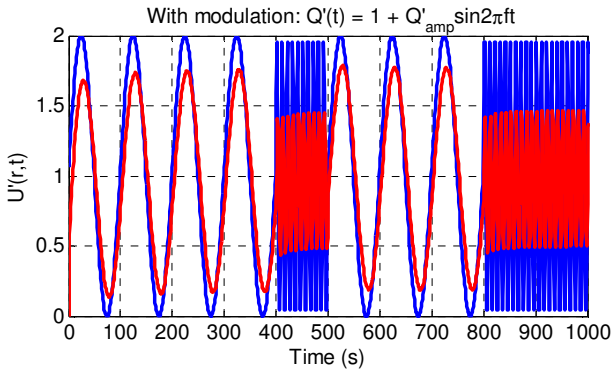

(a)

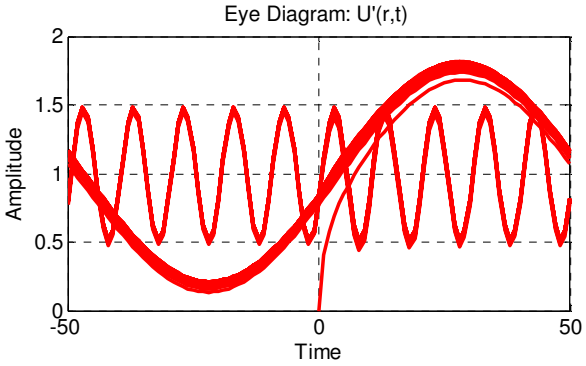

(b)

Figure 3.9 Input (blue line) and output (red line) of FSK-modulated CEMC (a), and the corresponding eye diagram representation of the output (b). Here sinusoidal signals with frequecies $f_{\text{Bit-1}}$ = 0.1 Hz and $f_{\text{Bit-0}}$ = 0.01 Hz are used to represent bits 1 and 0 respectively, when bit rate f = 0.01 bps and r = 1 μm.

3.8 Peformance of CEMC System

Results obtained in this work have been grouped into two categories: first, the spatiotemporal distribution $U(r,t)$ is examined under several different scenarios. Then, the signal intensity and strength based on OOK and FSK modulation schemes are presented in terms of *steady state amplitude loss* and *interference to total energy ratio*.

3.8.1 Diffusion-dependent Communication Ranges

Considering molecular diffusion, first, efforts have been made to define the range intervals for ‘short-range’, ‘medium-range’, and ‘long-range’ molecular communications for air,

water, and human body (blood plasma) media. Here, $U(r,t)$ has been calculated numerically as a convolution, in time domain, of transmission rate and impulse response of the molecular propagation channel. Through extensive numerical simulations, a possible set of diffusion-dependent communication ranges in air, water, and human body media has been identified and is shown in Table 3.1. This is one major contribution of our research and was reported in [MAH-10b]. The reader should note that suggested communication range depends on the specific medium of interest, and also on the diffusion constant D the medium of interest has. Interested readers may see [BOS-63], [BER-93]. In addition, it should also be noted here that diffusion of molecules also depends on the size of the messenger molecules, which is independent of propagation medium. In this research, we have not considered the effects of the size of the molecules. Figure 3.10 shows the available signal intensity $U(r,t)$ for short-range, medium-range, and long-range CEMC respectively when air (Fig. 3.10(a) and 3.10(b)), water (Fig. 3.10(c) and 3.10(d)), or human body (blood plasma) (Fig. 3.10(e) and 3.10(f)) are the propagation media. The displayed results confirm that distance has significant impact on signal intensity for all three propagation media. The differences among air, water, and blood plasma media were reflected in the performance of the system. This is because the propagation of molecules in the selected three media can be characterized by their respective diffusion constant values. As a result of different diffusion constants, the discovered short-range, medium-range, and long-range values for the corresponding media were different. As shown in Fig. 3.10, the performances in water and blood plasma media are different from that of air medium, which result in different communication ranges. However, the performances in water and blood plasma media did not show much difference.

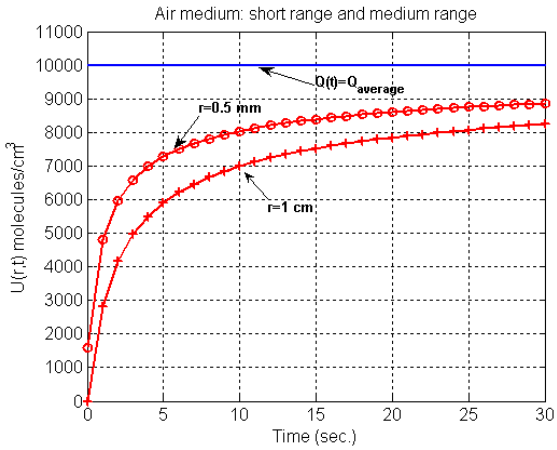

(a) Short and medium range, in air medium

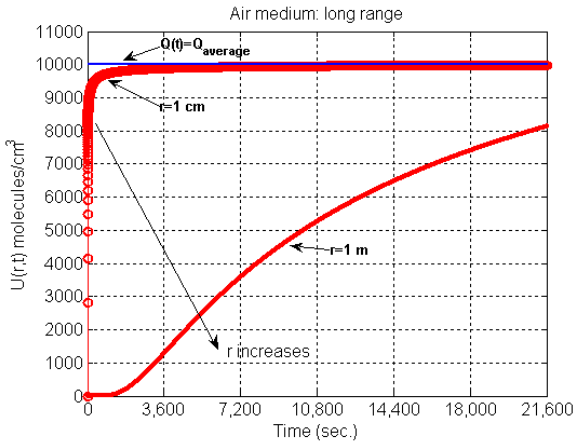

(b) Long range, in air medium

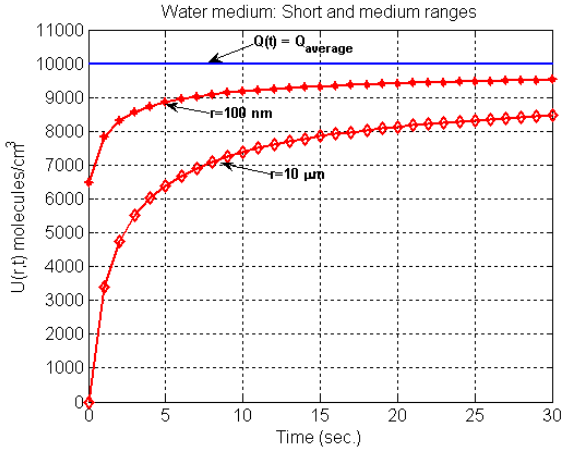

(c) Short and medium range, in water medium

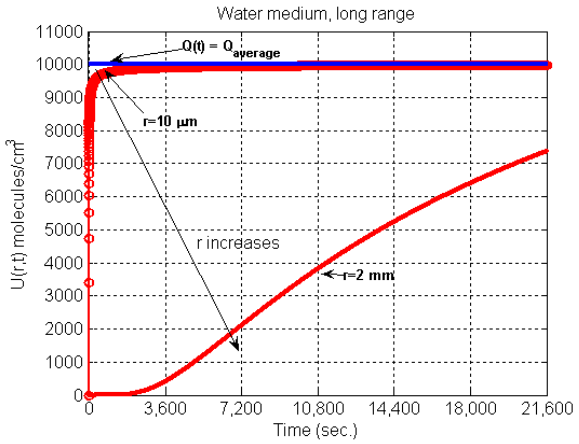

(d) Long range, in water medium

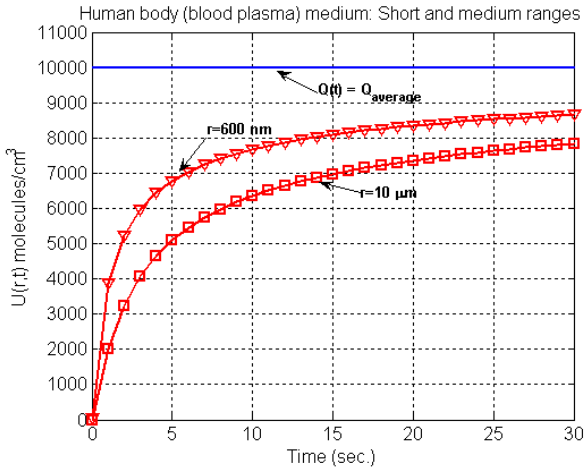

(e) Short and medium range, in human body medium

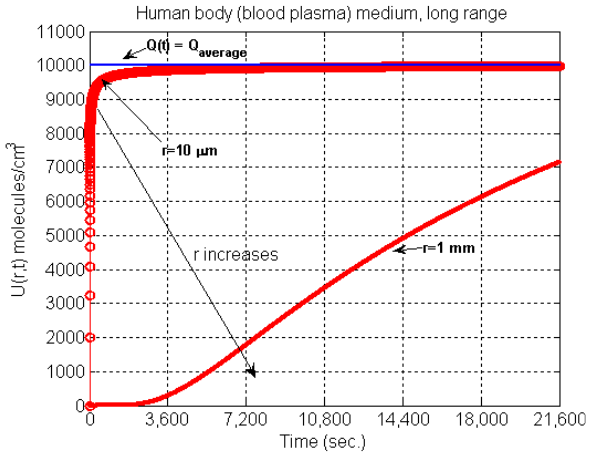

(f) Long range, in human body medium

Figure 3.10 Available signal strength for short-range, medium-range, and long-range CEMC in air (D = 0.43 cm^2/s), water (D = 10^{-6} cm^2/s), and human body (blood plasma (D = 2.2×10^{-7} cm^2/s)) media with constant transmission rate.

Table 3.1 Range of diffusion for air, water, and blood plasma media

Type	Discovered distance range		
	Air medium (D = 0.43 cm^2/s)	Water medium (D = 10^{-6} cm^2/s)	Human body (blood plasma) medium[7] (D = 2.2×10^{-7} cm^2/s)
Short-range	< 0.5 mm	< 800 nm	< 400 nm
Medium-range	0.5 mm to 1 cm	800 nm to 10 μm	400 nm to 5 μm
Long-range	> 1 cm	> 10 μm	> 5 μm

3.8.2 Steady-state Amplitude Loss

The results shown in this chapter determine the concentration of molecules at the position of RN. The exact molecule-receptor binding process is not considered here, which simplifies the analysis. Referring to Eq. (3.10), when $Q_{amp} = 0$, the sinusoidal transmission with $Q_{average}$ reduces to constant transmission $Q(t) = Q_{average}$. The quantities $Q_{average}$, Q_{amp}, and f_{sin} can be varied in order to generate different versions of the signal, each carrying a certain message. Figures 3.11–3.14 show that the molecular concentration at the location of RN captures the characteristics of the transmitted signal. This holds for a wide range of $Q_{average}$ values when Q_{amp} is kept unchanged, as can be concluded from Fig. 3.11.

Alternatively, we can vary Q_{amp} while keeping $Q_{average}$ fixed. This results in a multilevel amplitude modulation (M-AM) signal format. As shown in Fig. 3.12, for TN-RN distance r = 0.5 mm in air medium, r = 800 nm in water medium, and r = 400 nm in blood plasma medium, there is some misalignment initially. It is due to the transient period the signal goes through; however, the signal strength performs almost the same in water and blood plasma media. When this initial misalignment increases in accordance to the level of $Q_{average}$, Fig. 3.13 shows how the sinusoidal component of the signal behaves at certain distance in comparison to the input. The curves shown in Fig. 3.13 correspond to distance r = 0.5 mm and the medium is air. It is evident that the molecular concentration at the location of RN closely resembles the sinusoidal input even when the frequency changes, thus, an RN node containing reception functionalities implementing FSK detection should be able to extract

[7] For simple messages in blood plasma medium, the diffusion constant value is $D = 2.2\times10^{-7}$ cm^2/s. For complex messages in blood plasma medium, $D = 10^{-9}$ cm^2/s [LAC-09].

the information that is encoded in the frequency values. However, increase of the distance r between TN and RN can impact the behaviour drastically.

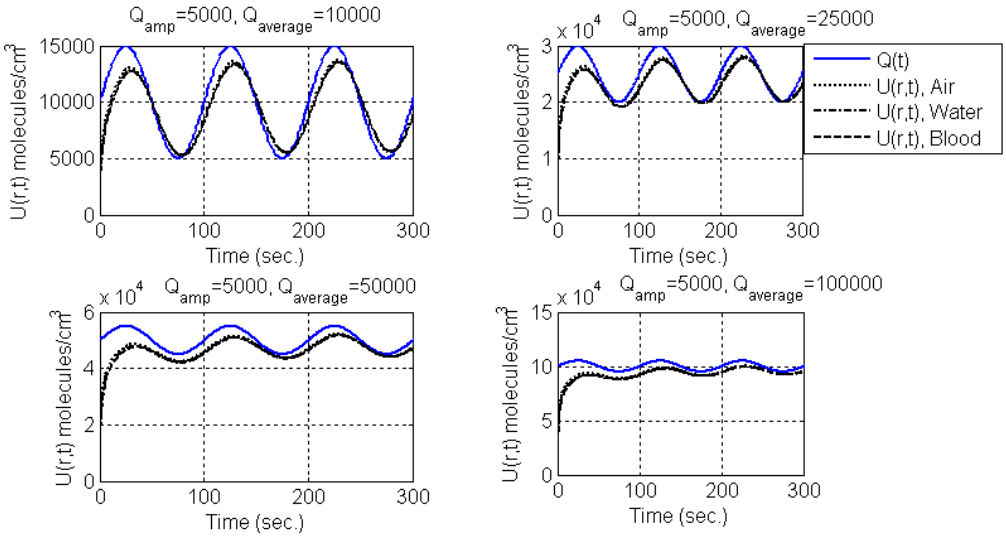

Figure 3.11 Signal intensity when Q_{average} varies while Q_{amp} remains fixed at 5000 molecules/sec. in air medium at r = 0.5 mm, water medium at r = 800 nm, and in blood plasma medium at r = 400 nm.

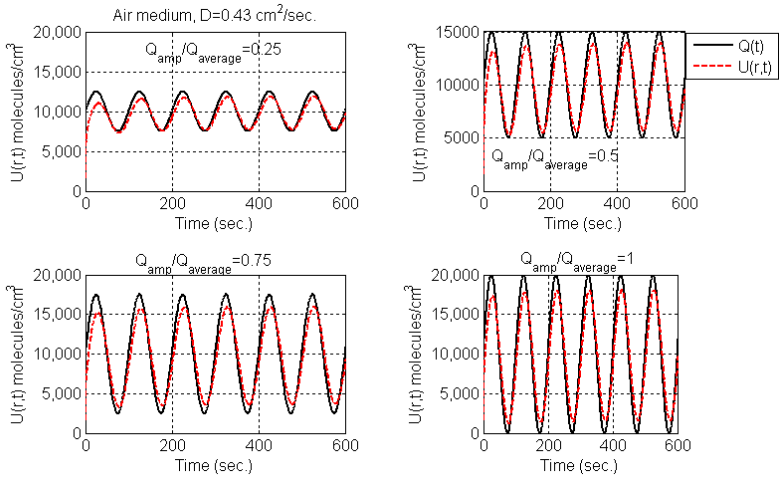

(a) Air medium

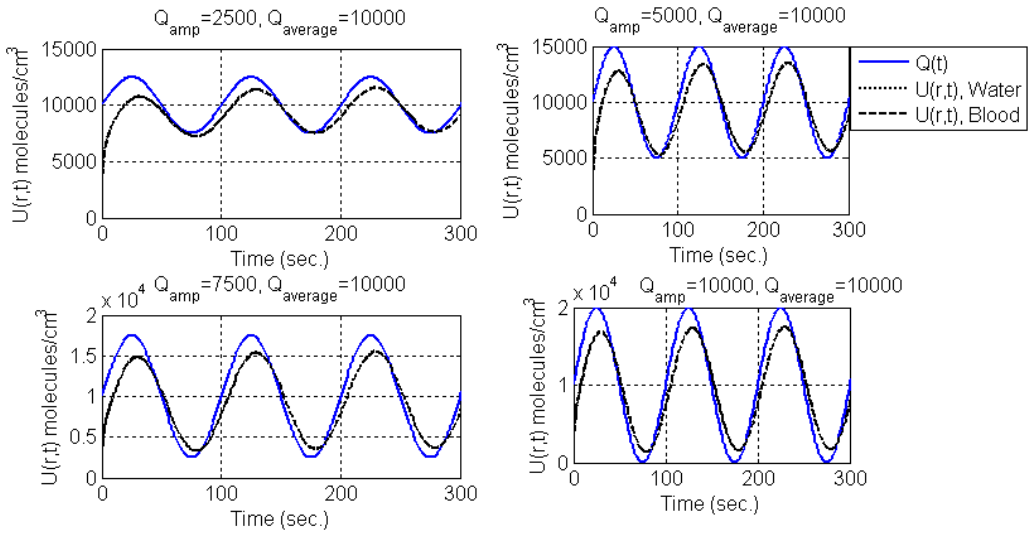

(b) Water and human body (blood plasma) media

Figure 3.12 Signal intensity when Q_{amp} varies while $Q_{average}$ remains unchanged at 10,000 molecules/sec. in (a) air medium at r = 0.5 mm, (b) water medium at r = 800 nm, and blood plasma medium at r = 400 nm.

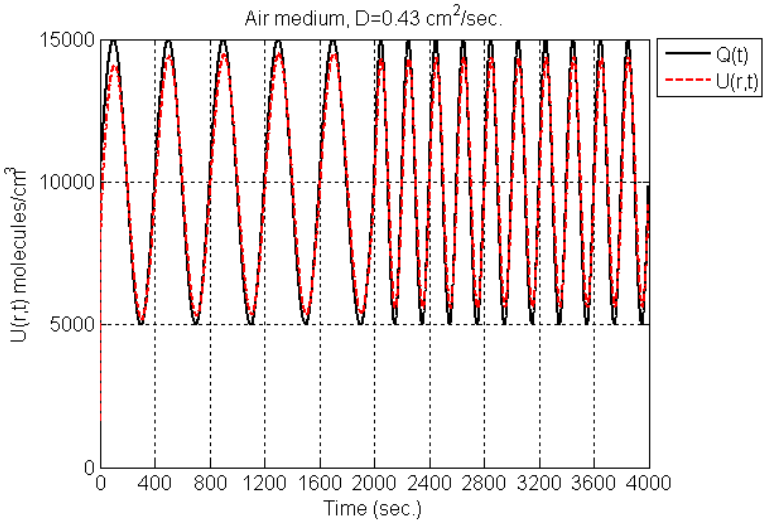

Figure 3.13 Signal intensity for FSK modulation at TN-RN distance r = 0.5 mm, Q_{amp} = 0.5 × $Q_{average}$, $f_{Bit\text{-}0}$ = 0.0025 Hz (i.e. $T_{Bit\text{-}0}$ = 400 seconds), $f_{Bit\text{-}1}$ = 0.005 Hz (i.e. $T_{Bit\text{-}1}$ = 200 seconds), in air medium. Information bits 0 and 1 are shown during (0–2000 seconds) and (2001–4000 seconds) intervals respectively.

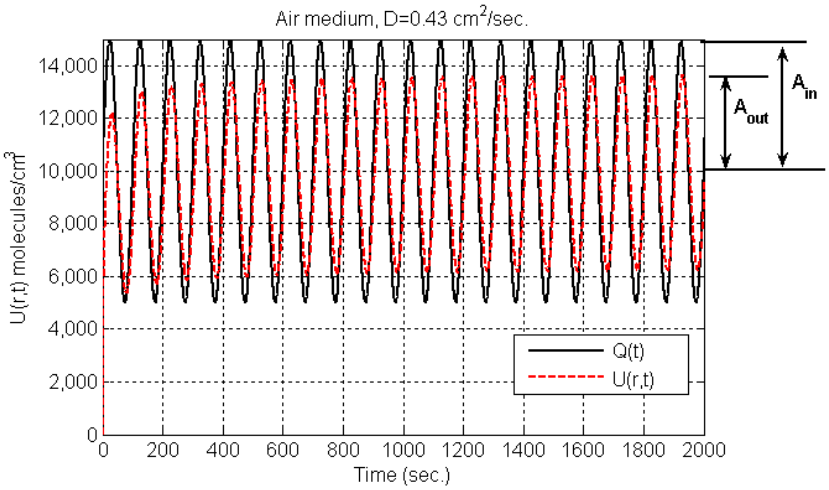

Figure 3.14 Signal intensity at RN for sinusoidal transmission at TN-RN distance r = 1 cm, Q_{amp} = 0.5 × $Q_{average}$, f_{sin} = 0.01 Hz. Steady state A_{in} and A_{out} can be used to calculate the steady state amplitude loss AL (in dB) = $10\log_{10}(A_{in}/A_{out})$.

The results shown in Fig. 3.14 correspond to r = 1 cm. Two conclusions can be drawn from the comparison of Fig. 3.13 and Fig. 3.14: the peak amplitude of the sinusoidal variation drops. In addition, it takes longer for the molecular concentration to reach steady state behaviour. Referring to Fig. 3.14, the metric for amplitude loss AL (measured in dB) is defined as $AL = 10\log_{10}(A_{in}/A_{out})$ where A_{in} and A_{out} represent maximum amplitudes (measured from the average value) of the transmitted (input) and received (output) concentrations respectively at steady-state. Thus AL expresses the amount of attenuation the molecular signal suffers at certain distance. The relation between AL and TN-RN distance provides an insight of the change rate of attenuation. These results are helpful in deciding the required strength of transmitted signal and/or required level of receiver's sensitivity.

Figure 3.15 shows the amplitude loss AL (in dB) for all ranges of TN-RN distance, starting from 100 μm and going up to 1 metre for air medium (Fig. 3.15(a)), starting from 10 nm and going up to 1 mm for water medium (Fig. 3.15(b)), and starting from 10 nm and going up to 1 mm for blood plasma medium (Fig. 3.15(c)). For short-range and up to r = 0.5 mm in air medium (Fig. 3.15(a)), r = 800 nm for water medium (Fig. 3.15(b)), and r = 400 nm for blood plasma medium (Fig. 3.15(c)), the molecular concentration shows negligible loss. For medium-range in air, water, and blood plasma media, the amplitude loss is about 1 dB (i.e. $A_{out} \approx 0.8A_{in}$). However, for long-range values, the attenuation of the molecular concentration signal increases further, and the rate of deterioration with distance becomes

considerable, reaching values close to 100 dB. For long distances, a different encoding technique such as pheromone-based *molecular encoding* [LAC-09] [ECK-07] seems to be more appropriate. It has been shown in [MAH-10a] that at longer distances the impulse response of the CEMC channel becomes smaller in its peak value and flat in time. In addition, the peak value of the impulse response occurs at a definite amount of delay in time for long distances. As a result, for the case shown in Fig. 3.15, the signal intensity *U(r,t)* cannot reach a higher steady state value (measured from the average value), and sometimes *U(r,t)* does not reach a steady state value at all. This phenomenon results in a high value of *AL* (in dB) for long ranges. In addition, this indicates that the metric *AL* is not a suitable way to evaluate the performance of such a CEMC system at long ranges.

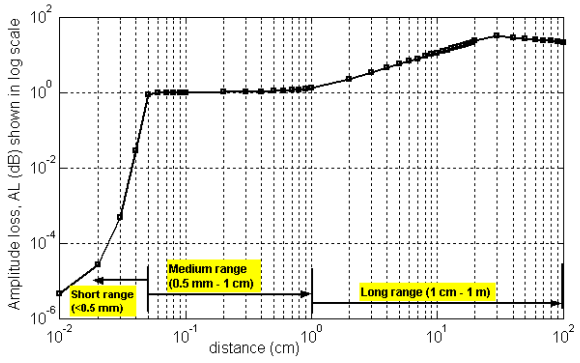

(a) Air medium

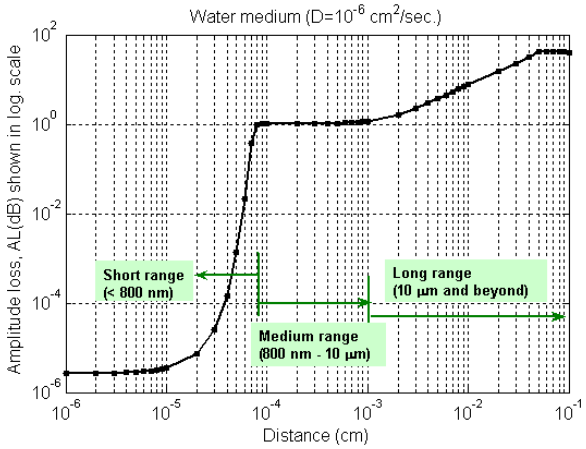

(b) Water medium

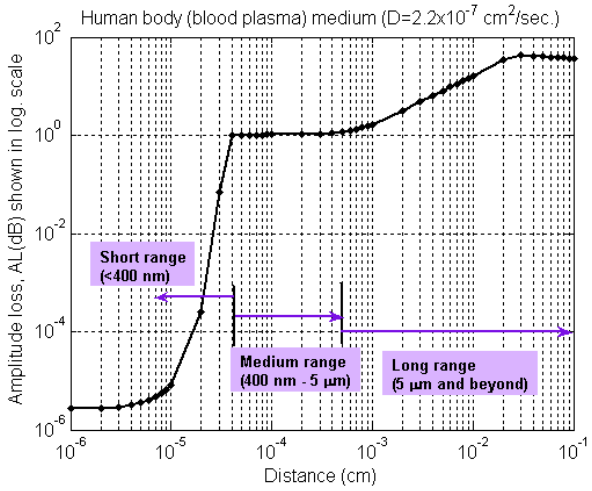

(c) Human body (blood plasma) medium

Figure 3.15 Steady state amplitude loss *AL* (dB) for different TN-RN distances, $Q_{amp} = 0.5 \times Q_{average}$ with sinusoidal transmission rate. Note that *AL* (dB) is shown in logarithmic scale.

3.8.3 Interference energy to Total available Energy Ratio (ITER)

Signal intensity and strength are also dependent on distance r and transmission data rate f of the system. OOK modulation with random 1 or 0 bits is shown in Fig. 3.16. Close examination reveals that the level gap[8] L_g is dependent on r and the communication speed $f = (1/T_{sym})$, T_{sym} being the pulse duration of OOK signaling system. Even if the bit duration is unchanged, the molecular concentration is impacted. This behaviour can be seen in Fig. 3.16(a) for r = 0.6 mm to r = 8 cm in air medium, in Fig. 3.16(b) for r = 800 nm to r = 1 mm in water medium, and in Fig. 3.16(c) for r = 800 nm to r = 1 mm in blood plasma medium. Depending on the consecutive number of 1s or 0s the concentration level rises or falls respectively, and this varies the level gap L_g. When frequent changes between 1 and 0 occur, L_g decreases, reducing the ability of RN to make a correct decision when some form of additive noise is present. It should be noted that, in determining the intensity, an RN will be picking up molecules belonging to previous bits, which are present due to the "spreading" in time of the original input. This will act as interference on the present symbol,

[8] Level gap is the difference between levels of *U(r,t)* for maximum and minimum concentrations during a bit change.

known in conventional communications as ISI. This gives us the motivation to compute the *interference energy to total available energy ratio (ITER).*

As shown in Fig. 3.17, interference energy corresponds to the total concentration of molecules during all 0 bits for that T_{obs} period, whereas total available energy is the total energy available for all 1 and 0 bits for that entire T_{obs} period. We use numerical simulations and, for the results shown in Fig. 3.18, we used an observation time T_{obs} = 10 hours (i.e. 36000 seconds). Figure 3.18 shows how *ITER* increases as the TN-RN distance *r* increases, which also implies that more than 40% of the received molecules act as interferers when RN is located at more than 10 cm in air medium, more than 35% of the received molecules act as interferers when RN is located at more than 0.1 mm in water medium, and more than 50% of the received molecules act as interferers when RN is located at more than 0.1 mm in blood plasma medium. This supports the results regarding long-range communications presented in Figs. 3.15(a), 3.15(b), and 3.15(c), corresponding to air, water, and blood plasma media respectively. In addition, it is also to be concluded that at long ranges the performance of $U(r,t)$ degrades (see Fig. 3.16), which in turn degrades communication capability of TN and RN, as shown in Fig. 3.18.

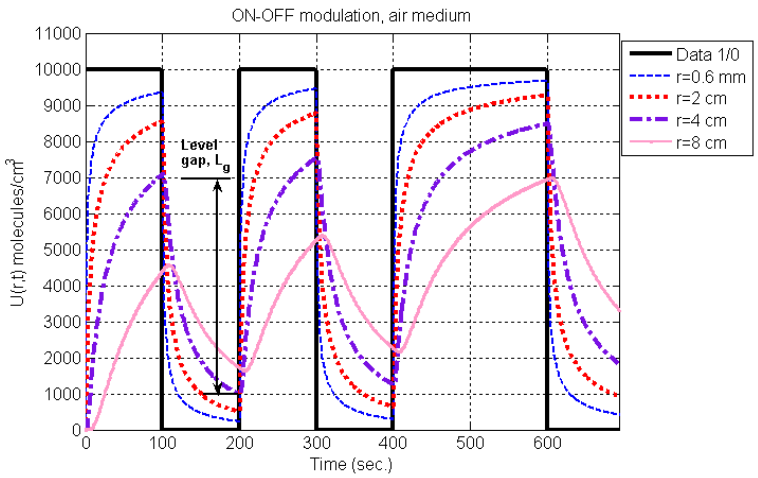

(a) Air medium

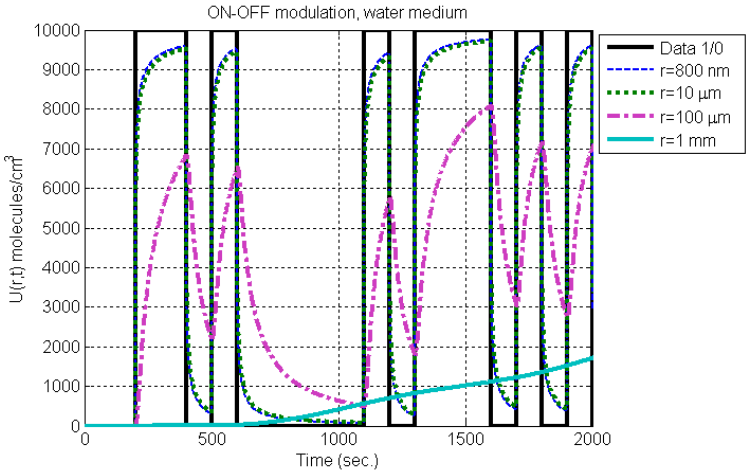

(b) Water medium

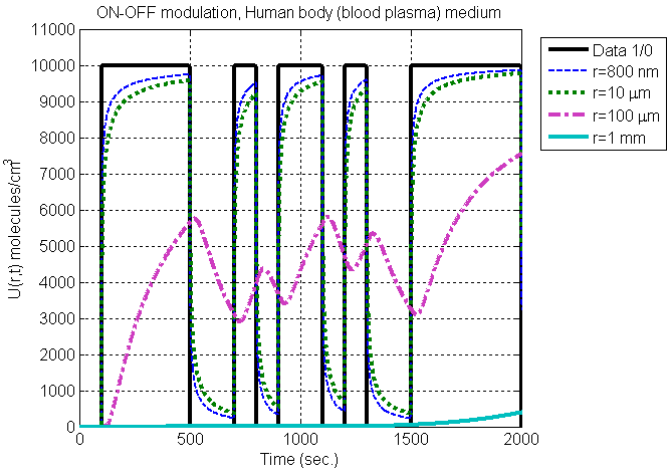

(c) Blood plasma medium

Figure 3.16 Variations of $U(r,t)$ in the case of pulse-based OOK modulation with random transmitted bits in (a) air medium, (b) water medium, and (c) blood plasma medium.

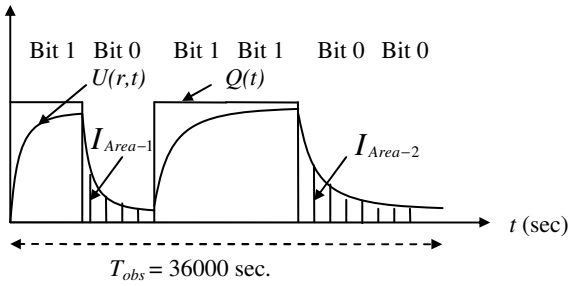

Interference Energy, $\text{Area}_I = \sum_{i=1}^{All} I_{Area-i}$

Total available energy at a given r, $\text{Area}_{Total} = \int_0^{T_{obs}} U(r,t)dt$

Interference to total energy ratio, $ITER = \dfrac{\text{Area}_I}{\text{Area}_{Total}}$

Figure 3.17 Signal strength causing interference to bit decision in pulse-based OOK modulation.

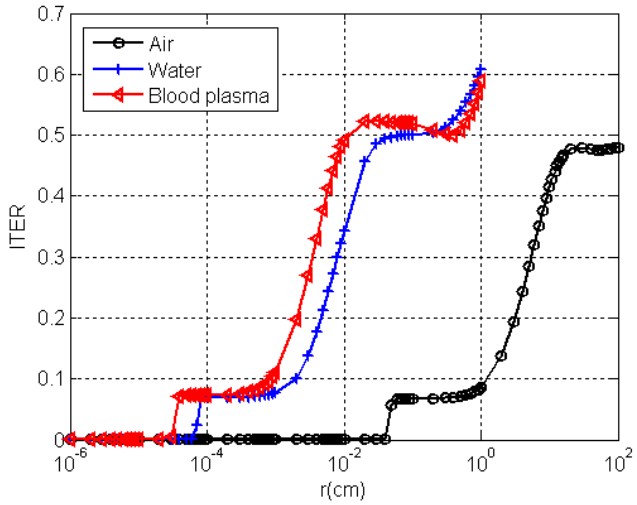

Figure 3.18 Interference to total energy ratio as a function of r in pulse-based OOK modulation in air, water, and blood plasma media.

3.8.4 Observations in FSK Modulation

Figure 3.13 shows that use of FSK modulation is possible in CEMC, however, the following results explain some important observations characteristic to the FSK modulation and their impact on the communication process in CEMC. In Fig. 3.19, we display $U(r,t)$ for distance r in the range from 0.6 mm to 8 cm in air medium (Fig. 3.19(a)), from 800 nm to 100 µm in water medium (Fig. 3.19(b)), and from 800 nm to 100 µm in blood plasma medium (Fig.

3.19(c)), while all other parameters were kept unchanged. As seen from Fig. 3.19, for short-range communication, the molecular concentration can follow the transmitted data reasonably well, but as the distance increases molecular concentration gradually cannot follow the input data well. This observation is important in the sense of correct bit decision following FSK demodulation at the RN.

Another element affected by the distance is the transient behavior of signal strength *U(r,t)* as shown in Figs. 3.10, 3.16, and 3.19. As the distance *r* increases, the spreading of the CIR grows, and thus generates more severe transient effects for both OOK and FSK modulations. The distance dependence of transient behavior shows how fast a molecular channel can be thought of behaving in order to have reliable communication. Based on the presented results we can conclude that the quality of molecular concentration signal is impacted mainly by three factors, namely, TN-RN distance *r*, data rate in case of OOK modulation, and the modulation frequencies $f_{\text{Bit-0}}$ and $f_{\text{Bit-1}}$ in case of FSK modulation.

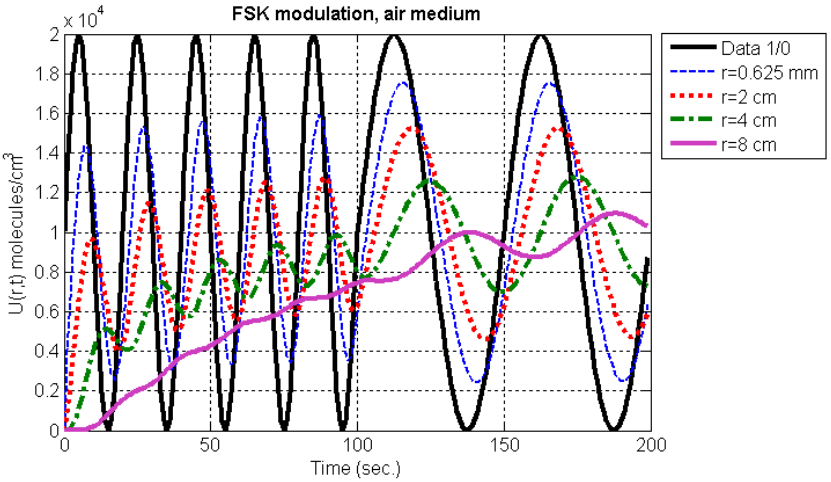

(a) Air medium

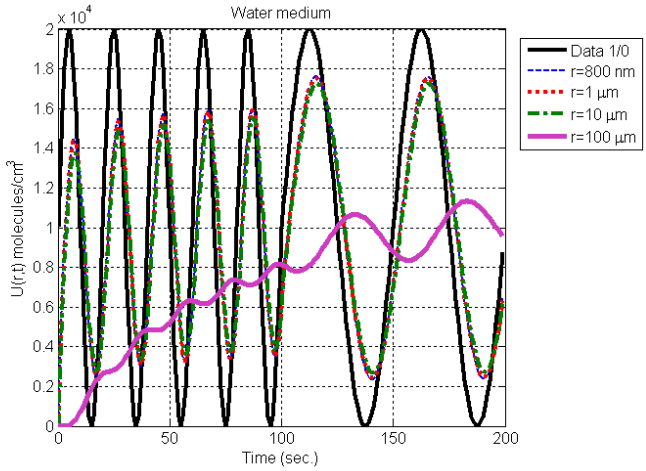

(b) Water medium

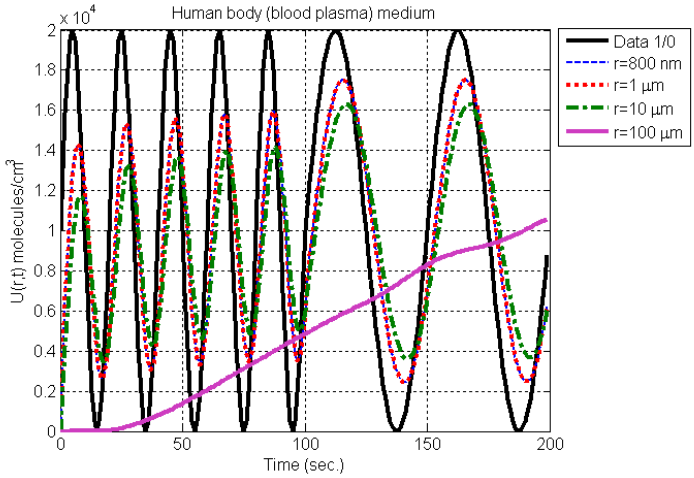

(c) Blood plasma medium

Figure 3.19 FSK modulation of transmission rate when r is varied, $f_{\text{Bit-0}} = 0.02$ Hz, $f_{\text{Bit-1}} = 0.05$ Hz. Information bits 1 and 0 are shown during (0-100 seconds) and (101-200 seconds) intervals respectively.

A reasonable assumption is that D remains unchanged over the entire observation interval T_{obs} [MAH-10b]. In addition, it should be noted that in ideal (i.e. free) diffusion, theoretically, molecules undergoing ideal diffusion mechanism can reach the RN even after infinite (∞) time, so ideally, $T_{obs} = \infty$. However, for practical cases we keep T_{obs} to 1–10 hours, reasonable enough [MAH-11] [MAH-10b] to perform the numerical simulations presented in this chapter, even after accepting the fact that the impulse response of the

CEMC channel suffers from temporal spreading in ideal diffusion. It should also be noted that D depends on size and molecular weight of the molecules, and the structural characteristics of the CEMC channel, and that the exact amount of molecules actually received by the RN depends on the MRBP between the molecules and the receptors of RN. However, in order to focus only on the characteristics of communication channel we have not considered the MRBP in this chapter, implying that in our case $U(r,t)$ is the signal intensity available at the location of the RN.

3.9 Conclusion

This chapter provided an in-depth analysis of the general characteristics of spatiotemporal distribution and modulation schemes for binary CEMC. The overall contributions of this chapter are as follows: first, the chapter has made a detailed analysis of short-range, medium-range and long range molecular communication, by describing the spatial and temporal distribution of concentration of received molecules. In that relation, corresponding ranges have been identified. In addition, a performance metric named as *steady state amplitude loss* (*AL*) has been used to illustrate the characteristics of the CEMC system. The chapter has also introduced the concept of interference energy in CEMC and explained the corresponding effects of communication range on interference energy. Interference energy in the form of *ITER* considers the effects of molecules from the previous transmissions on the concentration of molecules at the current symbol.

Numerical results obtained in this chapter conclude that TN-RN distance r is an important factor that affects the spatiotemporal distribution of CEMC signal. This chapter investigated into short-range, medium-range, and long-range molecular communications for air, water, and human body (blood plasma) media. The first two media (air, water) have already been used by many researchers for MC experiments among insects [BOS-63] or in numerical analyses [KRI-02]. Parameterization is a complicated process for CEMC because a large number of parameters need to be fine-tuned in order to get desired characteristics. We expect that the results presented in this chapter will help to better characterize the parameterization process and performance analyses of a binary CEMC system. In the following chapters, more results have been presented in detail for the CEMC system.

Chapter 4: Sampling-based Optimum Signal Detection in CEMC

4.1 Introduction

As mentioned in Chapters 2 and 3, in CEMC the probabilistic nature of the diffusion process makes it difficult to detect the information symbols correctly at the RN. This is because in the ideal case, information molecules can arrive at the RN even after infinite time, thereby causing ISI at the RN. In CEMC, the detection of transmitted symbols is quite challenging because the information molecules are of single type and ISI plays a negative role in the correct detection of the current symbols. In this thesis, we propose two detection schemes, namely, *sampling-based* and *strength-based* detection schemes, for the CEMC system between a pair of nanomachines. Sampling-based detection (SD) is presented in this chapter, followed by strength (or energy)-based detection (ED) presented in the next chapter.

Since CEMC is a new communication paradigm for molecular nanonetworks, the area of sampling-based optimum signal detection in CEMC is very new. Acknowleding this fact, in this chapter we focus on presenting and analysing a sampling-based optimum signal detection model for CEMC system. In SD, the RN samples the molecular concentration intensity for a very short duration of time, single or multiple times, in each symbol duration, and decides on the basis of the value(s) of the almost instantaneous sample(s). The decision is made based on the value of the test statistic being greater or smaller than a set threshold.

In this chapter, a comprehensive analysis of the sampling-based optimum signal detection in ideal (i.e. free) diffusion-based CEMC system has been presented. A generalized ASK-based CEMC system has been considered in diffusion-based noise and ISI conditions. Information is encoded by modulating the amplitude of the transmission rate of information molecules at the TN. The critical issues involved in the sampling-based receiver thus developed are addressed in detail, and its performance in terms of the number of samples per symbol, communication range, and transmission data rate is evaluated. ISI produced by the residual molecules deteriorates the performance of the CEMC system, which is further deteriorated when the communication range and/or the transmission data rate increase(s). In addition, the performance of the optimum receiver depends on the

receiver's ability to compute the ISI accurately, thus providing a trade-off between receiver complexity and achievable BER. Exact and approximate detection performances are derived. Finally, it is found that the sampling-based signal detection scheme thus developed can be applied to both binary and multilevel (M-ary) ASK-based CEMC systems, although M-ary systems suffer more from the BER.

Our results on sampling-based optimum signal detection in CEMC presented in this chapter have been published in [MAH-13] and [MAH-14a]. The four major contributions of our research on SD in CEMC that have been presented in this chapter are as follows.

- A detailed mathematical model of an optimum receiver of sampling-based signal detection in diffusion-based CEMC system has been presented for both binary and M-ary CEMC systems. This suggests that the binary receiver developed in [MAH-13] can also be extended to detect M-ary CEMC signals with appropriate modification in the receiver architecture. In addition, with simulation results, the BER characteristics of both binary and M-ary receivers have been explained when several influencing factors, e.g. the number of samples per symbol, communication range, and transmission data rate vary.
- The performance of the proposed receiver has also been evaluated in terms of the RN's ability to compute the ISI-producing molecules for three factors, namely, number of samples per symbol, communication range, and transmission data rate.
- The exact expressions of the detection performance of the proposed SD receiver have been developed and evaluated analytically with the receiver operating characteristics (ROC) curves.
- Finally, a novel single-sample detection scheme in case of the sampling-based binary CEMC system has been developed and analyzed in terms of ROC, probability of molecule availability, and the number of transmitted molecules.

This chapter is organized as follows: Section 4.2 describes the related work. Section 4.3 briefly discusses the system model. Section 4.4 describes the sampling-based signal detection in detail, followed by Section 4.5 explaining the simulation model and results. The exact detection performance of the binary optimum receiver has been presented in Section 4.6, followed by Section 4.7 discussing the single-sample binary CEMC detection. Finally, Section 4.8 concludes the chapter with possible future research directions.

4.2 Related Work

In CEMC, since the information molecules are of single type, they make signal detection process quite challenging due to the fact that ISI increases the probability of incorrect decoding of the transmitted symbols [MAH-10b] [MAH-12a] [MAH-11a]. To the best of the our knowledge, the concept of sampling-based detection in CEMC was first reported in [MAH-10] [MAH-10b], which proposed that the concentration sample be taken at a suitable time instant within the symbol duration, without mentioning when exactly the temporal sample should be taken. The early works in [MAH-10b] and [MAH-10] were later elaborated for a binary CEMC system in [MAH-11b] that provided the threshold values of *known-reference* and *blind-reference* sampling-based detection schemes in CEMC, but did not provide the appropriate receiver structure to decode the CEMC signals. Based on the work reported in [MAH-11b], the authors further investigated into sampling-based detection in [MAH-13] that provided the receiver structure of binary sampling-based detection in CEMC systems. However, the earlier works reported in [MAH-10b], [MAH-13], and [MAH-11b] were not complete, lacking the details of the receiver characteristics and subsequent further details that relate the sampling-based receiver to the M-ary signal detection scheme.

Available open literature also include related works on signal detection at the microscopic level dealing with only one or a few molecules when a molecule is removed from the system as soon as it hits the RN after the first hitting time [LIN-12] [MEN-12], and the detection of molecular signal using different types of molecules to represent different transmitted symbols [SHA-12]. However, the works in [LIN-12], [MEN-12], and [SHA-12] are different from ours in this chapter in the sense that we consider the macroscopic theory of ideal (i.e. free) normal diffusion process, where the TN transmits a large number of single type of information molecules and none of the molecules is removed from the environment, providing a concentration-encoded ideal (i.e. free) diffusion-based propagation environment.

4.3 System Model Overview

As shown in Fig. 2.1, diffusion-based unicast CEMC system consists of a TN that transmits information molecules, e.g. proteins [ALB-08] and ions [SUD-05] that contain information

to be transmitted, a propagation channel [MAH-10a], e.g. air, water, blood plasma, through which the molecules propagate in the environment, and an RN that decodes the transmitted information. We assume that the TN is a point source of information molecules located at (0,0,0) and transmits the information molecules in an impulsive manner, i.e. $Q_0\delta(t)$, where $\delta(t)$ is the *Dirac delta function* [HAY-02]. The TN can release at a time the contents of a vesicle, or vesicles of various sizes, that can contain the required numbers of information molecules to encode different information symbols [NAK-11a] [MOO-13].

Propagation of molecules in this case is governed by the ideal (i.e. free) diffusion process [BER-93] in an unbounded aqueous medium in three dimensions. In the system model based on ideal (i.e. free diffusion), none of the information molecules are removed from the system [ATA-10] and, therefore, they can be available to the RN multiple times.

The RN is a sampling-based receiver that samples the concentration of molecules available at its receptors [ALB-08]. The receptors on the surface of the RN are of same type, which ensures that only a single type of information molecules can bind to them. The RN senses continually [BER-77] the concentration of information molecules at its receptors and thus counts the number of available molecules at the location of its receptors at one or more time instants, i.e. the SD approach [MAH-13], and compares the test statistic [KAY-93] to a given threshold in order to determine the transmitted symbol. The concentration of receptors on the surface of RN is assumed to be sufficiently high such that all the molecules inside the sensing volume come in contact with a receptor [MOO-12b]. For the sake of simplicity, in this chapter we assume that the molecules that become available at the receptors are sensed and received by the RN. The information molecules can bind with the receptors with high specificity [BUS-10] [NAK-13], providing a reliable and robust CEMC by not allowing other types of molecules to bind with the receptors. We also assume that the TN and the RN are synchronized in time [MOO-09a] and that the RN is located at the centre of a small volume known as the VRV [ATA-10] at a distance denoted by the vector $\vec{r} = \hat{i} \cdot x_r + \hat{j} \cdot y_r + \hat{k} \cdot z_r$ from the origin. The TN and the RN are assumed to not move in space. Time-synchronization between the TN and the RN can be achieved by using external signals [MOO-13] [NAK-13] [MOO-11].

4.3.1 Signal Intensity and Signal Strength

As shown in Chapter 3, the temporal evolution of concentration of the information molecules available at the location of the RN can be explained by solutions to Fick's laws of ideal diffusion [BER-93]. The mean CIR in molecules per unit volume at a three-dimensional space $\vec{r}$ and at time t changes with time and space as below [BER-93] [BOS-63].

$$G(\vec{r},t) = \frac{Q_{b_j}}{(4\pi Dt)^{\frac{3}{2}}} \exp \frac{-\left(x_r^{\,2} + y_r^{\,2} + z_r^{\,2}\right)}{4Dt} = \frac{Q_{b_j}}{(4\pi Dt)^{\frac{3}{2}}} \exp \frac{-r^2}{4Dt} \tag{4.1}$$

where r is the distance representing the vector $\vec{r}$ between the TN and the RN, $r^2 = x_r^2 + y_r^2 + z_r^2$ when a Cartesian coordinate system is assumed. We assume that $D = 10^{-6}$ cm^2/s of small protein molecules [ALB-08] in water medium remains unchanged over the entire observation time and that the effects of size of the information molecules and the physical conditions of the propagation environment on D are negligible [MAH-10b]. Here, $G(\vec{r},t)$ is the response of the CEMC channel to the impulsive transmission of molecules $Q_{b_j}\delta(t)$. With the assumption of isotropic diffusion in three-dimensional homogenous medium, the vector notation in $G(\vec{r},t)$ can be dropped hereafter. The mean number of the available molecules in the volume VRV can be obtained by integrating $G(r,t)$ over the volume VRV of the RN as below.

$$G_{RN}(r,t) = \iiint_{\text{VRV}} \frac{Q_{b_j}}{(4\pi Dt)^{3/2}} \exp\left(-\frac{x_r^{\,2} + y_r^{\,2} + z_r^{\,2}}{4Dt}\right) dXdYdZ \tag{4.2}$$

Here VRV denotes the *receiver sensing volume* at the location of the RN and $dXdYdZ$ is the differential volume in the VRV. Expressing $G_{RN}(r,t)$ in energy-normalized CIR quantity [MAH-13] [MAH-13d], the mean number of molecules available at the RN can be expressed as [MAH-13]

$$s_{b_j}(r,t) = Q_{b_j} \frac{G_{RN}(r,t)}{\int_0^\infty G_{RN}(r,t)dt} = Q_{b_j}\, p(r,t) \text{ where } p(r,t) = \frac{G_{RN}(r,t)}{\int_0^\infty G_{RN}(r,t)dt} = \frac{\frac{1}{(4\pi Dt)^{\frac{3}{2}}} \exp\left(\frac{-r^2}{4Dt}\right)}{\int_0^\infty \frac{1}{(4\pi Dt)^{\frac{3}{2}}} \exp\left(\frac{-r^2}{4Dt}\right) dt} \tag{4.3}$$

is the energy-normalized CIR of the CEMC channel. Eq. (4.3) implies that $p(r,t)$ refers to *the probability of getting a molecule* at the location r of the RN at time t [BER-93], provided that the molecule was transmitted by the TN located at (0,0,0) at $t = 0$.

Considering that the observation time for the molecule is sufficiently larger than the delay spread of the CEMC channel, energy-normalizing the CIR would normalize the probability of getting the molecule at any time instant within the observation time [MAH-13]. Here $s_{b_j}(r,t)$ is considered as the mean concentration *signal intensity* of the available molecules at any TN-RN distance *r* at time *t*, and any integral of $s_{b_j}(r,t)$ over time is considered as the mean *signal strength* [MAH-11] [MAH-13].

In this chapter, the sensing of the concentration signal intensity by the RN is performed by sampling-based signal detection [MAH-13] meaning that the RN takes samples of the concentration signal at regular temporal intervals known as *sampling time intervals* t_s. The samples are taken uniformly at regular (i.e. equal) time intervals based on the number of samples per symbol in the design of the CEMC scheme. Fig. 4.1(a) shows the effects of the number of samples per symbol on the *p(r,t)*. Correspondingly, the less the number of samples per symbol is, the larger the sampling interval and the more the effects of ISI become in the sampling-based signal detection in CEMC.

4.3.2 Significance of *p*(*r*,*t*)

Clearly, $p(r,t)$ is a function of r and t, which causes the spatial (r-domain) and the temporal (t-domain) dependence of the $s_{b_j}(r,t)$. For a given r, since we consider the temporal samples of the concentration signal intensity only, from now on, the spatial functional dependence can be dropped and so correspondingly these quantities can be written as $s_{b_j}(t)$ and $p(t)$ respectively. In diffusion-based CEMC, each of the molecules travel independently from the TN to the RN [BER-93], therefore, as shown in Eq. (4.3), the total number of transmitted molecules Q_{b_j} times the quantity $p(t)$ would provide the mean number of molecules available at the RN.

In ideal case, information molecules may arrive at the RN even after infinite time, making the observation time T_{obs} ideally infinite. However, in realistic cases, considering the fact that $p(t)$ varies spatially and temporally, observation times of 1 to 10 hours [MAH-10b] would be reasonable enough in order to perform the numerical analyses in this chapter. The symbol duration is denoted as T_{sym}. Both T_{obs} and T_{sym} are expressed in units of seconds

(s). Figure 4.1(a) shows the characteristics of $p(t)$ when r is kept at 800 nm and various numbers of samples per symbol are taken by the RN in the symbol duration. Since the samples are taken at equal time intervals, as shown in Fig. 4.1(a), with less number of samples per symbol, $p(t)$ becomes more temporally spread, causing interference to the next symbols. Fig. 4.1(b) shows that $p(t)$ also becomes temporally-spread when r increases from 800 nm to 100 μm, while N is kept unchanged at $N = 100$.

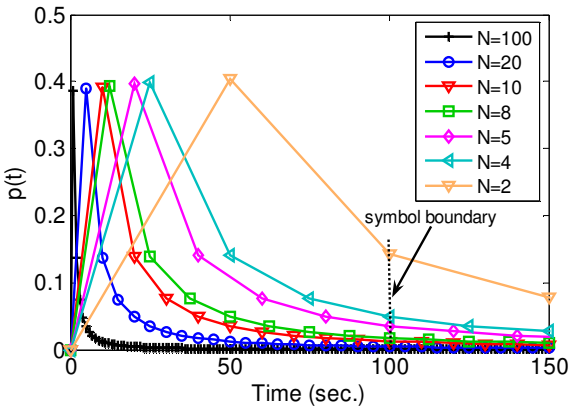

(a) *p(t)* when *N* varies

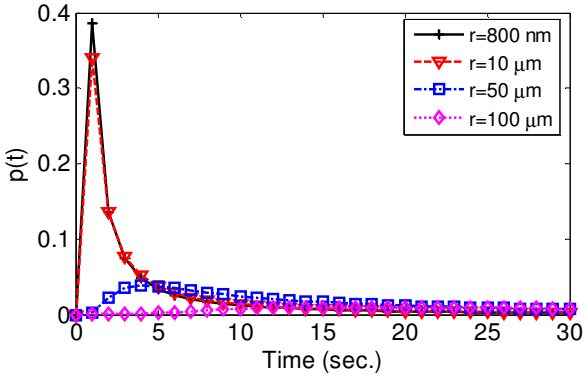

(b) *p(t)* when *r* varies

Figure 4.1 Time domain characteristics of *p(t)* when $T_{sym} = 100$ s, $T_{obs} = 10{,}000$ s, and (a) $r = 800$ nm and the number of samples N varies from 2 to 100 samples per symbol, and (b) r varies and N is kept unchanged at $N = 100$.

4.4 Sampling-based Signal Detection

4.4.1 Transmission of Molecules

As shown in Fig. 4.2, the impulsive transmission of a symbol is based on time-slotted manner meaning that the TN transmits each symbol at the beginning of the T_{sym}. In binary scheme, each *symbol* is represented as a 1 or a 0 and known as a *bit*, while in M-ary scheme, each symbol consists of $\log_2$M bits where M is the alphabet size in M-ary sheme [HAY-00]. In binary ASK-based IM transmission scheme, in the general case, the TN transmits an impulsive transmission of $Q_0\delta(t)$ molecules when it wants to send a bit 0 (hypothesis H_0) and it transmits $Q_1\delta(t)$ molecules when it wants to send a bit 1 (hypothesis H_1). As a result, in binary transmission scheme, the transmitted signal can be expressed as $\sum_{j=0}^{(N_b-1)} Q_{b_j}\delta(t-jT_{\text{sym}})$. The TN transmits Q_{b_j} molecules where $Q_{b_j} \gg 1$, and $b_j \in \{0,1\}$ denotes the binary alphabet, $j = \{0,1,2,\ldots,(N_b-1)\}$ is the index of bits to be transmitted, $\mathbf{b} = [b_0, b_1, b_2, ..., b_{(N_b-1)}]$ is the transmitted sequence of bits, and N_b is the total number of bits to be transmitted, T_{sym} is the symbol duration. Note that in binary scheme the alphabet of the transmitted symbols consists of two bits only, namely, 1 and 0, and can be expressed as $b_j \in \{0,1\}$, $j = \{0,1,2,\ldots,(N_b-1)\}$, and represented by sending $Q_{b_j} \in \{5000,10000\}$ molecules respectively. Figure 4.2 shows such a time-slotted binary ASK-modulated CEMC transmission scheme. Note that in Fig. 4.2, the amplitudes Q_{b_j} depend on the specific symbols (i.e bits in binary case) to be transmitted.

However, in M-ary scheme, each symbol consisting of $\log_2$M bits is taken from $\mathbf{b}$, ASK-modulated with $Q_{b_j^M}$ molecules, finally, transmitted with IM into the propagation medium. For example, in quaternary (M = 4) scheme, the alphabet of the transmitted symbols consists of four symbols, namely, $b_j^M \in \{00,01,10,11\}$, and is represented by sending $Q_{b_j^M} \in \{5000,10000,15000,20000\}$ molecules respectively. As a result, in M-ary scheme, the transmitted signal is $\sum_{j=0}^{(N_{\text{sym}}-1)} Q_{b_j^M}\delta(t-jT_{\text{sym}})$ where N_{sym} denotes the total number of $\log_2$M bit-long symbols.

4.4.2 Diffusion-based Propagation of Molecules

According to the microscopic theory of diffusion [BER-93], when a number of molecules are transmitted by the TN each of them propagates independently and reaches the RN in a probabilistic manner [BER-93]. Referring back to Eq. (4.1), Figs. 4.3(a) and 4.3(b) show the signals at the output of the CEMC channel with N = 10 samples taken in each symbol duration for binary and M-ary schemes respectively. The number of molecules that would be available and possibly received by the RN in the VRV would represent the deterministic amplitude $s_{b_j}(t)$ of the *signal intensity*, as shown in Eq. (4.3), following binomial distribution. In binary CEMC system, when the TN sends $Q_{b_j}, b_j \in \{0,1\}$, molecules in the medium for each symbol, the probability of having k_b molecules at the RN out of the Q_{b_j} transmitted molecules during the j-th symbol interval (i.e. whether each of those k_b molecules arrives the RN during the j-th symbol interval or not) can be expressed by the binomial distribution function as below.

$$\Pr\left(k_b; Q_{b_j}, p(t)\right) = \frac{Q_{b_j}!}{k_b!(Q_{b_j}-k_b)!} p^{k_b}(t)\left(1-p(t)\right)^{(Q_{b_j}-k_b)} \tag{4.4}$$

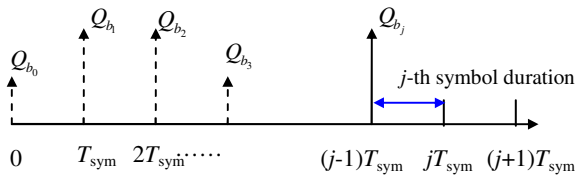

Figure 4.2 Time-slotted binary ASK-modulated CEMC signaling. The amplitudes Q_{b_j} correspond to the bits to be transmitted.

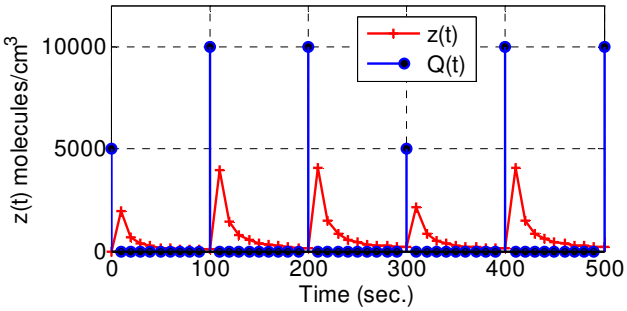

(a) Binary ASK

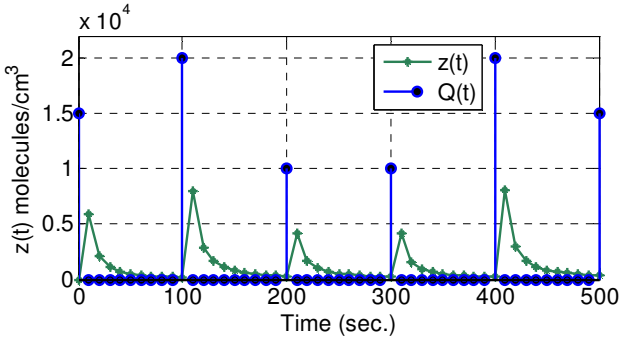

(b) M-ary ASK

Figure 4.3 Input $Q(t)$ and output $z(t)$ concentration signals at r = 10 μm, in ASK-based CEMC system. (a) Binary: bit 1 and bit 0 are represented by sending 10,000 and 5,000 molecules respectively at the beginning of each symbol duration, and (b) Quaternary: When M = 4, the symbols 00, 01, 10, and 11 are represented by sending 5000, 10000, 15000, and 20000 molecules respectively.

4.4.3 Signal, Noise, and Interference Models

For a reasonably large value of $Q_{b_j} \gg 1$, when $p(t)$ is not close to 1 or 0 and $p(t)$ is finite such that as $Q_{b_j} \to \infty$, $Q_{b_j} p(t) \to \infty$, the binomial distribution on the right side of Eq. (4.4) can be approximated to a *normal* distribution $\mathcal{N}(\mu_s, \sigma_s^2)$ where the mean (μ_s) and the variance (σ_s^2) can be expressed as

$$\begin{aligned} &\mu_s = Q_{b_j} p(t) = s_{b_j}(t), \quad \sigma_s^2 = Q_{b_j} p(t)\left(1-p(t)\right) = s_{b_j}(t)\left(1-p(t)\right) \\ &\text{and so, } \mathcal{N}\left(Q_{b_j} p(t), Q_{b_j} p(t)\left(1-p(t)\right)\right) \Rightarrow \mathcal{N}\left(s_{b_j}(t), s_{b_j}(t)\left(1-p(t)\right)\right). \end{aligned} \tag{4.5}$$

In addition, as shown in Figs. 4.1 and 4.3, since Q_0 and Q_1 are 5000 and 10000 molecules respectively, when Q_{b_j} is large (e.g. $Q_{b_j} > 5$), the spatiotemporal variation of

$p(t)$ provides $Q_{b_j}\,p(t)$ such that $\left|\left(1/\sqrt{Q_{b_j}}\right)\left(\sqrt{(1-p(t))/p(t)}-\sqrt{p(t)/(1-p(t))}\right)\right|<0.3$ is satisfied, where $|\bullet|$ denotes the absolute value of any quantity. This in turn validates that the *normal* approximation to the binomial distribution is "adequate" [BOX-78], p. 130.

As a result, the mean of the number of molecules available for reception is actually the deterministic signal $s_{b_j}(t)$ found previously as the mean signal intensity in Eq. (4.3) using the *macroscopic theory* of the diffusion [BER-93]. Therefore, the total number of molecules $y(t)$ available for reception as a result of diffusion only can be expressed as a *normal* distributed random variable that is the sum of the deterministic part $s_{b_j}(t)$ and a zero-mean *normal*-distributed random variable $n_{s_{b_j}}(t)$ with variance $s_{b_j}(t)\left(1-p(t)\right)$ as shown below.

$$\begin{aligned} &y(t)=s_{b_j}(t)+n_{s_{b_j}}(t) \text{ where} \\ &n_{s_{b_j}}(t)\sim\mathcal{N}\left(0,s_{b_j}(t)\left(1-p(t)\right)\right)=\sqrt{s_{b_j}(t)\left(1-p(t)\right)}\,\mathcal{N}\left(0,1\right) \end{aligned} \tag{4.6}$$

During the j^{th} symbol interval, the RN would receive some of the molecules that were transmitted by the TN at the beginning of the j^{th} symbol interval, plus some of the molecules that were transmitted by the TN during the previous symbols, i.e. from the first symbol up to the $(j\text{-}1)^{\text{th}}$ symbol. The former constitutes the desired signal part, while the latter constitutes the ISI part of the received signal.

In Eq. (4.6), the number of molecules available to the RN at any time t during the j^{th} symbol is a random variable with signal-dependent mean and variance, and therefore, incorporating the ISI, the received concentration signal intensity can be expressed as

$$z(t)=s_{b_j}(t)+n_{s_{b_j}}(t)+n_{\text{ISI}}(t) \tag{4.7}$$

where $n_{s_{b_j}}(t)$ is as shown in Eq. (4.6) and $n_{\text{ISI}}(t)$ denotes the residual molecules due to ISI and can be expressed as $n_{\text{ISI}}(t)\sim\mathcal{N}(\mu_{\text{ISI}},\sigma^2_{\text{ISI}})$.

4.4.4 Binary Optimum Receiver

Considering the signal, the noise, and the interference models explained above, the binary signal detection problem in CEMC system can be formally written as below.

$$z(t)\sim\begin{cases}\mathcal{N}\left(s_1(t)+\mu_{\text{ISI}},s_1(t)\left(1-p(t)\right)+\sigma^2_{\text{ISI}}\right); & \text{H}_1\\ \mathcal{N}\left(s_0(t)+\mu_{\text{ISI}},s_0(t)\left(1-p(t)\right)+\sigma^2_{\text{ISI}}\right); & \text{H}_0\end{cases} \tag{4.8}$$

An optimum receiver is the one that gives the *minimum probability of error* [KAY-93]. We develop optimum receiver architectures of the binary and the M-ary CEMC systems in this and the following subsections respectively. We consider the *minimum probability of error* criterion to derive a *test statistic* by calculating the logarithm of the likelihood ratio using the Neyman-Pearson theorem [KAY-93] with equal prior probabilities as below

$$\frac{\ell(z \mid \mathrm{H}_1)}{\ell(z \mid \mathrm{H}_0)} > 1 \;\Rightarrow \ln \frac{\ell(z \mid \mathrm{H}_1)}{\ell(z \mid \mathrm{H}_0)} > 0. \tag{4.9}$$

where the conditional probabilities can be expressed as below.

$$\ell(z \mid \mathrm{H}_1) = \frac{1}{\sqrt{2\pi\left(s_1(t)(1-p(t)) + \sigma_{\mathrm{ISI}}^2\right)}} \exp\left[-\frac{\left\{z - \left(s_1(t) + \mu_{\mathrm{ISI}}\right)\right\}^2}{2\left(s_1(t)(1-p(t)) + \sigma_{\mathrm{ISI}}^2\right)} \right] \tag{4.10}$$

$$\ell(z \mid \mathrm{H}_0) = \frac{1}{\sqrt{2\pi\left(s_0(t)(1-p(t)) + \sigma_{\mathrm{ISI}}^2\right)}} \exp\left[-\frac{\left\{z - \left(s_0(t) + \mu_{\mathrm{ISI}}\right)\right\}^2}{2\left(s_0(t)(1-p(t)) + \sigma_{\mathrm{ISI}}^2\right)} \right]$$

Note that for any prior probability the optimum receiver is termed as the *maximum a posteriori probability* (MAP) detector, which for equal prior probability, $\Pr(\mathrm{H}_0) = \Pr(\mathrm{H}_1)$, reduces to *maximum likelihood* (ML) detector [MAH-13] [KAY-93]. Each concentration sample value sensed by the RN represents one independent observation. As shown in Eqs. (4.7) and (4.8), each temporal sample represents the concentration signal intensity as an independent *normal*-distributed random variable whose mean and variance depend on two quantities, namely, the signal value itself and the probability that one molecule becomes available at the RN, i.e. $p(t)$. Therefore, for N observations in each symbol duration, $n = [1, 2, ..., N]$, combining Eqs. (4.9) and (4.10) and simplifying yield the test statistic $T(z)$ as shown in Eq. (4.11), and the resulting sampling-based binary receiver architecture is shown in Fig. 4.4.

$$T(z)=\sum_{n=1}^{N}\left\{a_{\mathrm{SD}}[n]z^2[n]+b_{\mathrm{SD}}[n]z[n]-\gamma[n]\right\}\underset{\text{Select H}_0}{\overset{\text{Select H}_1}{\gtrless}}0,\ \text{where} \tag{4.11}$$

$$a_{\mathrm{SD}}[n]=\left\{\frac{1}{2\left(s_0[n](1-p[n])+\sigma_{\mathrm{ISI}}^2\right)}-\frac{1}{2\left(s_1[n](1-p[n])+\sigma_{\mathrm{ISI}}^2\right)}\right\}$$

$$b_{\mathrm{SD}}[n]=\left\{\frac{\left(s_1[n]+\mu_{\mathrm{ISI}}\right)}{\left(s_1[n](1-p[n])+\sigma_{\mathrm{ISI}}^2\right)}-\frac{\left(s_0[n]+\mu_{\mathrm{ISI}}\right)}{\left(s_0[n](1-p[n])+\sigma_{\mathrm{ISI}}^2\right)}\right\}$$

$$-\gamma[n]=\left\{\frac{1}{2}\ln\frac{\left(s_0[n](1-p[n])+\sigma_{\mathrm{ISI}}^2\right)}{\left(s_1[n](1-p[n])+\sigma_{\mathrm{ISI}}^2\right)}-\frac{\left(s_1[n]+\mu_{\mathrm{ISI}}\right)^2}{2\left(s_1[n](1-p[n])+\sigma_{\mathrm{ISI}}^2\right)}+\frac{\left(s_0[n]+\mu_{\mathrm{ISI}}\right)^2}{2\left(s_0[n](1-p[n])+\sigma_{\mathrm{ISI}}^2\right)}\right\}$$

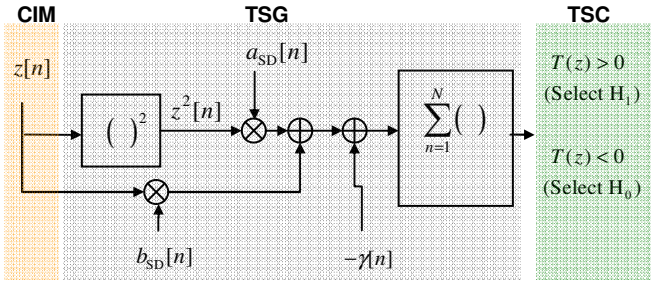

CIM – Concentration Intensity Measurement
TSG – Test Statistic Generator
TSC – Test Statistic Comparator

Figure 4.4 Sampling-based optimum receiver of binary CEMC system.

4.4.5 M-ary Optimum Receiver

In a similar way, a generalized ASK-based M-ary signal detection model can be shown as

$$z(t)\sim\mathcal{N}\left(s_k(t)+\mu_{\mathrm{ISI}},s_k(t)\left(1-p(t)\right)+\sigma_{\mathrm{ISI}}^2\right);\quad \text{when } \mathrm{H}_k \text{ is true, and } k=\{1,2,...,M\}. \tag{4.12}$$

Using the conditional probabilities in a similar way as shown in Eq. (4.10) the M-ary signal can be detected as shown below.

$$\textbf{Decide}:\ \mathrm{H}_k \text{ when } \log\ell\left(z\,|\,\mathrm{H}_k\right)\text{is the } \textbf{greatest}$$
$$\text{where}\quad \ell\left(z\,|\,\mathrm{H}_k\right)=\frac{1}{\sqrt{2\pi\left(s_k(t)\left(1-p(t)\right)+\sigma_{\mathrm{ISI}}^2\right)}}\times\exp\left[-\frac{\left\{z-\left(s_k(t)+\mu_{\mathrm{ISI}}\right)\right\}^2}{2\left(s_k(t)\left(1-p(t)\right)+\sigma_{\mathrm{ISI}}^2\right)}\right] \tag{4.13}$$

For N observations (i.e. concentration samples), finding the **greatest** $\log\ell(z\,|\,\mathrm{H}_k)$ is equivalent to finding the **smallest** equivalent test statistic T_k as shown in Eq. (4.14). The resulting sampling-based M-ary optimum receiver for CEMC is shown in Fig. 4.5.

$$\max\left[\log \ell\left(z \mid \mathrm{H}_k\right)\right] = \max\left[-\frac{1}{2}T_k\right] \Rightarrow \min\left(T_k\right) \quad \text{where}$$
$$\text{where } T_k(z) = \sum_{n=1}^{N}\left\{a_{\mathrm{SD},k}[n]z^2[n] + b_{\mathrm{SD},k}[n]z[n] + \gamma_k[n]\right\} \tag{4.14}$$
$$a_{\mathrm{SD},k}[n] = \frac{1}{s_k[n]\left(1-p[n]\right)+\sigma_{\mathrm{ISI}}^2}$$
$$b_{\mathrm{SD},k}[n] = -\frac{2\left(s_k[n]+\mu_{\mathrm{ISI}}\right)}{s_k[n](1-p[n])+\sigma_{\mathrm{ISI}}^2} \text{ and}$$
$$\gamma_k[n] = \frac{\left(s_k[n]+\mu_{\mathrm{ISI}}\right)^2}{s_k[n](1-p[n])+\sigma_{\mathrm{ISI}}^2} + \ln\left[2\pi\left(s_k[n](1-p[n])+\sigma_{\mathrm{ISI}}^2\right)\right]$$

4.4.6 ISI Characteristics

When the TN-RN distance is kept unchanged, the exact number of molecules that causes ISI depends on the previously transmitted symbols as well as the sampling time interval. For example, in binary CEMC system, in the *j*-th symbol at its *n*-th sample, when the RN considers all of the previous $\mathrm{M_{RN}} = (j-1)$ bits, the ISI-producing molecules can be found as $n_{\mathrm{ISI}}(j,n) \sim \mathcal{N}\left(\mu_{\mathrm{ISI}}^{(j,n)}, \sigma_{\mathrm{ISI}}^{2(j,n)}\right)$, where the mean ($\mu_{\mathrm{ISI}}^{(j,n)}$) and the variance ($\sigma_{\mathrm{ISI}}^{2(j,n)}$) can be expressed as shown in below,

$$\mu_{\mathrm{ISI}}^{(j,n)} = \sum_{i=1}^{\mathrm{M_{RN}}=(j-1)} Q_{b_{j-i}} p_{\tilde{\upsilon}}\left(iT_{\mathrm{sym}} + nt_{\mathrm{s}}\right)$$
$$\sigma_{\mathrm{ISI}}^{2(j,n)} = \sum_{i=1}^{\mathrm{M_{RN}}=(j-1)} Q_{b_{j-i}} p_{\tilde{\upsilon}}\left(iT_{\mathrm{sym}} + nt_{\mathrm{s}}\right)\left[1 - p_{\upsilon}\left(iT_{\mathrm{sym}} + nt_{\mathrm{s}}\right)\right] \tag{4.14a}$$

where $Q_{b_j}, \forall j$ denotes the number of molecules transmitted at the beginning of the *j*-th symbol, $p_{\tilde{\upsilon}}(t)$ is the $\tilde{\upsilon}$-th realization of the energy-normalized CIR of the CEMC channel [MAH-13], and t_{s} is the sampling time interval of the system such that $T_{\mathrm{sym}} = Nt_{\mathrm{s}}$. However, the quantity $\mathrm{M_{RN}}$ is known as the memory size of the receiver, expressed in terms of previous symbols (i.e. bits in case of binary system) , and can be varied to derive several receiver configurations as shown next.

4.4.7 Receiver Configurations

As shown in Eq. (4.14a), for binary CEMC, in order to compute $\mu_{\mathrm{ISI}}^{(j,n)}$ and $\sigma_{\mathrm{ISI}}^{2(j,n)}$ from the previous symbols, the RN needs to have in store the following quantities: $Q_0, Q_1, p_{\tilde{\upsilon}}, T_{\mathrm{sym}}, t_{\mathrm{s}}$ and $\mathrm{M_{RN}}$ where $\mathrm{M_{RN}}$ is the receiver memory in terms of the number of previous bits detected by the RN. For a transmitted bit sequence, the RN would require to store the samples of $p_{\tilde{\upsilon}}$

for use in the ISI computation. However, the accuracy of the M_{RN} previously detected bits would also impact the accuracy of the BER results. In this paper, we assume that RN can detect the previous M_{RN} bits correctly, thus the results shown would be the best case BER in each simulation setting. Based on the capability of the RN in determining the number of the ISI-producing molecules accurately, we consider three cases as shown in the following.

Case 1–The Simplest Receiver Configuration: In this receiver configuration, the RN is not at all able to determine the number of the ISI-producing molecules present in the current symbol. Since the symbol duration in this case is acceptably larger than the delay spread [RAP-02] of the CEMC channel, the RN can safely assume that a minimum ISI level present in the system can be represented as $\mu_{\text{ISI}} = 1$, $\sigma^2_{\text{ISI}} = 1$, i.e. $n_{\text{ISI}}(t) \sim \mathcal{N}(1,1)$. Considering RN's knowledge of the ISI in the system, this case can be known as the *simplest* case in terms of the complexity required at the RN, yet the *worst* case scenario in terms of the BER. Therefore, assuming that the RN is capable of doing simple tasks only, this scheme provides relatively lower complexity in the RN because the RN does not at all compute the number of ISI-producing molecules in the sample of the current bit. As a result, this scheme will provide an upper limit in the BER of the system under the scenario when the RN cannot compute the ISI at all.

Case 2–Reduced Complexity (RC) Receiver Configuration: In this receiver configuration, the RN considers the ISI-producing molecules originating from the immediately previous symbol only, i.e. $M_{RN} = 1$. Performance-wise, this scheme should be better than Case 1 because the RN now considers only the immediately previous symbol in order to compute the ISI-producing molecules. For the j-th symbol, when $1 < M_{RN} < (j-1)$, this configuration can be improved in terms of BER, though at the cost of design complexity. For example, when $M_{RN} = 4$ is plugged into Eq. (4.14a), at the 6^{th} sample of the 50^{th} symbol, both $\mu_{\text{ISI}}^{(50,6)}$ and $\sigma_{\text{ISI}}^{2(50,6)}$ will consist of 4 terms involving the previous 4 symbols, i.e. the 49^{th}, 48^{th}, 47^{th}, and 46^{th} bits in case of binary CEMC system. We also investigate how memory size M_{RN} impacts the BER performance of the receiver as shown in Section 4.5.

Case 3–Full Complexity (FC) Receiver Configuration: In this receiver configuration, the RN can accurately determine the number of ISI-producing molecules originating from

all the previous symbols at the current j-th symbol, i.e. $M_{RN} = (j - 1)$. This means the RN has the most accurate (exact) knowledge of the ISI taking place in the current symbol. The ISI-producing molecules can be accurately known to the RN at any temporal sample by computing the mean and the variance of ISI-producing molecules using Eq. (4.14a). Considering the most accurate (exact) knowledge of the ISI-producing molecules in the current symbol, this case can be known as the *best* case scenario in terms of BER. However, in this scheme the RN needs to know all the previously transmitted symbols correctly, thereby making the scheme excessively heavy in terms of memory and complexity of the RN. Nevertheless, being the *best* case for the RN, this scheme provides a lower limit in the BER of the system.

As shown in Fig. 4.4, the RN handles the received concentration of molecules by passing it through TSG and TSC blocks. The TSG block consists of a squarer, a multiplier, summer, and a threshold computer sub-blocks. The TSC block consists of a comparator sub-block only. Based on literature on biological computations and components, it is likely that the RN would be able to implement such building blocks, either by engineering the RN itself [NAK-11a] or by applying variable memory size techniques to reduce computations [MAH-13c]. Since accurate detector design was beyond of the focus of this chapter, some insights on the feasibility of designing a sampling-based detector can be found in Chapter 6. Although the work in Chapter 6 deals with optimum receiver based on SCK, we believe that the procedures, component blocks, and implementations of the sets of computations in bionanomachines should be able to provide necessary insights to system designers.

4.5 Simulation Model and BER Results

In this section, we explain the performances of the sampling-based binary and M-ary receivers using numerical simulations in terms of three factors, namely, number of samples per symbol (N), communication range (r), and transmission data rate (f).

4.5.1 Simulation Setup

An ideal diffusion-based CEMC system is simulated by assuming a point source TN located at the origin (0,0,0). A randomly generated bit sequence of 100,000 bits, following a time-slotted binary and M-ary IM scheme, as shown in Figs. 4.2 and 4.3, is transmitted into the

propagation medium. The diffusion coefficient, $D = 10^{-6}$ cm^2/s [BER-93] [LAC-09] [FRE-99], of information molecules is assumed to remain unchanged during the entire observation time [MAH-10b]. In ASK-based binary and M-ary systems, three scenarios are considered: when r varies from 400 nm up to 100 μm [MAH-10b], when N varies from 1 to 100, and finally, when f varies from 0.01 bps up to 1 bps (i.e. bit duration varies from 100 s down to 1 s). Since nanomachines are viewed as tiny machines of extremely limited capabilities [SUD-05], the minimum sampling time interval, on which basis the RN senses the concentration of the information molecules at its receptors, is chosen as at least 1 s [MAH-13]. The parameters of the numerical simulations are shown in Table 4.1. The transmitted bit sequence is tested by using 30 to 50 different randomly generated CIR realizations such that the probability that the sample mean of the CIR at the RN differs from the true mean by less than one standard deviation is at least 0.96 [LEO-94], and thus the average BER is computed.

Table 4.1 Parameters for numerical simulations

Symbol	Quantity	Parameter value
D	diffusion constant	10^{-6} cm^2/s
f	data rate	0.01 bps – 0.1 bps
r	communication range	400 nm – 100 μm in water medium
t	time	up to 10,000,000 s
M	ASK modulation type	M = 2 (binary), M = 4 (quaternary)
M_{RN}	receiver memory	M_{RN} = 1, 2, 5, 10, 20, 40, 60, 80, 99
$Q_{b_j}, Q_{b_j^M}$	amplitude levels	[5000,10000] molecules (binary), [5000, 10000,15000,20000] molecules (quaternary)
t_s	sampling time interval at RN	1 s – 100 s
K_{ch}	no. of random channel realizations considered	50

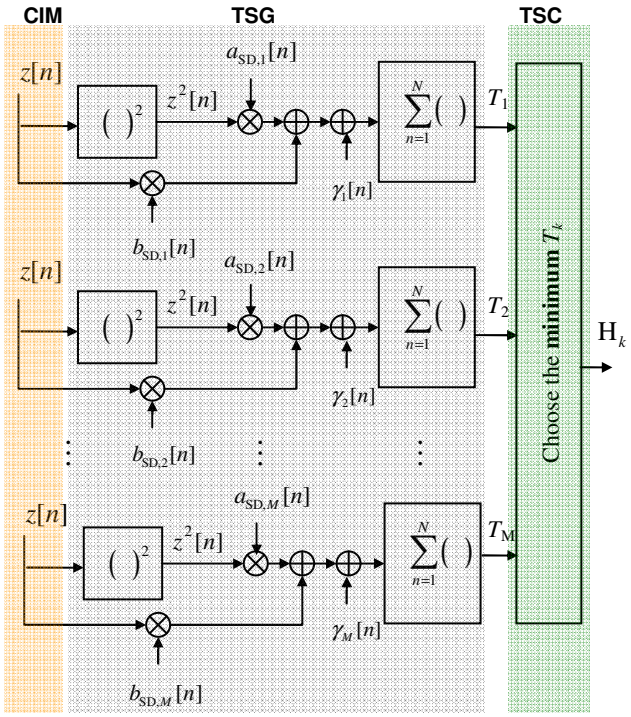

Figure 4.5 Sampling-based optimum receiver of M-ary CEMC system.

4.5.2 Results with the Simplest Receiver (Case 1)

Effects of sample number

Figure 4.6 shows the effects of N on BER for both binary and quaternary (i.e. M = 4) systems. As shown in Fig. 4.6, when a larger number of samples are used by the RN, the average BER at the RN decreases. For instance, when 4 samples per symbol are used at the receiver, a high BER of approximately 46% for both systems is observed, meaning that approximately 46% of the bits are decoded incorrectly for both binary and quaternary systems, and therefore, using the binary system with the reduction in the alphabet size from quaternary to binary does not provide any BER improvement in CEMC system when $1 \leq N \leq 4$. For both binary and quaternary systems, when r is fixed, as N increases the BER decreases. This can be explained by referring to Fig. 4.1 such that as N increases, the sampling time interval at the RN decreases and, as a result, the value of $p(t)$ at any sampling

time instant during T_{sym} decreases, meaning that signal experiences less ISI effects measured by the RN.

However, it is found that at any values of r and N, the binary CEMC system provides potentially lower BER than the quaternary system for any $N > 4$, which can be explained as follows: when N and r are fixed, in the quaternary (M = 4) system, the current symbol is affected much by the previous symbols (severely when the immediately previous symbol is larger than the current symbol, providing higher amplitude level in ASK-based modulation and so a higher number of residual molecules to interfere with the current symbol), and therefore, the RN cannot correctly distinguish among the 4 amplitude levels of the quaternary system. This results in the higher number of incorrectly decoded symbols at the RN, which causes a higher BER. As shown in Fig. 4.6, numerical results show that for binary system, when communication range and transmission data rate are fixed at r = 800 nm and f = 0.01 bps respectively, the receiver can decode all the bits correctly (BER = 0) when $N > 10$. However, for the same scenario and $N > 10$, as N increases, the quaternary system provides decreasing BER, although compared to the binary system, the BER performance of the quaternary system is considered worse. Since the CEMC system under consideration is subject to diffusion noise and ISI, it may not be possible to have BER exactly equal to zero. However, the simulation results, presented in this and the following chapters, showing that the receiver can detect all the bits correctly (i.e. BER = 0) actually mean that the BER in fact approaches zero in this case.

Effects of communication range

When the number of samples and transmission data rate are kept fixed at N = 10 and f = 0.01 bps respectively, Fig. 4.7 shows the effects of r on BER such that when r increases the BER increases. This means that the sampling-based detection approach can become limited by the communication range of operation. Even when N and f are kept unchanged, the degradation of the BER performance is due to the temporal spreading of the $p(t)$ and, correspondingly, the higher level of ISI that the signal experiences as r increases in the diffusion-based CEMC channel. The communication range investigated is in the range from 400 nm up to 100 μm, which covers a wide range of TN-RN distances in water as the propagation medium as reported in [MAH-10b].

As shown in Fig 4.1(b), when r increases the symbols become temporally spread and, therefore, cause more ISI to the system. In addition, in M-ary system, as explained earlier the current symbol is affected by the previous symbols of higher amplitude, thus causing a higher BER in the quaternary system compared to the binary system. The effects of r on BER are shown in Fig. 4.7. For instance, up to 10 μm, the BERs of the binary and the quaternary systems remain almost unchanged at approximately 7% and 30% respectively.

In addition, as shown in Fig. 4.1(b), when r is very large, e.g. 100 μm, the effects of diffusion of molecules is so slow such that $p(t)$ observes no peak in its amplitude within the symbol duration and, therefore, provides an almost flat $p(t)$ over time. In such cases, the sampling-based detector cannot detect any desired signal (in both binary and quaternary systems) and so provides high BER. In general, MC is an extremely slow communication system [NAK-11a] and, therefore, in CEMC using a quaternary system, keeping the symbol duration unchanged, can be considered as a trade-off between communication speed by increasing the alphabet size and BER to be achieved.

In Case 2 with a variable memory size receiver, the BER performance is shown in Fig. 4.7(c) for binary and quaternary systems when $N = 4$ and $f = 0.01$ bps. Comparing Fig. 4.7(b) with Fig. 4.7(c) shows that increasing the memory size improves the BER performance of both binary and quaternary systems.

Effects of transmission data rate

Finally, the effects of transmission data rate on BER are shown in Fig. 4.8 such that transmission data rate has no significant influence on the BER when the number of samples per symbol and the TN-RN distance are kept unchanged. For each transmission data rate shown in Fig. 4.8, the sampling intervals are adjusted such that total number of samples per symbol remains unchanged. For example, when the transmission data rate doubles, the symbol interval becomes half, which necessitates that the sampling interval be half in order for the number of samples per symbol to remain unchanged.

In sampling-based detection, r and N are two main factors that influence the BER of the CEMC system. However, as shown in Fig. 4.8, when r and N are kept unchanged, the binary and the quaternary systems can provide constant BER when f varies, although the BER performance of the quaternary system is worse than that of the binary system. While for

both binary and quaternary systems, to achieve a preset BER, the memory requirement increases when r increases, the performance of the quaternary system is considered worse than that of the binary system when r remains unchanged. However, when $M_{RN} > 10$, both systems can detect all the bits correctly, providing zero BER.

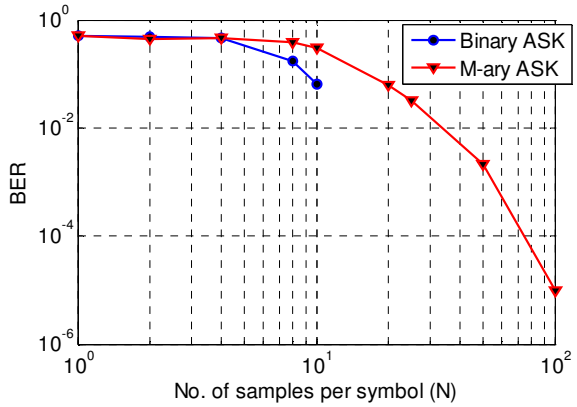

Figure 4.6 In Case 1, the effects of the number of samples per symbol (N) on BER when r = 800 nm and f = 0.01 bps.

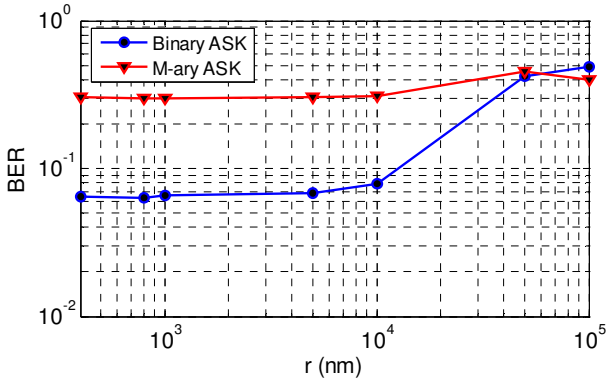

(a) Case 1: when RN does not compute the effects of ISI.

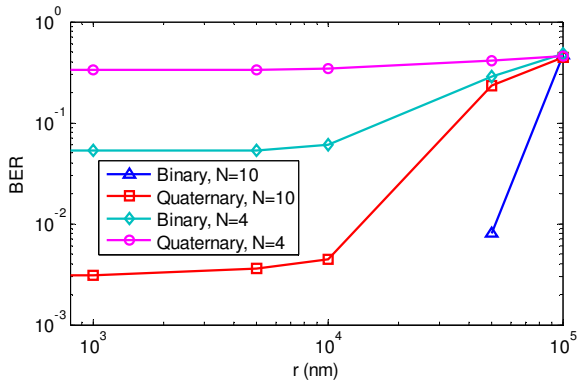

(b) Case 2: when the RN computes the ISI from the immediately previous symbol only.

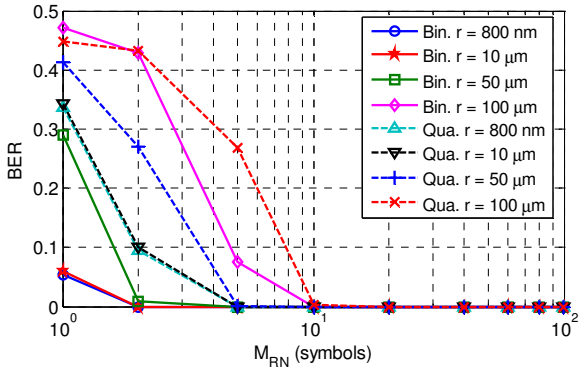

(c) Effects of memory size on BER when $f = 0.01$ bps and $N = 4$.

Figure 4.7 Effects of communication range r on BER when (a) $N = 10$ and $f = 0.01$ bps, (b) $N = 4$, 10, and $f = 0.01$ bps, and (c) memory size varies, $f = 0.01$ bps and $N = 4$.

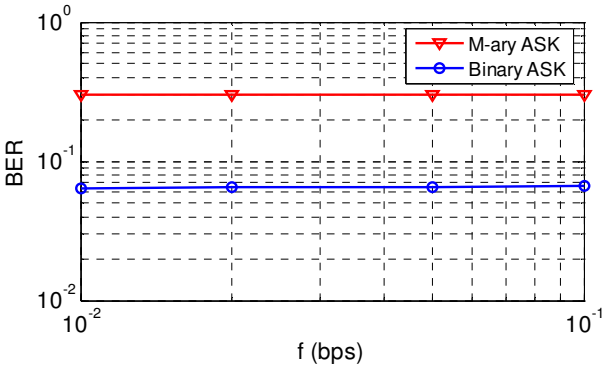

Figure 4.8 In Case 1, the effects of transmission data rate f on BER when $N = 10$ and $r = 800$ nm.

4.5.3 Results with RN's Knowledge of the ISI from the Immediately Previous Symbol Only (Case 2)

When the RN knows the number of ISI-producing molecules from the immediately previous symbol only, Fig. 4.7(b) shows the results of both binary and quaternary systems with $N = 4$ and $N = 10$ samples per symbol. As shown in Fig. 4.7(b), at any communication range with a given sampling rate, the binary system performs better than the quaternary system. However, using a higher sampling rate provides an improved BER in both binary and quaternary systems. As a result, of the four schemes as shown in Fig. 4.7(b), at any r the

binary system with $N = 10$ performs the best and, correspondingly, the quaternary system with $N = 4$ performs the worst. Note that in Fig. 4.7(b), with $N = 10$, when $r < 50$ μm, the binary CEMC system can detect all the transmitted bits correctly and thus gives zero BER. As a result, with $N = 10$, when $r < 50$ μm, the blue line with triangular marks does not exist in the logarithmic scale shown for BER in Fig. 4.7(b).

Comparing the performances of the binary and the quaternary systems in Figs. 4.6 and 4.7, it is evident that if BER is traded off with the complexity of the RN (i.e. whether or not the RN computes the ISI from the immediately previous symbol) then an improvement in the BER could be made for a given N and r. For example, when $N = 4$ and $r = 800$ nm are kept unchanged, for the binary system, the BER improves from ~45% to ~5%, providing approximately a ten-fold improvement in the BER of the binary system. Therefore, a system can surely choose to adopt an RN with a moderate complexity so as to compute the ISI-producing molecules from the immediately previous symbol only and thus improve the BER performance of the system.

4.5.4 Results with the Most Complex Receiver (Case 3)

When the RN is able to accurately compute all the ISI-producing molecules originating from all the previous information symbols, the RN has been found to detect all the symbols correctly (BER = 0) in both binary and M-ary systems. This is achieved at the cost of the complexity of the RN, by keeping the information of all the previously detected symbols in the memory of RN. Although the RN may not detect all the previous symbols correctly and/or may not store all the previously detected symbols in its memory, BER = 0 found with Case 3 can obviously prove that the developed sampling-based detector structure is correct, meaning that when all the previous symbols are correctly input to the RN, the RN is able to correctly detect all the transmitted symbols with BER = 0. As shown in Fig. 4.6, the more the number of samples per symbol, the better is the BER performance of the system. In addition, Fig. 4.6 also shows that for the binary system when $N > 10$, no bit errors take place even with the simplest RN (Case 1) when $r = 800$ nm and $f = 0.01$ bps. Therefore, Case 3 has been simulated for $r = 400$ nm, 800 nm, 1 μm, 5 μm, 10 μm, 50 μm, 100 μm, and $N = 2, 4, 5, 10$, and the obtained results show that the RN can correctly detect all the transmitted symbols in both binary and quaternary systems, providing BER = 0. Another notable

observation is that, within the mentioned ranges of *r* and *N*, when Case 3 provides BER = 0, the system designer can evaluate the situation and decide whether or not to use Case 3 and thereby compare the BER improvement achievable by using Case 2 instead of Case 3 in these ranges of *r* and *N*. This also means that a reduction in the complexity of the RN would be possible by using Case 2 instead of Case 3, which would be a better option than Case 1 in the BER performance but with less complexity in the RN than in Case 3.

4.5.5 Possibilities of Bio-inspired Design of the Detector

In this section, a brief introduction of some of the inspirations found in nature has been provided, which provides the motivation for the bio-inspired design of the sampling-based detectors using biological nanomachines (e.g. biological cells). For instance, biological cells can be viewed as *sensors* [LIU-12a] that are already available in the nature and can be engineered in order to realize the CEMC among nanomachines [NAK-11a]. It has been experimentally demonstrated that the extra-cellular agonist[9] concentration can encode the biological information and transmit it to the intra-cellular Ca^{+2} oscillations by providing variations in Ca^{+2} amplitude and frequency, and as a result, the intra-cellular Ca^{+2} concentration signal can be controlled by the extra-cellular agonist concentration signals received at the cell membrane [SCH-93]. In addition, it is well known from the biological signal transduction principles that it is possible to amplify [BUS-10] [LIU-11] the intra-cellular signaling effects due to extra-cellular signal concentration, which is also promising to possibly build detection-related cellular functionalities, e.g. addition, subtraction, multiplication, and square operations. For instance, in molecular biology, enzyme-based amplification methods are known to be the most sensitive amplification methods and can produce many thousands of molecules of the product from each enzyme when it acts in catalytic reaction [ALB-08]. In protein-based amplification, a small number of information proteins reacting with the receptor at the cell membrane can generate a large intracellular response by either producing large number of “small intracellular mediators” or by activating other signaling proteins [ALB-08], see p. 895. In addition, when an information molecule reacts with the receptor proteins at the cell boundary, the signal is relayed to the

[9] Hormone or any other ligand molecules.

cytoplasm of the cell through second messengers that influence the action of other enzymes inside the cell, and finally, releasing the enzymatic product molecules [ALB-08]. The effects of signaling molecules inside a cell can be amplified by using the chain of many protein messengers [ALB-08].

In addition, it is well known that logic functions can also be implemented inside the cytoplasm of a biological cell [NAK-11a] [MOO-07], which would be useful in implementing necessary functionalities focusing on the required detector design. Therefore, based on the knowledge available from the cellular and molecular biology domains, it would be possible to engineer a biological cell to implement the test statistic as shown in Eqs. (4.11) and (4.14) and further compare it to decide on the transmitted symbols. The detailed implementation of the sampling-based detector using biological components inside a cell is beyond the current focus of this research, and so it is not included in this chapter; however, as shown above, appropriate references to the relevant works have been made that support the possibility of cellular computations and implementation of the detector using biological components.

4.6 Exact Detection Performance

In this section, we present an approach to derive the exact ROC of the optimum binary receiver in terms of the probabilities of false alarm (P_{FA}) and probability of detection (P_{D}) [KAY-93]. Following a similar procedure the ROC of the M-ary receiver can be investigated, and hence the P_{FA} and the P_{D} of the M-ary receiver are not shown in this chapter.[10]

4.6.1 Probability of False Alarm ($\mathbf{P_{FA}}$)

At H_0: Since $z(t) \sim \mathcal{N}\left(\mu_{z_0}, \sigma_{z_0}^2\right)$ where $\mu_{z_0} = s_0(t) + \mu_{\mathrm{ISI}}$ and $\sigma_{z_0}^2 = s_0(t)\left(1 - p(t)\right) + \sigma_{\mathrm{ISI}}^2$, by converting $z[n]$ into a standard normal variable $x[n] \sim \mathcal{N}(0,1)$ the first term in the expression of $T(z)$, as shown in Eq. (4.11), yields

[10] The interested reader may refer to [KAY-93].

$$\sum_{n=1}^{N} a_{\mathrm{SD}}[n] z^2[n] \Rightarrow \sum_{n=1}^{N} \left\{ \begin{matrix} a_{\mathrm{SD}}[n]\mu_{z_0}^2 + 2a_{\mathrm{SD}}[n]\mu_{z_0}\sigma_{z_0} x[n] \\ + a_{\mathrm{SD}}[n]\sigma_{z_0}^2 x^2[n] \end{matrix} \right\} \tag{4.15}$$

$$\Rightarrow \mathcal{N}\left(\sum_{n=1}^{N} a_{\mathrm{SD}}[n]\mu_{z_0}^2, \sum_{n=1}^{N} \left(2a_{\mathrm{SD}}[n]\mu_{z_0}\sigma_{z_0} \right)^2 \right) + H_{z_0}(\mathbf{x})$$

where

$$H_{z_0}(\mathbf{x}) = \sum_{n=1}^{N} a_{\mathrm{SD}}[n]\sigma_{z_0}^2 x^2[n] = \sum_{n=1}^{N} \bar{a}_{\mathrm{SD}}[n] x^2[n] \tag{4.16}$$

and $\bar{a}_{\mathrm{SD}}[n] = a_{\mathrm{SD}}[n]\sigma_{z_0}^2$; $n = \{1, 2, ..., N\}$. In ideal (i.e. free) diffusion-based propagation, the temporal samples taken at $n = \{1, 2, ..., N\}$ time instants are independent and uncorrelated with each other. The chi-square term $H_{z_0}(\mathbf{x})$ has characteristic function expressed as

$$\phi_{H_{z_0}(\mathbf{x})}(\omega) = \prod_{n=1}^{N} \phi_{x^2[n]}\left(\omega \bar{a}_{\mathrm{SD}}[n] \right) \tag{4.17}$$

(see [KAY-93], p. 184) where the characteristic function of any quantity $\tilde{C}$ is $\phi_{\tilde{C}}(\omega) = E\left[\exp(j\omega\tilde{C}) \right]$, the operator $E(\cdot)$ denoting the expected value of the quantity in the parentheses. Therefore, $H_{z_0}(\mathbf{x})$ has the probability density function (pdf) expressed as the inverse Fourier Transform [HAY-02] of its characteristic function [KAY-93] and can be expressed as

$$p_{H_{Z_0}}(h) = \begin{cases} \dfrac{1}{2\pi} \displaystyle\int_{-\infty}^{+\infty} \phi_{H_{z_0}}(\omega) \exp(-j\omega h)\, d\omega & h \geq 0 \\ 0 & h < 0 \end{cases} \tag{4.18}$$

Although $H_{z_0}(\mathbf{x})$ is a sum of squares, as shown in Eq. (4.11), for the binary ASK-modulated CEMC scheme considered in general, $s_1[n] > s_0[n]$, and therefore, it can be implied that $a_{\mathrm{SD}}[n] > 0$, so $\bar{a}_{\mathrm{SD}}[n] > 0$, and $p_{H_{Z_0}}(h) = 0$ for $h < 0$. Since $x^2[n] \sim \chi_1^2$ its characteristic function can be shown as below [KAY-93].

$$\phi_{\chi_1^2}(\omega) = \frac{1}{\sqrt{1 - 2j\omega}}. \tag{4.19}$$

Therefore,

$$\phi_{H_{z_0}(\mathbf{x})}(\omega) = \prod_{n=1}^{N} \phi_{x^2[n]}\left(\omega \bar{a}_{\mathrm{SD}}[n] \right) = \prod_{n=1}^{N} \frac{1}{\sqrt{1 - 2j\omega \bar{a}_{\mathrm{SD}}[n]}} \tag{4.20}$$

where $\bar{a}_{\mathrm{SD}}[n] = a_{\mathrm{SD}}[n]\sigma_{z_0}^2$; $n = \{1, 2, ..., N\}$, and as a result,

$$p_{H_{Z_0}}(h) = \frac{1}{2\pi} \int_{-\infty}^{+\infty} \prod_{n=1}^{N} \frac{1}{\sqrt{1 - 2j\omega \bar{a}_{\mathrm{SD}}[n]}} \exp(-j\omega h)\, d\omega \tag{4.21}$$

The second term in the expression of $T(z)$ in Eq. (4.11) yields

$$\sum_{n=1}^{N} b_{\mathrm{SD}}[n] z[n] \Rightarrow \sum_{n=1}^{N} \left\{ b_{\mathrm{SD}}[n]\mu_{z_0} + b_{\mathrm{SD}}[n]\sigma_{z_0} x[n] \right\} \Rightarrow \mathcal{N}\left(\sum_{n=1}^{N} b_{\mathrm{SD}}[n]\mu_{z_0}, \sum_{n=1}^{N} \left(b_{\mathrm{SD}}[n]\sigma_{z_0} \right)^2 \right). \tag{4.22}$$

As a result, $T(z)$ becomes a sum of two *normal*-distributed random variables, and a weighted sum of N independent χ_1^2 random variables. Therefore, $T(z)$ is a random variable whose pdf can be expressed as

$$T_{Z_0}(z) \sim \mathcal{N}\left(\mu_{\text{Normal}(\mathrm{H}_0)}, \sigma^2_{\text{Normal}(\mathrm{H}_0)} \right) + p_{H_{Z_0}}(h) \underset{\text{Select } \mathrm{H}_0}{\overset{\text{Select } \mathrm{H}_1}{\gtrless}} \gamma \text{ where} \tag{4.23}$$

$$\mu_{\text{Normal}(\mathrm{H}_0)} = \sum_{n=1}^{N} \left\{ a_{\mathrm{SD}}[n]\mu_{z_0}^2 + b_{\mathrm{SD}}[n]\mu_{z_0} \right\}$$

$$\sigma^2_{\text{Normal}(\mathrm{H}_0)} = \sum_{n=1}^{N} \left\{ \left(2a_{\mathrm{SD}}[n]\mu_{z_0}\sigma_{z_0} \right)^2 + \left(b_{\mathrm{SD}}[n]\sigma_{z_0} \right)^2 \right\}.$$

Therefore, the P_{FA} can be expressed as

$$P_{FA} = \int_{\gamma}^{\infty} T_{Z_0}(z) dt_Z \tag{4.24}$$

where t_Z is any value of the $T(z)$ at a specified hypothesis shown in the subscript of $T(z)$.

4.6.2 Probability of Detection (P_D)

Similarly, at H_1, since $z(t) \sim N\left(\mu_{z_1}, \sigma_{z_1}^2\right)$ where $\mu_{z_1} = s_1(t) + \mu_{\mathrm{ISI}}$ and $\sigma_{z_1}^2 = s_1(t)\left(1 - p(t)\right) + \sigma_{\mathrm{ISI}}^2$, by converting $z[n]$ into $x[n] \sim \mathcal{N}(0,1)$, the first term yields

$$\sum_{n=1}^{N} a_{\mathrm{SD}}[n] z^2[n] \Rightarrow \sum_{n=1}^{N} \begin{Bmatrix} a_{\mathrm{SD}}[n]\mu_{z_1}^2 + 2a_{\mathrm{SD}}[n]\mu_{z_1}\sigma_{z_1} x[n] \\ + a_{\mathrm{SD}}[n]\sigma_{z_1}^2 x^2[n] \end{Bmatrix} \Rightarrow \mathcal{N}\left(\sum_{n=1}^{N} a_{\mathrm{SD}}[n]\mu_{z_1}^2, \sum_{n=1}^{N} \left(2a_{\mathrm{SD}}[n]\mu_{z_1}\sigma_{z_1} \right)^2 \right) + H_{z_1}(\mathbf{x}) \tag{4.25}$$

where

$$H_{z_1}(\mathbf{x}) = \sum_{n=1}^{N} a_{\mathrm{SD}}[n]\sigma_{z_1}^2 x^2[n] = \sum_{n=1}^{N} \beta[n] x^2[n] \tag{4.26}$$

and $\beta[n] = a_{\mathrm{SD}}[n]\sigma_{z_1}^2$; $n = \{1, 2, ..., N\}$. As mentioned earlier, the temporal samples taken at $n = \{1, 2, ..., N\}$ are independent and uncorrelated with each other. Likewise, the second term yields

$$\sum_{n=1}^{N} b_{\mathrm{SD}}[n] z[n] \Rightarrow \sum_{n=1}^{N} \left\{ b_{\mathrm{SD}}[n]\mu_{z_1} + b_{\mathrm{SD}}[n]\sigma_{z_1} x[n] \right\} \Rightarrow \mathcal{N}\left(\sum_{n=1}^{N} b_{\mathrm{SD}}[n]\mu_{z_1}, \sum_{n=1}^{N} \left(b_{\mathrm{SD}}[n]\sigma_{z_1} \right)^2 \right) \tag{4.27}$$

As a result, like in H_0, $T(z)$ becomes a sum of two *normal*-distributed random variables, and a weighted sum of *N chi-square* distributed χ_1^2 random variables. Therefore,

$$T_{Z_1}(z) \sim \mathcal{N}\left(\mu_{\text{Normal (H}_1\text{)}}, \sigma^2_{\text{Normal (H}_1\text{)}}\right) + p_{H_{Z_1}}(h) \underset{\text{Select H}_0}{\overset{\text{Select H}_1}{\gtrless}} \gamma \tag{4.28}$$

where

$$\mu_{\text{Normal (H}_1\text{)}} = \sum_{n=1}^{N} \left\{ a_{\text{SD}}[n]\mu_{z_1}^2 + b_{\text{SD}}[n]\mu_{z_1} \right\}, \tag{4.29}$$

$$\sigma^2_{\text{Normal (H}_1\text{)}} = \sum_{n=1}^{N} \left\{ \left(2a_{\text{SD}}[n]\mu_{z_1}\sigma_{z_1}\right)^2 + \left(b_{\text{SD}}[n]\sigma_{z_1}\right)^2 \right\}, \text{ and}$$

$$p_{H_{Z_1}}(h) = \begin{cases} \dfrac{1}{2\pi}\displaystyle\int_{-\infty}^{+\infty} \phi_{H_{z_1}}(\omega)\exp(-j\omega h)\,d\omega & h \geq 0 \\ 0 & h < 0. \end{cases}$$

is the pdf of $H_{z_1}(\mathbf{x})$. Here, $\phi_{H_{z_1}}(h)$ is the characteristic function [KAY-93] of $H_{z_1}(\mathbf{x})$ and can be expressed as

$$\phi_{H_{z_1}}(\omega) = \prod_{n=1}^{N} \frac{1}{\sqrt{1-2j\omega\beta[n]}} \tag{4.30}$$

where $\beta[n] = a_{\text{SD}}[n]\sigma_{z_1}^2$; $n = \{1, 2, ..., N\}$. As a result, this yields

$$p_{H_{Z_1}}(h) = \frac{1}{2\pi}\int_{-\infty}^{+\infty} \prod_{n=1}^{N} \frac{1}{\sqrt{1-2j\omega\beta[n]}} \exp(-j\omega h)\,d\omega \tag{4.31}$$

Therefore, P_{D} can be expressed as the following.

$$P_D = \int_{\gamma}^{\infty} T_{Z_1}(z)dt_Z \tag{4.32}$$

And correspondingly, in a binary system for equiprobable transmitted symbols 1 and 0, the BER can be expressed as

$$\text{BER} = \frac{(1-P_D) + P_{FA}}{2} \tag{4.33}$$

meaning that, for a given P_{FA}, BER decreases as P_{D} increases and vice versa. Therefore, for a given P_{FA}, a higher P_D would be desired, which would ensure a lower BER in the system.

Since individual nanomachines are of extremely limited capabilities and can perform very simple tasks only [AKY-08] [NAK-12], they should be very simple in design. As mentioned earlier, although there exists the possibility of bio-inspired design of the detectors, it is not known yet how the above detection functionality can actually be implemented in the RN, and so there exists open research questions in this area. However,

the exact detection performance derived above can act as an exact reference in order to evaluate the detection performance of the sampling-based binary CEMC receivers.

4.7 Single Sample Detection with Minimum ISI

4.7.1 Approximate ROC

For a large number of samples, it is difficult to determine the exact detection performance analytically in terms of P_{FA} and P_D. This is because $T(z)$ is a sum of a *normal*-distributed random variable and a weighted sum of independent χ_1^2 random variables. However, in the following, assuming $N=1$ sample and that $\mathcal{N}\left(\mu_{\text{ISI}},\sigma_{\text{ISI}}^2\right)=\mathcal{N}\left(1,1\right)$, i.e. minimum level of ISI, we derive the approximate expressions of P_{FA} and P_D under this scenario. Due to the extremely limited capability of an individual nanomachine, it is important to know how single-sample detection would perform in terms of several factors, namely, TN-RN distance, number of samples per symbol, and the number of molecules transmitted for each symbol. The assumption $\mu_{\text{ISI}}=\sigma_{\text{ISI}}^2=1$ allows us to derive a baseline result for the detector when the RN can assume that minimum ISI is present in the system. Such a scenario can be ensured by keeping intersymbol intervals larger than the delay spread [RAP-02] of the CEMC channel such that no or minimum number of the residual molecules are present in the system. From Eqs. (4.15) and (4.16), by analyzing the ratios of the means of the *normal* part and the *chi-square* part in the pdf of $T(z)$ it becomes clear from Eq. (4.34) that the mean and the variance of the normal part is much larger than that of the chi-square part.

$$\begin{aligned}&\text{H}_0\text{: } \mu_{\text{Normal (H}_0\text{)}} \gg \mu_{\text{Chi-square (H}_0\text{)}} \text{ and } \sigma^2_{\text{Normal (H}_0\text{)}} \gg \sigma^2_{\text{Chi-square (H}_0\text{)}} \\ &\text{H}_1\text{: } \mu_{\text{Normal (H}_1\text{)}} \gg \mu_{\text{Chi-square (H}_1\text{)}} \text{ and } \sigma^2_{\text{Normal (H}_1\text{)}} \gg \sigma^2_{\text{Chi-square (H}_1\text{)}}\end{aligned} \tag{4.34}$$

This provides an approximation to the pdf of $T(z)$ such that the effect of the chi-square part on $T(z)$ remains negligible and so the normal part in $T(z)$ may only be considered in order to derive the expressions of P_{FA} and P_D. Therefore, the approximate detection performance of single-sample detector can be found as shown below, where $\mathcal{Q}$ denotes the right-tail probability and can be expressed as $\mathcal{Q}(x_{\mathcal{Q}})=\int_{x_{\mathcal{Q}}}^{\infty}\frac{1}{\sqrt{2\pi}}\exp\left(-\frac{1}{2}q^2\right)dq$ [KAY-93], p. 21.

$$P_D = \mathcal{Q}\left(\mathcal{Q}^{-1}(P_{FA}) \frac{\sigma_{\text{Normal (H}_0\text{)}}}{\sigma_{\text{Normal (H}_1\text{)}}} - \frac{\left(\mu_{\text{Normal (H}_1\text{)}} - \mu_{\text{Normal (H}_0\text{)}}\right)}{\sigma_{\text{Normal (H}_1\text{)}}} \right) \tag{4.35}$$

For $\mathcal{N}\left(\mu_{\text{ISI}}, \sigma^2_{\text{ISI}}\right) = \mathcal{N}\left(1,1\right)$ and $N = 1$, from Eq. (4.11) we can find that $b_{\text{SD}}[n] \approx 0$, which yields the following simplification.

$$\frac{\sigma_{\text{Normal (H}_0\text{)}}}{\sigma_{\text{Normal (H}_1\text{)}}} = \left(\frac{s_0(t)}{s_1(t)}\right)^{3/2} \text{ and } \frac{\left(\mu_{\text{Normal (H}_1\text{)}} - \mu_{\text{Normal (H}_0\text{)}}\right)}{\sigma_{\text{Normal (H}_1\text{)}}} = \frac{1 - \left(\frac{s_0(t)}{s_1(t)}\right)^2}{2\sqrt{\frac{1-p(t)}{s_1(t)}}} \tag{4.36}$$

Therefore, Eqs. (4.5), (4.35) and (4.36) yield the detection performance as shown below

$$P_D = \mathcal{Q}\left(\mathcal{Q}^{-1}(P_{FA}) \left(\frac{s_0(t)}{s_1(t)}\right)^{3/2} - \frac{1 - \left(\frac{s_0(t)}{s_1(t)}\right)^2}{2\sqrt{\frac{1-p(t)}{s_1(t)}}} \right) \tag{4.37}$$

$$\Rightarrow P_D = \mathcal{Q}\left(\mathcal{Q}^{-1}(P_{FA}) \left(\frac{Q_0}{Q_1}\right)^{3/2} - \frac{1 - \left(\frac{Q_0}{Q_1}\right)^2}{2\sqrt{\frac{1-p(t)}{Q_1 p(t)}}} \right)$$

where $s_0(t) = Q_0 p(t)$ and $s_1(t) = Q_1 p(t)$.

As shown in Eq. (4.37), the key factors that affect the detection performance are P_{FA}, *p(t),* and amplitude levels Q_0 and Q_1, i.e. the number of molecules transmitted when the TN wants to send 0 and 1 respectively. The P_D increases when P_{FA} increases and/or *p(t)* increases. However, the dependence of P_D on Q_0 and Q_1 provides the system designer with an option of *transmission-controlled* approach to increase P_D. Therefore, in order to improve the detection performance, we can increase P_{FA} and/or *p(t)* as well as vary (Q_0,Q_1) pair.

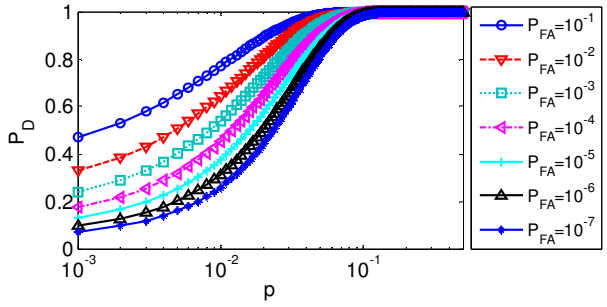

(a) P_D versus p characteristics

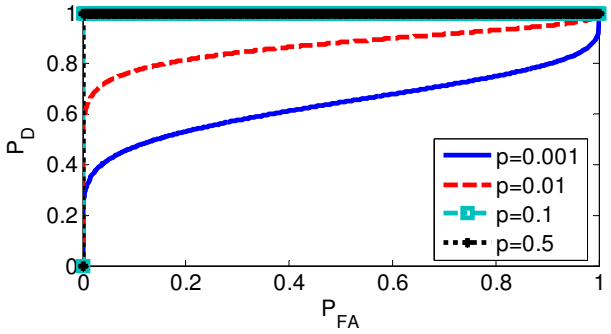

(b) P_D versus P_{FA} characteristics

Figure 4.9 Detection performance of single-sample binary receiver when Q_0 = 500 and Q_1 = 1000 molecules.

4.7.2 Effects of *p(t)*

Since P_D is a function of *p(t)*, it provides an option to choose a suitable *p(t)* for given values of TN-RN distance and time. As shown earlier, *p(t)* is a function of both *r* and *t*. Referring to Figs. 4.1 and 4.9(a), it is wise to choose the single sample when *p(t)* is maximum. For a given P_{FA}, when *p(t)* increases, the argument of $\mathcal{Q}(.)$ function in Eq. (4.37) decreases, and so P_D increases and vice versa. Depending on the choice of *r*, the value of the *p(t)* can be chosen in order to meet the targeted detection probability. Observations on *p(t)* suggest that it is wise to choose the sample at the beginning part of the symbol. As a result, when remaining factors are kept unchanged, the detection performance depends only on *p(t)*, which can be chosen by the CEMC system designer depending on several other system settings, e.g. communication range and sampling rate. Note that when the single sample is chosen from the beginning part of the symbol duration (e.g. as shown in Eq. (4.2), a better

choice would be when the peak of $G_{RN}(t)$ occurs), it can offer better detection performance. In addition, note that as shown in Eq. (4.3), due to the less number of samples and the energy-normalization process, the choice of the $p(t)$ would not be based on the choice of the peak amplitude value of $p(t)$, but rather be based on the peak amplitude value of unnormalized $G_{RN}(t)$. In order to ensure a higher $p(t)$ value, the choice of the temporal sampling instant should be such that it gives a higher value of $G_{RN}(t)$. Note that $G_{RN}(t)$ becomes temporally flat at higher time instants and hence although energy-normalization of $G_{RN}(t)$ may give a higher $p(t)$, it would result in the spreading of the $p(t)$ and so a decrease in P_D.

4.7.3 Effects of (Q_0,Q_1)

In order to investigate the analytical results, in the following we consider three scenarios to check the detection performance of the *single-sample* sampling-based detector, namely, when

- both Q_0 and Q_1 increase, the ratio Q_0/Q_1 remains constant,
- Q_0 is fixed and Q_1 increases, and
- $Q_0 = 0$ and Q_1 increases, i.e. the OOK[11] scheme with different numbers of transmitted molecules.

In each of the three scenarios mentioned above, P_D versus p and P_D versus P_{FA} characteristics are analyzed. As shown in Fig. 4.10, OOK-based detection is independent of P_{FA}, which is desired when $Q_0 = 0$ is plugged into Eq. (4.37), and hence P_D depends on p and Q_1 only. This also implies that the independence on P_{FA} can be achieved by using an OOK-based system.

[11] OOK is a special case of ASK modulation when the TN does not transmit any molecules at all in order to send bit 0, and so the TN remains off [HAY-00].

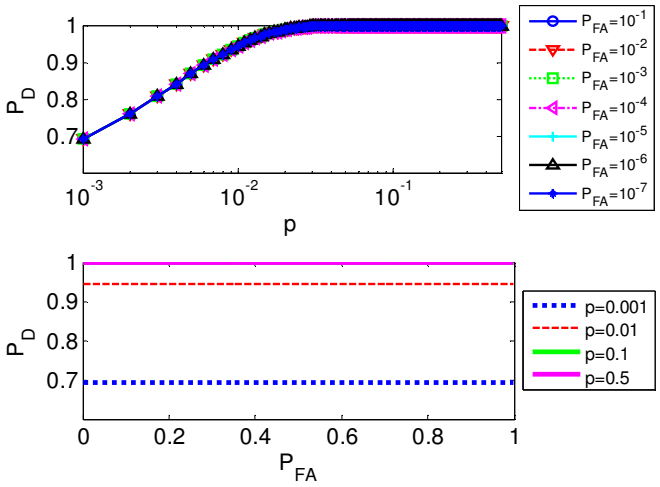

Figure 4.10 Detection performance of an OOK-based detector when $Q_0 = 0$ and $Q_1 = 1000$ molecules are sent to represent bits 0 and 1 respectively.

However, unlike an OOK-based system, in binary ASK system P_D depends on the values of P_{FA}, $p(t)$, and (Q_0,Q_1) pair. Figure 4.11 shows the detection performance in terms of the dependences on P_{FA} and p when the (Q_0,Q_1) pair is kept unchanged. As shown in Fig. 4.11, when the ratio Q_0/Q_1 remains at 1/2, increasing the Q_1 provides higher P_D.

For a set of given values of (p, P_{FA}, Q_0), Fig. 4.12 shows the detection performance when the value of the Q_1 varies. As shown in Fig. 4.12, while all the remaining system parameters are kept unchanged, P_D increases when Q_1 increases. Therefore, the results shown in Figs. 4.11 and 4.12 suggest that the transmitter parameters can be fine-tuned in order to achieve a targeted detection performance in a given scenario of the CEMC system. In the design of a CEMC system, when a preset P_{FA} is provided, the rest of the system design depends on the choices of p and (Q_0,Q_1) pair. As mentioned earlier, in order to achieve a better P_D, p should be chosen at a sampling time instant in the earlier portion of the symbol duration, and the choice of the (Q_0,Q_1) values would further allow the system designer to achieve the P_D of a desired operating point by varying the (Q_0,Q_1) values within the allowable limits of the TN.

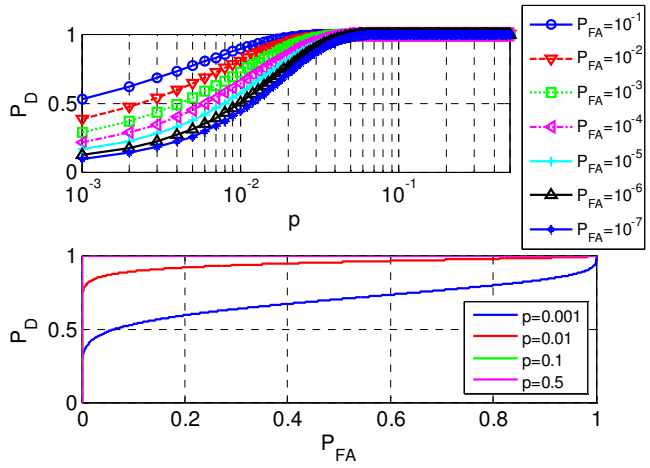

(a) $Q_0 = 1000$, $Q_1 = 2000$ (i.e. $Q_0/Q_1 = 1/2$)

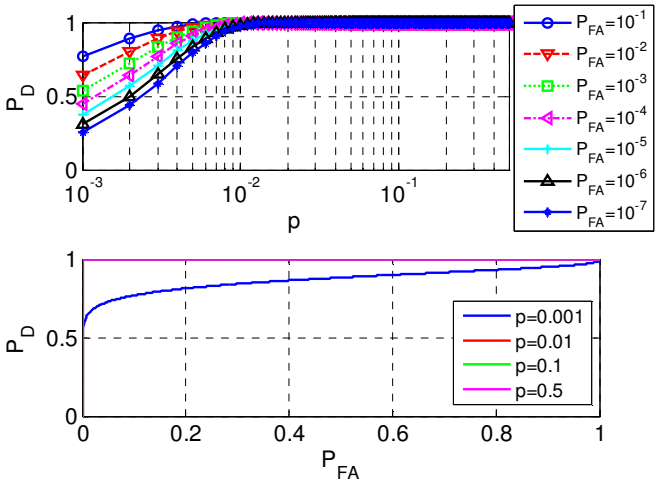

(b) $Q_0 = 5000$, $Q_1 = 10000$ (i.e. $Q_0/Q_1 = 1/2$)

Figure 4.11 Detection performance of binary ASK system (i.e. $s_0(t)$ and $s_1(t)$) when the Q_0/Q_1 ratio remains unchanged at ½.

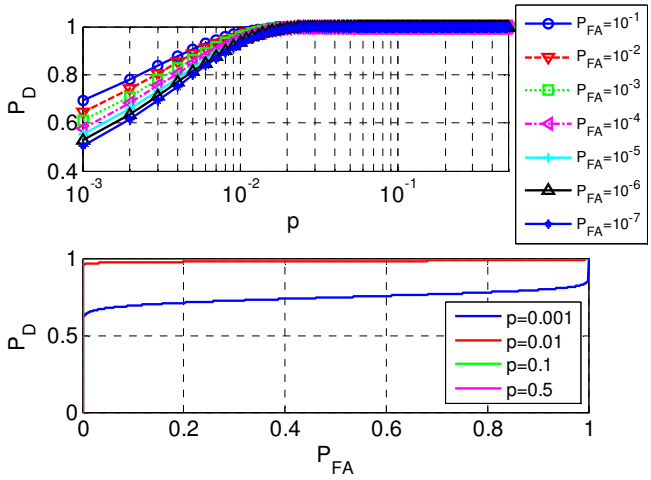

(a) $Q_0 = 500$, $Q_1 = 2000$ (i.e. $Q_0/Q_1 = 1/4$)

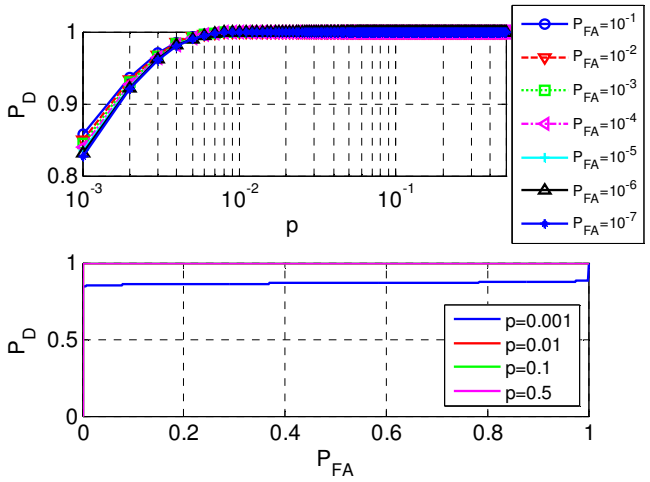

(b) $Q_0 = 500$, $Q_1 = 5000$ (i.e. $Q_0/Q_1 = 1/10$)

Figure 4.12 Detection performance of binary ASK system (i.e. $s_0(t)$ and $s_1(t)$) when the Q_0 is fixed and Q_1 varies.

4.8 Conclusion

A comprehensive analysis of sampling-based optimum receiver architecture of CEMC system has been presented in this chapter. The optimum receiver models of diffusion-based binary and M-ary CEMC systems have been developed and evaluated, first analytically and then numerically to study BER using 100,000 randomly generated bits at each simulation scenario when two key design parameters, namely, number of samples per symbol and communication range vary. The optimum receiver model is also evaluated for three cases depending on the RN's ability to accurately compute the ISI-producing molecules originating from the previous symbols.

With the most accurate computation of the ISI-producing molecules from all the previous symbols (the most complex RN structure), the optimum receiver is found to correctly detect all the symbols in both binary and multilevel (M-ary) transmissions. However, when the computation of the ISI-producing molecules is not accurate (the less complex RN structure), this gives the CEMC system designer options to make a trade off between achievable BER and complexity in RN. In the next chapter, we develop the strength-based (ED) detection model for CEMC.

Chapter 5: Strength-based Optimum Signal Detection in CEMC

5.1 Introduction

While Chapter 4 discussed the sampling-based optimum detection for CEMC systems, this chapter presents a comprehensive analysis of *strength (or energy)-based* detection (ED) for CEMC. The strength-based optimum signal detection problem in diffusion-based CEMC systems has been investigated in detail in the presence of both diffusion noise and ISI. Both ASK- and OOK-modulated CEMC systems have been considered with impulsive transmission scheme. The receiver for optimum signal detection has been developed theoretically and explained with both analytical and simulation results of binary signal detections in ASK and OOK schemes. Results obtained show that the receiver thus developed can detect CEMC symbols effectively; however, the performance is influenced by three main factors, namely, communication range, transmission data rate, and receiver memory. For both ASK and OOK receivers, exact and approximate detection performances have been derived analytically depending on the probabilistic nature of molecular availability and the relationship between mean and variance of signal strengths. Correspondingly, BER performance of the optimum receiver in a single CEMC link is further evaluated under various scenarios through extensive simulation experiments.

In CEMC, the *strength* of signal means the total number of accumulated molecules in the entire symbol duration [MAH-11]. Unlike sampling-based detection [MAH-13], in strength (i.e. energy)-based signal detection [MAH-13b], the RN accumulates the received molecules during the entire symbol interval, produces a test statistic and decides based on its strength compared to a threshold. In CEMC, strength-based detection can equivalently be termed as energy-based detection (ED)[12] [MAH-10b] [MAH-11b]. This is because concentration strength of a symbol is represented as the energy of the symbol in terms of the total number of accumulated molecules during that symbol.

As mentioned previously, due to effects of ISI in ideal (i.e. free) diffusion-based propagation of molecules, optimum signal detection in CEMC is an extremely challenging

[12] We use the term ED to denote strength-based detection in short and the subscript "$_{ED}$" to denote the quantities related to strength-based signal detection in the later sections of this chapter.

problem. In this chapter, we present the optimum detection of CEMC signals from signal strength point of view.

Our results on strength-based optimum signal detection in CEMC presented in this chapter have been published in [MAH-13b] and [MAH-14]. The main contributions of this chapter are the following:

• The generalized optimum ED receiver model has been investigated thoroughly for both ASK- and OOK-based transmission schemes, with and without the effects of ISI. Signal detection models have been presented in detail in order to offer detection capabilities for both ASK- and OOK-modulated CEMC schemes.

• Detection performance of the optimum receiver has been derived theoretically with and without the effects of ISI. For the optimum receiver, the exact and the approximate detection performances have been derived analytically and explained in detail in two realistic scenarios where the optimum receiver can be built and analyzed with some level of approximation.

• The optimum receiver has been built in MATLAB® software by incorporating the effects of ISI-producing molecules at the RN by considering the memory capability of the RN. Correspondingly, BER performance of the optimum receiver thus developed has been presented in detail when communication range, transmission data rate, and receiver memory vary. Based on receiver memory in the form of the number of previously decoded bits that the RN is capable of decoding correctly, three versions of the receiver have been investigated, and the corresponding BER characteristics have been evaluated.

The chapter is organized as follows: Section 5.2 provides the related work, followed by Section 5.3 detailing the strength-based optimum signal detection in CEMC. Section 5.4 presents a comprehensive analysis of the theoretical detection performances for ASK and OOK signal detections in CEMC. Analytical results of the detection performances have been shown in Section 5.5. Simulation results of the BER performance of the optimum and the suboptimum receivers have been presented in Section 5.6. Finally, Section 5.7 concludes the chapter with a summary of the findings.

5.2 Related Work

Strength-based signal detection was first conceptualized in [MAH-10] that first proposed ED technique as a means to determine the effective communication ranges in CEMC between a pair of nanomachines. Later on, the idea of ED scheme was further investigated in [MAH-11b] that provided threshold-based ED schemes in CEMC. Taking into account the effects of stochastic molecule-receptor binding based on chemical Langevin equation [GIL-00], the ED scheme with mean concentration of molecules at the RN was later investigated in terms of performances depending on communication ranges and transmission rates [MAH-12a] as well as variable threshold-based CEMC detection depending on SCK and receiver memory considerations [MAH-13c]. However, the works presented in [MAH-10], [MAH-12a], and [MAH-11b] were based on mean signal intensity only and did not consider diffusion-based noise [MAH-13] at the RN while developing the ED scheme.

The mechanism of energy-based signal detection in MC has also been investigated with communication metric-based approach in [LLA-13], however, without providing any performance evaluation in the form of information/detection theoretical or BER analyses.

A sequence detector-based receiver design for MC has been presented in [KIL-13] that focuses on high data rate MC and reports that sequence detectors can be possible at the expense of high computational complexity at the RN. Though sequence detection methods are widely seen in the traditional high-speed digital wireless communications, there is still inadequate evidence that such sequence detectors would be possible for MC, especially at high rates, given the fact that diffusion-based molecular propagation is an extremely slow process [NAK-11a]. In addition, since nanomachines generally are of extremely low functional capacity [NAK-11a], [NAK-13], p. 2, it is not clear yet in the literature whether nanomachines would be able to implement such computationally intensive sequence detectors. Unlike [KIL-13], our work in this chapter focuses on strength-based scalar symbol detection, and not signal vector detection, for low rate MC systems that are more biologically suitable, e.g. in calcium signaling [SCH-02], liver cells [SCH-93], and endocrine systems [PRA-00].

Apart from these, other related works include finding the optimum threshold-based detection with a prior signal transmission probability and without considering the diffusion

noise as reported in [MEN-12a], and in a noiseless scenario as in [MEN-12a] but from the microscopic perspective with only one molecule transmitted as shown in [MEN-12]. In addition, optimum molecule-shift keying (MoSK) receiver was presented in [SHA-12], where the TN encodes information symbols in different types of information molecules. A signal detection scheme based on multiple amplitude modulation dealing with the diffusion channel from microscopic perspective, where the molecule with drift velocity [KAD-12] is removed from the system once it hits the RN, has been reported in [LIN-12]. The work in [PIE-11] identified the noise in diffusion-based propagation of molecules as *particle-counting noise* and developed the expression of the concentration signal perturbed by the diffusion noise at the location of the RN.

Our work presented in this chapter is different from the works presented in [MEN-12], [MEN-12a], [SHA-12], and [LIN-12] in the sense that we consider the CEMC system from the macroscopic perspective dealing with the *concentration* of a large number of transmitted molecules, all of which are of a single type and the molecules propagate in an unbounded three-dimensional propagation medium. In our system model, none of the molecules is removed from the system upon its first hit at the RN, thereby providing an ideal (i.e. free) diffusion-based propagation environment. In addition, we also consider both diffusion noise and ISI in detail while developing the ED scheme in CEMC.

5.3 Strength-based Optimum Signal Detection Model

As shown in Fig. 2.1, the TN and the RN communicate with a single type of information molecules that bind with a single type of receptors located on the surface of the RN. The system model is as described in Chapter 4 in the case of sampling-based optimum detection in CEMC. In this chapter, we consider two modulation schemes, namely, ASK and OOK, both based upon spike (i.e. impulsive) transmission.

ASK: In the generalized ASK-modulated scheme, the TN emits $Q_m\delta(t)$ information molecules in impulsive fashion at the beginning of each symbol duration T_{sym}, where $m \in \{0,1\}$, $Q_m \gg 1$, and $\delta(t)$ denotes the Dirac delta function [HAY-02]. As a result, in a time-slotted fashion, the TN transmits Q_0 and Q_1 molecules at the beginning of each T_{sym} when it wants to transmit bit 0 and bit 1 respectively. Therefore, $\sum_{j=0}^{N_b} Q_m\delta(t - jT_{\text{sym}})$ represents the

transmitted signal, where $b_j \in \{0,1\}$, $j = \{1,2,\ldots,N_b\}$, is the bit to be transmitted, N_b being the total number of bits in the bit sequence. Hence $\mathbf{b} = [b_0, b_1, b_2, ..., b_{(N_b-1)}]$ denotes the bit sequence transmitted by the TN.

OOK: In the OOK-modulated scheme, in a time-slotted fashion, the TN emits Q_1 molecules at the beginning of each T_{sym} when it wants to transmit bit 1 and no molecules at all when it wants to transmit bit 0. As a result, the TN apparently remains "off" while bit 0 is being transmitted. OOK is a special case of ASK when $Q_0 = 0$.

In the ED scheme, after the RN has sensed the molecules available at its receptors at regular time intervals of t_s seconds, it accumulates all the molecules that become available at the RN during that symbol. As a result, the output variable (i.e. test statistic) of strength-based detection scheme in diffusion noise only can be expressed as below, where N_{samp} denotes the number of samples per symbol.

$$y_{\text{ED}} = \sum_{n=0}^{N_{\text{samp}}} t_s y(nt_s) \Rightarrow y_{\text{ED}} \sim \mathcal{N}\left(s_{\text{ED}}, \sigma^2_{\text{S(ED)}}\right) \text{ where} \tag{5.1}$$

$$s_{\text{ED}} = \sum_{n=0}^{N_{\text{samp}}} t_s s_m(nt_s) \text{ and } \sigma^2_{\text{S (ED)}} = \sum_{n=0}^{N_{\text{samp}}} t_s^2 s_m(nt_s)\left(1 - p(nt_s)\right)$$

Therefore,

$$y_{\text{ED}} = s_{\text{ED}} + n_{\text{ED}}^{\text{Noise}} \quad \text{where } n_{\text{ED}}^{\text{Noise}} \sim \mathcal{N}\left(0, \sigma^2_{\text{S (ED)}}\right) = \sigma_{\text{S (ED)}} \mathcal{N}(0,1) \tag{5.2}$$

In the accumulated molecules during the *i*-th symbol, in addition to the molecules that were intended for the *i*-th symbol only, the RN would also receive some of the molecules that were not intended for the *i*-th symbol. This means some of the molecules that were transmitted during the first to the $(i\text{-}1)^{\text{-th}}$ symbols would become available at the RN during the $i^{\text{-th}}$ symbol, causing ISI to the $i^{\text{-th}}$ symbol. Therefore, the intensity $z(t)$ and the strength z_{ED} of the CEMC signal including the effects of ISI can be written as

$$z(t) = y(t) + n_{\text{ISI}}(t) \quad \Rightarrow \quad z_{\text{ED}} = s_{\text{ED}} + n_{\text{ED}}^{\text{Noise}} + n_{\text{ED}}^{\text{ISI}} \tag{5.3}$$

where $n_{\text{ED}}^{\text{Noise}}$ is as shown in Eq. (5.2) and $n_{\text{ED}}^{\text{ISI}}$ denotes the accumulated number of residual molecules causing ISI. Since the concentration *intensity* [MAH-11] at any time instant *t* is a normal-distributed random variable [MAH-13] and concentration *strength* can be found as the integral of concentration intensity over the symbol duration, $n_{\text{ED}}^{\text{ISI}}$ can also be expressed as a normal-distributed random variable as $n_{\text{ED}}^{\text{ISI}} \sim \mathcal{N}\left(\mu_{\text{ISI (ED)}}, \sigma^2_{\text{ISI (ED)}}\right)$. Figure 5.1 shows the

mean CIR of the molecular channel. Figure 5.2 shows the input signal and υ-th realization $z_\nu(t)$ of the output signal $z(t)$. Therefore, strength-based binary detection problems in ASK- and OOK-modulated CEMC systems can be formally written as below, where hypotheses H_1 and H_0 denote the cases when bits 1 and 0 are to be transmitted respectively.

$$\text{ASK:}\quad z_{\text{ED}} = \begin{cases} \mathcal{N}\left(s_{\text{ED}}^{(1)} + \mu_{\text{ISI (ED)}}, \sigma_{\text{S (ED)}}^{2(1)} + \sigma_{\text{ISI (ED)}}^2\right); & \text{H}_1 \\ \mathcal{N}\left(s_{\text{ED}}^{(0)} + \mu_{\text{ISI (ED)}}, \sigma_{\text{S (ED)}}^{2(0)} + \sigma_{\text{ISI (ED)}}^2\right); & \text{H}_0 \end{cases} \tag{5.4a}$$

$$\text{OOK:}\quad z_{\text{ED}} = \begin{cases} \mathcal{N}\left(s_{\text{ED}}^{(1)} + \mu_{\text{ISI (ED)}}, \sigma_{\text{S (ED)}}^{2(1)} + \sigma_{\text{ISI (ED)}}^2\right); & \text{H}_1 \\ \mathcal{N}\left(\mu_{\text{ISI (ED)}}, \sigma_{\text{ISI (ED)}}^2\right); & \text{H}_0 \end{cases} \tag{5.4b}$$

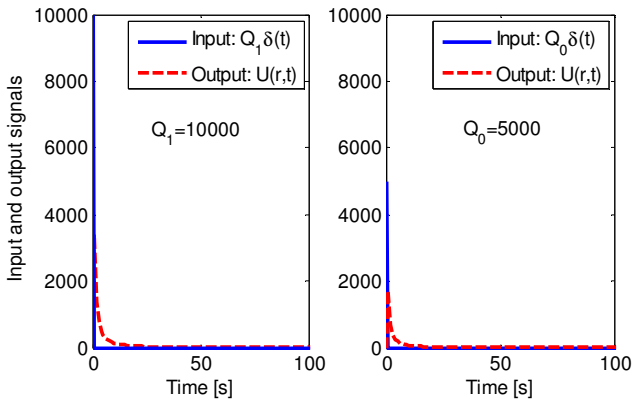

Figure 5.1 Mean concentration signal intensity $U(r,t)$ at r = 10 μm in response to impulse transmissions $Q_1\delta(t)$ and $Q_0\delta(t)$ when bits 1 and 0 are transmitted respectively.

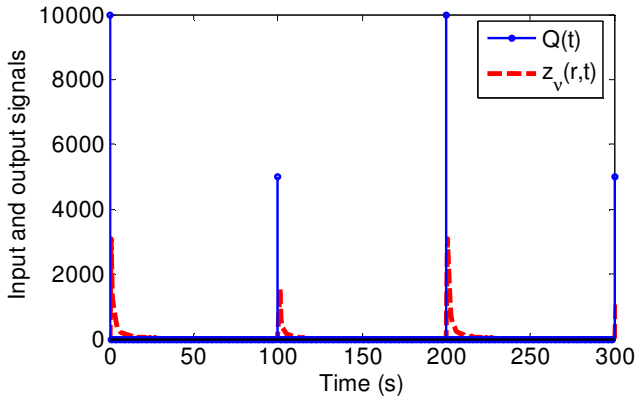

(a) ASK: $Q_1 = \xi Q_0$ when Q_0 = 5000 and ξ = 2 [MAH-13b].

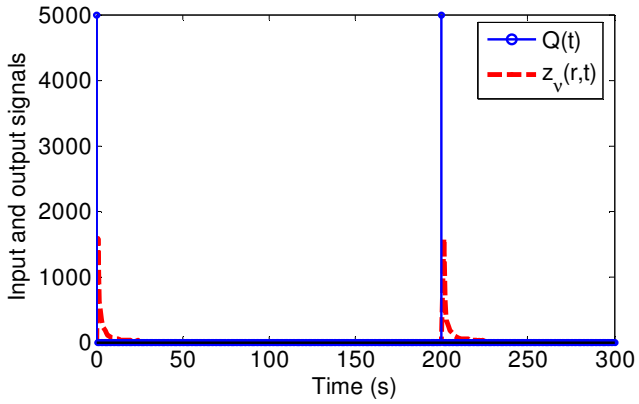

(b) OOK: $Q_1 = 5000$ and $Q_0 = 0$.

Figure 5.2 Input $Q(t)$ and one realization $z_v(t)$ of the output signal at $r = 10$ μm in (a) binary ASK and (b) OOK CEMC systems with diffusion noise and ISI, where $T_{sym} = 100$ s and transmitted bits are {1010…}.

5.4 Strength-based Optimum Receivers

5.4.1 Optimum ASK Receiver Architecture

In this section, the optimum ASK receiver is developed first in subsections 5.4.1–5.4.3, followed by the development of the optimum OOK receiver in subsection 5.4.4. An optimum receiver provides the minimum probability of error in detecting the transmitted bits. Therefore, we consider Neyman-Pearson theorem [KAY-93] and calculate the logarithm of the likelihood ratio under the *minimum probability of error criterion* using equal prior probabilities $\Pr(\mathrm{H}_0) = \Pr(\mathrm{H}_1)$ in order to derive the test statistic $T(z_{\mathrm{ED}})$ as shown below

$$\frac{\ell\left(z_{\mathrm{ED}} \mid \mathrm{H}_1\right)}{\ell\left(z_{\mathrm{ED}} \mid \mathrm{H}_0\right)} > 1 \;\Rightarrow \ln \frac{\ell\left(z_{\mathrm{ED}} \mid \mathrm{H}_1\right)}{\ell\left(z_{\mathrm{ED}} \mid \mathrm{H}_0\right)} > 0 \tag{5.5}$$

where, for ASK system, the conditional probabilities can be expressed as shown below.

$$\ell\left(z_{\mathrm{ED}} \mid \mathrm{H}_1\right) = \frac{1}{\sqrt{2\pi\left(\sigma^{2(1)}_{\mathrm{S\,(ED)}} + \sigma^{2}_{\mathrm{ISI\,(ED)}}\right)}} \exp\left[-\frac{\left\{z_{\mathrm{ED}} - \left(s^{(1)}_{\mathrm{ED}} + \mu_{\mathrm{ISI\,(ED)}}\right)\right\}^2}{2\left(\sigma^{2(1)}_{\mathrm{S\,(ED)}} + \sigma^{2}_{\mathrm{ISI\,(ED)}}\right)}\right] \tag{5.6}$$

$$\ell\left(z_{\mathrm{ED}} \mid \mathrm{H}_0\right) = \frac{1}{\sqrt{2\pi\left(\sigma^{2(0)}_{\mathrm{S\,(ED)}} + \sigma^{2}_{\mathrm{ISI\,(ED)}}\right)}} \exp\left[-\frac{\left\{z_{\mathrm{ED}} - \left(s^{(0)}_{\mathrm{ED}} + \mu_{\mathrm{ISI\,(ED)}}\right)\right\}^2}{2\left(\sigma^{2(0)}_{\mathrm{S\,(ED)}} + \sigma^{2}_{\mathrm{ISI\,(ED)}}\right)}\right]$$

The strength-based detector computes the test statistic $T(z_{\mathrm{ED}})$ at the end of symbol duration after the RN has produced a resultant concentration of all the molecules sensed during that symbol. Therefore, in each symbol the detection processing unit of the RN would generate one observation of $T(z_{\mathrm{ED}})$ and the detection of the symbol would be based on that observation. Combining Eqs. (5.5) and (5.6) and simplifying yields the test statistic for an ASK system as follows.

$$T\left(z_{\mathrm{ED}}\right)=a_{\mathrm{ED}}z_{\mathrm{ED}}^{2}+b_{\mathrm{ED}}z_{\mathrm{ED}}-\gamma_{\mathrm{ED}}\underset{\text{Select H}_0}{\overset{\text{Select H}_1}{\gtrless}}0,\ \text{where} \tag{5.7}$$

$$a_{\mathrm{ED}}=\left\{\frac{1}{2\left(\sigma_{\mathrm{S\,(ED)}}^{2(0)}+\sigma_{\mathrm{ISI\,(ED)}}^{2}\right)}-\frac{1}{2\left(\sigma_{\mathrm{S\,(ED)}}^{2(1)}+\sigma_{\mathrm{ISI\,(ED)}}^{2}\right)}\right\}$$

$$b_{\mathrm{ED}}=\left\{\frac{\left(s_{\mathrm{ED}}^{(1)}+\mu_{\mathrm{ISI\,(ED)}}\right)}{\left(\sigma_{\mathrm{S\,(ED)}}^{2(1)}+\sigma_{\mathrm{ISI\,(ED)}}^{2}\right)}-\frac{\left(s_{\mathrm{ED}}^{(0)}+\mu_{\mathrm{ISI\,(ED)}}\right)}{\left(\sigma_{\mathrm{S\,(ED)}}^{2(0)}+\sigma_{\mathrm{ISI\,(ED)}}^{2}\right)}\right\}$$

$$-\gamma_{\mathrm{ED}}=\left\{\frac{1}{2}\ln\frac{\left(\sigma_{\mathrm{S\,(ED)}}^{2(0)}+\sigma_{\mathrm{ISI\,(ED)}}^{2}\right)}{\left(\sigma_{\mathrm{S\,(ED)}}^{2(1)}+\sigma_{\mathrm{ISI\,(ED)}}^{2}\right)}-\frac{\left(s_{\mathrm{ED}}^{(1)}+\mu_{\mathrm{ISI\,(ED)}}\right)^{2}}{2\left(\sigma_{\mathrm{S\,(ED)}}^{2(1)}+\sigma_{\mathrm{ISI\,(ED)}}^{2}\right)}+\frac{\left(s_{\mathrm{ED}}^{(0)}+\mu_{\mathrm{ISI\,(ED)}}\right)^{2}}{2\left(\sigma_{\mathrm{S\,(ED)}}^{2(0)}+\sigma_{\mathrm{ISI\,(ED)}}^{2}\right)}\right\}$$

As a result, the strength-based optimum receiver can be shown in Fig. 5.3. The main difference between a conventional energy-detector in EM wave-based signals and the strength-based detector in CEMC signals is that in CEMC the numbers of molecules causing diffusion noise and ISI depend on the signal value itself under the specific hypothesis. This makes the strength-based detection of CEMC signals and its receiver implementation challenging. However, the detection models presented in this chapter are able to provide theoretical performance and numerical simulation results that describe the BER performance of the optimum receiver in CEMC as well as the effects of any suitable simplifications that may be possible in the detection signal processing unit of the RN.

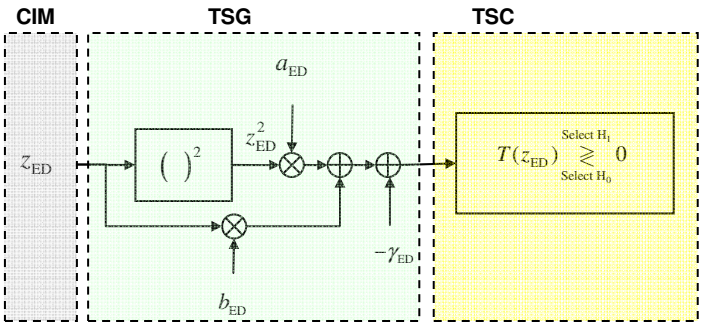

CIM – Concentration Intensity Measurement
TSG – Test Statistic Generator
TSC – Test Statistic Comparator

Figure 5.3 Strength-based optimum receiver architecture in binary CEMC system with diffusion noise and ISI. The selection of the quantities a_{ED}, b_{ED}, and γ_{ED} determines the type of the receiver, i.e. ASK or OOK.

5.4.2 Optimum ASK Receiver (Exact Detection Performance)

In this section, we derive the exact detection performance of the optimum ASK receiver first, followed by its approximate detection performance, which leads to the *suboptimum ASK receiver* in the next section. Dividing both sides of Eq. (5.7) yields the following.

$$\frac{T(z_{ED})}{a_{ED}} = z_{ED}^2 + c_{ED} z_{ED} - \gamma'_{ED} \underset{\text{Select H}_0}{\overset{\text{Select H}_1}{\gtrless}} 0 \tag{5.8}$$

where $c_{ED} = b_{ED}/a_{ED}$ and $\gamma'_{ED} = \gamma_{ED}/a_{ED}$. At H_0, since $z_{ED} \sim \mathcal{N}\left(s_{ED}^{(0)} + \mu_{ISI\,(ED)}, \sigma_{S\,(ED)}^{2(0)} + \sigma_{ISI\,(ED)}^2\right)$, by converting z_{ED} into a standard normal variable $x_{ED} \sim \mathcal{N}(0,1)$, i.e. $z_{ED} = \left(s_{ED}^{(0)} + \mu_{ISI\,(ED)}\right) + \sqrt{\sigma_{S\,(ED)}^{2(0)} + \sigma_{ISI\,(ED)}^2}\,(x_{ED})$, the data dependent terms of $T(z_{ED})/a_{ED}$, as shown in Eq. (5.8), yields the following modified test statistic $T'(z_{ED})$ as shown below.

$$T'(z_{ED}) = z_{ED}^2 + c_{ED} z_{ED} \underset{\text{Select H}_0}{\overset{\text{Select H}_1}{\gtrless}} \gamma'_{ED} \tag{5.9}$$

Plugging the expression of z_{ED} as a function of x_{ED} into Eq. (5.9) and simplifying the results further yields the modified test statistic $T''(z_{ED})$ as shown below.

$$T''(z_{\text{ED}}) = \frac{T'(z_{\text{ED}})}{\sigma^{2(0)}_{\text{S (ED)}} + \sigma^{2}_{\text{ISI (ED)}}} \sim \mathcal{N}\left(\mu_{T'(\text{H}_0)}, \sigma^{2}_{T'(\text{H}_0)}\right) + \chi^2_1 \tag{5.10}$$

$$\text{where } \mu_{T'(\text{H}_0)} = \frac{\left(s^{(0)}_{\text{ED}} + \mu_{\text{ISI (ED)}}\right)\left(s^{(0)}_{\text{ED}} + \mu_{\text{ISI (ED)}} + c_{\text{ED}}\right)}{\left(\sigma^{2(0)}_{\text{S (ED)}} + \sigma^{2}_{\text{ISI (ED)}}\right)}$$

$$\text{and } \sigma^{2}_{T'(\text{H}_0)} = \frac{4\left(s^{(0)}_{\text{ED}} + \mu_{\text{ISI (ED)}}\right)^2 + c^2_{\text{ED}}}{\left(\sigma^{2(0)}_{\text{S (ED)}} + \sigma^{2}_{\text{ISI (ED)}}\right)}$$

Here χ^2_1 is a chi-square distributed random variable with one degree of freedom with mean and variance equal to 1 and 2 respectively [KAY-93]. The expression of $T''(z_{\text{ED}})$ in terms of the data-dependent terms is important because it will show the dominance of the normal distributed part over the chi-square distributed part, as will be shown later.

Similarly, it can be shown that, at H_1, the test statistic can be found as the following.

$$T''(z_{\text{ED}}) = \frac{T'(z_{\text{ED}})}{\sigma^{2(1)}_{\text{S (ED)}} + \sigma^{2}_{\text{ISI (ED)}}} \sim \mathcal{N}\left(\mu_{T'(\text{H}_1)}, \sigma^{2}_{T'(\text{H}_1)}\right) + \chi^2_1 \tag{5.11}$$

$$\text{where } \mu_{T'(\text{H}_1)} = \frac{\left(s^{(1)}_{\text{ED}} + \mu_{\text{ISI (ED)}}\right)\left(s^{(1)}_{\text{ED}} + \mu_{\text{ISI (ED)}} + c_{\text{ED}}\right)}{\left(\sigma^{2(1)}_{\text{S (ED)}} + \sigma^{2}_{\text{ISI (ED)}}\right)}$$

$$\text{and } \sigma^{2}_{T'(\text{H}_1)} = \frac{4\left(s^{(1)}_{\text{ED}} + \mu_{\text{ISI (ED)}}\right)^2 + c^2_{\text{ED}}}{\left(\sigma^{2(1)}_{\text{S (ED)}} + \sigma^{2}_{\text{ISI (ED)}}\right)}.$$

Therefore, by using *Proposition 1* in the Appendix B, see Section B.3, it can be shown that, in Eqs. (5.10) and (5.11), the effects of χ^2_1 on $T''(z_{\text{ED}})$ can be neglected and the test statistic can be simplified as below

$$T''(z_{\text{ED}}) \sim \begin{cases} \mathcal{N}\left(\mu_{T'(\text{H}_0)}, \sigma^{2}_{T'(\text{H}_0)}\right), & \text{H}_0 \\ \mathcal{N}\left(\mu_{T'(\text{H}_1)}, \sigma^{2}_{T'(\text{H}_1)}\right), & \text{H}_1 \end{cases} \tag{5.12}$$

where the quantities are as described earlier. As a result, the probability of false alarm (P_{FA}) can be obtained as follows.

$$P_{\text{FA}} = \Pr\left\{T'(z_{\text{ED}}) > \gamma'_{\text{ED}};\ \text{H}_0\right\} = \Pr\left\{T''(z_{\text{ED}}) > \frac{\gamma'_{\text{ED}}}{\sigma^{2(0)}_{\text{S (ED)}} + \sigma^{2}_{\text{ISI (ED)}}};\ \text{H}_0\right\} \tag{5.13}$$

$$\Rightarrow \gamma'_{\text{ED}} = \left(\mathcal{Q}^{-1}(P_{\text{FA}})\sigma_{T'(\text{H}_0)} + \mu_{T'(\text{H}_0)}\right)\left(\sigma^{2(0)}_{\text{S (ED)}} + \sigma^{2}_{\text{ISI (ED)}}\right)$$

Here $\mathcal{Q}(\bullet)$ denotes the right tail probability that can be expressed as $\mathcal{Q}(\zeta_{\mathcal{Q}}) = \int_{\zeta_{\mathcal{Q}}}^{\infty} \left(1/\sqrt{2\pi}\right)\exp\left(-q^2/2\right)dq$ [KAY-93], p. 21, and $\mathcal{Q}^{-1}(\bullet)$ is the inverse of $\mathcal{Q}(\bullet)$.

Therefore, the exact expression of the probability of detection (P_D) of the optimum ASK receiver can be found as the following.

$$P_D = \Pr\{T'(z_{ED}) > \gamma'_{ED}; H_1\} = \Pr\left\{T''(z_{ED}) > \frac{\gamma'_{ED}}{\sigma^{2(1)}_{S(ED)} + \sigma^2_{ISI(ED)}}; H_1\right\} \tag{5.14}$$
$$= \mathcal{Q}\left(\frac{\mathcal{Q}^{-1}(P_{FA})\sigma_{T''(H_0)} + \mu_{T''(H_0)}}{\sigma_{T''(H_1)}}\left(\frac{\sigma^{2(0)}_{S(ED)} + \sigma^2_{ISI(ED)}}{\sigma^{2(1)}_{S(ED)} + \sigma^2_{ISI(ED)}}\right) - \frac{\mu_{T''(H_1)}}{\sigma_{T''(H_1)}}\right)$$

Signal-dependent means and variances of $T''(z_{ED})$ as shown in Eqs. (5.10) and (5.11) result in the complicated structure of the detection performance of the optimum receiver as shown in Eq. (5.14). Even if the chi-square term χ^2_1 can be ignored in the expression of $T''(z_{ED})$ as shown in Eq. (5.12), regardless of whether the impact of ISI is significant in the system or not, deriving the detection performance from Eq. (5.14) is very difficult and it may not be feasible to derive a simpler structure of the detection performance in this case. Hence effort has been made to simplify the exact detection performance with reasonable approximations as shown next.

5.4.3 Suboptimum ASK Receiver (Scenario 1)

To develop suboptimum receiver, two scenarios have been considered, the first one, *Scenario 1*, being the most general in nature has been shown in this section, and the second one, *Scenario 2*, which can be derived from the first one, is shown in Appendix B. At each temporal instant, the ratio of mean signal intensity to its variance can be expressed as $s(t)/\{s(t)(1-p(t))\} = 1/(1-p(t))$ [MAH-13] where, as mentioned in Section 5.3 and Appendix B, for a receiver that samples the concentration intensity at intervals of t_s s, $p(t)$ varies in the range $0 \le p(t) \le 0.5$, the higher value of $p(t)$ occurring at the shorter communication ranges. Referring to Eqs. (4.1)-(4.5), the quantity $1/(1-p(t))$ varies from ≈ 1 (when $p(t) \to 0$, e.g. at comparatively longer communication ranges or at long temporal instants) to ≈ 2 (when $p(t) \to 0.5$, e.g. at comparatively shorter communication ranges or at earlier temporal instants) [MAH-13]. In the most general form, no assumption is imposed on the value of $p(t)$, i.e. $p(t) \neq 0$ and so the results obtained in this section can be applied to all communication ranges, including long-range CEMC. However, at long communication ranges and/or long temporal instants with $T_{obs} \to \infty$, $p(t) \approx 0$ can also be considered as an

additional assumption that offers possible simplifications in the expression of P_{D}, as shown in Appendix B.4.

Scenario 1

In general, when $\mu_{\mathrm{ISI}} \ll s_{\mathrm{ED}}^{(i)}$, $\sigma_{\mathrm{ISI\,(ED)}}^2 \ll \sigma_{\mathrm{S\,(ED)}}^{2(i)}$, $i \in \{0,1\}$, and from Eq. (5.1) $s_{\mathrm{ED}}^{(1)} = \xi s_{\mathrm{ED}}^{(0)}$ and $\sigma_{\mathrm{S\,(ED)}}^{2(1)} = \xi \sigma_{\mathrm{S\,(ED)}}^{2(0)}$, this results in c_{ED} not exactly equal to zero but $c_{\mathrm{ED}} \approx 0$, and at the same time, $c_{\mathrm{ED}} \ll s_{\mathrm{ED}}^{(i)} + \mu_{\mathrm{ISI\,(ED)}}$, where $i \in \{0,1\}$ denotes the index of hypothesis H_i shown in the subscript. This in turn provides a more general case when the mean and the variance of signal strength at H_0 and H_1 are not approximately equal, i.e. $s_{\mathrm{ED}}^{(0)} \neq \sigma_{\mathrm{S\,(ED)}}^{2(0)}$, $s_{\mathrm{ED}}^{(1)} \neq \sigma_{\mathrm{S\,(ED)}}^{2(1)}$, and $\mu_{\mathrm{ISI\,(ED)}} \neq \sigma_{\mathrm{ISI\,(ED)}}^2$.

Therefore, at H_0, from Eq. (5.10) we get the mean and the variance of the test statistic as the following.

$$\mu_{T^*(\mathrm{H}_0)} = \frac{\left(s_{\mathrm{ED}}^{(0)} + \mu_{\mathrm{ISI\,(ED)}}\right)^2}{\sigma_{\mathrm{S\,(ED)}}^{2(0)} + \sigma_{\mathrm{ISI\,(ED)}}^2} \text{ and } \sigma_{T^*(\mathrm{H}_0)}^2 = \frac{4\left(s_{\mathrm{ED}}^{(0)} + \mu_{\mathrm{ISI\,(ED)}}\right)^2}{\sigma_{\mathrm{S\,(ED)}}^{2(0)} + \sigma_{\mathrm{ISI\,(ED)}}^2} \tag{5.15}$$

Similarly, at H_1, from Eq. (5.11), we get the corresponding quantities as the following.

$$\mu_{T^*(\mathrm{H}_1)} = \frac{\left(s_{\mathrm{ED}}^{(1)} + \mu_{\mathrm{ISI\,(ED)}}\right)^2}{\sigma_{\mathrm{S\,(ED)}}^{2(1)} + \sigma_{\mathrm{ISI\,(ED)}}^2} \text{ and } \sigma_{T^*(\mathrm{H}_1)}^2 = \frac{4\left(s_{\mathrm{ED}}^{(1)} + \mu_{\mathrm{ISI\,(ED)}}\right)^2}{\sigma_{\mathrm{S\,(ED)}}^{2(1)} + \sigma_{\mathrm{ISI\,(ED)}}^2} \tag{5.16}$$

Following a similar procedure as shown in Section 5.4.1, by using Eq. (5.15), the threshold γ'_{ED} can be obtained as follows.

$$\gamma'_{\mathrm{ED}} = 2\mathcal{Q}^{-1}(P_{\mathrm{FA}})\left(s_{\mathrm{ED}}^{(0)} + \mu_{\mathrm{ISI\,(ED)}}\right)\sqrt{\sigma_{\mathrm{S\,(ED)}}^{2(0)} + \sigma_{\mathrm{ISI\,(ED)}}^2} + \left(s_{\mathrm{ED}}^{(0)} + \mu_{\mathrm{ISI\,(ED)}}\right)^2 \tag{5.17}$$

Therefore, using Eqs. (5.16) and (5.17), P_{D} of the suboptimum ASK receiver can be obtained as below.

$$P_{\mathrm{D}} = \mathcal{Q}\left(\frac{\mathcal{Q}^{-1}(P_{\mathrm{FA}})}{\xi^{3/2}}\left(\frac{1+R_\mu^{(0)}}{1+R_\mu^{(1)}}\right)\sqrt{\frac{1+\left(R_\sigma^{(0)}\right)^2}{1+\left(R_\sigma^{(1)}\right)^2}} - \frac{\Lambda^{(0)}}{2}\left\{\frac{\xi^2\left(1+R_\mu^{(1)}\right)^2 - \left(1+R_\mu^{(0)}\right)^2}{\xi^{3/2}\left(1+R_\mu^{(1)}\right)\sqrt{1+\left(R_\sigma^{(1)}\right)^2}}\right\}\right) \tag{5.18}$$

where $\Lambda^{(0)} = \dfrac{s_{\mathrm{ED}}^{(0)}}{\sigma_{\mathrm{S}}^{(0)}}, R_\mu^{(i)} = \dfrac{\mu_{\mathrm{ISI\,(ED)}}}{s_{\mathrm{ED}}^{(i)}}, R_\sigma^{(i)} = \dfrac{\sigma_{\mathrm{ISI\,(ED)}}}{\sigma_{\mathrm{S}}^{(i)}}, i \in \{0,1\}$.

Here, $R_\mu^{(i)}$ and $R_\sigma^{(i)}$ are the *mean strength ratio* and the *standard deviation strength ratio* of ISI-producing molecules to desired signal molecules respectively at a specific hypothesis.

Note that, $\xi\left(R_{\sigma}^{(1)}\right)^2 = \left(R_{\sigma}^{(0)}\right)^2$, and $\xi R_{\mu}^{(1)} = R_{\mu}^{(0)}$. As shown in Eq. (5.18), P_{D} depends on P_{FA}, ξ, $\Lambda^{(0)}$, $R_{\mu}^{(i)}$, and $R_{\sigma}^{(i)}$, where $i \in \{0,1\}$ denotes the index of H_0 and H_1 hypotheses respectively. Keeping P_{FA}, $R_{\mu}^{(i)}$, $R_{\sigma}^{(i)}$, $i \in \{0,1\}$, and $\Lambda^{(0)}$ fixed, when ξ increases, the argument of $\mathcal{Q}(\bullet)$ in the right side of Eq. (5.18) decreases and so P_{D} increases. The effects of increasing the strength factor ξ is shown in Section 5.5.3. An increase in any one or more of P_{FA}, ξ, and $\Lambda^{(0)}$ decreases the argument of $\mathcal{Q}(\bullet)$ in Eq. (5.18), hence increases P_{D}. These three quantities are either related to transmission or detection systems and diffusion-based noise, but not related to ISI-producing molecules.

The quantities $R_{\mu}^{(i)}$ and $R_{\sigma}^{(i)}$ indicate the effects of ISI-producing molecules at the current symbol. Note that $R_{\mu}^{(i)}$ and $R_{\sigma}^{(i)}$ also depend on the mean signal strength and the variance of diffusion-noise respectively, as mentioned earlier in Eq. (5.18). Therefore, expressing the effects of ISI at the current symbol in terms of signal-dependent quantities can be considered as a convenient way to illustrate the effects of ISI by varying the quantities $R_{\mu}^{(i)}$ and $R_{\sigma}^{(i)}$, $i \in \{0,1\}$. As mentioned earlier, signal-dependence of diffusion-noise and ISI makes the CEMC signal detection extremely challenging. Therefore, Eq. (5.18) provides the system designer with a useful expression to study the effects of ISI on P_{D} as well as a means to distinguish the role of ISI from that of diffusion-based noise in the system. For instance, in the absence of ISI, plugging $R_{\mu}^{(i)} = 0$ and $R_{\sigma}^{(i)} = 0$, $i \in \{0,1\}$ in Eq. (5.18) provides the detection performance without the effects of ISI.

5.4.4 Suboptimum OOK Receiver (Scenario 1)

In this subsection, we extend the detection of ASK system to OOK scheme. The derivation of optimum OOK receiver follows a similar procedure shown in Sections 5.4.1-5.4.3. Note that, for an OOK system, considering $s_{\mathrm{ED}}^{(0)} = 0$ and $\sigma_{\mathrm{S\,(ED)}}^{2(0)} = 0$ in Eqs. (5.7)–(5.11) and following a similar procedure as shown in Section 5.4.3 yield the detection performance of the suboptimum OOK receiver in *Scenario 1* as the following.

$$P_{\mathrm{D}} = \mathcal{Q}\left(\mathcal{Q}^{-1}(P_{\mathrm{FA}}) \left(\frac{R_{\mu}^{(1)}}{1+R_{\mu}^{(1)}} \right) \frac{R_{\sigma}^{(1)}}{\sqrt{1+\left(R_{\sigma}^{(1)}\right)^2}} - \frac{\Lambda^{(1)}}{2} \left\{ \frac{1+2R_{\mu}^{(1)}}{\left(1+R_{\mu}^{(1)}\right)\sqrt{1+\left(R_{\sigma}^{(1)}\right)^2}} \right\} \right) \tag{5.19}$$

where $\Lambda^{(1)} = \frac{s_{\mathrm{ED}}^{(1)}}{\sigma_{\mathrm{S(ED)}}^{(1)}}, R_{\mu}^{(1)} = \frac{\mu_{\mathrm{ISI\,(ED)}}}{s_{\mathrm{ED}}^{(1)}}, R_{\sigma}^{(1)} = \frac{\sigma_{\mathrm{ISI\,(ED)}}}{\sigma_{\mathrm{S(ED)}}^{(1)}}$.

The detection performance of the OOK receiver can be explained in a similar way as shown earlier in terms of P_{FA}, $\Lambda^{(1)}$, $R_{\mu}^{(1)}$, and $R_{\sigma}^{(1)}$.

5.5 Analytical Results

In this section, based on Section 5.4 we show the analytical results of the optimum signal detection with the effects of diffusion noise and ISI in CEMC. We describe these analytical results in three main categories: first, we describe the characteristics of the quantities related to signal and ISI in terms of their dependence on *r* over a wide range as shown in Fig. 5.4 in Section 5.5.1. Then we describe the variations of P_{D} at different scenarios as shown in Figs. 5.5 and 5.6 in Sections 5.5.2 and 5.5.3. Finally, we describe the asymptotic detection performance in Section 5.5.4.

Since $\mathrm{P_D}$ is affected by the signal and ISI-related quantities as well as diffusion-noise, for various signal strengths, ISI strengths, and diffusion-noise variances, the achievable P_{D} would change accordingly. For instance, when ISI-producing molecules from one or more of the previous bits become available at the RN, P_{D} decreases. In this relation, we consider two cases, namely, when 1 and 5 previous bits cause ISI at the current bit. Figure 5.4 shows the characteristics of the quantities related to signal and ISI in terms of their dependence on *r* over a wide range. In this section, based on Sections 5.4.1 to 5.4.4 we also show the analytical results of P_{D} of the optimum receivers with the effects of diffusion noise and ISI produced by 1 and 5 previous bits, as shown in Fig. 5.5.

5.5.1 Characteristics of Signal- and ISI-related Quantities

As shown in Fig. 5.4, in short-range and medium range CEMC when $r \leq 10$ μm, Λ remains almost unchanged, while the quantities $R_{\mu}^{(i)}$ and $\left(R_{\sigma}^{(i)}\right)^2$, $i \in \{0,1\}$, remain almost unchanged up to $r \leq 100$ μm. However, when $r > 10$ μm, Λ decreases, and when $r > 100$ μm, both $R_{\mu}^{(i)}$ and $\left(R_{\sigma}^{(i)}\right)^2$, $i \in \{0,1\}$ increase. The quantity Λ represents signal to diffusion noise strength

ratio. The decrease in Λ indicates the severity of diffusion-based noise when r increases. Regardless of mean signal strength and diffusion-noise, the values of $R_{\mu}^{(i)}$ and $\left(R_{\sigma}^{(i)}\right)^2$, $i \in \{0,1\}$ depend on the ISI-producing molecules contributed from the previous symbols. Therefore, in order to see the detection performance, we consider two cases, where the ISI is produced by the residual molecules from the previous 1 and 5 bits. In the latter case, the effect of ISI is large, and so P_{D} provides degraded performance as shown in Fig. 5.5. The increasing trends of $R_{\mu}^{(i)}$ and $\left(R_{\sigma}^{(i)}\right)^2$, $i \in \{0,1\}$, with the increase of communication range denote the fact that the effects of ISI are more severe at longer communication ranges. More importantly, another notable feature is that $R_{\mu}^{(i)} \approx \left(R_{\sigma}^{(i)}\right)^2$, $i \in \{0,1\}$ when $r \leq 100$ μm, which provides us with the possible justification that a simpler version of suboptimum receiver, known as *Scenario 2*, can be made possible and is shown in Appendix B.4. When $r > 100$ μm, it is found that $R_{\mu}^{(i)} > \left(R_{\sigma}^{(i)}\right)^2$, $i \in \{0,1\}$, which can be explained as follows: when $r > 100$ μm, the CIR spreads very much temporally, and so there occur more temporal samples with $p(t) > 0$ when $t \geq T_{\mathrm{sym}}$, and, therefore, when $t \geq T_{\mathrm{sym}}$, the effects of $\mu_{\mathrm{ISI\,(ED)}} > \sigma^2_{\mathrm{ISI\,(ED)}}$ becomes more dominant than that of $s_{\mathrm{ED}} > \sigma^2_{\mathrm{S\,(ED)}}$.

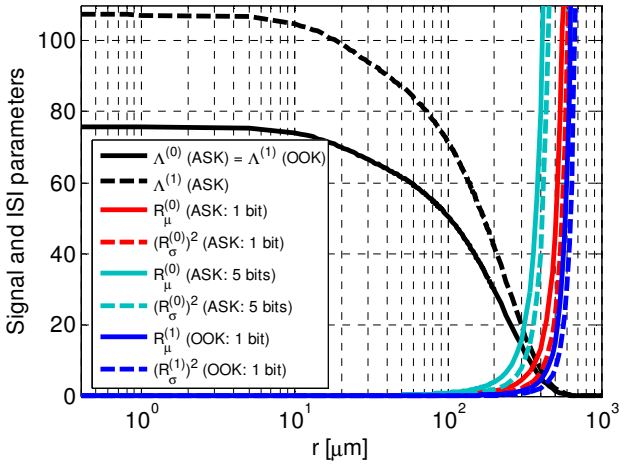

Figure 5.4 Quantities related to and expressing signal and ISI statistics when T_{sym} = 100 s. In the legends of Figs. 5.4 and 5.5, "1 bit" and "5 bits" denote the scenarios when ISI-producing molecules from the previous 1 and 5 bits are considered respectively.

5.5.2 Detection Performance

The detection performances derived in Eqs. (5.18), (5.19), and in Appendix B.4, are very useful in the sense that they offer the versatility of using $R_{\mu}^{(i)}$ and $\left(R_{\sigma}^{(i)}\right)^2$, $i \in \{0,1\}$ in studying the role of ISI in the system, e.g. as shown in Fig. 5.5 plugging $R_{\mu}^{(i)} = 0$ and $R_{\sigma}^{(i)} = 0$, $i \in \{0,1\}$ would provide the detection performance in the ISI-free situation with the effects of diffusion-noise only and plugging any other values of $R_{\mu}^{(i)}$ and $R_{\sigma}^{(i)}$, $i \in \{0,1\}$ would produce the detection performance correspondingly. As shown in Fig. 5.5, in the absence of ISI, P_{FA} does not affect P_{D} in OOK receiver, though it affects the same in ASK receiver, the reason being the fact that the ASK receiver sends Q_0 molecules even when it sends bit 0, causing a non-zero probability of false detection. In the absence of ISI, the OOK receiver provides superior performance to the ASK receiver. Here P_{D} increases as r decreases, meaning that, when r decreases, an improved signal to noise strength ratio provides better detection capabilities in both ISI-free and ISI-affected situations. Figure 5.5(a) shows the detection performance of both ASK and OOK systems in three cases, namely, ISI-free and ISI from previous 1 bit and 5 bits when $P_{\mathrm{FA}} = 10^{-2}$ and 10^{-7}. As shown in Fig. 5.5(a), increased level of ISI produces a decrease in P_{D}.

5.5.3 Role of the Strength Factor

The role that strength factor plays in the detection performance can be shown by varying either or both of ξ and Q_0. However, as shown in Fig. 5.6, in the absence of ISI the detection performance of the ASK receiver can be made even better than the OOK receiver if ξ is increased, e.g. from $\xi = 2$ to $\xi = 4$ or 8 at the TN when the remaining quantities are kept unchanged. For instance, as shown in Fig. 5.6, when r is in the range from 400 μm to 700 μm, using the ASK system with $\xi = 8$ provides higher P_{D} than with the OOK system. Increasing ξ and/or Q_0 can help increase the P_{D} even in presence of ISI; however, the results being straight-forward and similar, the data for the ISI-affected scenario are not shown in this chapter. In addition, note that in Figs. 5.4 to 5.6, the quantities showing the results have been computed when r varies from as short as 400 nm up to as long as 1000 μm and $T_{\mathrm{sym}} = 100$ s. For a different data rate (i.e. a different T_{sym}), the quantities would change correspondingly, and so would the P_{D}.

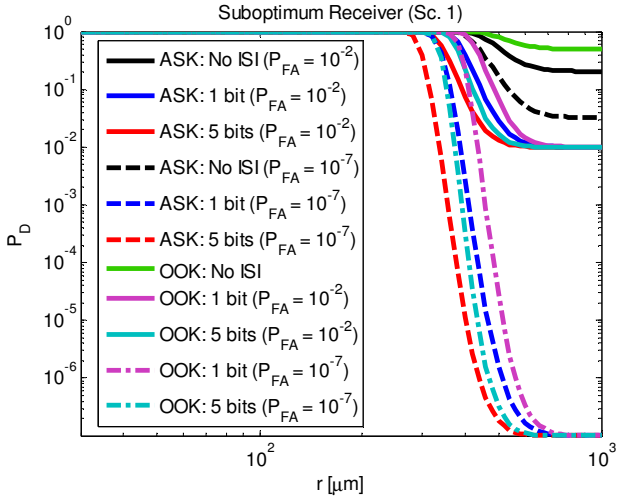

(a) Suboptimum receiver (*Scenario 1*)

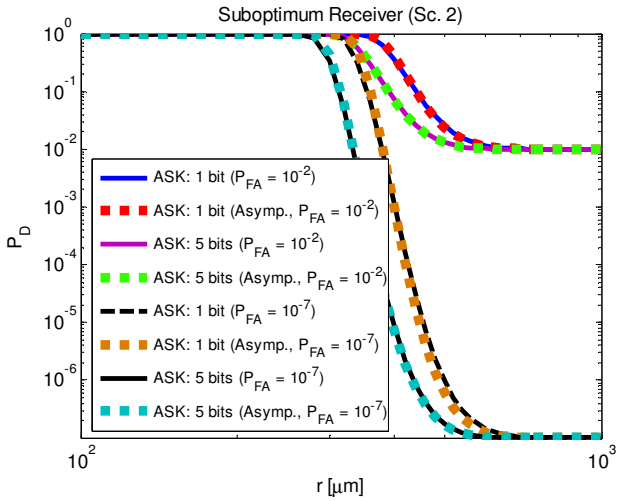

(b) Suboptimum receiver (*Scenario 2*)

Figure 5.5 P_{D} versus r characteristics of the suboptimum receivers: Scenario 1 in (a) and Scenario 2 in (b), in ISI-free and ISI-affected scenarios when f = 0.01 bps (i.e. T_{sym} = 100 s), ξ = 2, and Q_0 = 5000 molecules. ISI is produced by the previous 1 and 5 bits respectively. Note that $\Lambda^{(i)}$, $i = \{0,1\}$, can be computed at each r.

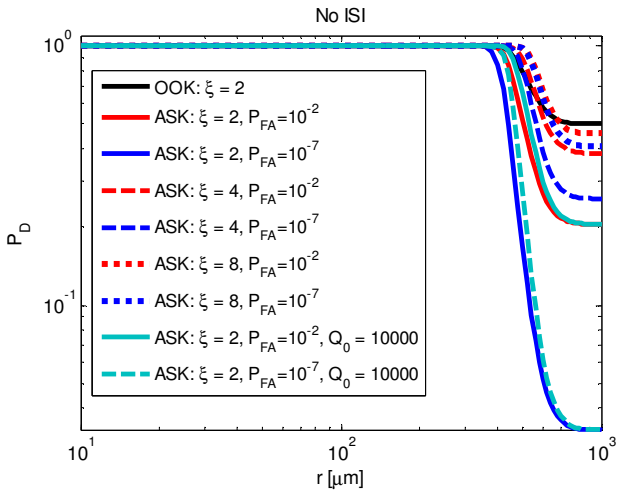

Figure 5.6 Effects of ξ on P_D versus r characteristics when $f = 0.01$ bps (i.e. $T_{sym} = 100$ s), $\xi = 2$, 4, and 8, $Q_0 = 5000$ (not marked in the legend) and $Q_0 = 10000$ (marked in the legend) without the presence of ISI.

5.5.4 Asymptotic Performance

For the ASK system, the asymptotic behavior of the *exact* detection performance of the optimum receiver as shown in Eq. (5.14) is difficult to be found analytically, mainly due to its complicated structure. However, when $r \to 0$, $\mu_{ISI} \to 0$ and $\sigma_{ISI}^2 \to 0$, and as a result, since $s_{ED}^{(1)} = \xi s_{ED}^{(0)}$ and $\sigma_{S(ED)}^{2(1)} = \xi \sigma_{S(ED)}^{2(0)}$, it can be shown from Eq. (5.7) that $b_{ED} \to 0$ and $a_{ED} \to (1-\xi^{-1})/2\sigma_{S(ED)}^{2(0)}$, and therefore, in the limit $r \to 0$, $c_{ED} \to 0$, i.e. $\lim_{r\to 0}[c_{ED}] = 0$, where lim denotes the limit operator. In addition, when $r \to 0$, since both $s_{ED}^{(i)}$ and $\sigma_{S(ED)}^{2(i)}$ are non-zero, this yields $R_\mu^{(i)} \to 0$ and $R_\sigma^{(i)} \to 0$, $i \in \{0,1\}$.

As shown in Fig. 5.4, when $r \to \infty$, because of the diffusion process and the extremely large temporal spreading of the CIR, μ_{ISI} and σ_{ISI}^2 become very large and show asymptotic behavior when $r \to \infty$: $\mu_{ISI} \to \infty$ and $\sigma_{ISI}^2 \to \infty$, and as a result, after plugging the expressions of b_{ED} and a_{ED} from Eq. (5.7) into $c_{ED} = b_{ED}/a_{ED}$ and performing algebraic simplifications, it can be shown that $\lim_{r\to\infty}[c_{ED}] = \lim_{r\to\infty}[(1/a_{ED})/(1/b_{ED})] = 0$. In addition, when $r \to \infty$, both $s_{ED}^{(i)}$ and $\sigma_{S(ED)}^{2(i)}$ tend to zero, and so $R_\mu^{(i)} \to \infty$ and $R_\sigma^{(i)} \to \infty$, $i \in \{0,1\}$.

As a result, both the asymptotic cases, when $r \to 0$ and $r \to \infty$, allow us to show that the optimum receiver shown in Eq. (5.14) actually turns into a suboptimum receiver as shown in Eq. (5.18). Therefore, this also allows us to show the asymptotic detection performance of the suboptimum receiver shown in Eq. (5.18) to explain the same of the optimum receiver shown in Eq. (5.14). Applying these limiting conditions into Eq. (5.18) and Eq. (B.9) and simplifying the algebraic expressions, the asymptotic detection performance for the ASK system in Scenario 1 and Scenario 2 can be obtained as shown in Eq. (5.20).

$$\lim_{r\to 0}\left[P_{\mathrm{D}}\right]=\begin{cases}\mathcal{Q}\left(\dfrac{\mathcal{Q}^{-1}(P_{\mathrm{FA}})}{\xi^{3/2}}-\dfrac{\Lambda^{(0)}}{2}\left\{\dfrac{\xi^{2}-1}{\xi^{3/2}}\right\}\right) & \text{(Sc. 1: ASK)}\\ \mathcal{Q}\left(\dfrac{\mathcal{Q}^{-1}(P_{\mathrm{FA}})}{\xi^{1/2}}-\Lambda^{(0)}\left\{\dfrac{\xi-1}{\xi^{1/2}}\right\}\right) & \text{(Sc. 2: ASK)}\end{cases} \tag{5.20}$$

$$\lim_{r\to \infty}\left[P_{\mathrm{D}}\right]=\begin{cases}P_{\mathrm{FA}} & \text{(Sc. 1: ASK)}\\ P_{\mathrm{FA}} & \text{(Sc. 2: ASK)}\end{cases}$$

By applying a similar approach, the asymptotic performance of the OOK system can also be found. However, the approach being very straight-forward, we have not shown that in this chapter.

Note that, as shown in Eq. (5.20), when $r \to 0$, the asymptotic detection performance is affected a lot by $\Lambda^{(0)}$ and for the range of values of $\Lambda^{(0)}$ as shown in Fig. 5.4, this yields $P_{\mathrm{D}} \to 1$. When $r \to \infty$, in the case of suboptimum receiver, both in Scenario 1 and Scenario 2, see Eq. (5.18) and Eq. (B.9) respectively, since $R_{\mu}^{(i)} \to \infty$ and $R_{\sigma}^{(i)} \to \infty$, i.e. $1/R_{\mu}^{(i)} \to 0$ and $1/R_{\sigma}^{(i)} \to 0$, $i \in \{0,1\}$, after algebraic simplifications, P_{D} becomes independent of $\Lambda^{(0)}$ and equals the chosen value of P_{FA}. Such asymptotic results of P_{D} can be verified as shown in Fig. 5.5 when $r \to 0$ and $r \to \infty$.

As shown in Eqs. (5.7), (5.13), (5.17), and (B.8), the mean and the variance of ISI-producing molecules originating from one or more of the previous bits, as estimated by the RN, can vary based on receiver memory and cause the detection threshold setting vary accordingly [VAN-68]. Therefore, in Figs. 5.5 and 5.6 we particularly focus on the P_{D} versus r characteristics for two P_{FA} settings, where at each r the signal to diffusion noise strength ratio Λ can be computed. And for equiprobable bits transmitted by the TN, when P_{D} and P_{FA} values are found from Eqs. (5.18), (5.19), (B.9) and (B.10), BER can also be expressed as the following.

$$\text{BER} = \frac{(1-P_{\text{D}})+P_{\text{FA}}}{2} \tag{5.21}$$

For a given P_{FA}, BER decreases as P_{D} increases and vice versa. Therefore, keeping P_{FA} unchanged a detector that maximizes P_{D} would be desired. The most noteworthy feature of the detection performances of the optimum ASK and OOK receivers and their suboptimum versions in CEMC as shown in Eqs. (5.14), (5.18), (5.19), (B.9), and (B.10) is that detection performances are affected by signal values themselves, unlike many traditional AWGN-affected communication signals, e.g. see [KAY-93]. Note that the variances of the diffusion noise in both H_1 and H_0 hypotheses are functions of the signal values themselves respectively (see Eq. (4.5)).

Comparing Fig. 5.5(a) with Fig. 5.5(b), the suboptimum receiver in Scenario 2 can effectively follow the similar curves for the same in Scenario 1. This implies, in Scenario 1, when $s_{\text{ED}}^{(0)} \approx \sigma_{\text{S (ED)}}^{2(0)}$, $s_{\text{ED}}^{(1)} \approx \sigma_{\text{S (ED)}}^{2(1)}$, and $\mu_{\text{ISI (ED)}} \approx \sigma_{\text{ISI (ED)}}^{2}$, it turns into the threshold-based receiver as shown in Scenario 2 in Appendix B (see Eqs. (B.8) and (B.9)).

5.6 Simulation Results on Bit Error Rate

5.6.1 Simulation Setup

The purpose of simulation experiments used here is to test the functionality of the strength-based optimum receiver model thus developed at various system settings with sequences of randomly transmitted bits. Based on Eq. (5.7), the optimum and the suboptimum receivers for CEMC system have been implemented in the software platform and tested at several scenarios using simulation experiments.

We explain the optimum receiver in terms of three main factors, namely, communication range (r) and transmission data rate (f), and receiver memory size (M_{RN}). The optimum receivers thus developed have been evaluated by using Monte Carlo simulations with at least 10,000 and up to 100,000 randomly generated bits at each setting of the experiment and BER results are obtained. Information molecules having a diffusion constant of 10^{-6} cm^2/s, i.e. 100 $\mu\text{m}^2/\text{s}$, in water medium has been assumed [ALB-08]. An observation time up to 10,000,000 simulated seconds (≈ 2777 simulated hours) is considered. Communication ranges from 400 nm up to 100 μm [MAH-10b] covering short, medium, and long-range CEMC in water medium are considered with transmission data rates of 0.01

bps up to 0.1 bps [MAH-11c]. In the ASK scheme, TN emits 5000 and 10000 molecules when it wants to send bits 0 or 1 respectively, while in the OOK scheme, it sends 0 and 5000 molecules to send bits 0 and 1 respectively. These are feasible numbers of molecules to be released from a vesicle to generate a spike (impulse) [MOO-13]. Each transmitted bit is tested by using 30 different randomly generated CIR realizations such that the probability that the sample mean of the CIR at the RN at time instant t differs from the true mean by less than one standard deviation is 0.96 [LEO-94]. The output concentration intensity signal is computed numerically by taking time domain convolution of the input transmission rate and the energy-normalized [MAH-13] [MAH-13d] randomly generated CIR of the CEMC channel. A sampling-based receiver [MAH-13] has been considered here that samples the output concentration signal, i.e. senses the occupancy of its receptors, uniformly at intervals of 1 second (s) [MAH-10b] [BER-77]. Based on the concept of an *ideal molecule* monitor [BER-77] [END-08] [MOO-13], we consider the concentration of molecules, i.e. the number of molecules available per unit sensing volume of the RN.

5.6.2 Receiver Configurations

As described in Chapter 4, we consider the same three receiver configurations, namely, the simplest receiver, the RC receiver, and FC receiver, in this chapter. In the *simplest receiver* configuration, since the RN is so simple in its structure that it is not at all able to determine $\mu_{\text{ISI (ED)}}$ and $\sigma^2_{\text{ISI (ED)}}$ in the current symbol. Therefore, referring to Eq. (5.3), it assumes that on average one ISI-producing molecule (with unity variance) is present at the current symbol, i.e. $n_{\text{ED}}^{\text{ISI}} \sim \mathcal{N}\left(\mu_{\text{ISI (ED)}}, \sigma^2_{\text{ISI (ED)}}\right) = \mathcal{N}(1,1)$. Due to the inherent nature of the diffusion process itself, in the ideal case, the molecules can arrive at the RN even after infinite time. In addition, in CEMC, the presence of a large number of molecules in the system makes it very likely that one or more molecules from the previous symbols can be present at the RN. Therefore, we investigate into the simplest receiver configuration where the RN assumes that a minimum level of ISI is present in the system where $n_{\text{ED}}^{\text{ISI}}$ is a normal-distributed random variable with unity mean and unity variance. Note that Eq. (4.6) shows the variance of concentration intensity affected by diffusion-noise.

In this configuration, the receiver is the simplest in terms of functional complexity required to detect the information symbols. This version of the receiver can be considered

useful in view of the extremely limited tasks and capabilities of a nanomachine [AKY-08] such that the RN may not have the ability to compute the ISI-producing molecules at all. With the *simplest* receiver configuration, the RN does not have to estimate the ISI correctly on per symbol basis, nor maintain a memory of the previous symbols, which allows implementing the RN with the simplest receiver circuitry. Therefore, the RN can avoid complicated procedures to estimate ISI correctly, but acknowledges the effects of diffusion-based propagation by assuming that there is one ISI-producing molecule present with unity variance. The *simplest receiver* configuration might be useful when estimating ISI correctly at the RN through complicated signal processing techniques might not be necessary, depending on the communication range of operation, e.g. in short-range CEMC when attenuation and temporal spreading of concentration signal is found minimum at the RN [MAH-10b], or when determining the ISI correctly might not be possible due to the limited capability of the RN itself.

As described previously, the RC receiver configuration computes the mean and the variance of ISI-producing molecules by using a number of previously transmitted symbols that is less than the total number of all previous symbols. To make an in-depth investigation, we assume 9 different settings of the RN based on the complexity of the RN, i.e. how many of the previous symbols would be processed by the RN in order to determine $\mu_{\text{ISI (ED)}}$ and $\sigma^2_{\text{ISI (ED)}}$ at the current symbol. For instance, at the i^{th} symbol, the FC receiver and the RC receiver compute $\mu_{\text{ISI (ED)}}$ and $\sigma^2_{\text{ISI (ED)}}$ by using *all of* $(i-1)$ and $\text{M}_{\text{RN}} < (i-1)$ previously transmitted symbols respectively. When $\text{M}_{\text{RN}} = (i-1)$, the RC receiver turns into the FC receiver. Therefore, in terms of complexity in the RN circuitry, the RC receiver is comparatively simpler than the FC receiver. In this chapter, we extend the functionality of the RC receiver such that in the simulation experiments the RN can determine $\mu_{\text{ISI (ED)}}$ and $\sigma^2_{\text{ISI (ED)}}$ at the current symbol by processing the previous M_{RN} = 1, 2, 5, 10, 20, 40, 60, 80, and 99 symbols.

5.6.3 BER Performance

Despite its simple structure, the simplest receiver configuration has been found to detect the bits in CEMC quite effectively. Fig. 5.7 shows the BER performance of the optimum and

the suboptimum versions of ASK and OOK receivers at various communication ranges and data rates. As shown in Fig. 5.7, the suboptimum version of the receiver performs almost equally well as the optimum receiver. In other words, this means the approximation shown in Section 5.4.3 can be considered as acceptable and thus provides with almost the same performance as the optimum receiver, even though the derivation of the exact detection performance shown in Eq. (5.14) seems quite difficult analytically.

As shown in Fig. 5.7(a), for data rates of 0.01 bps and 0.05 bps, the optimum ASK simplest receiver can detect all the bits correctly (BER = 0) up to 30 μm and 10 μm respectively, and beyond this range the BER increases as r increases, meaning that the higher transmission data rate suffers from higher BER at longer communication ranges. Please note that in this chapter BER = 0 in fact means that the simulation results indicate BER approaching zero in this case. Recall the comments regarding this in chapter 4. At higher data rates, symbol duration becomes shorter and the effect of ISI becomes dominant and hence an increased BER. Since the simplest receiver is not able to estimate the ISI accurately, this increases the BER. For example, when the transmission data rate increases to 0.1 bps, being closer to the TN does not help the RN to recover from the higher BER, and the performance degrades causing approximately 22% of the bits to be detected erroneously when r = 800 nm. The suboptimum ASK receiver has been implemented by plugging c_{ED} = 0 in Eq. (5.7) and thereby after implementing the resulting suboptimum receiver in software, the simulation results of the BER have been shown in Fig. 5.7(a). Results show that the suboptimum receiver is able to provide the BER performance almost the same as that of the optimum receiver. Finally, the comparison between the optimum and the suboptimum RC receivers with 1 and 5 bit memories has also been shown in Fig. 5.7(a). BER results show that the suboptimum RC receiver can perform reasonably well as the optimum receiver. In addition, the RC receiver provides less BER than the simplest receiver, which is because the RC receiver can estimate the ISI molecules with a better accuracy, while the simplest receiver cannot estimate that at all.

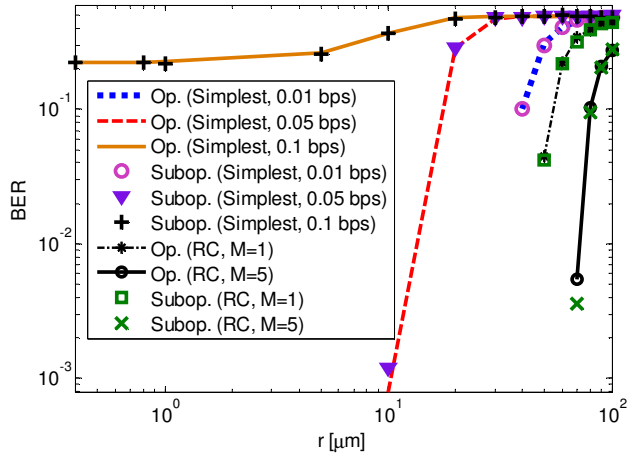

(a) ASK modulation

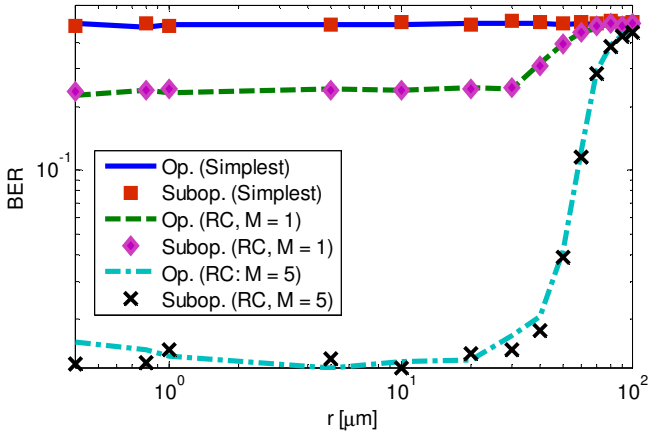

(b) OOK modulation with $f = 0.05$ bps.

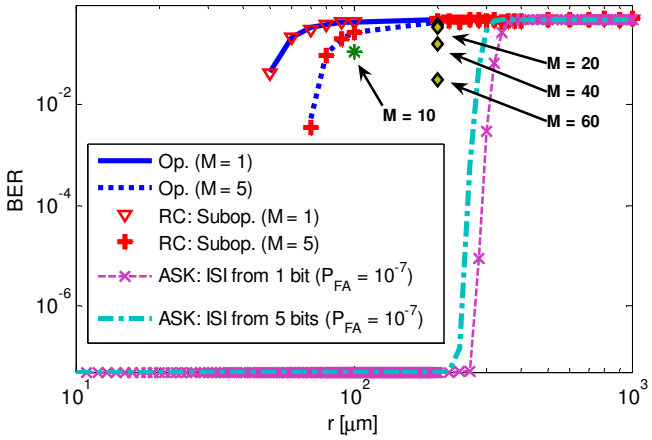

(c) ASK modulation

Figure 5.7 BER Performance of the optimum and suboptimum versions of the *simplest* and the *reduced-complexity* (RC) receivers with (a) ASK modulation and (b) OOK modulation at various communication ranges and data rates, and (c) BER performance at extended communication ranges beyond 100 μm.

Fig. 5.7(b) shows the performances of the optimum and the suboptimum versions of the simplest and the RC receivers based on OOK modulation when f = 0.05 bps. As shown in Fig. 5.7(b), the *simplest* OOK receiver performs worse than the *simplest* ASK receiver shown in Fig. 5.7(a). This is because, in OOK, since the TN sends no molecules at all when it transmits bit 0, the simplest OOK receiver produces bit errors in the detection process, which can be explained from the values of the coefficients a_{ED}, b_{ED}, and γ_{ED} in Eq. (5.7) for OOK and ASK systems when $\mu_{\mathrm{ISI\,(ED)}} = 1$ and $\sigma^2_{\mathrm{ISI\,(ED)}} = 1$. This in turn suggests that the optimum OOK receiver based on the simplest receiver configuration should not be a good choice for CEMC, which necessitates an investigation into the optimum RC and FC receivers with a finite memory size, as shown in Fig. 5.8. In addition, Fig. 5.7(b) also shows that the suboptimum version of the OOK receiver provides reasonably consistent BER results like the optimum OOK receiver, which again suggests that the approximation of the optimum receiver to its suboptimum version is reasonably acceptable.

Finally, Fig. 5.7(c) shows the comparison between the optimum and the suboptimum receivers, as well as these and the theoretical BER performances at $P_{\mathrm{FA}} = 10^{-7}$ when ISI is considered to be produced from the previous 1 and 5 bits. At extended communication

ranges beyond 100 μm, more specifically when 400 μm < r < 1000 μm, the temporal spreading becomes so large that theoretical and simulation results coincide at BER = 0.5, i.e. a random guess. This can be explained from the analytical results as follows: when $r \to \infty$, from Eq. (5.20) $P_D \to P_{FA}$, and as a result from Eq. (5.21) BER → 0.5. When r < 200 μm approximately, the theoretical BER performance depends on the allowed P_{FA} of the detector. For example, when $P_{FA} = 10^{-7}$ and r < 200 μm, as shown from Figs. 5.5(a) and 5.5(b), $P_D \approx 1$, and from Eq. (5.21), BER ≈ $P_{FA}/2$, which can be verified in Fig. 5.7(c).

Regarding the simulation results on BER, for the optimum RC receivers with $M_{RN} = 1$ and $M_{RN} = 5$, BER = 0 is found when r < 50 μm and r < 70 μm respectively, which is consistent with the theoretical results as shown in Fig. 5.7(c). However, when 50 μm ≤ r ≤ 400 μm, the performances of the optimum and the suboptimum receivers compared to the corresponding theoretical results are mainly controlled by the RN's memory size. For instance, when r = 100 μm, an increase in M_{RN} to $M_{RN} = 10$ yields the BER as denoted by the green asterisk (*), and $M_{RN} > 10$ yields BER = 0. Similarly, when r = 200 μm, if M_{RN} increases, BER decreases, as denoted by the diamond marks (♦) in Fig. 5.7(c) for $M_{RN} = 20$, 40, and 60, where for $M_{RN} > 60$, BER = 0 is achieved. Therefore, for 50 μm ≤ r ≤ 400 μm, the simulation results on BER tend to match with the theoretical BER results if M_{RN} increases. This is because when M_{RN} increases, the RC receiver can estimate the ISI quantities $\mu_{ISI(ED)}$ and $\sigma^2_{ISI(ED)}$ reasonably accurately such that when the estimated values of $\mu_{ISI(ED)}$ and $\sigma^2_{ISI(ED)}$ are plugged into Eq. (5.7) in implementing the optimum receiver in software, the RC receiver provides less BER. Therefore, a larger receiver memory yields a close match between the simulation and the theoretical results for 50 μm ≤ r ≤ 400 μm.

In addition, as shown in Fig. 5.7(c), the sharp increase in the theoretical BER when 200 μm ≤ r ≤ 400 μm can be explained as follows: as shown in Fig. 5.4, when 200 μm ≤ r ≤ 400 μm, for the ASK system the quantities $\Lambda^{(i)}$, $i \in \{0,1\}$, decrease sharply, and the quantities $R_\mu^{(i)}$, and $\left(R_\sigma^{(i)}\right)^2$, $i \in \{0,1\}$, increase sharply. When this happens, as shown in Section 5.4.3, a decrease in $\Lambda^{(i)}$, $i \in \{0,1\}$, decreases the P_D and at the same time an increased level of ISI-producing molecules dominates and hence causes a decrease in P_D, which finally yields

BER $\rightarrow$ 0.5 when $r \rightarrow \infty$. Note that the asymptotic performance of P_D when $r \rightarrow \infty$ is shown in Eq. (5.20).

As shown in Fig. 5.8, with the RC receiver, more reliable CEMC can be achieved for the OOK system at the cost of larger memory size at the RN. For example, when a bit sequence of length 100 is transmitted, M_{RN} = 99 would indicate the FC receiver configuration when all the previous bits would be considered while determining the ISI statistics at the current symbol. As a result, this yields zero BER. The effect of memory size of the receiver on the performance of optimum RC receiver has been shown in Fig. 5.8 in terms of the quantity $r_{BER=0}$ that indicates the *communication range up to which zero BER can be obtained* for given memory size and transmission data rate. Thus, Fig. 5.8 shows how the performance of an RC receiver can be obtained by using a larger memory size when compared to the simplest receiver.

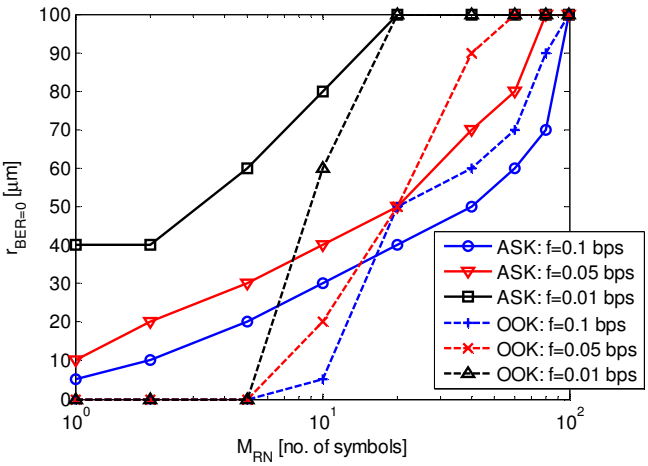

Figure 5.8 Performance of the optimum RC receiver in terms of $r_{BER=0}$ at various receiver memory sizes and transmission data rates.

It is observed that with smaller memory size M_{RN} < 20, ASK system provides better BER performance than the OOK scheme, while the opposite is true when M_{RN} > 20. The crossover point in memory size is important because it shows that, at a given transmission data rate, the performances of the ASK and the OOK schemes change. In OOK system, at M_{RN} < 20, some of the bits get detected erroneously when both the current bit and all the M_{RN} previous bits are 0s, thereby the optimum receiver finds $\mu_{ISI\,(ED)} = 0$ and $\sigma^2_{ISI\,(ED)} = 0$. When this happens, given $s^{(0)}_{ED} = 0$ and $\sigma^{2(0)}_{S\,(ED)} = 0$ in the case of OOK, in order to avoid

divide-by zero problem in Eq. (5.7), the optimum receiver thus implemented switches from the RC receiver to the simplest receiver and hence results in an increased probability of erroneous detection of the current bit. Such a degraded performance in OOK can be overcome by increasing M_{RN}, because it makes it more unlikely for all the M_{RN} previous bits to be 0s at the same time.

Finally, the FC receiver can detect all the transmitted bits correctly over a wide communication range from 400 nm up to 100 μm when the transmission data rate varies from 0.01 bps up to 0.1 bps. Completely error-free communication using the FC receiver can be attributed to the fact that RN now determines the ISI statistics using all of the previously transmitted bits.

Note that the RC and the FC receivers assume that the RN can detect the previous M_{RN} bits correctly and, based on that, computes the ISI statistics at the current symbol and then applies them to the detection signal processing unit of the optimum and the suboptimum receivers. Such a scenario is important because it provides the most achievable detection performances of the optimum and the suboptimum receivers when M_{RN} varies. In more realistic scenarios, when one or more of the previously transmitted bits are detected incorrectly, it would impact the ISI statistics computed by the RN and so the BER performance of the system. However, we have not considered this in this chapter.

Apart from this, since the receiver is based upon statistically independent, uncorrelated samples of the concentration signal intensity, the effect of sampling time t_s on the BER performance of the optimum receiver is worth investigating. Figures 5.9(a) and 5.9(b) show the BER performances achieved by the optimum simplest receiver and the optimum RC receiver with $M_{RN} = 1$ respectively. Due to the very nature of the diffusion process itself, the CIR peaks at the RN at some time and decays gradually over time. When t_s increases, the RN samples the concentration intensity at longer temporal intervals. Since the CIR at a given r and time t is normalized to the total energy, i.e. the total number of molecules received during the entire observation time [MAH-13] [MAH-13d], when t_s increases, the relative amplitudes of the normalized CIR at temporal sampling instants increase in magnitude. This spreads the CIR and hence the RN senses more ISI. As a result, when $t_s > 1$ s, this produces higher BER to both ASK and OOK systems than that when $t_s = 1$ s. In this chapter, to ensure statistically independent, uncorrelated concentration samples, we have

considered $t_s \geq 1$ s at the RN [BER-77] [END-08]. When t_s remains unchanged, the performance of the optimum RC receiver with $M_{RN} = 1$ is better than the optimum simplest receiver because the RC receiver can make a better estimate of the ISI in the system. Note that sampling intervals of $t_s = 1$ s has been considered all through this chapter except for Fig. 5.9 where, in addition to $t_s = 1$ s, $t_s = 2$ s, 5 s, 10 s, 20 s, and 50 s have also been investigated.

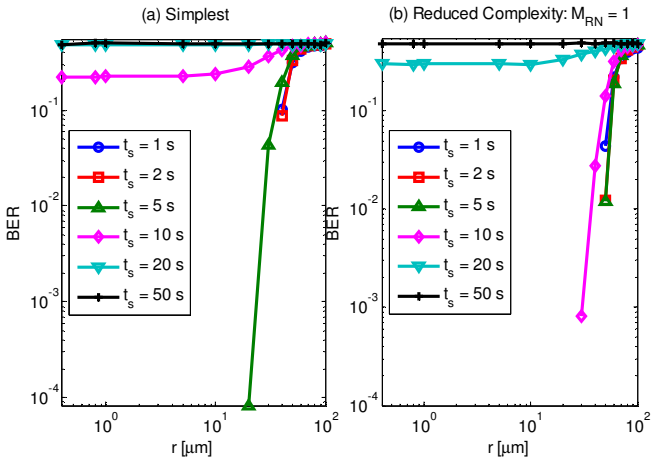

Figure 5.9 Effects of sampling time on BER with the optimum simplest receiver in (a) and the optimum RC receiver with $M_{RN} = 1$ in (b) when $f = 0.01$ bps.

5.7 Conclusion

In this chapter, we have presented detailed theoretical formulations and architectures of the strength-based optimum receivers based on spike transmission of molecules. Expressions of detection probability of the suboptimum receivers have been derived analytically and explained in detail. The optimum and suboptimum versions of ASK and OOK receivers have also been implemented in software and their BER performances, based on three receiver configurations (the simplest, RC, and FC), have been evaluated through simulation experiments. Although this chapter has mainly focussed on spike (or impulse)-based modulation in binary CEMC, the receiver model developed in this chapter can be applied to detect multi-level (M-ary) and pulse amplitude modulated (PAM) CEMC signaling by properly modifying the signal processing blocks of the optimum receiver. In the next chapter, we present the results of the CEMC receiver based on the stochastic nature of the chemical reactions between information molecules and receptors.

Chapter 6: Strength-based Optimum Receiver with Stochastic Chemical Kinetics

6.1 Introduction

In this chapter, a strength-based optimum signal detection scheme, based on stochastic chemical kinetics (SCK), for binary CEMC system has been presented. We consider a pair of nanomachines communicating by means of OOK transmission protocol in a three-dimensional ideal (i.e. free) diffusion-based unbounded propagation environment. First, based on SCK of the reaction events between information molecules and receptors, we develop a mathematical receiver model of strength-based detection scheme for OOK CEMC system. Using an analytical approach, we explain the ROC curves of the receiver thus developed. Finally, we propose a *variable threshold* (VT)-based detection scheme and explain its communication range and rate dependent characteristics. We show that it provides an improvement in the communication ranges compared to *fixed threshold* (FT)-based detection scheme.

While Chapters 4 and 5 described optimum signal detection based on sampling-based and strength-based approaches respectively, this chapter investigates into the optimum receiver based on the interactions between the information molecules and the receptors in the form of SCK. In this chapter, in order to present the SCK-based optimum receiver for CEMC, we consider a pulse-transmitted CEMC system with OOK modulation. Pulse-transmitted OOK modulation is widely used in biochemical receptor systems due to its simplicity and suitability [KRI-02] [ROS-04] [ROS-00].

Detection schemes presented in Chapters 4 and 5 did not consider the interactions between the information molecules and the receptors, as explained by the SCK. The strength-based detection model presented in Chapter 5 is different from the one presented in this chapter in that the former considers diffusion-based noise and ISI only in developing the receiver, without considering the effects of the interactions between the information molecules and the receptors that this chapter has investigated.

Our results on the strength-based optimum signal detection based on SCK in CEMC presented in this chapter have been published in [MAH-12a] and [MAH-13c]. The main contributions of this chapter are the following:

• First, based on SCK of the reaction events between information molecules and receptors, a detailed mathematical model of the strength-based optimum detection scheme for pulse-transmitted OOK-based CEMC system has been developed and analyzed.

• Second, a new VT-based detection scheme has been proposed, which incorporates the ISI-causing molecular concentrations from the previously transmitted symbols in each symbol duration. The possible advantage of increasing the effective communication ranges by using the proposed VT-based detection scheme has been explained.

The remainder of this chapter is organized as follows: Section 6.2 presents the related work. Section 6.3 discusses the strength-based optimum detection based on SCK and presents a detailed mathematical model of the strength-based optimum receiver based on such stochastic molecule-receptor binding. Section 6.4 explains the detection characteristics of the receiver thus developed in the form of ROC curves. A VT-based signal detection scheme is introduced in Section 6.5. Section 6.6 discusses the feasibility and design of VT-based signal detector in CEMC. Finally, Section 6.7 concludes the chapter with a summary of the findings and possible future research directions.

6.2 Related Work

Development of a CEMC receiver based on SCK was first conceptualized in [MAH-12a]. However, the work reported in [MAH-12a] did not consider the mean values of the normal and chi-square parts of the test statistic. The work reported in [MAH-13c] provides a complete analysis and the development of the strength-based receiver architecture based on SCK in two scenarios, depending on whether the chi-square part of the test statistic is included or neglected, and in the following cases: a) when the variance of the normal part of the test statistic is comparatively larger than that of the chi-square part, b) when the number of observations is much larger than or equal to unity, and c) when the mean values of the normal and chi-square parts are taken into consideration.

In [PIE-11b], reception noise characteristics at the input of the receiver has been investigated from the viewpoints of ligand-reception binding based on ligand-receptor kinetics and stochastic chemical kinetics, where the authors developed both physical and statistical models of the reception noise at the input of the receiver and derived expressions of the variance of the received signal perturbed with reception noise. In our research, we

consider SCK [GIL-00] and have developed an optimum receiver that considers the SCK, separates the noise and the interference components of the received signal part at the RN, and thereby detects the transmitted symbols with the proposed detection schemes.

In [NOE-13], an active enzyme-based technique has been shown where the enzymes deactivate the effects of ISI-producing molecules and thus the destructive effects of ISI are reduced. The enzymes introduced in the system facilitate eliminating the long tail of diffused molecular concentration at the receiver. The particle-based technique adopted there assumes all particle locations to be known, which may not be feasible in a real case [SHA-13]. The work in [NOE-13] is on particle-based approach and is different from ours presented in this chapter in the sense that, among other contributions, in order to model the random interactions between the information molecules and the receptors, we base our approach on SCK [GIL-00] [GIL-07] and have developed a VT-based detector scheme for the OOK CEMC system to decode the transmitted symbols at the receiver side.

In [PIE-11], diffusion noise has been explained as "particle counting noise" in the way by considering the effects of random movements of the molecules in the diffusion process. Based on non-homogeneous Poisson process, the work in [PIE-11] presented a stochastic model of diffusion-based propagation and developed the expression of root mean square (RMS) signal corrupted with diffusion noise at the location of the RN. Our work in this chapter is different from the work in [PIE-11] in the sense that we develop an optimum signal detector by considering the interactions between information molecules and the receptors stemming from SCK and provide separate signal and noise models based on the probabilistic treatment of the number of chemical reactions that take place between the information molecules and receptors. In general, we have explained the performance of the detector thus developed by considering the randomness in molecule-receptor binding based on SCK without the presence of diffusion noise (i.e. by considering mean concentration signal only). However, we have also pointed out how the detector architecture can be modified in order to incorporate the diffusion noise at the location of the RN.

6.3 Optimum Receiver with Stochastic Chemical Kinetics

6.3.1 System Model Overview

The basic system model considered in this chapter is the same as the one considered in Chapters 4 and 5. However, in addition, based on SCK we consider the interactions between information molecules and the receptors in this chapter. As shown in Fig. 2.1, the size of the VRV is sufficiently small [ATA-10] such that it can surround the RN to exactly follow the stochastic chemical reactions between the information molecules and the receptors based on SCK [GIL-00]. There are a finite number of receptors on the surface of the RN. In the ideal diffusion process, some of the transmitted molecules become available at the RN and collide with the receptor sites of the RN, and when this happens, the colliding molecule and the receptor react with each other producing a chemical reaction between them. Each collision between a molecule and a receptor triggers a chemical reaction [ATA-10]. Each chemical reaction is an instantaneous physical event [GIL-07] and produces an infinitesimally small electrochemical pulse in order to deliver information through molecules [ATA-10]. A set of such chemical reactions are required in order for the RN to perceive the biologically meaningful information in the form of action potentials [ATA-10]. The receptors react with the information molecules according to *propensity function* [GIL-00] [ATA-10], which can also be thought of as probabilistic *molecule−receptor binding process* (MRBP) that depends on the affinity of information molecules to the receptors. The RN senses the concentration signal strength [MAH-11] with its receptors and thus decodes the information symbol based on MRBP by incorporating the effects of the SCK [GIL-00]. The molecule that has already hit and collided with the receptor is not removed from the system, meaning that the molecule continues its free diffusion in the propagation medium [ATA-10] and, therefore, can contribute to the ISI-producing molecules in the detection of the succeeding symbols.

Two ways to characterize the temporal evolution of the molecular species population are *classical chemical kinetics* (CCK) and SCK. In CCK, the evolution is assumed to be continuous and deterministic [GIL-07] [ATA-10], which is not true because the population of molecular species in a chemically reacting system evolves stochastically as an integer variable [GIL-07]. In CCK, the evolution of chemical species is explained by a set of coupled ordinary differential equations known as *reaction rate equations* (RRE) [GIL-07].

SCK is the study of the temporal evolution of the "well stirred" chemically reacting systems where the populations of chemical species evolve because of the chemical reactions taking place within the system [GIL-07]. In SCK, the time evolution of the chemical species populations is explained on the basis of random-walk process and characterized by a single differential equation known as the *chemical master equation* (CME) [GIL-07]. CME explains the populations of the chemical species that take part in chemical reactions. In a chemically reacting system, tracking the positions and the velocities of all the molecules over time, and therefore, changing the populations of the chemical species when a chemical reaction occurs would provide the most accurate results of the temporal evolution of the chemical species populations. Hence, the chemically reacting system would not evolve deterministically with the molecular species populations only, unless the positions and the velocities of all the molecules are known correctly [GIL-07]. Since it is not always possible to have the information of the positions and the velocities of all the molecules in the system, as a result, the system shows stochastic behavior and the number of reactions taking place between molecules and receptors during a time interval becomes a random variable [ATA-10]. In this chapter, our objective is to describe the statistics of the number of reactions that take place between the molecules and the receptors during a symbol duration, and develop a strength-based optimum signal detection model, as shown in the next subsections.

6.3.2 Symbol-wise Probabilities Based on Single Pulse Transmission

The performance of a single pulse transmission in an ideal diffusion-based CEMC channel has been shown in Fig. 6.1. Since this chapter has focused on pulse-transmitted OOK scheme, it is important that the characteristics of a single pulse transmission are understood in detail first before explaining the performance of a random sequence of bits transmission. In addition, the signal and the noise models of the strength-based detection presented in this chapter are based on the single pulse transmission, as shown later. For instance, when a pulse of molecules are sent in the water medium, the concentration profile at different TN-RN distances are shown in Fig. 6.1(a), which shows clearly that the desired mean signal strength (in number of molecules) during the pulse interval reduces when TN and RN are comparatively far apart. This also means that, in cases when RN is far apart from the TN, the level of ISI caused by the residual molecules would be higher than that when RN is

located close to TN. The residual molecules that originated in previous symbol durations but become available at the current symbol duration cause ISI in the symbol detection process.

We express the *desired* and the *undesired (interference)* signals by the symbol-wise probabilities. For the single pulse transmission, the symbol-wise probabilities s_{SCK} and $n_{\mathrm{SCK},j}$, where j is a positive integer, at a particular symbol duration, are defined as the fraction of the total number of molecules available at the RN for reception on average in the corresponding symbol duration and can be expressed as Eq. (6.1). This means, at a particular symbol transmission, the symbol-wise probability would be the ratio of the average number of molecules available at the RN during that particular symbol duration to the average number of molecules available at the RN during the entire observation time.

$$s_{\mathrm{SCK}} = \frac{\int_{0}^{T_b} U(r,t)\,dt}{\int_{0}^{T_{obs}} U(r,t)\,dt} \text{ and } n_{\mathrm{SCK},j} = \frac{\int_{jT_b,\, j\neq 0}^{(j+1)T_b} U(r,t)\,dt}{\int_{0}^{T_{obs}} U(r,t)\,dt} \tag{6.1}$$

For example, in Fig. 6.1(a) at r = 100 μm (i.e. the magenta dot-dashed line) s_{SCK} and $n_{\mathrm{SCK},j}$ (j = 1, 2,…, $N_b - 1$), where N_b is the total number of bits to be transmitted, indicate the fractions of the available mean number of molecules during the intervals (0–100 s), (100–200 s), (200–300 s), and, so on, respectively, when the bit duration T_b = 100 seconds, meaning that $s_{\mathrm{SCK}} + \sum_{j=1,\, j\neq 0}^{N_b-1} n_{\mathrm{SCK},j} = 1$ would represent the sum of the symbol-wise probabilities during the entire observation time from t = 0 to $t = T_{obs}$ seconds. Similarly, considering other values of T_b, the desired signal strength and ISI can be calculated. The signal and the noise models of the system constituted on the basis of symbol-wise probabilities s_{SCK} and $n_{\mathrm{SCK},j}$ (j = 1,2,… $N_b - 1$) for a given T_b are shown later in this chapter.

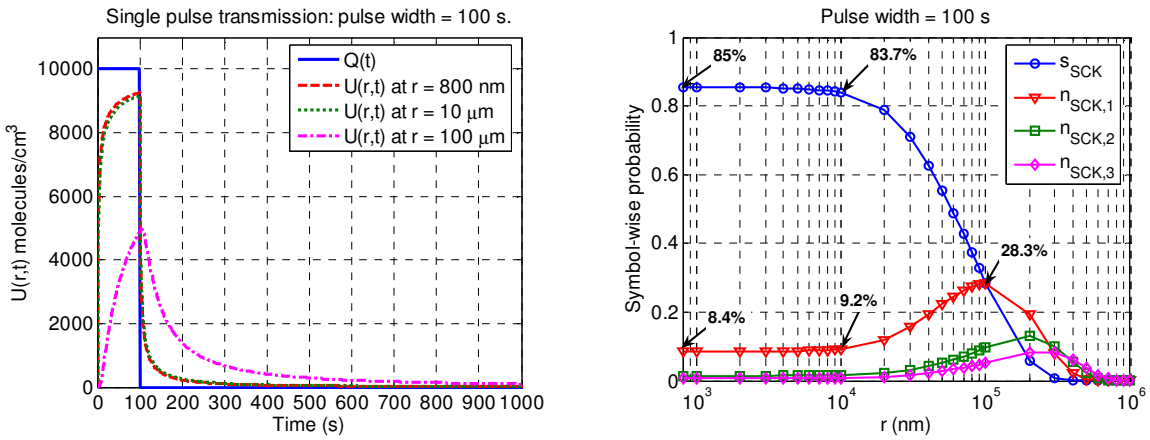

(a) (b)

Figure 6.1 (a) Available concentration of molecules at the RN in the water medium in response to single pulse transmission of pulse width $T_b = 100$ s. (b) The first four symbol-wise probabilities s_{SCK} and $n_{\text{SCK},j}$, $j = \{1, 2, 3\}$, when $T_b = 100$ seconds, and r varies, in water medium.

As shown, Fig. 6.1(a) displays the effects of TN-RN distance on the available molecular concentration at the location of the RN. It is understood from Fig. 6.1(a) that as r increases the desired signal component (s_{SCK}) at the current symbol duration decreases and, correspondingly, the number of residual molecules at the next symbol durations ($n_{\text{SCK},j}$) increases, thus creating ISI to the next symbols. However, Fig. 6.1(b) shows the impact of r on the available concentrations of molecules in the current and the next three symbols, denoted respectively as the symbol-wise probabilities s_{SCK}, $n_{\text{SCK},1}$, $n_{\text{SCK},2}$, and $n_{\text{SCK},3}$. For instance, according to Fig. 6.1(b), we find that at $r = 800$ nm approximately 85% and 8.4% of the molecules are received during the first (s_{SCK}) and second ($n_{\text{SCK},1}$) symbol durations, i.e. during the (0–100 s) and (100–200 s) intervals respectively[13]. The decay of the molecular concentration is due to the temporal spreading of the impulse response of the diffusion-based MC channel. The symbol-wise probability curves for $n_{\text{SCK},1}$, $n_{\text{SCK},2}$, and $n_{\text{SCK},3}$ have a peak and then drop down because of the nature of the diffusion process. Fig.

[13] The reader should note that by multiplying the symbol-wise probabilities by the total transmitted molecules (i.e. $Q_{avg}T_b$) one can calculate the total number of available molecules on average during that symbol duration. For instance, in Fig. 6.1(b) at $r = 800$ nm, the total number of available molecules on average during the first and second intervals are respectively

$s_{\text{SCK}}Q_{avg}T_b = 0.85(10000)(100) = 8.5\times10^5$ and

$n_{\text{SCK},1}Q_{avg}T_b = 0.084(10000)(100) = 8.4\times10^4$.

6.2 shows the concentration intensity and the corresponding symbol-wise probabilities of a single pulse transmission when the symbol duration is 50 s (Fig. 6.2(a) and Fig. 6.2(b)), 20 s (Fig. 6.2(c) and Fig. 6.2(d)), and 10 s (Fig. 6.2(e) and Fig. 6.2(f)), respectively.

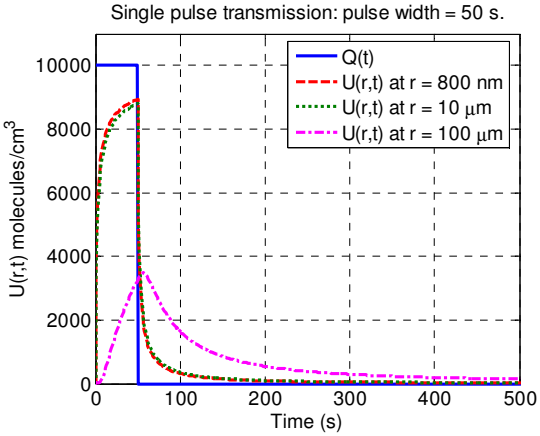

(a) $T_b = 50$ s.

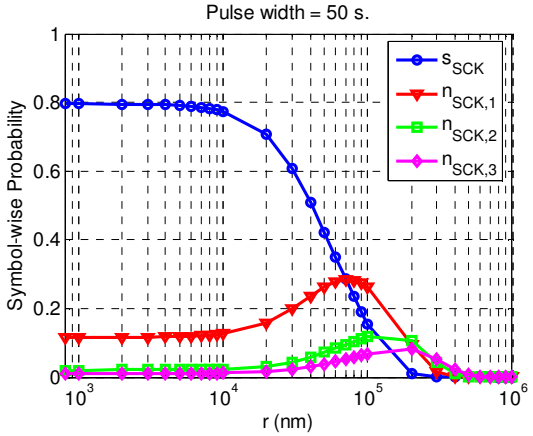

(b) $T_b = 50$ s.

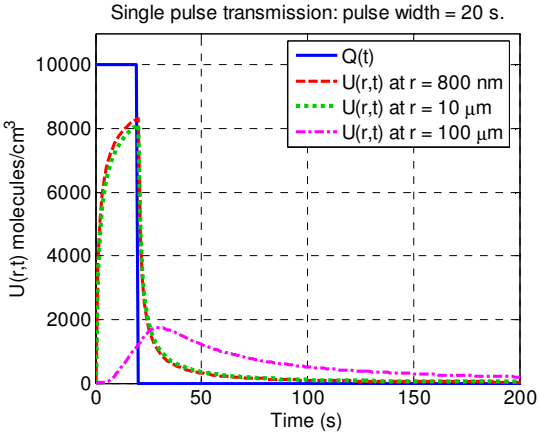

(c) $T_b = 20$ s.

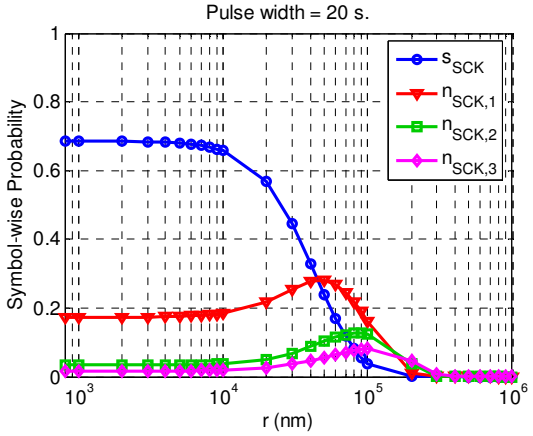

(d) $T_b = 20$ s.

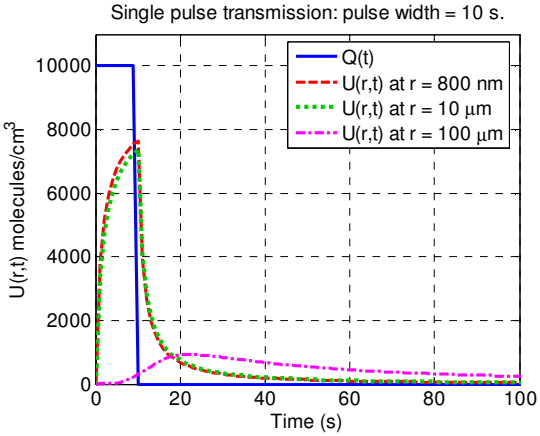

(e) $T_b = 10$ s.

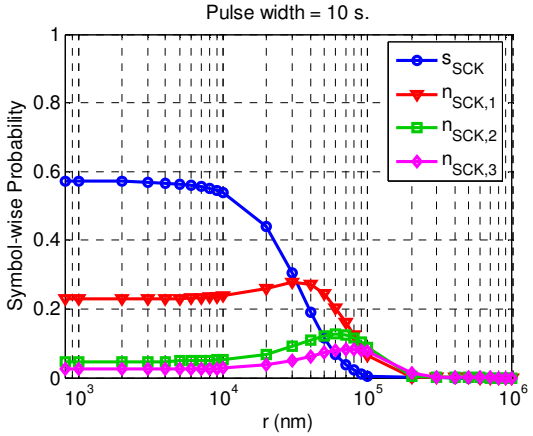

(f) $T_b = 10$ s.

Figure 6.2 Output concentration signals due to single pulse transmission with various pulse widths: 50 s (a), 20 s (c), and 10 s (e). In (a), (c), and (e), up to 10 symbol times are shown, although

observation time in each case is 100,000 s. The corresponding symbol-wise probabilities are shown in (b), (d), and (f), respectively.

6.3.3 Propensity Function-based MRBP Approach to Signal and Noise (Interference) Models

First, we describe the *propensity function*-based approach to compute the mean number of chemical reactions between the information molecules and the receptors of the RN in a given time duration. Then, we use the propensity function-based MRBP approach to derive the signal and the noise (interference) models and, thus, to develop the receiver architecture. The reception of molecules actually depends on the reactions between the molecules and the receptors of the RN. Since the system would contain a large number of molecules randomly moving by means of ideal diffusion mechanism, it may not be feasible to track the positions and velocities of all the molecules in the system. This makes the number of molecules received a *random* variable. It has been shown in the literature in the area of chemical reaction kinetics that the number of molecules that react with the receptors of the RN can be explained by means of the *propensity function* [GIL-00] [GIL-07], which can be explained as follows:

$a_{\mathrm{SCK}}\left(U\left(r,t\right)\right)dt \equiv$ the probability that a reaction occurs, somewhere in the small volume VRV surrounding the RN, between molecule and receptor, in the infinitesimally small time interval $[t,t+dt)$. Here $a_{\mathrm{SCK}}\left(U\left(r,t\right)\right)$ is known as the *propensity function* and can be explained as below.

$$a_{\mathrm{SCK}}\left(U\left(r,t\right)\right)=\eta_{\mathrm{SCK}}\rho_{\mathrm{SCK}}=\eta_{\mathrm{SCK}}\left(\Re U(r,t)\right)=\eta_{\mathrm{SCK}}\Re U(r,t) \tag{6.2}$$

where η_{SCK} is the specific probability rate constant for molecular reaction between an information molecule and a receptor in the VRV, thereby $\eta_{\mathrm{SCK}}dt$ denotes the probability that a randomly chosen molecule will react with a randomly chosen receptor during the infinitesimal time interval $[t,t+dt)$. The ρ_{SCK} denotes the distinct molecule and receptor pairs available in the VRV, and therefore, $\rho_{\mathrm{SCK}}=\Re U(r,t)$, where $\Re$ is the concentration of receptors on the surface of the RN. The stochastic nature of the molecule-receptor binding mechanism is provided by the chemical reaction kinetics as shown in Eq. (6.2). As shown in the next subsection, one key point of this stochastic molecule-receptor binding is that it

leads directly to the development of a strength-based receiver architecture that is based on *variable threshold* in the detection process. The developed receiver architecture shows that it is possible to incorporate the effects of the variable ISI into the *variable threshold* and, therefore, the bit detection process provides better results when compared to *fixed threshold*-based signal detection.

In order to develop the strength-based signal detection scheme by using the stochastic molecule-receptor binding approach, our principal focus is on the "number of reactions" between the molecules and the receptors on the surface of the RN. Let $K_{\mathrm{SCK}}\left(U(r,t),dt\right)$, for any $dt>0$, be the number of reactions that occur in the sub-sequent interval $[t,t+dt]$. Since $K_{\mathrm{SCK}}\left(U(r,t),dt\right)$ is a *random* variable, to compute this for arbitrary $dt>0$ is not only difficult through solving the stochastic CME, but also faces the fact that a stochastic CME does not always have a solution [GIL-00] [ATA-10]. However, it is possible to obtain an "excellent" approximation to $K_{\mathrm{SCK}}\left(U(r,t),dt\right)$ when the following two conditions are imposed [GIL-00].

(1) dt is required to be small enough such that the change in the system state would be so slight that none of the propensity functions changes its value "appreciably" and thereby it follows that $a_{\mathrm{SCK}}\left(U(r,t)\right)\cong a_{\mathrm{SCK}}\left(U(r,t')\right),\forall t'\in[t,t+dt]$. This requirement can easily be met by taking dt to be so small that no reactions will likely take place in the interval $[t,t+dt]$. This seems very strict in the sense that the same requirement can also be met by ensuring that all the reactant molecules populations are sufficiently larger than unity (i.e. 1), which is because propensity functions depend on the non-negative integer powers of the molecular species populations that never practically change by more than two molecules in one reaction event [GIL-00]. When this condition is fulfilled, the reactions that take place in the time interval $[t,t+dt]$ do not change any of the propensity functions, and therefore, all the reaction events occurring in the interval $[t,t+dt]$ are independent of each other, and as a result, $K_{\mathrm{SCK}}\left(U(r,t),dt\right)$ is a *statistically independent Poisson's* random variable with rate $\lambda_{\mathrm{SCK}}=a_{\mathrm{SCK}}\left(U(r,t)\right)dt$ [ATA-10].

(2) dt is required to be large enough such that the expected number of reactions in interval $[t,t+dt]$ is much larger than unity (i.e. 1), i.e. $a_{\mathrm{SCK}}\left(U(r,t)\right)dt\gg 1,$ which can, in

many practical circumstances, also be satisfied by having large molecular population numbers. When this condition is satisfied, the *Poisson's* random variable $K_{\text{SCK}}\left(U(r,t),dt\right)$ can be approximated to a *normal* distributed random variable of equal mean and variance $\mathcal{N}(\lambda_{\text{SCK}},\lambda_{\text{SCK}})$, i.e. $\mathcal{N}\left(a_{\text{SCK}}\left(U(r,t)\right)dt, a_{\text{SCK}}\left(U(r,t)\right)dt\right)$, where $\mathcal{N}(\mu,\sigma^2)$ denotes a *normal* distributed random variable with mean μ and variance σ^2 [GIL-00] [ATA-10]. Note that $\mathcal{N}(\mu,\sigma^2)$ can be simplified into a *standard normal* random variable [JOH-05] by $\mathcal{N}(\mu,\sigma^2)=\mu+\sigma\mathcal{N}(0,1)$.

The strength-based receiver architecture presented in this chapter is built upon the *propensity function*-based molecule-receptor interactions shown above and is introduced next.

6.3.4 Development of Strength-based Receiver Architecture

As shown earlier, according to the *propensity function*-based approach shown above, the total number of chemical reactions during an interval can be approximated to a *normal* distributed random variable of equal mean and variance. Based on OOK[14] modulation [HAY-00], where the TN has to transmit bits $b_i \in \{0,1\}$ for $i=1,2,...,N_b$, N_b being the total number of bits to be transmitted and T_b being the duration of each bit (in second), the TN releases a pulse of molecules at a fixed rate during the T_b (i.e. the ON time of the pulse) if it wants to transmit a bit 1, while it does not release any molecules at all if it wants to transmit a bit 0. The strength-based receiver for the CEMC system discussed in this chapter is based on an OOK CEMC system. In this relation, it is important to investigate into a single pulse transmission, as shown in Fig. 6.1, because the single pulse transmission provides with the mean numbers of molecules that would be available at the RN during the desired time interval $[0,T_b]$ and those that would be causing ISI during the time interval $[T_b,T_{obs}]$.

Referring back to Eq. (6.2), since η_{SCK} and $\Re$ are constant numbers, it is found that the propensity function can directly map to the concentration signal intensity $U(r,t)$ as below.

[14] OOK is a special case of PAM scheme [HAY-00].

$$a_{\text{SCK}}\left(U\left(r,t\right)\right) \Leftrightarrow U(r,t) \tag{6.3}$$

Considering a single pulse transmission starting at $t=0$ and using the *propensity function*-based approach, the number of desired reactions $N_{s_{\text{SCK}}}$ during the interval $[0,T_b]$ would constitute the desired signal and, based on the two approximations mentioned above, can be equivalently expressed as *normal* distributed random variable with equal mean and variance as below.

$$N_{s_{\text{SCK}}} \sim \mathcal{N}\left(\mu_{s_{\text{SCK}}}, \sigma^2_{s_{\text{SCK}}}\right) \text{ where } \mu_{s_{\text{SCK}}} = \int_0^{T_b} a_{\text{SCK}}\left(U\left(r,t\right)\right) dt \text{ and } \sigma^2_{s_{\text{SCK}}} = \int_0^{T_b} a_{\text{SCK}}\left(U\left(r,t\right)\right) dt \tag{6.4}$$

and, similarly, the number of undesired (i.e. ISI-causing) reactions $N_{n_{\text{SCK},j,j\neq 0}}$, where j is a non-zero positive integer, can be expressed as

$$N_{n_{\text{SCK},j,j\neq 0}} \sim \mathcal{N}\left(\mu_{n_{\text{SCK},j}}, \sigma^2_{n_{\text{SCK},j}}\right) \tag{6.5}$$

$$\text{where } \mu_{n_{\text{SCK},j}} = \int_{jT_b,j\neq 0}^{(j+1)T_b} a_{\text{SCK}}\left(U\left(r,t\right)\right) dt \text{ and } \sigma^2_{n_{\text{SCK},j}} = \int_{jT_b,j\neq 0}^{(j+1)T_b} a_{\text{SCK}}\left(U\left(r,t\right)\right) dt \cdot$$

In the strength-based binary symbol detection, the molecules during a bit interval are accumulated and the decision on which bit was transmitted is done by comparing that with a threshold. While the number of molecules that can be available at the RN is a random variable, the solution of Fick's laws, as shown in Eq. (3.1), provides the mean number of molecules that are available at the RN. Based on the *propensity function*, a particular realization of the concentration signal intensity would provide particular values of $N_{s_{\text{SCK}}}$ and $N_{n_{\text{SCK},j}}$. The TN is assumed to start transmission at the beginning of the *i*-th bit interval. The total number of molecules available for reception would possibly (based on the reaction rate constant) react with the receptors of the RN, which would constitute the quantity z_{SCK} and can be expressed as a *normal* distributed random variable [ATA-10] as shown in Eqs. (6.4)–(6.6). This results from the approximation that the number of chemical reactions corresponding to $N_{s_{\text{SCK}}}$ and $N_{n_{\text{SCK},j}}$ are all *normal* distributed random variables and any summation of them is also a *normal* distributed random variable. When $U(r,t)$, i.e. the mean concentration, is taken as the realization of the signal intensity, signal detection can be explained using the following hypotheses, when $i=1,2,...,N_b$:

$$z_{\text{SCK}} = \begin{cases} N_{s_{\text{SCK}}} + \sum_{j=1}^{i-1} b_{i-j} N_{n_{\text{SCK},j}}; & \text{H}_1 \\ \sum_{j=1}^{i-1} b_{i-j} N_{n_{\text{SCK},j}}; & \text{H}_0 \end{cases} \Rightarrow z_{\text{SCK}} \sim \begin{cases} \mathcal{N}\left(\mu_1, \sigma_1^2\right); & \text{H}_1 \\ \mathcal{N}\left(\mu_0, \sigma_0^2\right); & \text{H}_0 \end{cases} \tag{6.6}$$

where z_{SCK} is the total number of molecules received during the *i*-th bit duration, μ_m and σ_m^2 are the mean and variance of z_{SCK} when hypothesis H_m, $m = \{0,1\}$ is true. Therefore, for an OOK-based CEMC system it can be written that

$$\begin{aligned} \mu_1 &= \left(\mu_s + \sum_{j=1}^{i-1} b_{i-j} \mu_{n_{\text{SCK},j}} \right) \quad \sigma_1^2 = \left(\sigma_{s_{\text{SCK}}}^2 + \sum_{j=1}^{i-1} b_{i-j}^2 \sigma_{n_{\text{SCK},j}}^2 \right) \\ \mu_0 &= \sum_{j=1}^{i-1} b_{i-j} \mu_{n_{\text{SCK},j}} \qquad \sigma_0^2 = \sum_{j=1}^{i-1} b_{i-j}^2 \sigma_{n_{\text{SCK},j}}^2 \end{aligned} \tag{6.7}$$

where the subscripts of the means and the variances on the left hand side of the equations correspond to the appropriate hypotheses. Note that, in the development of the strength-based receiver, we have considered the realization of the mean concentration signal $U(r,t)$ as shown in Eqs. (3.1)–(3.4). Therefore, for this case, the *signal*, the *noise*, and the *interference* portions can be expressed as below, where z_{SCK} is the *test statistic* of the detection problem.

$$\begin{aligned} &z_{\text{SCK}} = \begin{cases} \mu_{s_{\text{SCK}}} + n_{s_{\text{SCK}}} + n_{\text{ISI}}; & \text{H}_1 \\ n_{\text{ISI}}; & \text{H}_0 \end{cases} \text{ where} \\ &n_{s_{\text{SCK}}} \sim \mathcal{N}\left(0, \sigma_{s_{\text{SCK}}}^2\right) \\ &n_{\text{ISI}} \sim \mathcal{N}\left(\mu_{\text{ISI}}, \sigma_{\text{ISI}}^2\right) \text{ where } \mu_{\text{ISI}} = \mu_0 = \sum_{j=1}^{i-1} b_{i-j} \mu_{n_{\text{SCK},j}}, \text{and } \sigma_{\text{ISI}}^2 = \sigma_0^2 = \sum_{j=1}^{i-1} b_{i-j}^2 \sigma_{n_{\text{SCK},j}}^2. \end{aligned} \tag{6.8}$$

Since $\mu_{n_{\text{SCK},j}} = \sigma_{n_{\text{SCK},j}}^2$ and $b_{i-j} = \{0,1\}$ where j is a non-zero positive integer and $i = 1,2,...,N_b$, it yields $\mu_{\text{ISI}} = \sigma_{\text{ISI}}^2$. However, for any realization $U_k(r,t)$ other than $U(r,t)$, the *signal*, the *noise*, and the *interference* portions can be shown as below.

$$\begin{aligned} &z_{\text{SCK}}[k] = \begin{cases} \mu_{s_{\text{SCK}}}[k] + n_{s_{\text{SCK}}}[k] + n_{\text{ISI}}[k]; & \text{H}_1 \\ n_{\text{ISI}}[k]; & \text{H}_0 \end{cases} \text{ where} \\ &n_{s_{\text{SCK}}}[k] \sim \mathcal{N}\left(0, \sigma_{s_{\text{SCK}}}^2[k]\right) \\ &n_{\text{ISI}}[k] \sim \mathcal{N}\left(\mu_{\text{ISI}}[k], \sigma_{\text{ISI}}^2[k]\right) \text{ where } \mu_{\text{ISI}}[k] = \mu_0[k], \text{and } \sigma_{\text{ISI}}^2[k] = \sigma_0^2[k]. \end{aligned} \tag{6.9}$$

However, in this chapter, we base our approach on the mean concentration signal intensity $U(r,t)$ of the single pulse transmission and, therefore, we consider the system model described by Eq. (6.6) only. Hence, Eq. (6.9) is just a more general case of the system model presented in Eq. (6.6).

The reader should note that in Eq. (6.8) the mean and the variance depend on the signal value itself. Considering the minimum probability of error criterion we can derive a *test statistic* by calculating the logarithm of the likelihood ratio using Neyman-Pearson formula [KAY-93] with equal prior probabilities as Eq. (6.10)

$$\frac{\ell\left(z_{\mathrm{SCK}} \mid \mathrm{H}_1\right)}{\ell\left(z_{\mathrm{SCK}} \mid \mathrm{H}_0\right)} > 1 \;\Rightarrow \ln \frac{\ell\left(z_{\mathrm{SCK}} \mid \mathrm{H}_1\right)}{\ell\left(z_{\mathrm{SCK}} \mid \mathrm{H}_0\right)} > 0 \tag{6.10}$$

where the conditional probabilities $\ell\left(z_{\mathrm{SCK}} \mid \mathrm{H}_m\right)$, $m = \{0,1\}$ can be given as below.

$$\begin{aligned} \ell\left(z_{\mathrm{SCK}} \mid \mathrm{H}_1\right) &= \frac{1}{\sqrt{2\pi\left(\sigma^2_{s_{\mathrm{SCK}}} + \sigma^2_{\mathrm{ISI}}\right)}} \exp\left[-\frac{\left\{z_{\mathrm{SCK}} - \left(\mu_{s_{\mathrm{SCK}}} + \mu_{\mathrm{ISI}}\right)\right\}^2}{2\left(\sigma^2_{s_{\mathrm{SCK}}} + \sigma^2_{\mathrm{ISI}}\right)}\right] \\ \ell\left(z_{\mathrm{SCK}} \mid \mathrm{H}_0\right) &= \frac{1}{\sqrt{2\pi\sigma^2_{\mathrm{ISI}}}} \exp\left[-\frac{\left\{z_{\mathrm{SCK}} - \mu_{\mathrm{ISI}}\right\}^2}{2\sigma^2_{\mathrm{ISI}}}\right] \end{aligned} \tag{6.11}$$

Therefore, for a total of N observations that z_{SCK} may take on, combining Eqs. (6.10) and (6.11) and simplifying yield the test statistic $T(z_{\mathrm{SCK}})$ as shown in Eq. (6.12).

$$T\left(z_{\mathrm{SCK}}\right) = \frac{N}{2} \ln \frac{\sigma^2_{\mathrm{ISI}}}{\left(\sigma^2_{s_{\mathrm{SCK}}} + \sigma^2_{\mathrm{ISI}}\right)} + \sum_{n=1}^{N} z^2_{\mathrm{SCK}}[n] \left\{\frac{1}{2\sigma^2_{\mathrm{ISI}}} - \frac{1}{2\left(\sigma^2_{s_{\mathrm{SCK}}} + \sigma^2_{\mathrm{ISI}}\right)}\right\} - \frac{N\mu_{s_{\mathrm{SCK}}}}{2} > 0 \tag{6.12}$$

The observation number N means that with mean concentration signal realization $U(r,t)$, there are N observations of the signal strength quantity z_{SCK} that the receiver would use in order to decide which bit had been transmitted by the TN. The resulting strength-based receiver architecture is shown in Fig. 6.3.

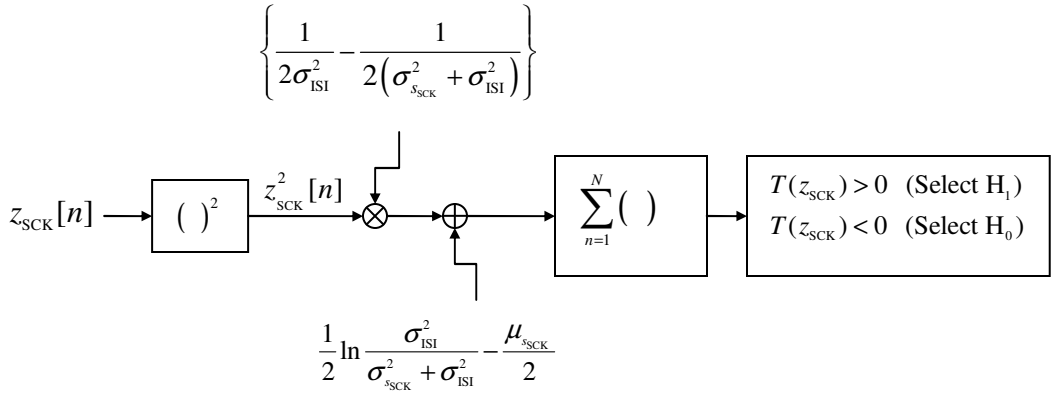

Figure 6.3 Strength-based optimum receiver architecture resulted from propensity function-based MRBP.

From Eq. (6.12), summing all the terms not involving z_{SCK} as γ in the right hand side and assuming that

$$\left\{\frac{1}{2\sigma_{\mathrm{ISI}}^2}-\frac{1}{2\left(\sigma_{s_{\mathrm{SCK}}}^2+\sigma_{\mathrm{ISI}}^2\right)}\right\}=\varpi_{\mathrm{SCK}} \text{ and}$$
$$\frac{N}{2}\ln\frac{\sigma_{\mathrm{ISI}}^2}{\left(\sigma_{s_{\mathrm{SCK}}}^2+\sigma_{\mathrm{ISI}}^2\right)}-\frac{N\mu_{s_{\mathrm{SCK}}}}{2}=-\gamma, \tag{6.13}$$

the modified test statistic can be written as the following.

$$T_1\left(z_{\mathrm{SCK}}\right)=\sum_{n=1}^{N}z_{\mathrm{SCK}}^2[n]>\gamma'$$
$$\text{where } \gamma'=\frac{\gamma}{\varpi_{\mathrm{SCK}}}=\left\{-\frac{N}{2}\ln\frac{\sigma_{\mathrm{ISI}}^2}{\left(\sigma_{s_{\mathrm{SCK}}}^2+\sigma_{\mathrm{ISI}}^2\right)}+\frac{N\mu_{s_{\mathrm{SCK}}}}{2}\right\}\Bigg/\left\{\frac{1}{2\sigma_{\mathrm{ISI}}^2}-\frac{1}{2\left(\sigma_{s_{\mathrm{SCK}}}^2+\sigma_{\mathrm{ISI}}^2\right)}\right\} \tag{6.14}$$

Therefore, the modified strength-based receiver architecture is shown in Fig. 6.4.

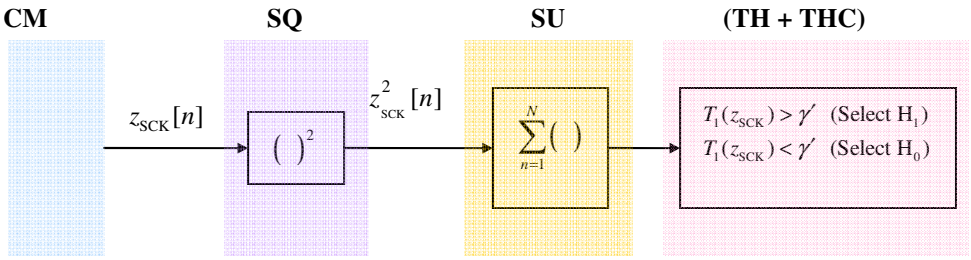

CM: Concentration Measurement
SQ: Square operation
SU: Summation
TH: Threshold computation
THC: Threshold comparator

Figure 6.4 A modified strength-based optimum receiver architecture resulted from propensity function-based MRBP.

6.4 Receiver Operating Characteristics

In this section, we present an analytical approach to derive the ROC of the optimum receiver that has been developed in Section 6.3 for the pulse-transmitted OOK CEMC system.

■ At H_0 : Since $z_{SCK}[n] = n_{ISI} \sim \mathcal{N}\left(\mu_{ISI}, \sigma^2_{ISI}\right)$ by converting $z_{SCK}[n]$ into a *standard normal* variable $x[n] \sim \mathcal{N}(0,1)$ as $z_{SCK}[n] = \mu_{ISI} + \sigma_{ISI} x[n]$, Eq. (6.14) yields

$$T_1\left(z_{SCK}\right) = \sum_{n=1}^{N} z^2_{SCK}[n] \Rightarrow \sum_{n=1}^{N}\left\{\mu^2_{ISI} + 2\mu_{ISI}\sigma_{ISI}x[n] + \sigma^2_{ISI}x^2[n]\right\} \tag{6.15}$$

$$\Rightarrow \mathcal{N}\left(N\mu^2_{ISI}, 4N\mu^2_{ISI}\sigma^2_{ISI}\right) + \sum_{n=1}^{N} w_0^2[n] \quad \text{where} \quad w_0[n] \sim \mathcal{N}\left(0, \sigma^2_{ISI}\right)$$

■ At H_1 : Since $z_{SCK}[n] = \left\{\mu_{s_{SCK}} + n_{s_{SCK}} + n_{ISI}\right\} \sim \mathcal{N}\left(\mu_{s_{SCK}} + \mu_{ISI}, \sigma^2_{s_{SCK}} + \sigma^2_{ISI}\right)$, by converting $z_{SCK}[n]$ into a *standard normal* variable $x[n] \sim \mathcal{N}(0,1)$ as mentioned earlier, we get

$$T_1\left(z_{SCK}\right) = \sum_{n=1}^{N} z^2_{SCK}[n] \Rightarrow \sum_{n=1}^{N}\left\{\left(\mu_{s_{SCK}} + \mu_{ISI}\right)^2 + 2\left(\mu_{s_{SCK}} + \mu_{ISI}\right)\sqrt{\left(\sigma^2_{s_{SCK}} + \sigma^2_{ISI}\right)}x[n] + \left(\sigma^2_{s_{SCK}} + \sigma^2_{ISI}\right)x^2[n]\right\}$$

$$\Rightarrow \mathcal{N}\left(N\left(\mu_{s_{SCK}} + \mu_{ISI}\right)^2, 4N\left(\mu_{s_{SCK}} + \mu_{ISI}\right)^2\left(\sigma^2_{s_{SCK}} + \sigma^2_{ISI}\right)\right) + \sum_{n=1}^{N} w_1^2[n]$$

where $w_1[n] \sim \mathcal{N}\left(0, \left(\sigma^2_{s_{SCK}} + \sigma^2_{ISI}\right)\right)$. (6.16)

As can be seen from above, in both H_0 and H_1, $T_1(z_{SCK})$ is a sum of one *normal* distributed random variable, and one *chi-square* distributed random variable with equal but

non-unity variances of the constituting normal random variables. We find that the pdf of $T_1(z_{\text{SCK}})$ depends not only on N but also on the coefficients of $x[n]$ and $x^2[n]$ terms that produce the normal and the chi-square parts respectively. Since $T_1(z_{\text{SCK}})$ is constituted of a non-zero-mean *normal* distributed component and a *chi-square* distributed component composed of individual zero-mean and non-unity variance *normal* distributed random variables, it is necessary to investigate into mean and variance of the *normal* distributed part (i.e. μ_{normal} and σ^2_{normal}) and those of the *chi-square* distributed part (i.e. $\mu_{\text{chi-square}}$ and $\sigma^2_{\text{chi-square}}$) of the $T_1(z_{\text{SCK}})$. We consider two scenarios as shown in Table 6.1.

Table 6.1 Scenarios considered in the analytical development of the ROC.

Scenario	Realization of the signal considered	No. of observations N	Mean and variance values
1.	Mean concentration signal $U(r,t)$	Large $N \gg 1$, and $N = 1$	$\mu_{\text{normal}} \gg \mu_{\text{chi-square}}, \sigma^2_{\text{normal}} \gg \sigma^2_{\text{chi-square}}$, and *chi-square* part is included in $T_1(z_{\text{SCK}})$.
2.	Mean concentration signal $U(r,t)$	Large $N \gg 1$	$\mu_{\text{normal}} \gg \mu_{\text{chi-square}}, \sigma^2_{\text{normal}} \gg \sigma^2_{\text{chi-square}}$, and *chi-square* part is neglected in $T_1(z_{\text{SCK}})$.

■ Scenario 1: This includes the contribution of the chi-square part in $T_1(z_{\text{SCK}})$. When N is large, the *chi-square* components can be approximated to a *normal* distributed random variable as follows.

$$\begin{aligned} &\text{At H}_0: && \sum_{n=1}^{N} w_0^2[n] \sim \mathcal{N}\left(N\sigma^2_{\text{ISI}}, 2N\left(\sigma^2_{\text{ISI}}\right)^2\right) \\ &\text{At H}_1: && \sum_{n=1}^{N} w_1^2[n] \sim \mathcal{N}\left(N\left(\sigma^2_{s_{\text{SCK}}} + \sigma^2_{\text{ISI}}\right), 2N\left(\sigma^2_{s_{\text{SCK}}} + \sigma^2_{\text{ISI}}\right)^2\right) \end{aligned} \tag{6.17}$$

Therefore, $T_1(z_{\text{SCK}})$ can be approximated to the following:

$$\text{At H}_0: T_1(z_{\text{SCK}}) \sim \mathcal{N}\left(N\mu_{\text{ISI}}^2 + N\sigma_{\text{ISI}}^2, \left[4N\mu_{\text{ISI}}^2\sigma_{\text{ISI}}^2 + 2N\left(\sigma_{\text{ISI}}^2\right)^2\right]\right) = \mathcal{N}\left(\mu_{T_1(H_0)}, \sigma_{T_1(H_0)}^2\right)$$

$$\text{where } \mu_{T_1(H_0)} = N\mu_{\text{ISI}}^2 + N\sigma_{\text{ISI}}^2 \text{ and } \sigma_{T_1(H_0)}^2 = 4N\mu_{\text{ISI}}^2\sigma_{\text{ISI}}^2 + 2N\left(\sigma_{\text{ISI}}^2\right)^2$$

$$\text{At H}_1: T_1(z_{\text{SCK}}) \sim \mathcal{N}\left(N\left(\mu_{s_{\text{SCK}}} + \mu_{\text{ISI}}\right)^2 + N\left(\sigma_{s_{\text{SCK}}}^2 + \sigma_{\text{ISI}}^2\right), \left[4N\left(\mu_{s_{\text{SCK}}} + \mu_{\text{ISI}}\right)^2\left(\sigma_{s_{\text{SCK}}}^2 + \sigma_{\text{ISI}}^2\right) + 2N\left(\sigma_{s_{\text{SCK}}}^2 + \sigma_{\text{ISI}}^2\right)^2\right]\right)$$

$$= \mathcal{N}\left(\mu_{T_1(H_1)}, \sigma_{T_1(H_1)}^2\right)$$

$$\text{where } \mu_{T_1(H_1)} = N\left(\mu_{s_{\text{SCK}}} + \mu_{\text{ISI}}\right)^2 + N\left(\sigma_{s_{\text{SCK}}}^2 + \sigma_{\text{ISI}}^2\right) \text{ and } \sigma_{T_1(H_1)}^2 = 4N\left(\mu_{s_{\text{SCK}}} + \mu_{\text{ISI}}\right)^2\left(\sigma_{s_{\text{SCK}}}^2 + \sigma_{\text{ISI}}^2\right) + 2N\left(\sigma_{s_{\text{SCK}}}^2 + \sigma_{\text{ISI}}^2\right)^2 \tag{6.18}$$

Correspondingly, P_{FA} and P_D can be calculated respectively as

$$P_{\text{FA}} = \Pr\left(T_1(z_{\text{SCK}}) > \gamma'; \text{H}_0\right) = \mathcal{Q}\left(\frac{\gamma' - \mu_{T_1(H_0)}}{\sigma_{T_1(H_0)}}\right) \tag{6.19}$$

and

$$P_{\text{D}} = \Pr\left(T_1(z_{\text{SCK}}) > \gamma'; \text{H}_1\right) = \mathcal{Q}\left(\frac{\gamma' - \mu_{T_1(H_1)}}{\sigma_{T_1(H_1)}}\right). \tag{6.20}$$

Here $\mathcal{Q}(\bullet)$ is the *right tail probability* [KAY-93]. Expressing γ' in terms of P_{FA}, the ROC of the receiver in this case can be expressed as the following.

$$P_{\text{D}} = \mathcal{Q}\left(\frac{\mathcal{Q}^{-1}(P_{\text{FA}})\sigma_{T_1(H_0)} + \mu_{T_1(H_0)} - \mu_{T_1(H_1)}}{\sigma_{T_1(H_1)}}\right) = \mathcal{Q}\left(\mathcal{Q}^{-1}(P_{\text{FA}})\frac{\sigma_{T_1(H_0)}}{\sigma_{T_1(H_1)}} - \frac{\mu_{T_1(H_1)} - \mu_{T_1(H_0)}}{\sigma_{T_1(H_1)}}\right) \tag{6.21}$$

Applying $\mu_{n_{\text{SCK},j}} = \sigma_{n_{\text{SCK},j}}^2$ and $b_{i-j} = \{0,1\}$ gives $\mu_{\text{ISI}} = \sigma_{\text{ISI}}^2$; and since $2\mu_{\text{ISI}} + 1 \approx 2\mu_{\text{ISI}}$ and $2\left(\mu_{s_{\text{SCK}}} + \mu_{\text{ISI}}\right) + 1 \approx 2\left(\mu_{s_{\text{SCK}}} + \mu_{\text{ISI}}\right)$, we find

$$\begin{aligned}\frac{\sigma_{T_1(H_0)}^2}{\sigma_{T_1(H_1)}^2} &= \frac{4N\mu_{\text{ISI}}^2\sigma_{\text{ISI}}^2 + 2N\left(\sigma_{\text{ISI}}^2\right)^2}{4N\left(\mu_{s_{\text{SCK}}} + \mu_{\text{ISI}}\right)^2\left(\sigma_{s_{\text{SCK}}}^2 + \sigma_{\text{ISI}}^2\right) + 2N\left(\sigma_{s_{\text{SCK}}}^2 + \sigma_{\text{ISI}}^2\right)^2} \\ &= \frac{2\mu_{\text{ISI}} + 1}{\left(1 + \frac{\mu_{s_{\text{SCK}}}}{\mu_{\text{ISI}}}\right)^2\left[2\left(\mu_{s_{\text{SCK}}} + \mu_{\text{ISI}}\right) + 1\right]} \\ &= \frac{1}{\left(1 + \frac{\mu_{s_{\text{SCK}}}}{\mu_{\text{ISI}}}\right)^3}\end{aligned} \tag{6.22}$$

where $2\mu_{\text{ISI}} + 1 \approx 2\mu_{\text{ISI}}$ and $2\left(\mu_{s_{\text{SCK}}} + \mu_{\text{ISI}}\right) + 1 \approx 2\left(\mu_{s_{\text{SCK}}} + \mu_{\text{ISI}}\right)$ are assumed.

Here $\left(\frac{\mu_{s_{\mathrm{SCK}}}}{\mu_{\mathrm{ISI}}}\right)$ denotes the *signal to interference strength ratio* (SIR) and $10\log_{10}\left(\frac{\mu_{s_{\mathrm{SCK}}}}{\mu_{\mathrm{ISI}}}\right)$ denotes the SIR in decibels (dB). On the other hand,

$$\begin{aligned}\frac{\mu_{T_1(H_1)}-\mu_{T_1(H_0)}}{\sigma_{T_1(H_1)}} &= \frac{N\left(\mu_{s_{\mathrm{SCK}}}+\mu_{\mathrm{ISI}}\right)^2+N\left(\sigma^2_{s_{\mathrm{SCK}}}+\sigma^2_{\mathrm{ISI}}\right)-N\mu^2_{\mathrm{ISI}}-N\sigma^2_{\mathrm{ISI}}}{\sqrt{4N\left(\mu_{s_{\mathrm{SCK}}}+\mu_{\mathrm{ISI}}\right)^2\left(\sigma^2_{s_{\mathrm{SCK}}}+\sigma^2_{\mathrm{ISI}}\right)+2N\left(\sigma^2_{s_{\mathrm{SCK}}}+\sigma^2_{\mathrm{ISI}}\right)^2}} \\ &= \frac{\sqrt{N}\mu_{s_{\mathrm{SCK}}}\left(\mu_{s_{\mathrm{SCK}}}+2\mu_{\mathrm{ISI}}+1\right)}{2\left(\mu_{s_{\mathrm{SCK}}}+\mu_{\mathrm{ISI}}\right)\sqrt{\left(\mu_{s_{\mathrm{SCK}}}+\mu_{\mathrm{ISI}}\right)+\frac{1}{2}}} \\ &= \frac{\sqrt{N}\sqrt{\mu_{s_{\mathrm{SCK}}}}\sqrt{\frac{\mu_{s_{\mathrm{SCK}}}}{\mu_{\mathrm{ISI}}}}\left(2+\frac{\mu_{s_{\mathrm{SCK}}}}{\mu_{\mathrm{ISI}}}\right)}{2\left(1+\frac{\mu_{s_{\mathrm{SCK}}}}{\mu_{\mathrm{ISI}}}\right)^{3/2}}\end{aligned} \tag{6.23}$$

where $\mu_{s_{\mathrm{SCK}}}+2\mu_{\mathrm{ISI}}+1\approx\mu_{s_{\mathrm{SCK}}}+2\mu_{\mathrm{ISI}}$ and $\left(\mu_{s_{\mathrm{SCK}}}+\mu_{\mathrm{ISI}}\right)+\frac{1}{2}\approx\left(\mu_{s_{\mathrm{SCK}}}+\mu_{\mathrm{ISI}}\right)$ are assumed.

Therefore, using Eqs. (6.21)–(6.23) the ROC can be expressed as the following.

$$\begin{aligned}P_{\mathrm{D}} &= \mathcal{Q}\left(\mathcal{Q}^{-1}(P_{\mathrm{FA}})\frac{\sigma_{T_1(H_0)}}{\sigma_{T_1(H_1)}}-\frac{\mu_{T_1(H_1)}-\mu_{T_1(H_0)}}{\sigma_{T_1(H_1)}}\right)=\mathcal{Q}\left(\frac{\mathcal{Q}^{-1}(P_{\mathrm{FA}})}{\left(1+\frac{\mu_{s_{\mathrm{SCK}}}}{\mu_{\mathrm{ISI}}}\right)^{3/2}}-\frac{\sqrt{N}\sqrt{\mu_{s_{\mathrm{SCK}}}}\sqrt{\frac{\mu_{s_{\mathrm{SCK}}}}{\mu_{\mathrm{ISI}}}}\left(2+\frac{\mu_{s_{\mathrm{SCK}}}}{\mu_{\mathrm{ISI}}}\right)}{2\left(1+\frac{\mu_{s_{\mathrm{SCK}}}}{\mu_{\mathrm{ISI}}}\right)^{3/2}}\right) \\ &= \mathcal{Q}\left(\frac{\mathcal{Q}^{-1}(P_{\mathrm{FA}})}{\left(1+\mathrm{SIR}\right)^{3/2}}-\frac{\sqrt{N}\sqrt{\mu_{s_{\mathrm{SCK}}}}\sqrt{\mathrm{SIR}}\left(2+\mathrm{SIR}\right)}{2\left(1+\mathrm{SIR}\right)^{3/2}}\right)\end{aligned} \tag{6.24}$$

The ROC expressed in Eq. (6.24) is quite complicated, and in addition, note that in Eq. (6.24) P_{D} depends not only on SIR but also on the number of observations and the mean value of the signal itself. Eq. (6.24) provides the ROC curves of the strength-based receiver in Scenario 1 shown in Table 6.1.

In the second term of the argument of $\mathcal{Q}(\bullet)$ in Eq. (6.24), the presence of the quantity $\sqrt{\mu_{s_{\mathrm{SCK}}}}$ originated from dealing with Eq. (6.23) given the fact that the mean and the variances of $z_{\mathrm{SCK}}[n]$ are equal in both H_0 and H_1 hypotheses, and so when Eq. (6.23) is used

to find the ROC, the quantity $\sqrt{\mu_{s_{\text{SCK}}}}$ still remains in the ROC expression. While a large value of $\sqrt{\mu_{s_{\text{SCK}}}}$ will decrease the value of the argument of $\mathcal{Q}(\bullet)$, the value of $\mu_{s_{\text{SCK}}}$ needs to be chosen, which, for $N=1$ observation, will yield the following theoretical ROC curves as shown in Figs. 6.5 and 6.6.

As discussed earlier, $\mu_{s_{\text{SCK}}}$ is a function of both *r* and data rate *f*, and according to Eq. (6.4), $N_{s_{\text{SCK}}} \sim \mathcal{N}\left(\mu_{s_{\text{SCK}}}, \sigma^2_{s_{\text{SCK}}}\right)$ where $\mu_{s_{\text{SCK}}} = \sigma^2_{s_{\text{SCK}}} = \int_0^{T_b} a_{\text{SCK}}\left(U\left(r,t\right)\right)dt$. Hence, assuming that $\eta_{\text{SCK}}\Re = (0.01)100 = 1$ [ATA-10] and using Eqs. (6.2) and (6.4) give the following.

$$\mu_{s_{\text{SCK}}} = \sigma^2_{s_{\text{SCK}}} = (\eta_{\text{SCK}}\Re)s_{\text{SCK}}Q_{avg}T_b = s_{\text{SCK}}Q_{avg}T_b\,. \tag{6.25}$$

When *r* = 10 μm, 100 μm, and *f* = 0.01 bps, considering $\mu_{s_{\text{SCK}}}$ as the mean number of reactions that take place during the symbol duration, we get the detection performance and the ROC as shown in the Fig. 6.5 below. Similarly, when *r* = 10 μm, 100 μm, and *f* = 0.1 bps, the detection performance is shown in Fig. 6.6.

While detection probability versus SIR characteristics for 0.01 bps have been shown in Figs. 6.5(a) and 6.5(c) for *r* = 10 μm and *r* = 100 μm respectively, similar results for 0.1 bps case have been shown in Figs. 6.6(a), 6.6(c) for *r* = 10 μm and *r* = 100 μm respectively. As shown in Fig. 6.5(b), for a transmission data rate of 0.01 bps when $\mu_{s_{\text{SCK}}} < \mu_{\text{ISI}}$ by 40 dB or less, P_{D} is close to unity for any value of P_{FA}. As shown in Fig. 6.6(b) when the data rate increases to 0.1 bps, then if $\mu_{s_{\text{SCK}}} < \mu_{\text{ISI}}$ by 40 dB or less then P_{D} is close to unity for any value of P_{FA}. In addition, at SIR = −60 dB, P_{D} decreases when *f* increases, as shown in Figs. 6.5(b) and 6.6(b) when *r* = 10 μm, and in Figs. 6.5(d) and 6.6(d) when *r* = 100 μm. This shows the effects of communication data rate on the detection probability of the symbol. The red curves in Fig. 6.5(b) and 6.6(b) show that the CEMC system becomes more affected by the ISI when the transmission data rate increases, and, therefore, the detection probability decreases, as shown in the red curve in Fig. 6.6(b) when compared to that in Fig. 6.5(b). Figs. 6.5 and 6.6 show that P_{D} depends on the chosen values of P_{FA} and SIR of the system. For instance, as shown in Fig. 6.5(a), with $P_{\text{FA}} = 10^{-5}$, when SIR starts to increase from −60 dB, P_{D} gradually increases, where an SIR of −50 dB or higher can ensure a P_{D} close to unity.

As shown in Figs. 6.5(b) and 6.5(d), keeping the data rate fixed at 0.01 bps, when the TN and the RN are comparatively far apart, the detection probability decreases, as shown by the decrease of the gap between the red and the blue curves in Figs. 6.5(b) and 6.5(d). A similar degraded detection performance is shown in Figs. 6.6(b) and 6.6(d) for the case of 0.1 bps. Keeping the data rate fixed at 0.01 bps, for any given SIR when the TN-RN distance increases from 10 µm to 100 µm, the detection performance deteriorates, as shown in Figs. 6.5(a) and 6.5(c) respectively. A similar deteriorated detection performance can be observed when the data rate is fixed at 0.1 bps for any given SIR as shown in Figs. 6.6(a) and 6.6(c), when the TN-RN distance increases from 10 µm to 100 µm respectively.

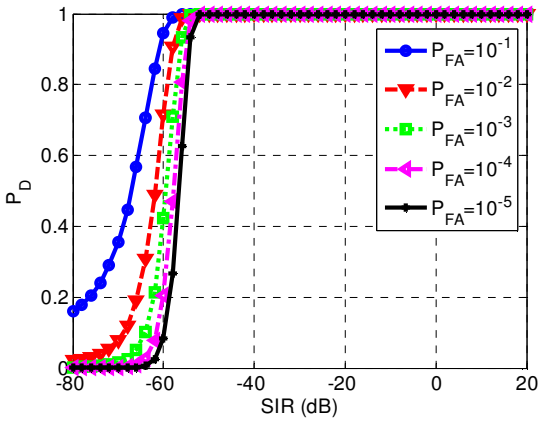

(a) r = 10 µm

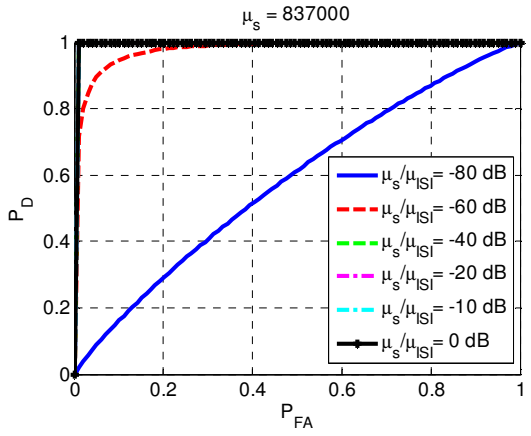

(b) r = 10 µm

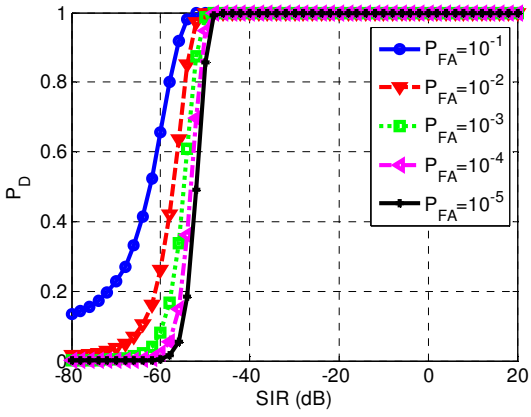

(c) r = 100 µm

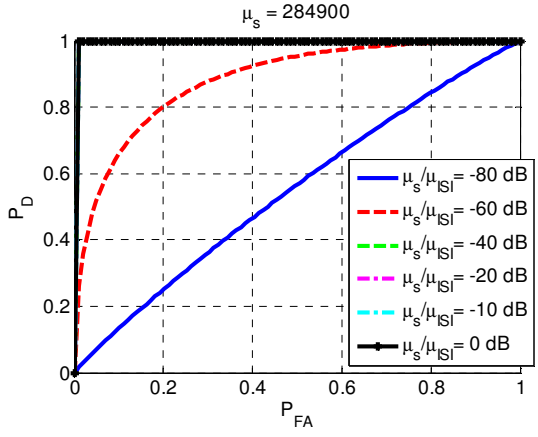

(d) r = 100 µm

Figure 6.5 Detection performance of strength-based optimum detector with stochastic molecule-receptor binding based on SCK, r = 10 µm (in (a) and (b)), and r = 100 µm (in (c) and (d)), when f

= 0.01 bps, N = 10, and $\mu_{s_{SCK}}$ is calculated[15] from Eq. (6.25). For the sake of visual clarity, the sub-subscript "SCK" has been dropped from the quantity $\mu_{s_{SCK}}$ in this figure.

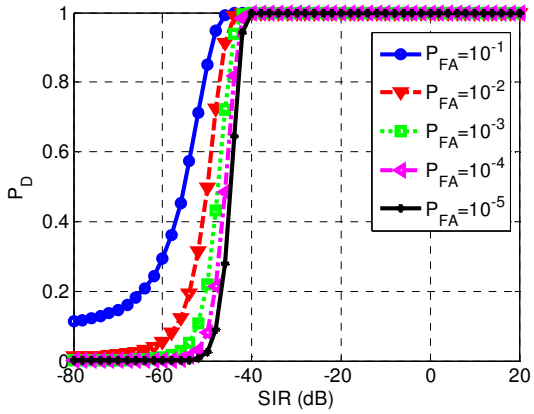

(a) r = 10 μm

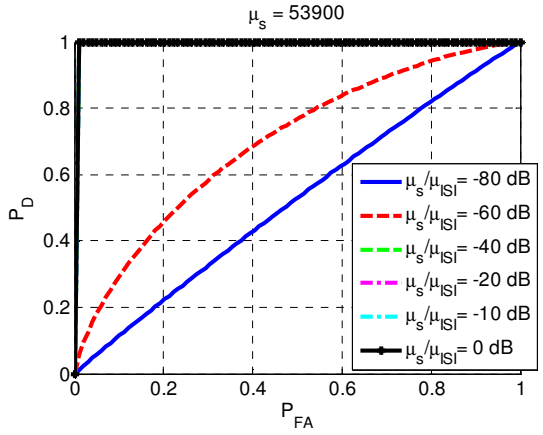

(b) r = 10 μm

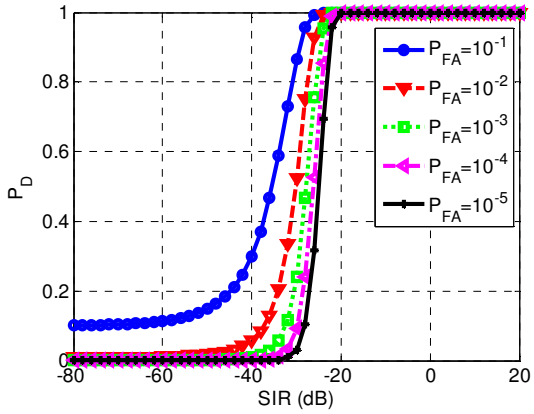

(c) r = 100 μm

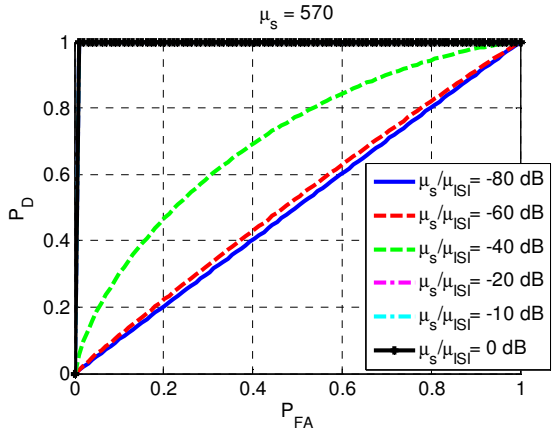

(d) r = 100 μm

Figure 6.6 Detection performance of strength-based optimum detector with stochastic molecule-receptor binding based on SCK, r = 10 μm (in (a) and (b)), and r = 100 μm (in (c) and (d)), when f = 0.1 bps, N = 10, and $\mu_{s_{SCK}}$ is calculated from Eq. (6.25). For the sake of visual clarity, the sub-subscript "SCK" has been dropped from the quantity $\mu_{s_{SCK}}$ in this figure.

[15] For example, given a transmission data rate of f = 0.01 bps, when r = 10 μm, $\mu_{s_{SCK}} = s_{SCK} Q_{avg} T_b$ = (0.837)(10,000)(100) = 837000. Note that from Fig. 6.1(b) we find s_{SCK} = 83.7% when r = 10 μm, and given that Q_{avg} = 10,000 molecules/second and $T_b = 1/f$ = 100 seconds.

■ Extension to Scenario 2: At H_0, since according to Eq. (6.5) $\mu_{n_{\mathrm{SCK},j}} = \sigma^2_{n_{\mathrm{SCK},j}}$, using Eqs. (6.15)–(6.18), when $N = \text{large}$, the mean and the variance ratios of the *normal* part to the *chi-square* part of the $T_1(z_{\mathrm{SCK}})$ can be expressed as the following,

$$\frac{\mu_{\text{normal}}}{\mu_{\text{chi-square}}} = \frac{N\mu^2_{\mathrm{ISI}}}{N\sigma^2_{\mathrm{ISI}}} = \mu_{\mathrm{ISI}} \gg 1; \quad \frac{\sigma^2_{\text{normal}}}{\sigma^2_{\text{chi-square}}} = \frac{4N\mu^2_{\mathrm{ISI}}\sigma^2_{\mathrm{ISI}}}{2N\left(\sigma^2_{\mathrm{ISI}}\right)^2} = 2\mu_{\mathrm{ISI}} \gg 1 \tag{6.26}$$

which shows that $\mu_{\text{normal}} \gg \mu_{\text{chi-square}}$ and $\sigma^2_{\text{normal}} \gg \sigma^2_{\text{chi-square}}$, provided that μ_{ISI} is in general a large number. Similarly, at H_1,

$$\begin{aligned} \frac{\mu_{\text{normal}}}{\mu_{\text{chi-square}}} &= \frac{N\left(\mu_{s_{\mathrm{SCK}}} + \mu_{\mathrm{ISI}}\right)^2}{N\left(\sigma^2_{s_{\mathrm{SCK}}} + \sigma^2_{\mathrm{ISI}}\right)} = \mu_{s_{\mathrm{SCK}}} + \mu_{\mathrm{ISI}} \gg 1 \\ \frac{\sigma^2_{\text{normal}}}{\sigma^2_{\text{chi-square}}} &= \frac{4N\left(\mu_{s_{\mathrm{SCK}}} + \mu_{\mathrm{ISI}}\right)^2\left(\sigma^2_{s_{\mathrm{SCK}}} + \sigma^2_{\mathrm{ISI}}\right)}{2N\left(\sigma^2_{s_{\mathrm{SCK}}} + \sigma^2_{\mathrm{ISI}}\right)^2} = 2\left(\mu_{s_{\mathrm{SCK}}} + \mu_{\mathrm{ISI}}\right) \gg 1 \end{aligned} \tag{6.27}$$

which, for the similar reason, shows that $\mu_{\text{normal}} \gg \mu_{\text{chi-square}}$ and $\sigma^2_{\text{normal}} \gg \sigma^2_{\text{chi-square}}$, provided that μ_{ISI} and $\mu_{s_{\mathrm{SCK}}}$ are, in general, large numbers. Since $\sigma^2_{\text{normal}} \gg \sigma^2_{\text{chi-square}}$, the effects of $\sigma^2_{\text{chi-square}}$ can be ignored. Following the similar steps as shown for Scenario 1, for Scenario 2 we can derive the exact same ROC as in Scenario 1 shown in Eq. (6.24). The derivation being very similar is not shown here.

6.5 Signal Detection Based on Variable Threshold

As shown in Eq. (6.14), the modified test statistic $T_1\left(z_{\mathrm{SCK}}\right)$ is compared with a threshold γ' that is a function of $N, \mu_{s_{\mathrm{SCK}}}$, and μ_{ISI} (known that $\mu_{s_{\mathrm{SCK}}} = \sigma^2_{s_{\mathrm{SCK}}}$ and $\mu_{\mathrm{ISI}} = \sigma^2_{\mathrm{ISI}}$) and for $N = 1$, γ' can be expressed as the following.

$$\gamma' = \frac{-\frac{1}{2}\ln\frac{\mu_{\mathrm{ISI}}}{\left(\mu_{s_{\mathrm{SCK}}} + \mu_{\mathrm{ISI}}\right)} + \frac{\mu_{s_{\mathrm{SCK}}}}{2}}{\frac{1}{2\mu_{\mathrm{ISI}}} - \frac{1}{2\left(\mu_{s_{\mathrm{SCK}}} + \mu_{\mathrm{ISI}}\right)}} = \frac{\mu_{s_{\mathrm{SCK}}} - \ln\frac{\mu_{\mathrm{ISI}}}{\left(\mu_{s_{\mathrm{SCK}}} + \mu_{\mathrm{ISI}}\right)}}{\frac{1}{\mu_{\mathrm{ISI}}} - \frac{1}{\left(\mu_{s_{\mathrm{SCK}}} + \mu_{\mathrm{ISI}}\right)}} \tag{6.28}$$

The threshold γ' shown above depends on both $\mu_{s_{\mathrm{SCK}}}$ and μ_{ISI}. Here $\mu_{s_{\mathrm{SCK}}}$ denotes the mean number of the reactions that take place during symbol duration and can be found by the *propensity function*-based approach using the concentration signal intensity $U(r,t)$. As

shown in Eq. (6.25), for $\eta_{\text{SCK}}\Re = (0.01)100 = 1$, $\mu_{s_{\text{SCK}}} = \sigma^2_{s_{\text{SCK}}} = s_{\text{SCK}} Q_{avg} T_b$, which is constant for a given set of Q_{avg}, TN-RN distance, and data rate f (i.e. $1/T_b$) values. As a result, it is shown that γ' depends on μ_{ISI} only, for a given set of Q_{avg}, TN-RN distance, and data rate f (i.e. $1/T_b$) values.

Unlike *fixed threshold*-based approach where the total accumulated number of the reactions is compared with a fixed threshold value, in the *variable threshold*-based approach, the threshold is calculated on per symbol basis (i.e. per bit in case of binary scheme), taking into account the ISI contributions from the previous bit transmissions, and hence this scheme is called the *variable threshold*-based detection scheme.

For example, when the RN considers all the previous bits, the threshold for the i-th bit is computed by taking into account the ISI contributions from the first bit up to the $(i-1)$-th bit. Different bits in the transmitted bit sequence suffer differently from the impacts of the ISI and, therefore, the threshold that the strength of the bit is compared with is different for each transmitted bit at the RN side. While the value of $\mu_{s_{\text{SCK}}}$ can be known from the single pulse transmission for a given TN-RN distance and transmission data rate, the impact of μ_{ISI} is different for different transmitted bits at the receiver side. The *variable threshold*-based approach identifies the impact of μ_{ISI} in a particular bit and thus computes the threshold for that bit in order to decide which bit was transmitted by the TN. In order to calculate the BER through numerical simulations, we consider transmitting a random sequence of bits and that mean concentration signal intensity *U(r,t)* is present at the location of the RN, which is the reason of considering $N = 1$ in Eq. (6.28).

A comparison between *fixed threshold*-based and *variable threshold*-based signal detection schemes in terms of communication range and rate-dependent characteristics is shown in Fig. 6.7. The BER characteristics of the *variable threshold*-based and the *fixed threshold*-based detectors have been shown for $f = 0.01$ bps, 0.02 bps, 0.05 bps, and 0.1 bps transmissions in Figs. 6.7(a), 6.7(b), 6.7(c), and 6.7(d) respectively. It is understood from Fig. 6.7 that in order to achieve a preset BER (or less than a preset BER), the *variable threshold*-based detector allows more TN-RN distance, which indicates the possibility of using the *variable threshold*-based detector to increase the effective communication range in

diffusion-based CEMC system. For example, as shown in Fig. 6.7(a), when the transmission data rate is 0.01 bps, with *fixed threshold*-based and *variable threshold*-based detectors, BER equal to or less than 0.1 can be achieved when the RN is at most 80 μm and 500 μm away from the TN respectively. This indicates the possibility of increasing the effective communication range by using the *variable threshold*-based detection approach in CEMC. Table 6.2 shows the increases in effective communication ranges by using the *variable threshold*-based detection scheme in CEMC such that in all the transmission data rates it is possible to have an extended communication range by using the *variable threshold*-based detection approach. However, the increase in effective communication ranges becomes less when the transmission data rate of the system is higher, which is mainly due to the fact that the RN cannot cope with the TN in decoding the bits correctly when the transmission data rate is higher. The chosen transmission data rates are in accordance with the previously published results [MAH-11c].

As shown in Figs. 6.7(a)–6.7(d), when r is comparatively shorter, the RN can avoid the complexity in the detection process by choosing the *fixed threshold*-based detection scheme. In such cases, at short distances, the difference between $\mu_{s_{\mathrm{SCK}}}$ and μ_{ISI} is big and the RN can distinguish between 1 and 0 comparatively easily. However, in those cases, the variable threshold-based scheme computes the threshold as a function of $\mu_{s_{\mathrm{SCK}}}$, μ_{ISI}, and the length of the bit sequence that is transmitted at a time. Therefore, when the memory size is very small, e.g. < 10, there arises a probability of getting all the bits in memory to be 0, which contributes to the BER by producing an undefined threshold value as per Eq. (6.28). Thus, at short communication ranges, *variable threshold*-based schemes would be carefully selected, if necessary, by choosing the memory size appropriately for a given communication range, whereas in other cases, in short communication ranges, *fixed threshold*-based detection scheme may be used.

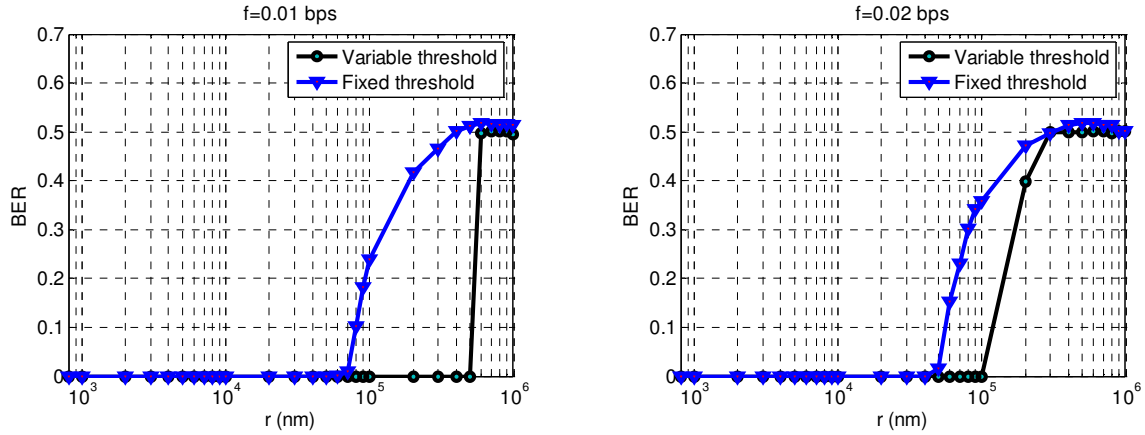

(a) $f = 0.01$ bps (b) $f = 0.02$ bps

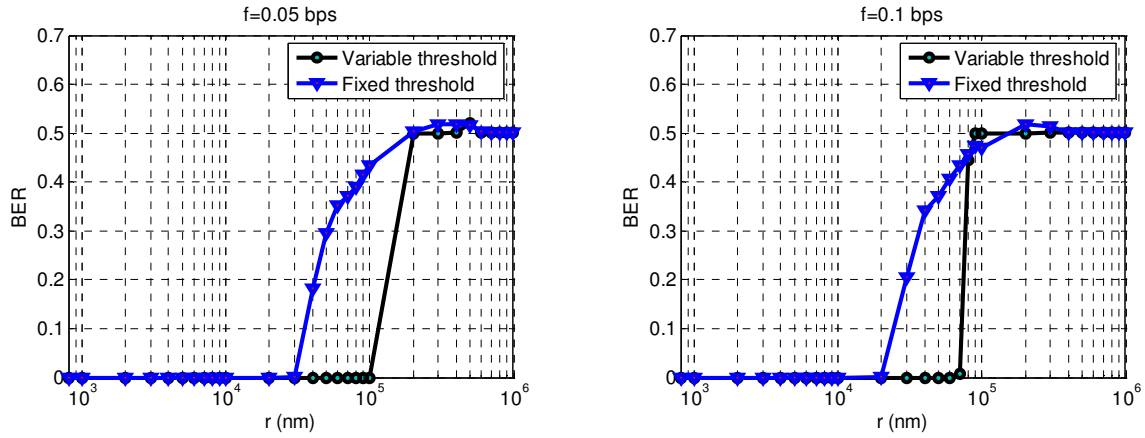

(c) $f = 0.05$ bps (d) $f = 0.1$ bps

Figure 6.7 BER performance of strength-based optimum detector based on SCK with $N = 1$ over different TN-RN distances and transmission data rates. *Full complexity variable threshold*-based detection scheme is considered, where memory size is 999 and the length of the bit sequence is 1000, i.e. providing the maximum memory size and maximum complexity in the RN.

Table 6.2 Possibility of increased communication range with *variable threshold*-based detection scheme and maximum memory size.

f (bps)	The value of r up to which all bits can be decoded correctly (i.e. BER = 0)	
	Fixed threshold-based scheme	Variable threshold-based scheme
0.01	70 µm	500 µm
0.02	40 µm	100 µm
0.05	30 µm	100 µm
0.1	20 µm	60 µm

6.6 Feasibility and Design of Variable Threshold-based Detector

In this section, we first provide the description of *variable threshold*-based detection scheme blocks, and then discuss its feasibility in design as well as possibilities with bionanomachines. We also explain the functionality of the detector block and show techniques to achieve it.

6.6.1 Description of the Detector Block Components

In order to implement the detector, as shown in Eq. (6.14) and Figure 6.4, the RN needs the following functionalities.

A **concentration measurement (CM)** block consists of RN, e.g. a biological entity, and can sense the concentration signal intensity continually, as shown in [BER-77].

A **square operation (SQ)** block makes a response to the effect of the square of the signal at the RN. As shown in [SCH-93], it may be possible to have an effect at the inside of a bionanonachine that is a function of the signal at the input to the receptors of the RN. Therefore, it is anticipated that the squarer function need not be exactly squaring the number of molecules; it can rather generate an effect proportional to the square of the concentration of molecules at the RN. In addition, as shown in [SCH-93], it has been experimentally demonstrated that the extra-cellular agonist[16] concentration can encode the biological information and transmit it to the intra-cellular calcium oscillations by providing variations in calcium amplitude and frequency. This means that extra-cellular agonist signaling corresponds to intra-cellular calcium signaling [SCH-93]. So, there exists an experimental mapping between the two. For this reason, it is likely that the intra-cellular effect may be expressed as a function of the extra-cellular agonist concentration.

A **summation (SU)** block may be a full adder implemented with logic functions in biological nanonachines [NAK-11a], depending on the number of previous symbols that would be considered. The detector structure would need two summation blocks, one for summing the squares of the observations, and the other for summing the ISI-producing molecules originating from the previous symbols. The former summation block is not necessary when the detector is based upon one sample (i.e. observation) only. Note that in

[16] Hormone or any other molecules.

the case of a single sample strength-based detection based on SCK, the squarer block followed by a threshold comparator can be reduced in design to a threshold comparator only that compares the concentration strength with the *square-root* of the detection threshold, since there is no SU block in the case of a single-sample strength-based detection.

Threshold computation (TH) block computes the threshold based on the contributions from the previous symbols. As a result, the threshold computation block needs memory as per the requirement that can also be adjusted based on the need of the scenario under investigation. As shown in Fig. 6.2, although the ISI caused by the previous symbol dominates, the ISI contributions from the symbols prior to the immediately previous symbol are also significant in computing the threshold. When the number of previous symbols that are considered in the RN is comparatively large (e.g. > 10), the BER performance becomes better than when the same becomes comparatively smaller (e.g. < 10). However, as memory size (in terms of the previous symbols) increases, the complexity in the RN to compute the threshold increases and, therefore, demands more computations in the RN. Similarly, smaller memory size requires less number of computations and simpler RN, but does not provide better BER results. The TH block can be implemented as shown in Fig. 6.8 below.

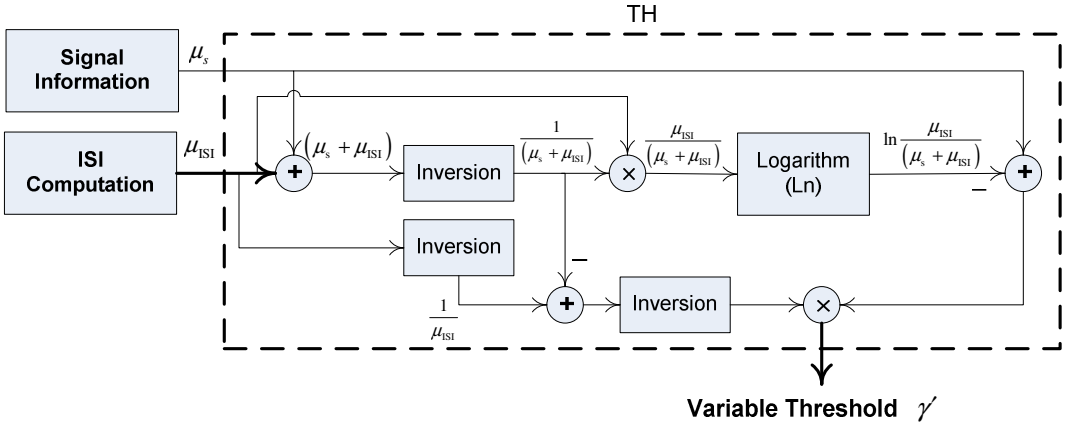

Figure 6.8 Structure of the threshold computation (TH) block. For the sake of visual clarity, the sub-subscript "$_{SCK}$" has been dropped from the quantity $\mu_{s_{SCK}}$ in this figure.

The TH block receives input from two sub-blocks, namely, the **Signal Information (SI)** block and the **ISI Computation (ISIC)** block. SI block stores the information of the deterministic number of information molecules, from where the RN fetches the required

value of $\mu_{s_{\text{SCK}}}$ in the process to compute the variable threshold. ISIC block computes the strength of the ISI, i.e. μ_{ISI} through a series of addition and multiplication operations using the symbol-wise probabilities stored in its memory and the previous symbols detected by the detector, in the process to compute the variable threshold.

For μ_{ISI} to be the correct estimate of the ISI-producing molecules present at the RN, the previously detected symbols need to be correctly determined. Therefore, the performance is limited by the ability of the detector in detecting the previous symbols correctly. Using, Eqs. (6.1)–(6.3), (6.5), and (6.8), μ_{ISI} at the i-th bit can be expressed as

$$\mu_{\text{ISI}}(i) = \sum_{j=1}^{i-1} b_{i-j}\mu_{n_{\text{SCK},j}} \Leftrightarrow \sum_{j=1}^{i-1} b_{i-j} n_{\text{SCK},j} \text{ , where } i \text{ is a positive integer.} \tag{6.29}$$

When $i = 1$, there is no previously transmitted symbol and so no computation is necessary to determine $\mu_{\text{ISI}}(1)$. However, for $i \geq 2$, where i is a positive integer, the computations necessary to determine μ_{ISI} are shown in Table 6.3. Therefore, it is understood that, as i increases, the numbers of *multiplication* and *summation* operations increase, which require more computations when the index i is large, due to the increased number of previously transmitted symbols considered in the computation of the ISI-producing molecules.

Finally, a **threshold comparator (THC)** block compares the square of the concentration signal intensity to the threshold γ' of detection. Both TH and THC blocks are shown as combined in Fig. 6.4. In view of the available literature [NAK-11a], it can be hoped that the basic computation blocks, e.g. *summation*, *multiplication*, and *comparator* blocks, can possibly be built by using biological logic functions.

Table 6.3 Number of *multiplication* and *summation* operations required to compute the ISI at i-th symbol.

Symbol index i	ISI-producing reactions $\mu_{\text{ISI}}(i)$	# Multiplications	# Summations
$i=1$	$\mu_{\text{ISI}}(1)=0$	0	0
$i=2$	$\mu_{\text{ISI}}(2)=b_1 n_{\text{SCK},1}$	1	0
$i=3$	$\mu_{\text{ISI}}(3)=b_2 n_{\text{SCK},1}+b_1 n_{\text{SCK},2}$	2	1
$i=4$	$\mu_{\text{ISI}}(4)=b_3 n_{\text{SCK},1}+b_2 n_{\text{SCK},2}+b_1 n_{\text{SCK},3}$	3	2
…	…	…	…
i	$\mu_{\text{ISI}}(i)=\sum_{j=1}^{i-1} b_{i-j} n_{\text{SCK},j}$ $=b_{i-1} n_{\text{SCK},1}+b_{i-2} n_{\text{SCK},2}+\ldots+b_2 n_{\text{SCK},i-2}+b_1 n_{\text{SCK},i-1}$	$(i-1)$	$(i-2)$

6.6.2 Possibilities of Computation Reduction

(a) Techniques related to receiver signal processing

The first approach that we would consider in reducing the computational burden and, therefore, the complexity of the proposed detector is through reducing the number of previous symbols that the RN would consider in estimating μ_{ISI}. We believe that this would be a viable option because as seen from Fig. 6.1(b), the effect of the immediately previous bit is the most significant on producing the ISI at the RN. So, as a first step of reducing the computation burden, we focus on limiting the number of previous symbols that the RN would consider to a smaller value. We focused on the fundamental modeling of the detector based on concentration signal strength and the chemical reactions produced by the SCK process at the RN. Therefore, our focus is not on the formal evaluation of the specific computational requirements at the RN, but principally on the structure of the detector and correspondingly, the BER performance of the variable threshold-based detector compared to fixed threshold-based detector at the RN. Therefore, we provide a preliminary investigation on the computational requirement including a description of the detector functionalities required at the RN, as well as a comparison of performance in terms of the *fixed threshold*-based, *full complexity variable threshold*-based, and *reduced complexity variable threshold*-based detectors.

Full complexity variable threshold-based detector processes the ISI-producing molecules from all the previous symbols. *Reduced complexity variable threshold*-based detector processes the ISI-producing molecules from a smaller number of previously

transmitted symbols in order to detect the current symbol. Such an approach using reduced number of transmitted symbols would be reasonable enough in terms of the study of complexity versus BER performance of the detector. In addition, since the performance of the detector also depends on the involvement of the receiving nanomachine's capability to implement the detection circuitry using the biological components, we also include a discussion on the possibilities of the bio-inspired design of the detector using biological nanomachines, e.g. a biological cell.

Figure 6.9 shows the performance of the reduced complexity variable threshold-based detector as compared to the full complexity variable threshold-based detector at transmission data rates of 0.01 bps, 0.02 bps, 0.05 bps, and 0.1 bps. The performance of variable threshold-based detector depends on the length of the bit sequence that is being transmitted. As shown in Fig. 6.9, for lower data rates, e.g. 0.01 bps (i.e. when $T_b = 100$ s), the communication range $r_{\text{BER=0}}$ up to which the RN can detect all the bits correctly (i.e. BER = 0) increases, compared to other scenarios when data rates are higher. Please note that in this chapter BER = 0 in fact means that the simulation results indicate BER approaching zero in this case. Recall the comments regarding this in chapter 4.

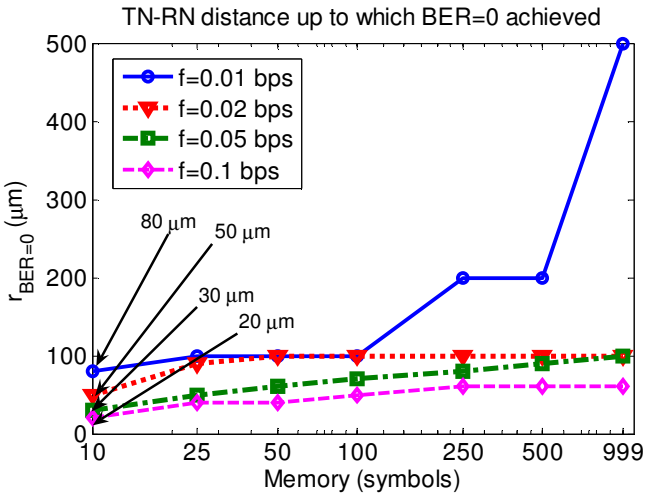

Figure 6.9 Performance of the reduced-complexity variable threshold-based detector at various transmission data rates.

The increase in $r_{\text{BER=0}}$ as shown in Fig. 6.9 indicates the possibility of increased communication range by using lower transmission data rates when the memory size is kept fixed, or adopting higher memory size when the transmission data rate is kept fixed. Using

lower transmission rates reduces the communication speed between the communicating nanomachines. Adopting a higher memory size increases the complexity of the RN to detect the symbols and hence requires a higher complexity in the design of the RN. We consider a random sequence of 1000 bits being transmitted by the TN in each simulation run with a total of 100 simulation runs, and, therefore, using the full complexity variable threshold-based detector scheme, the RN would require the threshold at the 1000^{th} transmitted bit to be computed using all the 999 previous bits of the bit sequence. As a result, the maximum memory size shown in Fig. 6.9 is 999. Figure 6.9 shows only the communication range up to which the RN can detect all the bits correctly with zero BER.

While Table 6.2 compares the fixed threshold-based detection scheme with full complexity variable threshold-based scheme, it can be seen from Fig. 6.9 that by reducing the memory size of the RN, it is also possible to achieve a communication range larger than that of the fixed threshold-based scheme but smaller than the same at full complexity variable threshold-based scheme, however, at a comparatively lower complexity in the detection processing circuitry at RN. For example, when memory length is that of 10 symbols, as shown in Fig. 6.9, although 0.05 bps and 0.1 bps schemes do not provide improvements in communication range compared to *fixed threshold*-based scheme, when data rate decreases below 0.05 bps, there is a significant improvement in the communication range compared to the *fixed threshold*-based scheme. However, if the communication range of operation increases beyond $r_{\text{BER=0}}$ at any particular setting, the BER performance depends on the data rate and the memory size, as will be shown in Fig. 6.10.

Figure 6.10 shows the BER performance of the variable threshold-based detector at extremely large communication ranges, when BER is found to be non-zero and varying according to TN-RN distance and memory size. An explanation of such cases is important in the sense that it provides the performance of the CEMC system when communication range needs to be increased. As shown in Figs. 6.10(a)–(d), $r_{\text{BER=0}}$, i.e. the communication ranges up to which BER is found to be zero, decreases as transmission data rate increases. The starting distances in the horizontal axes in Figs 6.10(a)–(d) are corresponding to the $r_{\text{BER=0}}$ values found in Fig. 6.9. When *r* is kept unchanged, reducing the memory size reduces the ISI-producing molecules being considered at the RN and thus reduces the threshold of

detection, as shown in Eq. (6.28). As a result, the RN incorrectly detects more bits as 1 when 0 may be true, thereby, increasing the BER.

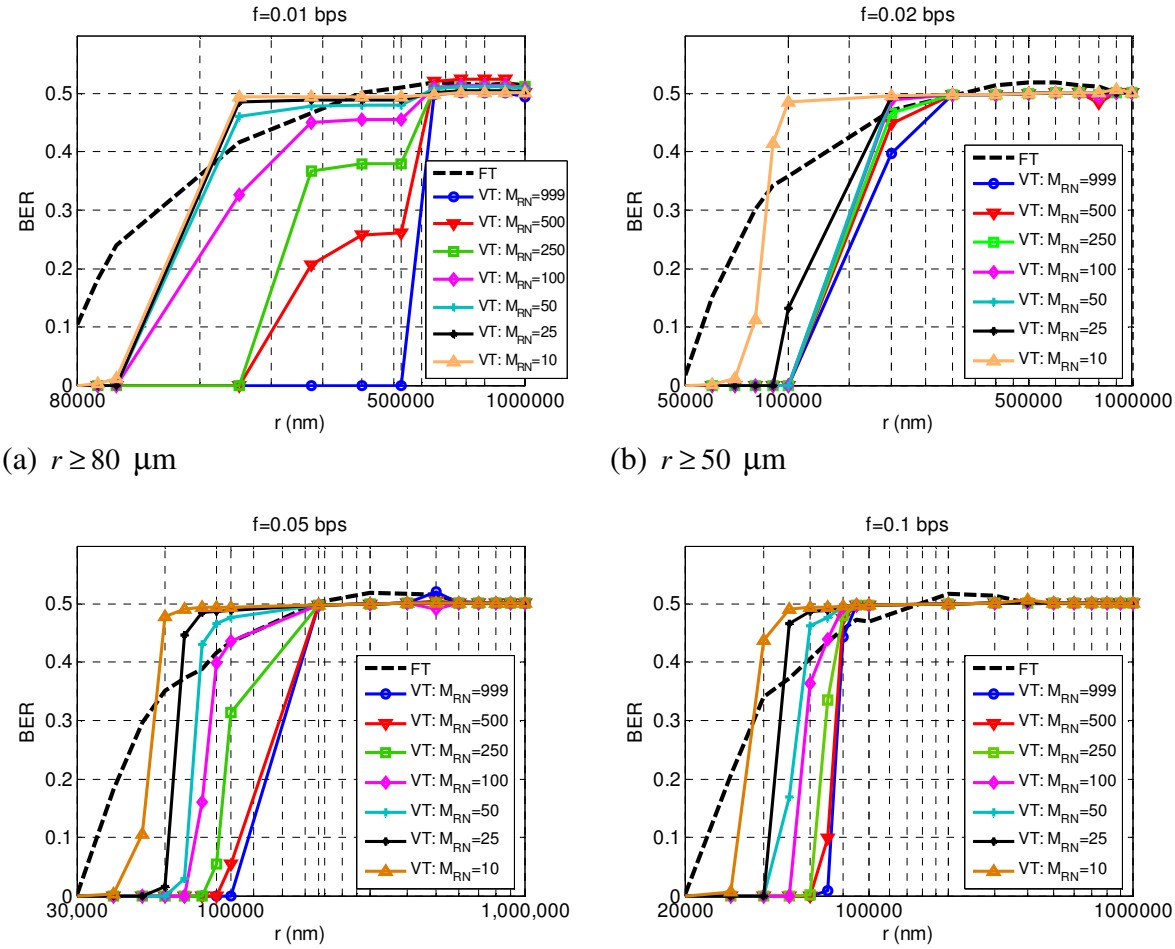

(a) $r \geq 80$ μm (b) $r \geq 50$ μm

(c) $r \geq 30$ μm (d) $r \geq 20$ μm

Figure 6.10 Performance of the reduced-complexity variable threshold-based detector at extremely large communication ranges. The communication ranges considered here are greater than the corresponding ones from Fig. 6.9. In this figure, FT, VT, and M_{RN} denote fixed threshold, variable threshold, and memory size respectively.

(b) By engineering the RN

Although an individual nanomachine is of limited capacity, the recent developments of engineered nanomachines [NAK-11a] [OZI-05] show a bright future for molecular nanonetworks [NAK-12] [AKY-08] [NAK-11a]. At the same time, in view of the current progresses on engineered nanomachines, it can be expected that advanced technologies of the future would promisingly be able to perform the required amount of tasks in implementing the variable threshold-based detector. For example, programmable molecular nanomachines [ATA-10] can be envisioned to perform the required tasks of the detector. In

addition, a network of communication nanomachines can be programmed to share information within a nanonetwork so that they can perform more complex tasks by sharing information among them [ATA-10]. Although the power-handling capacity of each nanomachine is very small requiring them to be very limited in tasks performed, genetic programming has opened the doors to *engineered nanomachines* [NAK-11a] in a much greater detail today than what was in the last decade. In addition, logic functions can be implemented today by using biological nanaomachines [NAK-11a].

It is now possible to engineer nanomachines to do required and controlled tasks, e.g. to achieve synchronization between the TN and the RN [MOO-07] [MOO-11] and control the release rate of molecules such that concentration-based modulation schemes become possible [SCH-93] [NAK-11a]. It is also possible to develop logic gates by using Belousov-Zhabotinsky (BZ) reactions [MOO-07], realize impulsive passive transportation and intercellular passive transportation [MOO-07], and produce some required functionalities in biological cells by applying genetic engineering [NAK-11a]. DNA logic gates can also be built by using single- and double-stranded DNA [KRO-11]. A square root operation circuit based on different DNA molecules has also been built by using molecular nanotechnology [KRO-11]. Therefore, based on a review of the available literature, all of the operational building blocks in the variable threshold-based detector can possibly be implemented by using the logical circuitry implemented with biological nanomachines and bio-materials. For instance, see [NAK-11a] for a detailed account of how an RN can be engineered in order to materialize MC.

(c) Networks of nanomachines

As mentioned above, since nanomachines in a nanonetwork can share information, it can be anticipated that in order to implement the detection functionality at the RN, if an individual nanomachine cannot implement the detector alone, if required, a nanonetwork of nanomachines can share the information among them, coordinate, and implement the detector functionality. In nature, coordinated action of biological nanomachines is quite common, e.g. biological cells in body tissues work cooperatively in order to perform specific task. Therefore, detection processing by a group of *networked* nanomachines also holds a bright prospect and may possibly help implement the signal detector in order to ensure reliable CEMC. In addition, with a similar analogy this can also be applicable to

components of an individual nanomachine, for example, the cellular organelles that can be in a network to implement the strength-based signal detector. However, this can be considered as an open area of research in this field.

6.7 Conclusion

In this chapter, strength-based optimum receiver architecture of pulse-transmitted OOK CEMC system has been presented by incorporating the stochastic molecule-receptor binding based on SCK between information molecules and receptors of the RN. The mathematical model of the receiver has been developed and the corresponding ROC curves have been presented. The proposed *variable threshold*-based optimum detection scheme shows that it is possible to increase the effective communication range by incorporating the effects of ISI in the calculation of the threshold on per symbol basis. The receiver model and the corresponding analyses presented in this chapter should be useful in evaluating the performance of the diffusion-based CEMC system under stochastic molecule-receptor binding mechanism based on SCK.

Chapter 7: Convolutional Coding Techniques in PAM CEMC

7.1 Introduction

In this chapter, we investigate the performance of convolutional coding techniques in ideal diffusion-based CEMC channel with PAM transmission scheme. Convolutional codes have shown to provide a significant amount of gain in the SIR between a pair of communicating nanomachines, and thus help increase the communication range and improve the end-to-end BER performance. We have also determined the impact of convolutional codes (CC) for several key performance factors, e.g. transmission data rate, communication range, and the constraint length of the convolutional code in the context of diffusion-based CEMC. In addition, we have compared the PAM system with the IM system in CEMC. We have found that the use of multilevel (M-ary) signaling scheme in CEMC system provides a degraded BER performance even in short communication ranges. Therefore, a convolutional coded scheme with larger alphabet size should not be recommended for CEMC system because of the stronger ISI produced within symbols. As an alternative, a convolutional coded scheme with binary alphabet and higher symbol rate was evaluated and found to provide a gain in the SIR of the system, and is, therefore, recommended for short-to-medium range CEMC. For long communication ranges, an uncoded system can be preferred over convolutional coded schemes.

In general, coding is applied in a communication system mainly for two reasons: *line coding* is used to control the power spectrum of the transmitted signal, whereas *channel coding* is used to detect and/or correct symbol errors in communication. In channel coding, CC has long been used in numerous applications, e.g. mobile communications, satellite communications, and digital video, in order to ensure reliable communication between the transmitter and the receiver. However, so far CC has not been considered for use in CEMC. This gives us the impetus to use CC in CEMC system.

Signal attenuation is a major challenge in diffusion-based CEMC system, and, therefore, any technique that can possibly increase the signal strength and communication range would be desired. Since CEMC suffers from the effects of ISI, in this chapter we address the issue of increasing effective communication range by applying the concepts of channel coding in CEMC system. To the best of our knowledge, our work on the application of convolutional

coding techniques in PAM CEMC system is one of first few works in this area that has explained the BER performance of the CEMC system in detail. In this chapter, the possibility of using CC in the diffusion-based CEMC channel has been explored. At the receiver a hard decision decoder is used. Coding schemes add redundant information bits in the transmitted bit sequence. This requires transmission using higher rate and/or a larger alphabet size.

Our results presented in this chapter have been published in [MAH-13d]. The main contributions of this chapter are the following:

- The concepts of convolutional codes applied to diffusion-based CEMC channel have been introduced. We show the performance of the convolutional codes especially in increasing the effective communication range based on the gain in the SIR.
- Through an in-depth performance analysis it has been shown that a potential benefit of applying convolutional coding at the TN in diffusion-based CEMC system is that effective communication ranges for a given BER can be increased. Performances of a simple convolutional encoder (CE) system with M = 2 (binary) and M = 4 (quaternary) amplitude levels have been investigated and compared in this regard.

The chapter is organized as follows: Section 7.2 presents the related work. Section 7.3 discusses the system model overview and the performance metrics used to analyze the impact on the system performance. Results obtained on BER performance at various scenarios are discussed in Section 7.4. Section 7.5 provides a brief description of the possibilities of developing the CE and decoder architectures required for the CEMC by using biological nanomachines. Finally, Section 7.6 concludes the chapter with a summary of the findings and future possibilities of this work. Since MC is a truly interdisciplinary research field, considering the readers with a good diversity of backgrounds, we also provide some fundamentals of CC in Appendix A.

7.2 Related Work

In literature, our work published in [MAH-13d] is one of the earliest works that investigated the use of convolutional coding scheme in PAM CEMC in ideal (i.e. free) diffusion-based propagation environment and explained its impact on the BER performance of the CEMC system. Apart from this, channel coding in the case of MC has also been reported in [LEE-

12] and [LEE-12a] that focused on the energy budget issue of simple block codes (hamming codes) with impulsive transmission of molecules. In [SHI-13], a new family of channel codes, namely, *ISI-free codes,* has been investigated for diffusion-based MC where bits 0 and 1 are represented by two distinguishable types of molecules and the molecules under Brownian motion with drift velocity are removed from the system upon their first hit at the RN. ISI-free channel codes have also been investigated in [SHI-12] where a system model similar to that reported in [SHI-13] has been assumed.

The works in [LEE-12], [LEE-12a], [SHI-12], and [SHI-13] are different from our work presented in this chapter in the sense that we consider convolutional coding with PAM scheme for ideal (i.e. free) diffusion process and focus on the BER performance based on diffusion dynamics of the system. In our system model, we consider ideal (i.e. free) diffusion of molecules where the molecules can propagate freely even after they first hit the RN, hence none of the molecules are removed from the system after they first hit the RN.

7.3 System Model Overview for Convolutional Coded OOK-based CEMC

In order to evaluate the performance of the CE systems in CEMC, we consider the system model as shown in Section 3.3. As the system has been described in detail in Chapter 3, the same is not re-described in this chapter. In order to evaluate the BER performance of the CE systems in diffusion-based CEMC channel, a random sequence of bits, which is modulated with OOK type of PAM scheme, is transmitted by the TN and the total number of desired (i.e. "signal") molecules and undesired (i.e. "interference") molecules are calculated during each symbol duration over the entire observation time $T_{\text{obs}} = N_b T_b$ where N_b is the total number of bits in the random bit sequence and T_b is the duration of each symbol[17] (or "bit" if the scheme is binary). When a random sequence of bits is transmitted in the CEMC channel, the *desired* and the *undesired* strengths of molecules at the current symbol can be computed as shown for the *bit sequence transmission* in Section 3.6.

As shown in Section 3.6, E_S and E_I can be expressed as a fraction of the E_U and denoted as $S_{(r,f)}$ and $I_{(r,f)}$ respectively as shown in Eq. (7.1). The $S_{(r,f)}$ and $I_{(r,f)}$ are functions of TN-RN distance r and transmission data rate f.

[17] For binary scheme a "symbol" is represented by a '1' or '0' bit, whereas a symbol comprises of $\log_2 M$ bits in M-ary scheme. M denotes the alphabet size of the system.

$$S_{(r,f)} = \frac{E_S}{E_U} \text{ and } I_{(r,f)} = \frac{E_I}{E_U}. \tag{7.1}$$

This yields the following metric named *approximate signal to interference strength ratio* denoted as $\widetilde{SIR}_{(r,f)}$ as shown in Eq. (7.2).

$$\widetilde{SIR}_{(r,f)} = 10\log_{10}\left(\frac{S_{(r,f)}}{I_{(r,f)}}\right) = 10\log_{10}\left(\frac{E_S}{E_I}\right) \text{dB}. \tag{7.2}$$

In this chapter, for convenience we prefer to use $\widetilde{SIR}_{(r,f)}$ as the metric for comparing the performance of the CE schemes with that of the uncoded scheme. In addition, in this case the encoded symbols are detected by using the strength-based detection (ED) method that accumulates the total number of molecules on average during a symbol duration and then decides in favour of a particular symbol by comparing the accumulated number of molecules with a predefined threshold. The concept and the functionality of such an ED method has been reported in our earlier works [MAH-11b].

Clearly, the quantity $\widetilde{SIR}_{(r,f)}$ is also a function of both *r* and *f*. The characteristics of this quantity are explained in detail in Section 7.4. We compare the performance of an uncoded system with that of a CE system (with 2 schemes) by considering the gain in $\widetilde{SIR}_{(r,f)}$ received by using a CE system compared to using an uncoded system for achieving a required BER value at a given TN-RN distance and a given transmission data rate. Alternatively, since each value of the $\widetilde{SIR}_{(r,f)}$ is computed for a particular TN-RN distance and transmission data rate, a gain in the $\widetilde{SIR}_{(r,f)}$ would indicate an improvement in communication range by using a CE system compared to using an uncoded system. Since the $\widetilde{SIR}_{(r,f)}$ incorporates the available molecules that interfere with the decoding of the current bit, this is a useful and convenient measure that indicates the ISI level of the system for a given set of system parameters.

However, in addition, the reader should note that the information molecules (of single type) undergo free diffusion in the unbounded propagation medium, and so the metric $\widetilde{SIR}_{(r,f)}$ does not guarantee that all the molecules received by the RN during the current symbol duration belong exactly to the transmitted signal from the TN during the same (current) symbol duration, rather the received molecules constituting the E_S portion (refer to

Eq. (7.1)) may contain some molecules originating from the previous symbols and thus also constitute the ISI in the E_S portion as well. E_I consists of the interfering molecules only from all the previous symbols when the currently received signal intensity $U(r,t)$ is larger than the $Q(t)$.

The definitions of $s_{approx}(t)$ and $i_{approx}(t)$ shown in Section 3.6, see Eq. (3.13), allow us to compute a "non-exact" or "fractional" amount of residual molecules that were originated from the previous symbol durations and that are present during the current symbol duration. By observing the definition of the $i_{approx}(t)$ in Eq. (3.13) we can find that the signal intensity is considered as interference only when it is greater than the transmission rate of molecules during the current symbol duration. Although the received desired signal intensity may (and possibly will) contain information molecules that are contributed by the earlier transmissions during previous symbol durations, the received signal intensity is not considered as interference as long as it is less than the $Q(t)$. Note that the received signal intensity is composed of both the desired signal intended for the current symbol and the interference signal originated from the previous symbol transmissions. Since the RN in this simple signaling and reception model shown in this chapter cannot distinguish between molecules specific to the current and the previous symbol transmissions, the RN only accumulates the total number of molecules during specific symbol duration and compares it with a preset threshold in order to detect the transmitted symbol.

Therefore, although the indication of the ISI level using the metric $\widetilde{SIR}_{(r,f)}$ is not exact, it gives a reasonable estimate of the effective signal strength taking into the effects of the ISI. The received molecules that not only cause the ISI but also constitute the E_S portion of E_U can be estimated by the approaches reported in [MAH-11] and [MAH-12a]. It is simple for the RN to compute the $\widetilde{SIR}_{(r,f)}$, without having to compute the individual interference signal portions contributed by all the previous symbol transmissions. This reduces the computational burden on the RN. In addition, when comparing the performances of the uncoded and the channel-coded CEMC systems, the gain in $\widetilde{SIR}_{(r,f)}$ (in dB) was investigated. As a result, we believe that the metric $\widetilde{SIR}_{(r,f)}$ is reasonable enough [MAH-11] [MAH-12a] to be used in evaluating the performances of the CE systems considered in this chapter. In addition, this tells us that BER versus $\widetilde{SIR}_{(r,f)}$ characteristics are, therefore,

necessary and this would provide us with the idea of how the residual molecules that are considered as the desired signal intensity during the calculation of the E_S impact the BER of the system. BER versus $\widetilde{SIR}_{(r,f)}$ characteristics curves will be used throughout this chapter in order to evaluate the CE systems through numerical simulations. The quantity $\widetilde{SIR}_{(r,f)}$ is different from the quantity SIR in Chapter 6 in that the latter denotes the exact value of signal to interference strength ratio, whereas the former denotes the approximate value of the same.

7.4 Performance Evaluation

We first describe the setup for the simulation experiment, which is followed by the simulation results obtained from the experiments with a randomly generated bit sequence. The results have been presented in two sections: first, the behaviour of the uncoded system is explained for various input bit rates, and then the key results of the CE systems are presented. In this chapter, although the channel encoder will principally be based on CE system [LIN-83], we also use simple block encoder (BE) as channel encoder just for comparison purposes with the performance of the CE systems. In this work, Viterbi decoding is used in detecting the message at the output of the CEMC channel. See Appendix A for the related basics of CC and its decoding fundamentals.

7.4.1 Simulation Setup

Each simulation experiment is conducted for a randomly generated bit sequence of 100,000 bits with various bit rates ranging from 0.01 bps to 0.1 bps, which gives an observation time of approximately 2778 simulated hours (10,000,000 seconds) and 278 simulated hours (1,000,000 seconds) for the former and the latter cases respectively. Rate ½ convolutional codes with constraint lengths of 2, 3, and 4 are considered for the CE system. To accommodate redundant bits in the CE system two schemes are followed:

- the first scheme uses the M-PAM with M = 4 amplitude levels (i.e. quaternary) with the same symbol rate as that of the uncoded system, and
- the second scheme uses 2-PAM with M = 2 amplitude levels (i.e. binary) with the symbol rate twice as much as that of the uncoded system.

The communication ranges r simulated are in the range from 800 nm to 1 mm for diffusion-based short-range, medium-range, and long-range CEMC as reported in our earlier works [MAH-10b] as shown in Chapter 3. The chosen transmission bit rates in the range from 0.01 bps to 0.1 bps have been shown previously in [MAH-11c] as biologically meaningful transmission data rates for CEMC. The chosen value of D of small size molecules in water medium is 10^{-6} cm^2/s [LAC-09] [MAH-10b].

7.4.2 Performance of the CE Systems

The BER versus $\widetilde{SIR}$ results at various transmission data rates for the uncoded system, the CE system with M = 2 levels, and the CE system with M = 4 levels have been shown in Fig. 7.1(a) in magenta, red, and blue sets of curves respectively. According to Fig. 7.1(a), the BER versus received $\widetilde{SIR}$ characteristics show similar patterns at different transmission bit rates of 0.01, 0.02, 0.05, and 0.1 bps. In the uncoded binary sequence, each symbol is a binary 1 or 0 and when the TN and the RN come closer to each other, the $\widetilde{SIR}$ increases and the BER decreases, meaning that a smaller portion of the received signal interferes with the decoding of the current symbol and thus constitutes less ISI. As a result, more signal energy constitutes the detection variable of the strength-based detection, which reduces the BER. A higher $\widetilde{SIR}$ is found when the RN is located comparatively closer to the TN and vice versa. The CIR of the concentration-encoded signal experiences temporal spreading and concentration attenuation loss in the diffusion-based propagation [MAH-10a], meaning that increasing the data rate (i.e. decreasing the symbol duration) may not receive enough molecules and so may cause more ISI at the RN. According to Fig. 7.1(a), when redundancy is provided in the transmitted bits it can be concluded from Fig. 7.1(a) that a CE system with higher M but with the same symbol rate as that of the uncoded system (i.e. blue curves in Fig. 7.1(a)) would definitely be a wrong choice from the BER point of view when compared with the CE system with M = 2 but with higher symbol rate (i.e. red curves in Fig. 7.1(a)). This also concludes that higher amplitude levels in 4-PAM signaling (i.e. when M = 4) provides higher BER compared to the 2-PAM (i.e. when M = 2) for any $\widetilde{SIR}$ level. In this analysis each $\widetilde{SIR}$ value is calculated at a location r of the RN and at a given data rate f by

computing the received desired and interference signal strengths as shown in Section 3.6, see Eq. (3.13).

As noted in [MAH-10a], when communication range increases there incurs concentration attenuation, and as a result, according to the definitions used in this chapter, the $\widetilde{SIR}$ decreases. The reader should note that in this analysis a decrease in the $\widetilde{SIR}$ will correspond to a scenario when the TN and the RN are located comparatively farther from each other. Therefore, each point of the horizontal axis in Figs. 7.1(a)–(c) corresponding to an $\widetilde{SIR}$ value will actually indicate a communication range for which the $\widetilde{SIR}$ has been calculated. As shown in Fig. 7.1(a) at f = 0.01 bps, for example, if a BER value of 10^{-2} is required at the RN, the $\widetilde{SIR}$ computed for the uncoded system (i.e. the magenta color curve with circle marks) and the CE system with M = 2 levels (the red color curve with circle marks) are approximately 5 dB and 4 dB respectively. This means that when the required BER is same (i.e. 10^{-2} here) the CE system with M = 2 levels can achieve the same BER at a TN-RN distance larger than that of an uncoded system. In other words, approximately 1 dB of $\widetilde{SIR}$ can be saved by using the CE system with M = 2 levels compared to using the uncoded system mentioned above. Thus, approximately 1 dB of $\widetilde{SIR}$ gain is possible by using the 2-PAM CE scheme with double the symbol rate. The observed ~1 dB gain in $\widetilde{SIR}$ by using the 2-PAM CE scheme can surely be translated to an increase of communication range, meaning that the TN can increase the communication range by using the 2-PAM CE scheme. This is unlike the case when f = 0.01 bps with 4-PAM CE scheme with the same symbol rate as that of the uncoded system where a BER value of 10^{-2} is not achievable at all because of the fact that a high level of ISI is present. The gain in the $\widetilde{SIR}$ is also dependent on the transmission data rate of the system. When the transmission data rate increases it means that the communication symbols have smaller symbol durations. The results for various transmission data rates as shown in Fig. 7.1(a) can be useful in determining the gain in $\widetilde{SIR}$ in the similar way when the transmission data rate of the system varies. Similar results for various constraint lengths of the CE system have been shown in Figs. 7.1(b) and 7.1(c) for transmission data rates f = 0.05 bps and f = 0.1 bps respectively.

The CE system with M = 2 amplitude levels as shown in Fig. 7.1(a) provides a better performance than the uncoded system especially in the comparatively higher $\widetilde{SIR}$ region,

e.g. above a cross-over[18] $\widetilde{SIR}$ of approximately 3 dB as shown in Fig. 7.1(a). For instance, when $\widetilde{SIR}$ = 4 dB, the uncoded system and the CE system with M = 2 give BER of 5×10^{-2} and 1×10^{-2} respectively at f = 0.01 bps. When the $\widetilde{SIR}$ increases further, the BER achievable by using the CE system with M = 2 drops sharply, meaning that it is possible to get better performance with a CE system with M = 2 at these comparatively higher $\widetilde{SIR}$ region when the TN and the RN are comparatively closer to each other.

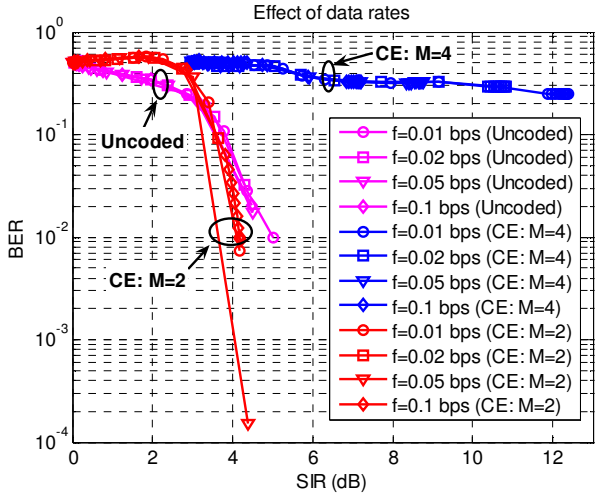

(a)

[18] By *cross-over* $\widetilde{SIR}$ we mean that at approximately 3 dB the performance curves of the uncoded system and the CE system with M = 2 cross over. Correspondingly, for $\widetilde{SIR}$ > ~3 dB the performance of 2-PAM CE system with M = 2 levels is better than that of the uncoded system, and for $\widetilde{SIR}$ < ~3 dB the performance of the 2-PAM CE system with M = 2 levels is worse than that of the uncoded system. The cross-over point at $\widetilde{SIR}$ = 3 dB indicates the condition when $E_S = 2E_I$ as shown in Eqs. (3.12) and (3.13) and occurs when the *signal strength* is twice as much as the *interference strength*. See [MAH-11] for relevant details.

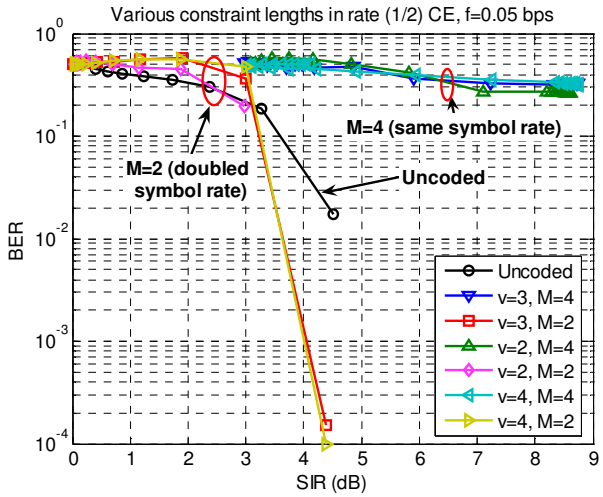

(b)

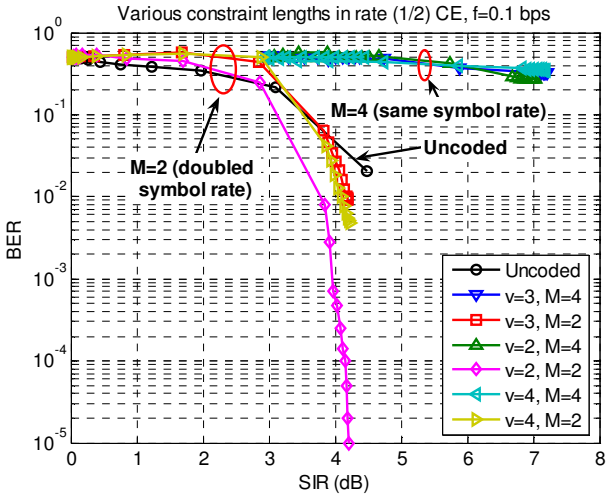

(c)

Figure 7.1 BER performance of an uncoded system and (2,1,3) CE systems with M = 2 and M = 4 amplitude levels with OOK modulation and code generator matrix $GM = \begin{bmatrix} 110 \\ 111 \end{bmatrix}$ (a), the impact of constraint lengths υ at f = 0.05 bps (b) and the impact of constraint lengths υ at f = 0.1 bps (c). In (b) and (c), υ = 2 with $GM = \begin{bmatrix} 11 \\ 10 \end{bmatrix}$, υ = 3 with $GM = \begin{bmatrix} 110 \\ 111 \end{bmatrix}$, and υ = 4 with $GM = \begin{bmatrix} 01111 \\ 10001 \end{bmatrix}$ are considered. The horizontal axis shows the approximate SIR, $\widetilde{SIR}$, at the RN without the symbol "~" for the sake of visual clarity in the figure.

As shown in Fig. 7.1(a), the set of blue curves display the performance of the CE system with M = 4 amplitude levels (i.e. 4-PAM CE system). It is evident from Fig. 7.1(a) that CE system with M = 4 provides worse BER performance than both the uncoded system and the

CE system with M = 2 levels (i.e. 2-PAM CE system). In the CE system with M = 4 levels, the encoder encodes symbols by increasing the alphabet size, meaning that more number of amplitude levels are used to encode a symbol (keeping the symbol rate unchanged). This produces stronger ISI effects in the current symbol duration due to the residual molecules originated from the previous symbol transmissions and, therefore, threshold-based strength detection [MAH-11b] produces higher BER. In CEMC, a single type of information molecules are used to encode symbols and thus the RN accumulates all the molecules it receives during the current symbol duration and cannot distinguish between molecules specific to the current symbol transmission and those from previous symbol transmissions. Thus an increased level of ISI is the main reason of the high BER in the CE system with M = 4 levels.

However, when the $\widetilde{SIR}$ is low, for example, less than approximately 3 dB as shown in Fig. 7.1(a) (i.e. when the TN and the RN are comparatively farther apart) the performance of the uncoded system is better than both of the CE systems with M = 2 and M = 4 levels. Therefore, for large communication ranges convolutional coding may not perform better, rather an uncoded system may be preferred.

Apart from this scenario, as shown in Figs. 7.1(b) and 7.1(c), it has been observed that constraint length has no significant influence on the BER for given values of r and f. The reader should note that choosing a higher value of υ would need more complexity in the molecular encoder circuit and thus higher values of υ are not desired. Increasing the constraint length means increasing the number of memory units in the encoder circuit and so a smaller value of υ is desired in the bio-inspired design of the encoder discussed in Section 7.5. The results shown in Fig. 7.1(b) show that the choice of υ does not impact the $\widetilde{SIR}$ significantly and so $\upsilon = 2$ or $\upsilon = 3$ would be a reasonable choice for the constraint length of the CE provided that a proper consideration to the design complexity of the decoder at the RN has been made. The reader should refer to Appendix A for the code generator structure of the CE.

While the results for the CE system with M = 2 are promising when compared with that of the uncoded system, the same is not true for the CE system with M = 4. The BER versus $\widetilde{SIR}$ curves as shown in Fig. 7.1 are not satisfactory for the CE system with M = 4

amplitude levels. The most significant observation from Fig. 7.1(a) is that the CE system with M = 4 experiences a higher BER in the range approximately from 0.23 to as high as 0.50 in the communication ranges from 800 nm (medium range) up to 60 μm (long range, see [MAH-10b]) respectively because of the fact that using multiple amplitude levels (M = 4) yields more residual molecules that become available at the current symbol duration and thus they add to the undesired ISI-producing molecules while detecting the current symbol, producing a higher BER.

Therefore, it can be concluded that in CEMC system convolutional codes have significant advantages in the sense that communication ranges can be increased by adopting the CE system with M = 2 amplitude levels. It is also found that a CE system with M = 4 amplitude levels performs worse than that with M = 2 amplitude levels or the uncoded system, and can never provide a BER of 10^{-1} or lower. The results also show that the CE system with M = 4 levels does not actually provide any benefit in getting a better BER at long ranges when the SIR is low.

In addition to the results presented above, this chapter also presents some results on an estimation of how much of the $\widetilde{SIR}$ is caused by the residual molecules during any symbol duration. In order to do this we compute only those molecules in the current symbol duration that become available at the RN from the pulse transmitted only at the beginning of the current symbol duration. As a result, all the molecules that originated from the previous symbol durations earlier than the beginning of the current symbol are ignored. Such a technique would give us an idea of how strongly the ISI is impacting the $\widetilde{SIR}$ and thus the BER of the system. In the uncoded system with f = 0.01 bps without the ISI, depending on the chosen r, the RN needs a minimum SIR of 0.94 dB (computed[19] from a single pulse of pulse-width T_b transmitted by the TN and r = 50 μm) in order to detect all the symbols correctly, whereas with the ISI in consideration the RN receives an $\widetilde{SIR}$ of approximately more than 5 dB (as shown in magenta color with circle marks in Fig. 7.1(a)) in order to detect all the symbols correctly.

[19] For a single pulse transmission, the SIR is the ratio of the percentage of total number of molecules "received" (w_C) during a symbol (pulse) duration to that "not received" (1-w_C) during the symbol duration [MAH-12a] and following Eq. (7.2) can be expressed as $\text{SIR}_{(r,f)} = 10\log_{10}\{w_C/(1-w_C)\}$.

Tables 7.1 and 7.2 summarize the $\widetilde{SIR}$ required to achieve the required BER for the stated scenario by adopting the CE systems with and without ISI in consideration respectively. As shown in Table 7.1, the CE system with M = 2 levels requires less $\widetilde{SIR}$ at the RN than the uncoded system and, therefore, provides an $\widetilde{SIR}$ gain meaning that the effective communication range can be increased using this scheme. Table 7.2 shows the SIR required to decode all the symbols correctly when there is no ISI present from the previous symbol transmissions. Note that the computed values shown in Table 7.2 correspond to f = 0.01 bps and r = 50 μm. Finally, referring to Fig. 7.1(a) Table 7.3 shows the effects of the transmission data rate on the $\widetilde{SIR}$ such that the CE system with M = 2 levels requires less $\widetilde{SIR}$ than the other two systems and, therefore, provides an $\widetilde{SIR}$ gain, which can be used to increase the effective communication range.

In addition to the results presented above, in Fig. 7.2 we present the results of (7,4) block encoded (BE) [LEE-94] system with M = 2 and M = 4 amplitude levels. As shown in Fig. 7.2, using multiple amplitude levels produces higher BER due to the increased level of the ISI, while using M = 2 amplitude levels shows better BER performance than that with M = 4 levels in BE system. A comparison of the performances of CE and BE systems at different transmission data rates has been shown in Table 7.3, showing that using M = 2 amplitude levels, the CE (M = 2) system requires less $\widetilde{SIR}$ at the RN than the BE (M = 2) system at different transmission data rates. This can equivalently mean that a CE system with M = 2 levels may be thought of as a better option than a BE system with M = 2 levels.

The comparison between PAM (M = 2) and IM (M = 2) schemes in CC for various transmission data rates has been shown in Fig. 7.3. The reason of comparing M = 2 schemes only is that the M = 4 schemes in both modulation schemes cannot provide the required BER at the RN, and, therefore, it is realistic enough to think that M = 2 scheme would be better-suited for the CEMC system. As seen from Fig. 7.3, the performance curves shift to left when IM scheme is used, which means that the CE (M = 2) system with IM scheme would provide better BER versus $\widetilde{SIR}$ characteristics compared to the CE (M = 2) system with PAM scheme. However, unlike the instantaneous nature of IM (which makes it somewhat the “ideal” case), this chapter has focused on the more realistic non-instantaneous

PAM scheme (i.e. based on pulses with finite pulse-width) in order to justify the use of CE systems in CEMC.

Table 7.1 $\widetilde{SIR}$ required to achieve the required BER when ISI is considered and f = 0.01 bps.

Required BER	$\widetilde{SIR}$ required to achieve the required BER		
	Uncoded system	CE system (M = 4)	CE system (M = 2)
$\leq 10^{-2}$	$\geq$ 5.01 dB	Never[20]	$\geq$ 4.1 dB
$\leq 10^{-1}$	$\geq$ 3.8 dB	Never	$\geq$ 3.6 dB

Table 7.2 SIR required to achieve the required BER when ISI is not present, f = 0.01 bps, and r = 50 μm.

BER	SIR required to achieve the BER		
	Uncoded system	CE system (M = 4)	CE system (M = 2)
0	0.94 dB	0.94 dB[21]	0.16 dB[22]

[20] The term "Never" in Table 7.1 denotes the fact that when the BER is required to be 10^{-2} and 10^{-1}, the $\widetilde{SIR}$ received at the RN needs to be so large that we can approximately say that the system can never provide the corresponding required BER.

[21] The reader should note that for the CE system with M = 4 levels the TN uses the same symbol duration as that of the uncoded system but with higher number of amplitude levels, i.e. increasing the alphabet size. When a pulse transmission with higher amplitude level is considered, the SIR can be calculated as $SIR_{(r,f)} = 10\log_{10}\{\varnothing_A w_C/\varnothing_A(1-w_C)\}=10\log_{10}\{w_C/(1-w_C)\} = SIR_{Uncoded}$ where $\varnothing_A$ is a constant that depends on the amplitude of the pulse transmission [MAH-12a].

[22] For the CE system with M = 2 amplitude levels the TN uses the half the symbol duration of the uncoded system (i.e. doubling the symbol rate) but with the same amplitude levels as that of the uncoded system. When a pulse transmission with double the symbol rate is considered, the SIR can be calculated as $SIR_{(r,f)} = 10\log_{10}\{w_{C1}/(1-w_{C1})\}$ where w_{C1} is the percentage of the total number of molecules "received" during the symbol duration when the pulse duration is half that of the uncoded system [MAH-12a].

Table 7.3 Effects of the transmission data rate when ISI is considered and BER required is ≤ 10^{-2}.

Transmission data rate	$\widetilde{SIR}$ received to achieve the required BER				
	Uncoded system	CE system (M = 4)	CE system (M = 2)	BE system (M = 4)	BE system (M = 2)
f = 0.01 bps	≥ 5.01 dB	Never[23]	≥ 4.1 dB	Never	≥ 4.19 dB
f = 0.02 bps	≥ 4.87 dB	Never	≥ 3.65 dB	Never	≥ 3.65 dB
f = 0.05 bps	≥ 4.51 dB	Never	≥ 3.6 dB	Never	≥ 4.15 dB
f = 0.1 bps	≥ 4.48 dB	Never	≥ 4.17 dB	Never	≥ 4.2 dB

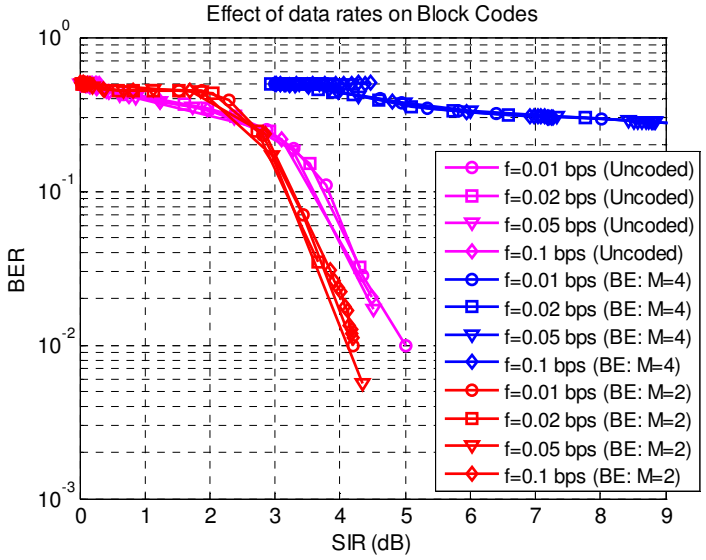

Figure 7.2 BER performance of an uncoded system and (7,4) block encoded (BE) systems using M = 2 and M = 4 amplitude levels with PAM. The horizontal axis shows the approximate SIR, $\widetilde{SIR}$, at the RN without the symbol "~" for the sake of visual clarity in the figure.

[23] The term "Never" in Table 7.3 denotes the fact that when the BER is required to be 10^{-2} the $\widetilde{SIR}$ received at the RN needs to be so large that we can approximately say that the system can never provide the BER of 10^{-2} at that transmission data rate.

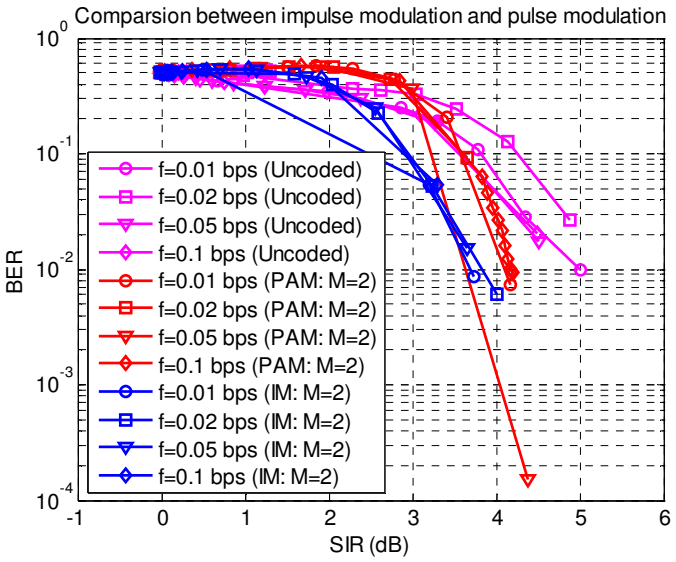

Figure 7.3 Comparison between CE (M = 2) systems with PAM and IM schemes at different data rates. The horizontal axis shows the approximate SIR, $\widetilde{SIR}$, at the RN, without the symbol "~" for the sake of visual clarity in the figure.

7.5 Bio-inspired Architecture of Convolutional Encoder and Decoder

In this section, the possibility of bio-inspired architecture of convolutional encoder and decoder has been briefly addressed without going into the details of component design. From MC point of view, nanomachines are capable of performing simple tasks, which is the motivation of using a simpler version of a CE system such as the (2,1,3) CE system. As shown in Appendix A, see Fig. A.2(b), the CE system requires two memory units and two XOR gates (one with two inputs and the other with three inputs). Since artificial nanomachines are not yet manufactured, an ideal example of a biological nanomachine for this purpose is a biological cell capable of signaling with CEMC [MOO-07] [NAK-11a]. In order to perform logic operations while transmitting the convolutional coded bit sequence nanomachines may use either of Belousov-Zhabotinsky (BZ) reaction, intracellular calcium signaling, or intercellular calcium signaling [MOO-07], as well as DNA transcription and translation processes, synthetic signaling protein, and biochemical delay units [NAK-11a].

As shown in Appendix A, according to the Viterbi decoding procedures based on path metrics and branch metrics, the update of the path metric involves an "add" operation (see. Eq. (A.10) such that an updated path metric is a sum of a previous path metric and a branch

metric [JIA-10]), a “compare” operation (choosing the minimum path metric), and a “select” operation (selecting the path with the minimum path metric as the survivor path). These three operations form the “add-compare-select” (ACS) system [JIA-10] that can also be built at the cellular scale in order to decode the convolutional coded signal at the RN. The “add” operation, the “select” operation, and the “compare” operation can be performed by using an adder, a multiplexer (MUX), and a comparator circuit respectively, all of which can be built using basic logic gates [MAN-02]. Therefore, in view of the above discussion it can be concluded that it would be possible to implement the convolutional encoder and the convolutional decoder circuits at the cellular level using a biological nanomachine, e.g. a bacterium.

7.6 Conclusion

Convolutional codes are one example of channel coding and are used in noisy channels in conventional communication systems in order to correct symbols and thus ensure reliable communication. However, their application to PAM-based CEMC systems is new. In this chapter, the results of the application of CC in PAM CEMC systems have been presented. In addition, the results show that it is possible to increase the effective communication ranges in CEMC by applying simple CC in the system. Therefore, it can be hoped that simple convolutional codes can improve the end-to-end performance of a CEMC-based nanonetwork where a huge number of nanomachines would be communicating among themselves. We strongly believe that the results presented in this chapter will certainly be useful to justify the concepts of convolutional coding techniques in the study of communication range improvement and the design and analysis of CEMC system suitable for nanonetworks applications.

Chapter 8: CEMC Based on Anomalous Diffusion – An Investigative Analysis

8.1 Introduction

While up to now all the results presented in the previous chapters dealt with CEMC system based on normal diffusion process, this chapter introduces anomalous diffusion process to CEMC system. Normal diffusion of a molecule is based on uncorrelated random walk where the direction of the new movement a molecule, suspended in the fluid medium, is independent of the direction of its previous movement and can follow any of the directions in its 3-dimensional space with equal probability [BER-93]. In the case of anomalous diffusion, the movement of the molecule is described by the correlated random walk model, that is placing higher probability, the molecule will maintain moving at its current direction, thereby generating unequal probabilities of taking the next step to right or left in each dimension [TAY-21].

Although correlated random walk-based anomalous diffusion can dramatically alter the rate of diffusion [LUT-13], to the best of our knowledge, no other work on MC in the past considered correlated random walk and presented its BER performance in CEMC. To the best of our knowledge, all investigations on MC [PAR-09] so far have considered normal diffusion based on the uncorrelated random walk model of the propagation of molecules in order to describe the physical channel of MC. We believe that the motivation for doing so has to do with the simplicity in modeling normal diffusion process as well as the suitability of the propagation models based on normal diffusion process in many realistic scenarios [BER-93] [EIN-05] [BOS-63] [LAC-09]. However, anomalous diffusion is a well-known phenomenon, and has been observed in many fields including amorphorous semiconductors, polymer materials, heterogeneous films, porous medium, and movement/dispersion of insects [RYA-03] [HÖF-13] [MET-00] [LUT-13a] [JOS-12] [AND-05]. Anomalous diffusion process can also take place in biological fields [HÖF-13] [WEI-04]. Recent research on molecular nanonetworks admits that similar anomalous diffusion situation can arise in the field of MC, too [GAR-11].

Almost all of the works mentioned above investigate anomalous diffusion from mathematical point of view only. However, as of today anomalous diffusion has not yet

been properly investigated in the field of molecular nanonetworks, thus, its role in molecular nanonetworks is not understood completely yet.

Normal diffusion has been reasonably well researched in the area of diffusion-based MC [BER-93]. However, for normal diffusion to occur, the concentration of solvent molecules must be considerably larger compared to the concentration of information molecules, thereby making a dilute solution [BER-93]. An example where this condition is valid is at the extra-cellular space of a biological cell. However, it may not be valid when the information molecules are confined within a small space, as is the case within the intra-cellular space, or when the molecules interact with each other, which occurs in the case of the charged particles [SCH-75].

In CEMC, due to several reasons molecules can experience anomalous diffusion. In normal diffusion, steps taken by a single molecule follow the Markovian rule, meaning that any future step does not depend on the history of previous steps, i.e. each step is statistically independent from all others, making the process memory-less [BER-93]. However, in anomalous diffusion, there are mechanisms affecting the movement of a molecule that makes its next movement dependent on earlier ones, thus introducing memory, which makes the system non-Markovian [LUT-13a]. Also, even when the diffusive propagation system can be modeled as Markovian, anomalous diffusion effects can occur either due to the presence of external forces [LUT-13a] and/or when the molecules can interact with each other [LUT-13] [LUT-08] [BOO-07]. Both cases can generate anomalous diffusion within the propagation medium.

The fractional diffusion equations (FDE) [JOS-12] describe accurately [RYA-03] the anomalous diffusion behaviour of molecules in the case of a continuous-time random walk (CTRW) model of molecular propagation. Representation of anomalous diffusion by using fractional diffusion dynamics was the outcome of research on the theory of particle diffusion [RYA-03] [HIL-00]. While several researchers have explained anomalous diffusion by using FDE based on fractional time derivatives [RYA-03] [MET-00] [JOS-12] [AND-05], most of the research contributions have been using the correlated random walk approach. Also, they don't deal with MC and the CEMC system. Furthermore, it is reported that the nature of anomalous diffusion is case-specific based on different physical models [SOK-12] and its onset could be found experimentally difficult [HOR-10]. Therefore, it is

necessary to investigate into the performance of anomalous diffusion-based CEMC system through numerical experiments.

To the best of our knowledge, so far no studies analyzed the performance of CEMC system based on anomalous diffusion in three-dimensional unbounded propagation medium and showed its time-dispersive properties as well as BER performance. Our results presented in this chapter have been published in [MAH-14b]. In this chapter, we have made the following contributions:

- A thorough investigation has been made into anomalous diffusion-based CEMC system using fractional diffusion approach. For pure subdiffusive molecular propagation, the CIR of CEMC channel has been identified, its temporal spreading properties in three-dimensional unbounded propagation medium are presented in terms of pdf and cumulative distribution function (cdf) of a molecule to be available at the RN.
- Symbol interval selection problem in subdiffusive CEMC system has been addressed from the viewpoints of signal strength and delay spread of CIR.
- Finally, BER performance of subdiffusive CEMC system has also been analyzed in detail from the viewpoints of varying communication range, transmission data rate, and receiver memory.

The chapter is organized as follows: Section 8.2 reviews the related works of anomalous diffusion in the field of CEMC. Section 8.3 describes the generalized anomalous diffusion molecular transport model. Section 8.4 discusses the results of channel characteristics, followed by Section 8.5 describing the BER results obtained through extensive numerical experiments. Finally, Section 8.6 concludes the chapter with a summary of the findings.

8.2 Related Work

In the context of CEMC, so far anomalous diffusion has been inadequately addressed in literature. As a result, research efforts on anomalous diffusion in CEMC are extremely limited. Only a few research publications that are currently available on anomalous diffusion in the context of CEMC are discussed in the following.

The work in [GAR-11a] identified the necessity of anomalous diffusion in MC in the form of correlated random walk [TAY-21] of information molecules and when information

molecules carry electrostatic charges. However, the work in [GAR-11a] did not provide any results on anomalous diffusion dynamics and its effects on BER of the system.

Apart from this, the work presented in [LLA-11] showed, based on a particular simulator named *N3Sim* [LLA-11], some results of concentration profile of anomalous diffusion-based MC system considering inertia and elastic collisions of molecules; however, without providing relevant details of the analytical channel model of molecular propagation and BER performance of the system. While the works mentioned above describe anomalous diffusion mainly from the simulation point of view, the analytical treatment of the same in CEMC is still missing in the open literature available today.

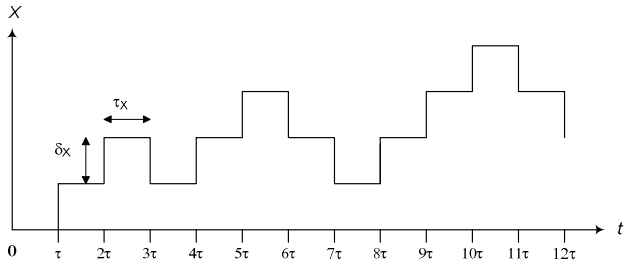

(a) Normal diffusion: Brownian random walk model. Here τ_X and δ_X are constants.

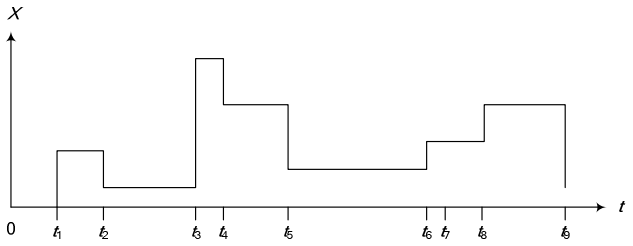

(b) Anomalous diffusion: CTRW model. Here time intervals $(t_{i+1} - t_i)$, where $i = \{0,1,2,3,\ldots\}$ and $t_0 = 0$, and displacement increments $\{X(t_{i+1}) - X(t_i)\}$ are random variables.

Figure 8.1 Displacement (X) versus time (t) diagrams of normal and anomalous diffusion processes in one dimension shown in (a) and (b) respectively.

8.3 Generalized Anomalous Diffusion-based Molecular Transport Model

8.3.1 Subdiffusive Propagation of Molecules

In this section, we provide a generalized anomalous diffusion transport model for information molecules transmitted by the TN. We base our analysis on the available literature on anomalous diffusion explained with *fractional time derivatives* [MET-00].

Ideal diffusion of molecules stemming from the Brownian motion [BRO-28], which was explained later by Einstein [EIN-05], is still one of the milestones in the physics of diffusion. However, due to correlated random walk, temporal correlation among the movements of the molecules at micro/nano-scale dimensions causes anomalous diffusion of molecules in the fluid medium [HÖF-13]. In this chapter, we explain anomalous diffusion in its most generality from the basics of CTRW model.

Figure 2.1 in Chapter 2 shows diffusion-based propagation of molecules in three-dimensional unbounded propagation medium. Fig. 8.1 shows the displacement X in one dimension versus time t characteristics for both normal diffusion and anomalous diffusion, shown in Figs. 8.1(a) and (b) respectively. In normal diffusion, between any two jumps, the time intervals, denoted as τ_X, and correspondingly, the displacement increments, denoted as δ_X, are constant numbers. In anomalous diffusion, between any two jumps, the corresponding quantities are random variables and can be expressed as $\tau_{X,i} = (t_{i+1} - t_i)$, where $i = \{0,1,2,3,\ldots\}$, $t_0 = 0$, and $\delta_{X,i} = \{X(t_{i+1}) - X(t_i)\}$ respectively.

The basic characteristic of normal diffusion is the linear dependence of mean square (MS) displacement of a molecule with time, $\langle X_{\text{AD}}^2 \rangle \sim K_1 t$, where K_1 denotes the diffusion constant of information molecules in the medium in normal diffusion process, where the *anomalous diffusion exponent* α is equal to unity. However, the principal feature of anomalous diffusion of molecular transport is that MS displacement of a molecule depends on the power law of time t, i.e. $\langle X_{\text{AD}}^2 \rangle \sim t^{\alpha}$, where α is known as the *anomalous diffusion exponent* [VLA-08]. The diffusion process is known as *subdiffusion* and *super-diffusion* when $0 < \alpha < 1$ and $\alpha > 1$ respectively [JOS-12]. As will be shown later, the quantity α determines the characteristics of anomalous diffusion-based CEMC channel and, as a result, affects its BER performance.

The role of anomalous subdiffusion in CEMC could be vital. For instance, several experimental studies show that deviations from normal diffusion are possible [VLA-08]. In those cases, the diffusion of molecules is either faster or slower than in normal diffusion. Slower molecular transportation is widely seen in bio-nanomachines, which results in subdiffusion of molecules. For instance, there are a large number of organelles inside a

biological nanomachine, e.g. a biological cell, that do not allow ideal diffusion to take place [HÖF-13], thus subdiffusion is a better fit. Apart from this, in order to design and implement modulation, transmission, and detection circuitries in CEMC as well as to engineer bio-nanomachines for intra-cellular activities, e.g. cellular functionalities controlling cellular activities [NAK-11a] [MOO-07] [MAH-13d] and building intra-cellular logical functionalities [NAK-11a], subdiffusion can affect CEMC-based intra-cellular nanomachine communication.

In CEMC, the local concentration of the information molecules might become very large in the vicinity of the nanomachines. Therefore, a large number of information molecules may gather at the receptor such that the normal diffusion-based propagation may become affected by molecular crowding [WEI-04] [SOK-12], resulting in subdiffusive CEMC. In addition, if the information molecules carry charges [ALB-08], they may interact with each other, which will change their behaviour compared to their behaviour under normal diffusion process, which may result in subdiffusive CEMC. All these scenarios being quite possible in bio-nanomachines provide us with sufficient reasons to pursue an investigative analysis into the performance of the CEMC system under conditions of subdiffusion.

8.3.2 Fractional Diffusion Equations (FDEs)

The mathematical techniques of *fractional time derivatives* have been used by researchers to describe the phenomenon of anomalous diffusion, e.g. see [RYA-03], [MET-00], [JOS-12], [AND-05], [HIL-00], [SUN-10]. This is why anomalous diffusion is also known as *fractional diffusion* after the name of this technique. In many of these works, anomalous diffusion is explained by replacing the integer time derivative of the first order in the differential equation with a fractional time derivative. The concepts of anomalous diffusion stemming from the CTRW model and the fractional Fokker-Planck equation (FFPE) model can be supported by using fractional time derivative [RYA-03]. Recent advances in fractional dynamics have been proved to be a valuable mathematical tool in the analysis of anomalous diffusion systems [JOS-12].

8.3.3 CTRW-based Anomalous Diffusion Transport Model

In order to develop a pure anomalous diffusion transport model, starting from the CTRW model we base our system on one-dimensional model [MET-00] and derive the FDEs. The solutions to one-dimensional system are then extended to a three-dimensional system based on the model shown in [RYA-03].

A remarkable advantage of using FDE-based approach to anomalous diffusion system is that it directly allows provisions for comparisons between the performances of anomalous diffusion (denoted by the quantity α, where $0 < \alpha < 1$) and normal diffusion ($\alpha = 1$) systems under the same set of assumptions. We consider CEMC system based on pure subdiffusion only and, in addition, assume that the other system components, namely, the TN and the RN, are working perfectly. This further allows us to assume that the particle sampling noise at TN [PIE-11] and the particle reception noise at RN [PIE-11b] are negligible. These assumptions isolate the effects of anomalous diffusion only and show its performance over normal diffusion-based CEMC system in more detail.

In CTRW model, jump length and waiting time of a molecule to remain at one state before it goes to the next state are both independent random variables, taken from distributions $\lambda_{\mathrm{AD}}(X)$ and $w_T(t)$ respectively [MET-00]. Despite the fact that the local jump lengths can be Markovian, the overall displacement $X = \sum_j X_j$, where j is the jump index, that the molecule traverses over the time duration $t = \sum_j t_j$ suffers from long-ranging correlations in space and time, which, therefore, makes the system semi-Markovian [JOS-12].

For decoupled jump length and waiting time distributions [MET-00], their joint pdf can be expressed as $\psi(X,t) = \lambda_{\mathrm{AD}}(X) w_T(t)$. Correspondingly, the characteristic time T_{Ch} and the jump length variance $\sum^2$ can be expressed as $T_{\mathrm{Ch}} = \int_0^\infty t w_T(t) dt$ and $\sum^2 = \int_{-\infty}^{\infty} X^2 \lambda_{\mathrm{AD}}(X) dX$ respectively [MET-00]. Independent of the details of the distributions $\lambda_{AD}(X)$ and $w_T(t)$, for $\lambda_{AD}(X)$ with finite variance $\sum^2$ and for $w_T(t)$ with mean waiting time T_{Ch}, applying central limit theorem (CLT), the CTRW model shown above yields Gaussian pdf that obeys normal diffusion equation [MET-00] [JOS-12].

Anomalous diffusion takes place when $\lambda_{\mathrm{AD}}(X)$ and $w_T(t)$ obey power laws as shown below [JOS-12]

$$\begin{aligned} w_T(t) &\sim A_\alpha \left(\mathfrak{T}/t\right)^{1+\alpha} \qquad 0<\alpha<1 \\ \lambda_{\mathrm{AD}}(X) &\sim A_{\tilde{\mu}} \sigma^{\tilde{\mu}} |X|^{-(1+\tilde{\mu})} \quad 1<\tilde{\mu}<2 \end{aligned} \tag{8.1}$$

where A_α and $A_{\tilde{\mu}}$ denote the coefficients related to $w_T(t)$ and $\lambda_{\mathrm{AD}}(X)$ distributions respectively, and $\mathfrak{T}$ is a time constant of relaxation in a complex system, e.g. in CTRW process in a subdiffusive system [MET-00]. In the specific case of subdiffusion, T_{Ch} diverges while $\sum^2$ is still kept finite. Therefore, the long-tailed waiting time distribution $w_T(t)$ as shown in Eq. (8.1) can be introduced [MET-00]. The power laws shown in Eq. (8.1) emerge because of the generalized CLT and have characteristic functions, with small *k* and *u* expansions and α and $\tilde{\mu}$ in the range of values shown in Eq. (8.1), as below [MET-00] [JOS-12].

$$w_T(u) = \exp\left(-[u\mathfrak{T}]^\alpha\right) \sim 1-(u\mathfrak{T})^\alpha \quad \text{and} \quad \lambda_{\mathrm{AD}}(k) = \exp\left(-[\sigma|k|]^{\tilde{\mu}}\right) \sim 1-\sigma^{\tilde{\mu}}|k|^{\tilde{\mu}}. \tag{8.2}$$

In its complete generality, based on the values of $\tilde{\mu}$ and α, the following four cases can be derived.

Case 1: Normal diffusion occurs when $\tilde{\mu} = 2$ and $\alpha = 1$, and jump length variance and characteristic waiting time exist.

Case 2: CTRW subdiffusion occurs when $\tilde{\mu} = 2$ and $0<\alpha<1$.

Case 3: Levy flight occurs when $1<\tilde{\mu}<2$ and $\alpha = 1$.

Case 4: Levy flight occurs with long-tailed waiting time distribution when $1<\tilde{\mu}<2$ and $0<\alpha<1$.

Based on a thorough research in the available literature, we find that the *subdiffusive* scenario of Case 2 is commonly seen [HÖF-13] in case of biological nanomachines, and therefore, in this chapter, we focus on pure subdiffusive transport of information molecules in the three-dimensional unbounded propagation environment.

Considering decoupled jump length $\lambda_{\mathrm{AD}}(X)$ and waiting time $w_T(t)$ distributions, i.e. $\psi(X,t) = \lambda_{\mathrm{AD}}(X) w_T(t)$, the pdf of a CTRW process in Fourier–Laplace (k,u) space,

meaning that the probability $F_\alpha(X,t)$ of having a molecule at position X and at time t can be expressed as the algebraic relation as shown below [JOS-12].

$$F_\alpha(k,u)=\frac{1-w_T(u)}{u}\frac{F_0(k)}{1-\psi(k,u)}\Rightarrow F_\alpha(k,u)=\frac{1-w_T(u)}{u}\frac{F_0(k)}{1-\lambda_{\text{AD}}(k)w_T(u)} \tag{8.3}$$

For uncoupled jump length and wait time distributions, the quantities can be expressed as

$$\psi(X,t)=\lambda_{\text{AD}}(X)w_T(t)\Rightarrow\psi(k,u)=\lambda_{\text{AD}}(k)w_T(u) \tag{8.4}$$

$$\text{where } \lambda_{\text{AD}}(k)=\Im\left[\lambda_{\text{AD}}(X)\right]\triangleq\int_{-\infty}^{\infty}\lambda_{\text{AD}}(X)\exp\left(-jkX\right)dX$$

$$F_0(k)=\Im\left[F_0(X)\right]=\Im\left[\delta(X)\right]=1$$

$$w_T(u)=\mathbb{L}\left[w_T(t)\right]\triangleq\int_0^{\infty}w_T(t)\exp\left(-ut\right)dt$$

where $F_0(X)=\delta(X)$ is the initial condition and $\Im$ and $\mathbb{L}$ denote the Fourier Transform and the Laplace Transform operators respectively [HAY-02] [JOS-12]. Therefore, in Fourier-Laplace space, the solution to the probability $F_\alpha(X,t)$ can be expressed as below.

$$F_\alpha(k,u)=\frac{1-w_T(u)}{u}\frac{1}{1-\lambda_{\text{AD}}(k)w_T(u)} \tag{8.5}$$

Using integration rule for fractional integrals, we obtain

$$F_\alpha(X,t)-F_{\alpha,0}(X)={}_0\mathcal{L}_t^{-\alpha}K_\alpha^{\tilde{\mu}}\frac{\partial^{\tilde{\mu}}}{\partial X^{\tilde{\mu}}}F_\alpha(X,t) \tag{8.6}$$

which, after applying the differential operator $\partial/\partial t$, finally yields the following.

$$\frac{\partial}{\partial t}F_\alpha(X,t)={}_0\mathcal{L}_t^{1-\alpha}K_\alpha^{\tilde{\mu}}\frac{\partial^{\tilde{\mu}}}{\partial X^{\tilde{\mu}}}F_\alpha(X,t) \tag{8.7}$$

Here ${}_0\mathcal{L}_t^{1-\alpha}$ is known as the *Rieman-Liouville operator* [RYA-03] and can be expressed as ${}_0\mathcal{L}_t^{1-\alpha}=\left(\partial/\partial t\right){}_0\mathcal{L}_t^{-\alpha}$, which for $0<\alpha<1$, can be defined as

$${}_0\mathcal{L}_t^{1-\alpha}F_\alpha(X,t)=\frac{1}{\Gamma(\alpha)}\frac{\partial}{\partial t}\int_0^t\frac{F_\alpha(X,t')}{(t-t')^{1-\alpha}}dt' \tag{8.8}$$

where $\Gamma(\cdot)$ denotes the gamma function [KAY-93], p. 24, $K_\alpha^{\tilde{\mu}}$ is the generalized diffusion constant of dimension $[K_\alpha^{\tilde{\mu}}]=\text{cm}^{\tilde{\mu}}/\text{s}^{\alpha}$. For Case 2, anomalous diffusion of molecules in pure subdiffusive transport can be expressed as below.

$$\frac{\partial}{\partial t}F_\alpha(X,t) = {}_0\mathcal{L}_t^{1-\alpha} K_\alpha^2 \frac{\partial^2}{\partial X^2} F_\alpha(X,t) \tag{8.9}$$

Extending the solutions in three dimensions, anomalous diffusion of a molecule can thus be expressed as [RYA-03]

$$\frac{\partial}{\partial t}F_\alpha(r,t) = K_\alpha^2 {}_0\mathcal{L}_t^{1-\alpha}\left[\nabla^2 F_\alpha(r,t)\right] \tag{8.10}$$

where ∇^2 denotes the differential Laplace operator [OLV-10] and K_α^2 denotes the diffusion constant of molecules in pure subdiffusion and has the dimension $\mathrm{cm}^2/\mathrm{s}^\alpha$.

Eq. (8.10) shows the spatiotemporal evolution of $F_\alpha(r,t)$, where $F_\alpha(r,t)$ denotes the probability of getting a molecule in a three-dimensional space at a distance r from the TN at time t, where the molecule experiences pure subdiffusion in three-dimensional unbounded propagation medium. As shown in Fig. 2.1, TN is located at the origin (0,0,0) and the vector to RN is $\vec{r} = \hat{i}\cdot x_r + \hat{j}\cdot y_r + \hat{k}\cdot z_r$ where $\hat{i}, \hat{j}$, and $\hat{k}$ are unit vectors along X, Y, and Z axes respectively.

Eq. (8.10) needs to be solved with appropriate initial condition in order to get the expressions of the temporal evolution of the concentration of information molecules at the location of the RN. In order to get the CIR of the anomalous diffusion channel, the appropriate initial condition is

$$F_\alpha(r,0) = F_0\delta(r)\delta(t) \tag{8.11}$$

where $\delta(r)$ and $\delta(t)$ are Dirac delta functions [HAY-02] in space and time domains respectively, and F_0 is the strength of the impulse function. The solution of Eq. (8.10) can be expressed in terms of Fox H function as below [MET-00] [RYA-03], where d_{dim} denotes the dimension of the propagation system and d_{dim} = 3 for the three-dimensional system shown in Fig. 2.1.

$$F_\alpha(r,t) = \frac{F_0}{(\pi r^2)^{d_{\mathrm{dim}}/2}} \mathrm{H}_{1,2}^{2,0}\left[\left.\frac{r^2}{4K_\alpha t^\alpha}\right|_{(d_{\mathrm{dim}}/2,1),(1,1)}^{(1,\alpha)}\right] \tag{8.12}$$

Since $\tilde{\mu}$ = 2 for subdiffusive scenario in Case 2, from now onwards, the generalized subdiffusion constant K_α^2 in anomalous diffusion is written as K_α.

Since the solution shown in Eq. (8.12) in terms of Fox H function is a bit difficult for numerical simulation in several software packages [ANS-12], this can conveniently be expressed in terms of the gamma function $\Gamma(\cdot)$ [KAY-93] for a three-dimensional system as shown in Eq. (8.13), where $\Upsilon = r^2/4K_\alpha t^\alpha$ [RYA-03].

$$F_\alpha(r,t) = \underbrace{\frac{F_0}{\left(4\pi K_\alpha t^\alpha\right)^{3/2}}}_{\text{First Term}} \underbrace{\sum_{i=0}^{\infty} \frac{(-\Upsilon)^i}{i!} \left(\frac{\Gamma(-\frac{1}{2}-i)}{\Gamma\left(1-\alpha\left(\frac{3}{2}+i\right)\right)} + \frac{\Gamma(\frac{1}{2}-i)}{\Gamma(1-\alpha(1+i))\sqrt{\Upsilon}} \right)}_{\text{Second Term}} \tag{8.13}$$

As a result, Eq. (8.13) shows the spatiotemporal evolution of the CIR $F_\alpha(r,t)$ of pure subdiffusive CEMC channel. Therefore, the output signal $U(r,t)$ denotes the concentration of molecules at the location of the RN, and can be expressed as the following,

$$U(r,t) = Q(t) \otimes F_\alpha(r,t) \tag{8.14}$$

where $Q(t)$ is the input signal transmitted by the TN and the symbol $\otimes$ denotes convolution operation [HAY-02] in time domain. When a unit impulse signal is transmitted by the TN, the CIR of the CEMC channel in anomalous diffusion process can be expressed as the following.

$$F_0 = 1, \quad Q(t) = \delta(r)\delta(t) \quad \Rightarrow \quad U(r,t) = F_\alpha(r,t) \tag{8.15}$$

Correspondingly, putting $F_0 = 1,$ Eq. (8.13) yields

$$F_\alpha(r,t) = \frac{1}{\left(4\pi K_\alpha t^\alpha\right)^{3/2}} \sum_{i=0}^{\infty} \frac{(-\Upsilon)^i}{i!} \left(\frac{\Gamma(-\frac{1}{2}-i)}{\Gamma\left(1-\alpha\left(\frac{3}{2}+i\right)\right)} + \frac{\Gamma(\frac{1}{2}-i)}{\Gamma(1-\alpha(1+i))\sqrt{\Upsilon}} \right). \tag{8.16}$$

In this chapter, first, we show the properties of the average CIR of the CEMC channel in subdiffusion process, as expressed in Eq. (8.16), followed by the BER performance of the channel with or without the receiver's ability to compute the ISI from the previous symbols.

In order to explain the properties of anomalous diffusion-based CEMC channel, we use the following quantities derived from the CIR of the channel as shown below:

(i) $F_\alpha(r,t)$ that denotes the pdf of getting one molecule at the location *r* at time instant *t*,

(ii) cdf $\left(F_\alpha(r,t)\right)$ that denotes the cdf of $F_\alpha(r,t)$ and can be expressed as

$$\text{cdf}\left(F_\alpha(r,t)\right) = \int_0^t F_\alpha(r,\zeta)d\zeta, \tag{8.17}$$

(iii) $\tau_{\text{D (RMS)}}$ that denotes the root mean square (RMS) delay spread [RAP-02] of the CEMC channel and can be expressed as

$$\tau_{\mathrm{D\,(RMS)}} = \sqrt{\overline{\tau_{\mathrm{E}}^{\,2}} - (\overline{\tau}_{\mathrm{E}})^2} \tag{8.18}$$

where $\overline{\tau_{\mathrm{E}}^{\,2}} = \sum_k F_\alpha(r,\tau_{\mathrm{E},k})\tau_{\mathrm{E},k}^2 \Big/ \sum_k F_\alpha(r,\tau_{\mathrm{E},k})$ and $\overline{\tau}_{\mathrm{E}} = \sum_k F_\alpha(r,\tau_{\mathrm{E},k})\tau_{\mathrm{E},k} \Big/ \sum_k F_\alpha(r,\tau_{\mathrm{E},k})$.

Here τ_{E} and $\overline{\tau}_{\mathrm{E}}$ denote the delay and the mean excess delay respectively [RAP-02], p. 199, and $\tau_{\mathrm{D\,(RMS)}}$ explains the time dispersion properties of the CIR.

(iv) $S_{\mathrm{sym\ (AD)}}$ that denotes the percentage strength of the symbol in anomalous diffusion and can be expressed as

$$S_{\mathrm{sym\ (AD)}} = \int_0^{T_{\mathrm{sym}}} F_\alpha(r,\zeta)d\zeta = \mathrm{cdf}\left(F_\alpha(r,T_{\mathrm{sym}})\right). \tag{8.19}$$

Here $S_{\mathrm{sym\ (AD)}}$ denotes the probability of getting one molecule available at the RN during the current symbol duration T_{sym}. This also denotes the cdf of $F_\alpha(r,t)$ at the temporal instant $t = T_{\mathrm{sym}}$. When the TN transmits Q_0 molecules at t = 0, the quantity $S_{\mathrm{sym\ (AD)}}Q_0$ denotes the total number of molecules that are expected to become available at the RN during T_{sym}. $S_{\mathrm{sym\ (AD)}}$ indicates the desired percentage signal strength for a given symbol duration based on a particular transmission data rate.

(v) $t_{\mathrm{EN\,(\%)}}$ that denotes the time to achieve a specified percentage of signal strength at the RN. Here, we consider $t_{50\%}$ and $t_{90\%}$ that mean the times to achieve 50% and 90% of the molecules being available at the RN respectively.

8.4 Anomalous Diffusion Channel Characteristics

In this section, the properties of the CIR of the subdiffusive CEMC channel have been explained. Based on the solutions to $F_\alpha(r,t)$ as shown in Eq. (8.13), channel characteristics and time dispersion parameters, as shown in Eqs. (8.17)–(8.19), have been derived numerically and the results have been shown in the following.

8.4.1 Normal Diffusion Scenario

Fig. 8.2 shows the pdf $F_\alpha(r,t)$ and its cdf at the RN when α = 1, meaning that normal diffusion taking place. As shown in Fig. 8.2, in case of ideal diffusion, as r increases, the CIR becomes temporally spread, although the amount of temporal spreading is less when r is less than 10 μm. The temporal spreading of the CIR is a function of communication range

r and time t, as can be seen from Eq. (8.13). As shown in Fig. 8.2, temporal spreading observed at $r \leq 10$ μm is more or less the same, however, when $r > 10$ μm, the diffusion of molecules experiences a significant amount of temporal spreading that causes reliability concerns in CEMC.

In addition, the validity of the solution shown in Eq. (8.13) can be explained mathematically as follows. In case of ideal diffusion, putting $\alpha = 1$ in Eq. (8.13) and plugging the gamma function [KAY-93] into it yields Eq. (8.20), which is the widely known solution to normal diffusion of molecules in three dimensions [BER-93]. In Eq. (8.20), K_1 denotes the diffusion constant when $\alpha = 1$. In addition, $K_1 = D$ for normal diffusion scenarios as shown in the previous chapters.

$$F_1(r,t) = \frac{F_0}{\left(4\pi K_1 t\right)^{3/2}} \sum_{i=0}^{\infty} \frac{(-\Upsilon)^i}{i!} = \frac{F_0}{\left(4\pi K_1 t\right)^{3/2}} \exp\left(-\frac{r^2}{4K_1 t}\right) \tag{8.20}$$

where $\Upsilon = r^2/4K_1 t$

In normal diffusion, Figs. 8.3(a) and (b) respectively show the variations of $S_{\text{sym (AD)}}$ when the symbol duration T_{sym} varies from 100 s up to 1000 s and that of $t_{\text{EN (\%)}}$ when 50% and 90% of the available number of molecules are expected to be available at the RN. The characteristics of normal diffusion ($\alpha = 1$) are shown first in Figs. 8.2 and 8.3 because they act as reference when the similar CIR properties of anomalous diffusion are compared. As shown in Fig. 8.3, since symbol durations are smaller with higher data rates, when data rate increases the RN can have less number of molecules at the desired symbol duration, especially when r increases. Figure 8.3(b) shows the effects of variations of r on the time required by the RN to collect 50% and 90% of the available molecules. As shown in Fig. 8.3(a), when r increases beyond 10 μm, T_{sym} needs to be increased in order to increase $S_{\text{sym (AD)}}$. This is due to the increased temporal spreading the signal goes through at longer r. Figure 8.3(b) shows that for increased r if the RN wants to collect more signal strength, e.g. 90%, T_{sym} needs to be increased, though at the cost of the data rate.

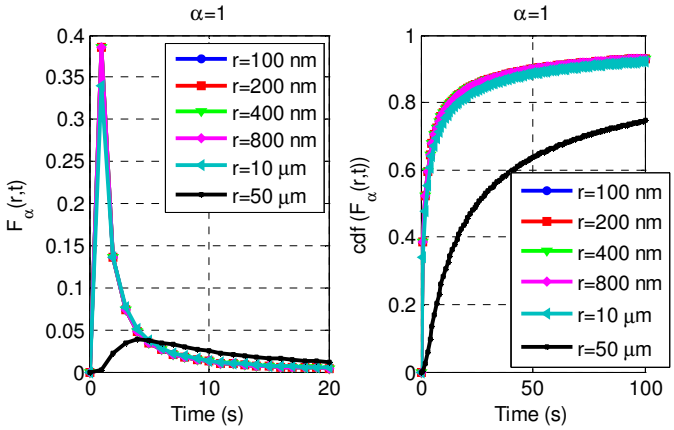

Figure 8.2 CIR and its cdf, as sensed by the sampling-based[24] RN based on uniform sampling of 1 s, when $\alpha = 1$ and r varies from 100 nm up to 50 μm.

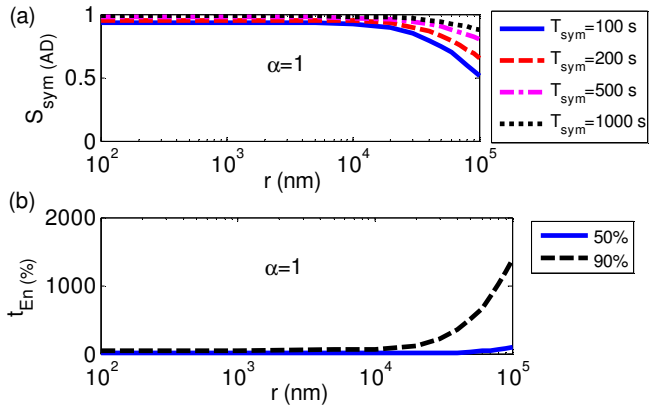

Figure 8.3 Variations of $S_{\text{sym (AD)}}$ and $t_{\text{EN (\%)}}$ in ideal diffusion ($\alpha = 1$) when r varies.

8.4.2 Anomalous Diffusion Scenario

Similar results of anomalous diffusion when $\alpha = 0.85$ and 0.70 and r varies in the range from 100 nm up to 10 μm are shown in Figs. 8.4–8.6. Figs. 8.4(a) and (b) show the pdf and the cdf of CIR in anomalous diffusion CEMC channel for $\alpha = 0.85$ and $\alpha = 0.7$ respectively. As seen from Fig. 8.4(a), when $\alpha = 0.85$ and $r = 10$ μm, it is seen that the CIR gets a bit strong in amplitude especially when t is small, e.g. $t \leq 20$ s. This characteristic feature of $F_\alpha(r,t)$ can be explained as a result of the subdiffusive phenomenon at $\alpha = 0.85$ and 1 μm < $r \leq 10$ μm. However, when the system recovers from the initial transient, e.g. when 20 s ≤ t

[24] Sampling-based receiver for CEMC has been investigated in detail in [MAH-13], [MAH-13d].

$\leq T_{obs}$,[25] no such behavior is seen further. Note that the second term in Eq. (8.13) is a function of r, t, and α, which influences the spatiotemporal distribution of $F_\alpha(r,t)$ when communication range is 1 μm < $r \leq$ 10 μm and hence the transient behavior of $F_\alpha(r,t)$. One constructive outcome of this behavior is that it increases the symbol strength $S_{sym\ (AD)}$ (see Eq. (8.19)), and provides improved BER performance as shown in the next section. However, as shown in Fig. 8.4(b), when α decreases further, e.g. $\alpha = 0.7$, no such behavior is observed and $F_\alpha(r,t)$ decreases as r increases during the initial transient period, e.g. $t \leq 10$ s.

In addition, it is also found that the impact of distance in the range from 100 nm up to 10 μm is not significant. This phenomenon can be explained by realizing the smaller impacts of r in Eq. (8.13) when $\alpha = 0.70$ and r varies in this range. In Figs. 8.4(a) and (b), the anomalous diffusion exponent, α, is chosen as 0.85 and 0.7 respectively because these values of α have proved to be valid from experiments with biological entities [HÖF-13]. In addition, it has been reported that molecular crowding results in a subdiffusive phenomenon in the cytoplasm and the nucleus of a eukaryotic cell when the value of α lies in the range $0.5 < \alpha < 1$ [GUI-08] [BAN-05]. Communication ranges from 100 nm up to 10 μm have been considered because CEMC based on anomalous diffusion transport process in intracellular environments at less than 10 μm range would be reasonably acceptable, provided that the size of a typical bionanomachine (e.g. a bacterium) is approximately 1 μm [ALB-08], p. 14.

Comparing Fig. 8.2 with Fig. 8.4 explains the fact that the CIR in subdiffusive molecular propagation experiences more temporal spreading when α decreases and vice versa. As a result, when r is kept fixed, subdiffusive CEMC is slower than that based on normal diffusion. The cdf in normal diffusion is much higher than that in subdiffusive propagation in Fig. 8.4, which means that a given T_{sym} would collect less number of molecules in the latter case, producing more ISI and thereby higher BER at the RN. In

[25] Since molecules in ideal (i.e. free) diffusion can be available at the RN even after infinite (∞) time, in the ideal case, the observation time T_{obs} is infinite. However, in the numerical simulations we considered T_{obs} = 10,000 simulated seconds (s) that is reasonable enough so as to provide negligible value of $F_\alpha(r,t)$ beyond T_{obs}.

addition, temporal spreading is an indication of higher RMS delay spread as shown in Fig. 8.7.

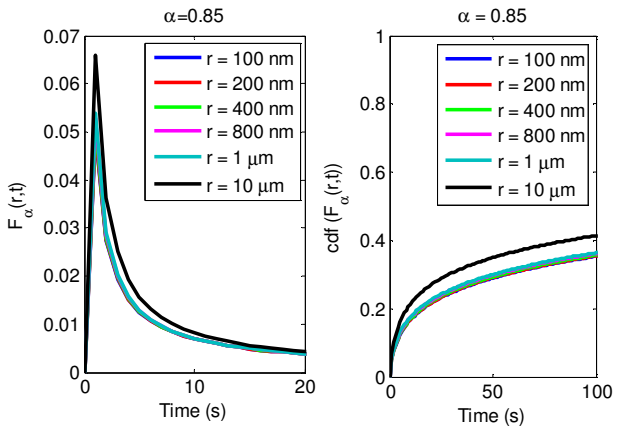

(a) $\alpha = 0.85$

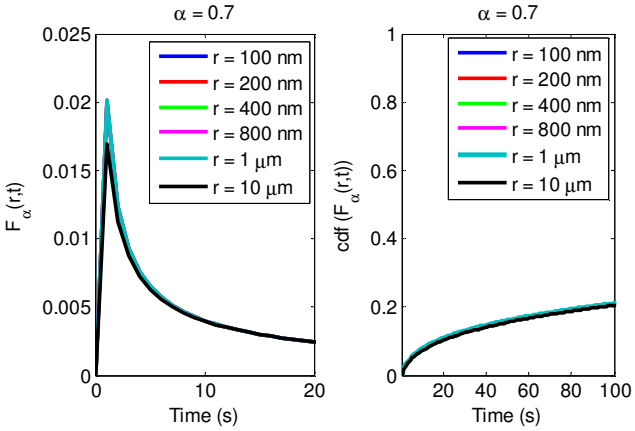

(b) $\alpha = 0.7$

Figure 8.4 The CIR and its cdf, as sensed by the sampling-based RN based on uniform sampling of 1 s, when $\alpha = 0.85$ (in (a)) and $\alpha = 0.7$ (in (b)) as well as r varies from 100 nm up to 10 μm.

Fig. 8.5 shows the variation of $S_{\text{sym (AD)}}$ when different symbol durations T_{sym} and α are considered. When $r \leq 10$ μm, $S_{\text{sym (AD)}}$ remains approximately fixed when T_{sym} and α are not varied. This can be explained by the observations from Fig. 8.4 such that the CIR does not vary much when $r \leq 10$ μm. For fixed values of r and α, $S_{\text{sym (AD)}}$ increases as T_{sym} increases, which is due to collecting additional molecules when T_{sym} increases. Increasing T_{sym} reduces the effective data rate and so is considered a trade-off with data rate when r and α are kept fixed. This, in turn, is an open challenge that T_{sym} needs to be optimized on a case-by-case basis.

Selection of T_{sym} can be done by observing the RMS delay spread of the CEMC channel in anomalous diffusion, which is discussed in the next subsection and shown in Fig. 8.7. When $S_{sym\ (AD)} < 0.5$, it can be understood that the RN would fail to collect even 50% of the available molecules, and so the detection of the information symbol would be unreliable even in the absence of ISI. When α decreases even more, e.g. $\alpha = 0.5$ and $\alpha = 0.3$, it is found that $S_{sym\ (AD)}$ can never reach 0.5 even with the longest symbol duration of 1000 s (data not shown). Therefore, based on the observations, it can be suggested that for comparatively lower values of α, CEMC based on anomalous diffusion will be extremely slow, and so we have not considered $\alpha < 0.7$ in the BER analysis shown in Section 8.5. In addition, Fig. 8.6 also shows that low values of $\alpha \leq 0.7$ would yield very low data rate in CEMC, even with the 50% strength threshold in the absence of ISI, which again suggests that $\alpha \geq 0.7$ can be considered acceptable in the analysis shown in this chapter.

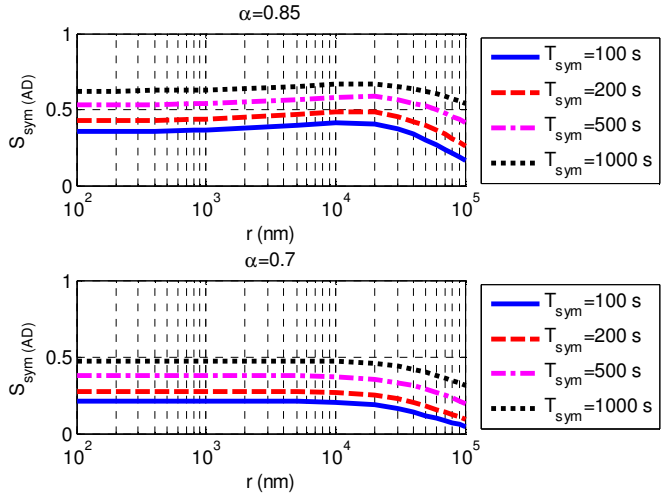

Figure 8.5 Variation of $S_{sym\ (AD)}$ for various T_{sym} when r varies, $\alpha = 0.85$ (top), and $\alpha = 0.7$ (bottom).

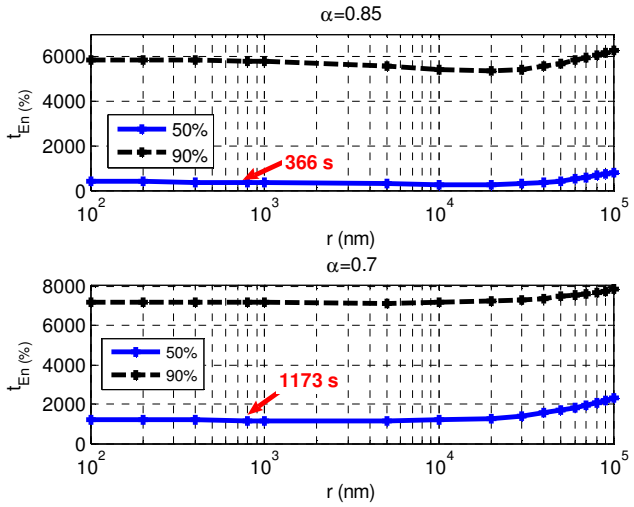

Figure 8.6 Variations of $t_{EN\ (\%)}$ when r varies and α is kept fixed at 0.85 (top) and 0.7 (bottom) respectively.

8.4.3 Symbol Interval Selection

Fig. 8.7 shows the time dispersion parameters in the form of RMS delay spread $\tau_{D(RMS)}$ for different values of α. The top and the bottom parts of Fig. 8.7 respectively show the variations of $\tau_{D(RMS)}$ for two cases, namely, when the amplitudes of $F_\alpha(r,t)$ that are respectively 10 dB and 13 dB less than the peak of $F_\alpha(r,t)$ are ignored.[26] Three general conclusions that can be drawn from Fig. 8.7 are as follows:

- First, when r increases, $\tau_{D(RMS)}$ increases, meaning that the CIR becomes more temporally spread.
- Second, for a given weak peak filtering (WPF) case, when r is kept fixed, as α decreases, $\tau_{D(RMS)}$ increases and vice versa, meaning that a lower value of α indicates a CEMC system to be more anomalous and thus the transmitted molecules become very slow in reaching the RN, which increases $\tau_{D(RMS)}$.
- Finally, with a lower WPF scheme, e.g. -13 dB, $\tau_{D(RMS)}$ increases compared to that in -10 dB WPF, although r and α are kept fixed. This means, with WPF of -13 dB, the RN is

[26] Ignoring the weak peaks in the CIR can be termed as *weak peak filtering* (WPF) [BEN-04], p. 355. WPF affects the computation of $\tau_{D\,(RMS)}$.

now able to incorporate the effects of the CIR contributions even weaker by 3 dB than those in the -10 dB case, hence increasing $\tau_{D(RMS)}$.

The results of $\tau_{D(RMS)}$ for a given set of system parameters are important in the sense that they help choose the most suitable symbol duration required at the TN so as to combat ISI at the RN. Table 8.1 shows the transmitted data rates and symbol durations used in the numerical experiments. Table 8.2 shows the RMS delay spreads of the CEMC channel in normal diffusion ($\alpha = 1$) and anomalous subdiffusion ($\alpha = 0.85$ and 0.7). Since selection of the appropriate symbol duration is related to minimizing ISI effects, we can assume that symbol duration should be at least 10 times the delay spread [RAP-02], p. 201.

Increasing the symbol duration decreases the effective transmission data rate, and so to ensure that speed of CEMC does not go down, the symbol interval needs to be optimized, making a trade-off with ISI and BER that can be tolerated. In this chapter, we consider symbol durations as shown in Table 8.1. Since we assume to not slow down the CEMC based on anomalous diffusion process, we tend to consider $T_{sym} \leq 100$ s and check the role that ISI plays in the BER performance. Another reasoning that supports the choice of $T_{sym} \leq 100$ s is that, for instance, as shown in Fig. 8.6, at 800 nm, even to collect 50% of the molecules the RN needs to wait 366 s and 1173 s when $\alpha = 0.85$ and $\alpha = 0.7$ respectively. This may make the selection of very long symbol durations quite unreasonable in anomalous subdiffusion-based CEMC, compared to compromising with the ISI. For example, when $T_{sym} = 100$ s is considered, the condition $T_{sym} \geq 10\tau_{D(RMS)}$ is met for all the values of $\tau_{D(RMS)}$ in Table 8.2 except the grey-shaded **bold**-formatted values. In either case, it is necessary to investigate into the BER performance as shown in Section 8.5.

Table 8.1 Transmitted data rates and symbol durations

f (bps)	0.01 bps	0.02 bps	0.05 bps	0.1 bps
$T_{sym} = 1/f$ (s)	100 s	50 s	20 s	10 s

Table 8.2 Delay spreads with sampling-based RN with uniform sampling interval of 1 s and -10 dB and -13 dB weak peak filtering

	$\alpha = 1$		$\alpha = 0.85$		$\alpha = 0.7$	
r = 800 nm	-10 dB	-13 dB	-10 dB	-13 dB	-10 dB	-13 dB
	0.95 s	1.6 s	3.57 s	8.4 s	7.4 s	**20.1 s**
r = 10 μm	-10 dB	-13 dB	-10 dB	-13 dB	-10 dB	-13 dB
	1.22 s	1.88 s	3.25 s	6.93 s	9.7 s	**26.2 s**

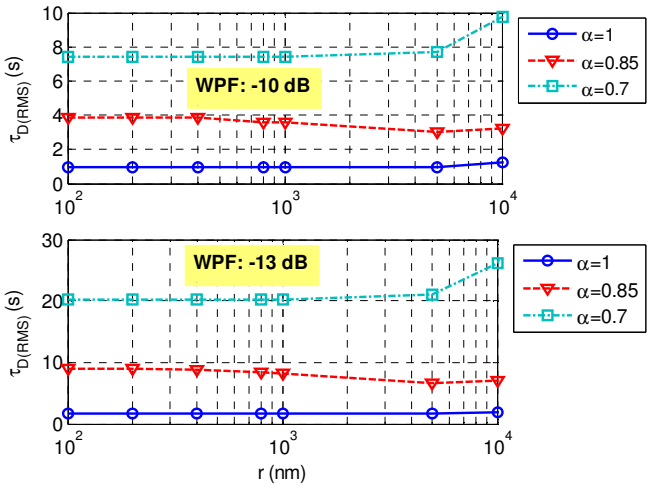

Figure 8.7 Variation of $\tau_{D\,(RMS)}$ when r varies for different α and WPF.

8.5 Performance of CEMC System Based on Anomalous Subdiffusion

In this section, we describe BER performance of a CEMC system when a random sequence of bits is transmitted in the three-dimensional unbounded propagation medium. The transmission, modulation, and detection schemes are introduced briefly first, followed by a description of simulation setup and numerical experiments. Finally, BER results obtained through extensive numerical experiments are presented.

8.5.1 Transmission, Modulation, and Detection

The TN transmits a single type of molecules as an impulsive fashion into propagation medium. The transmission of symbols is based on time-slotted generalized binary ASK modulation as shown in Fig. 8.8 where the TN transmits molecules at the beginning of each bit interval T_b such that $Q_0\delta(t)$ and $Q_1\delta(t)$ molecules transmitted at $t = 0$ indicate a bit 0 and

bit 1 being transmitted by the TN respectively. In binary system, each symbol is represented by a bit 1 or bit 0, and therefore, symbol duration and bit interval mean the same, i.e. $T_{\text{sym}} = T_b$.

A generalized strength-based optimum signal detection scheme for CEMC system has been presented in Chapter 5 and reported in one of our recent works [MAH-13b], and so the same has not been restated here.[27] In this chapter, in order to evaluate BER performance of anomalous subdiffusion-based CEMC system, we apply the strength-based optimum detector as described in Chapter 5. Figure 8.8 shows the input (transmitted) signal and a random realization $z_v(t)$ of the output (received) signal intensity $z(t)$ in anomalous subdiffusion-based CEMC system for different α. Figure 8.8 also shows that signal intensity becomes weak when α decreases from 1 to 0.85 or 0.7. The generalized strength-based optimum signal detector described in Chapter 5 accumulates the molecules during each symbol and makes an optimum decision on the transmitted symbols, providing the minimum BER [KAY-93]. Since the strength-based optimum ASK detector shown in Chapter 5 is a generalized version of the strength-based detector and can be modified into other CEMC signal detectors, it has been used in this chapter to evaluate the performance of anomalous diffusion-based CEMC.

[27] A generalized strength-based ASK detector can detect a transmitted signal when the TN transmits $Q_1\delta(t)$ and $Q_0\delta(t)$ molecules to represent bit 1 and bit 0 respectively. In OOK-modulated transmission, the TN does not transmit any molecule at all when it transmits bit 0, i.e. $Q_0 = 0$. For details on the development of the generalized strength-based detector, see Chapter 5 [MAH-13b].

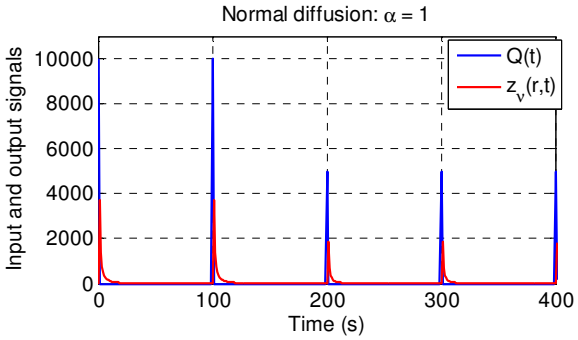

(a) Normal diffusion: $\alpha = 1$ when first 4 bits transmitted are {1100}.

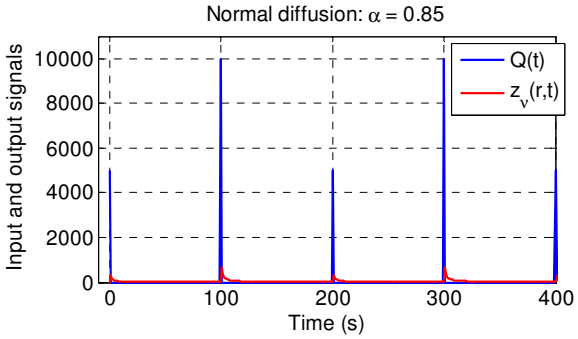

(b) Anomalous subdiffusion: $\alpha = 0.85$ when the first 4 bits transmitted are {0101}.

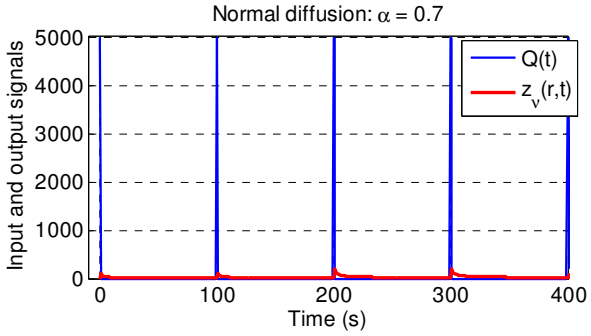

(c) Anomalous subdiffusion: $\alpha = 0.7$ when the first 4 bits transmitted are {0000}.

Figure 8.8 Input (transmitted) and output (available) concentration signal intensities in generalized binary ASK-based CEMC system when $r = 5$ μm. The TN encodes bits 1 and 0 by emitting 10,000 and 5,000 molecules respectively at the beginning of symbol duration of 100 s in this case.

8.5.2 Simulation Setup Overview

The simulation setup in case of anomalous subdiffusion-based CEMC is the same as that used for strength-based signal detection as shown in Chapter 5. By incorporating the diffusion-based propagation shown in Eqs. (5.1)–(5.4), we implement the strength-based optimum receiver model as shown in Eq. (5.7) in software, which takes as input the

concentration signal intensity $z(t)$, computes signal strength z_{ED} (see Eq. (5.3)), and finally detects the symbol by comparing the test statistic $T(z_{ED})$ with a threshold. The optimum receiver thus developed is based on minimum probability of error criterion [KAY-93] and provides minimum BER at the RN.

The performance of the optimum receiver has been tested in several simulation scenarios using numerical experiments. The BER results obtained from the simulation experiments have been explained in terms of three factors, namely, communication range (r), transmission data rate (f), and memory length M_{RN} of the RN measured in unit of *symbol*.

In each simulation experiment in this chapter, the TN transmits 10,000 randomly generated bits in the propagation channel by using a generalized binary ASK modulation as shown in Fig. 8.8. In order to investigate into the effects of ISI at the RN, based on the discussion on selection of appropriate symbol duration mentioned earlier and from our previous works [MAH-10b] [MAH-13d] [MAH-13] [MAH-13b], we prefer to consider transmission data rates in the range from $f = 0.01$ bps (i.e. $T_b = 100$ s) to $f = 0.1$ bps (i.e. $T_b = 10$ s). When $f = 0.01$ bps is adopted, it provides an observation time of 1,000,000 simulated seconds (i.e. approximately 277 simulated hours). The distance r between the TN and the RN is considered from as low as 100 nm to as high as 10 μm, covering a wide range of effective CEMC distances [MAH-10b]. As shown in Chapter 5, we consider three different receiver configurations at the RN, namely, *full complexity (FC)*, *reduced complexity (RC)*, and *simplest* receivers. For details of the simulation setup, please see Sections 5.6.1 and 5.6.2.

8.5.3 BER Performance

Figure 8.9 shows BER versus transmission data rate characteristics of pure subdiffusive CEMC system for the *simplest* receiver configuration of the RN. As shown in Fig. 8.9, for $\alpha = 1$, i.e. in the case of normal diffusion, when data rate is less than 0.05 bps, the RN can detect the symbols with low BER even with the simplest receiver configuration, thereby minimizing the requirements of high memory and complexities in the RN circuitry. However, when data rate is as high as 0.1 bps, BER increases, providing an even worse performance at larger communication ranges.

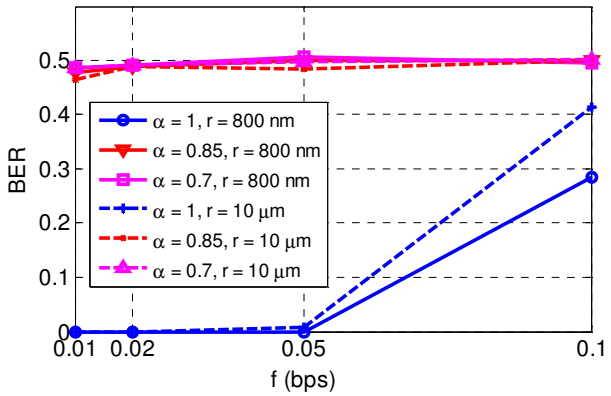

Figure 8.9 BER performance of subdiffusive CEMC system with the *simplest* receiver configuration.

In addition, another significant observation from Fig. 8.9 is that, with the simplest receiver configuration, the BER performances obtained for $\alpha = 0.85$ and $\alpha = 0.7$ are high enough to be close to 0.5, i.e. the performance of detector with random guess [KAY-93]. As a result, in order to provide better BER performance, it becomes necessary for the RN to compute the ISI-producing molecules by using one or more previously transmitted symbols, as shown in Fig. 8.10 for FC and RC receiver configurations.

Figs. 8.10(a) and (b) show the BER performance of the FC and the RC receiver configurations as a function of memory size of the RN when $\alpha = 0.85$ and $\alpha = 0.7$ respectively. As shown in Fig. 8.10, the BER performance of the system depends on the computational accuracy of the RN in computing ISI-producing molecules at the current symbol, and therefore, the memory size of the RN.

Numerical experiments show that in normal diffusion ($\alpha = 1$), the RN can detect all the bits correctly (zero BER) if the RN computes ISI from at least the immediately previous symbol. In normal diffusion, the ability of the RN to achieve zero BER can be attributed to the fact that in normal diffusion the RN is able to receive more signal strength that it can use in detection, unlike the scenarios with $\alpha = 0.85$ and $\alpha = 0.70$. However, when $\alpha = 0.85$ and $\alpha = 0.7$, BER performances degrade; and the performance is even worse for $\alpha = 0.5$ and so the results for $\alpha = 0.5$ are not shown in this chapter.

Fig. 8.10 also shows the BER performances of the system for different transmission data rates when memory length of the RC receiver configuration varies from 1 to 99. In the numerical simulations, 100 bits are sent at a time, and so a maximum of 99 previous

symbols can be considered by the RN while computing the ISI-producing molecules. As shown in Fig. 8.10, for a given α, when memory length increases, BER decreases, at the expense of complexity in the RN circuitry to accommodate the ISI processing involving more of the previous symbols.

In addition, for given α and memory length, transmitting symbols at a higher rate provides higher BER. This is because of the fact that in subdiffusion the received signal intensity becomes more temporally spread, which increases ISI-producing molecules in the current symbol. Comparing the BER performance shown in Fig. 8.10(a) with that shown in Fig. 8.10(b), it is found that when α decreases, BER increases. The BER performance becomes even worse when data rate increases while at the same time α decreases, providing higher BER close to 0.5 in the case of $\alpha = 0.7$, compared to the BER shown as the green lines in Fig. 8.10(a). For instance, when the RN uses the immediately previous symbol memory only to compute the ISI-producing molecules, the system shows high BER values close to the range from 0.45 to 0.50, which indicate poor performance, meaning that almost 50% of the bits are detected incorrectly by the detector. Such BER values should be too high to ensure reliable communication among communicating nanomachines in a nanonetwork.

Higher BER obtained in the numerical simulation experiments mean that at low α the desired signal strength at the current symbol duration becomes less and the estimate of the ISI-producing molecules computed from the immediately previous symbol only does not provide a reasonable estimate of the ISI so as to detect the current symbol correctly, and therefore, BER increases. As shown in Fig. 8.10, with large memory size, the estimate of the ISI becomes sufficient enough to provide improved BER performance at the RN.

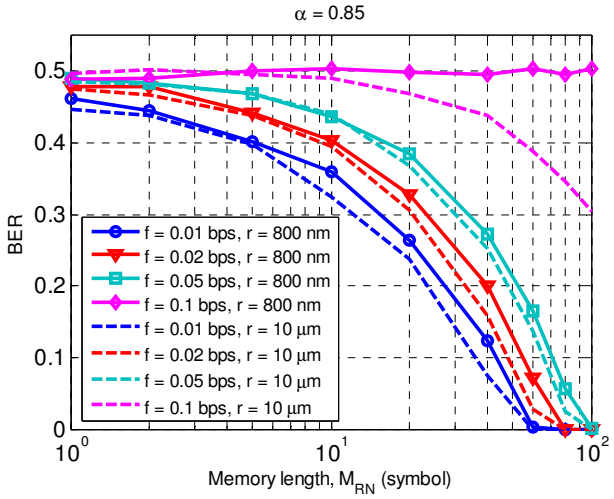

(a) $\alpha = 0.85$

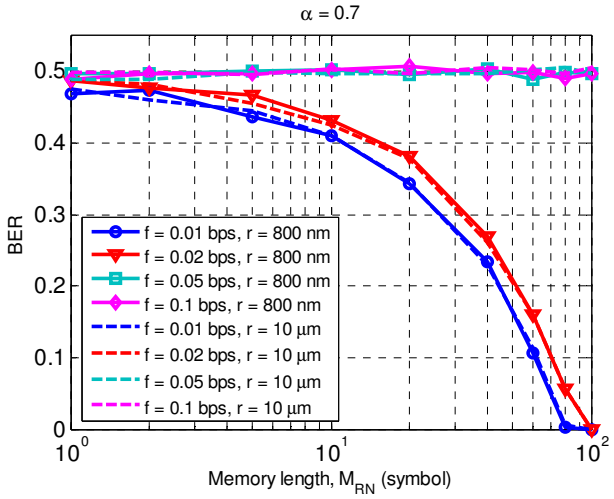

(b) $\alpha = 0.7$

Figure 8.10 Effects of memory length M_{RN} (in unit of symbols) on BER when $\alpha = 0.85$ and 0.70, shown in (a) and (b) respectively.

8.6 Conclusion

The performance of CEMC system based on anomalous subdiffusion has been presented in detail in this chapter. The time-dispersive properties of the CEMC channel are presented first, followed by an investigative analysis of the BER performance of the CEMC system with generalized binary ASK-modulated transmission and strength-based optimum signal detection.

In view of the relevance to biological nanomachines, only pure subdiffusive phenomenon of anomalous diffusion has been investigated in this chapter. Results show that, due to inherent properties of subdiffusion, CEMC system suffers from the slowness in propagation, which causes longer RMS delay spreads of the channel, and correspondingly, a high level of ISI and hence a higher BER at the RN. However, the results show that increasing the memory size at the RN while computing the ISI-producing molecules would be a wise choice in such cases in order to improve the BER.

Anomalous diffusion phenomena in general and subdiffusion in particular are widely seen in bionanomachines. Therefore, we strongly believe that the results obtained in this chapter would certainly be useful to further the study of anomalous diffusion in molecular nanonetworks for the future generation on information technology.

Chapter 9: Conclusions and Future Research

9.1 Concluding Remarks

In this thesis, we have presented an in-depth study of the characteristics and performance of concentration-encoded molecular communication (CEMC) system. Molecular communication (MC) is recently gaining a lot of interests in the research community as a new physical layer option for molecular nanonetworks. MC is a bio-inspired communication paradigm that is targeted for communication among a vast number of nanomachines in nanonetworks. Since MC is a new area standing at the crossroads of nanotechnology, biological sciences, and information and communication technologies, communication engineers mainly focus on the understanding of the communication process among nanomachines in general. Having said that, information communication in nanonetworks is a vast area of research.

In this thesis, we have focused on CEMC among nanomachines and studied the performance of the same in detail. In-depth investigations of the suitable modulation schemes, impacts of the intersymbol interference (ISI), and communication range- and rate-dependent characteristics have been presented.

Initially, three novel optimum signal detection techniques have been proposed and extensively investigated. These detection techniques rely on the concentration of molecules at the RN and develop receivers for CEMC signal detection in ideal diffusion-based propagation environment.

The first technique, namely, the *sampling-based detection* (SD), detects the information symbols by processing the individual sample or samples of concentration signal intensity at the RN. The second technique, namely, the *strength (or energy)-based detection* (ED), detects the information symbols by accumulating the molecules available at the RN and comparing it with a threshold. Finally, the strength-based receiver built upon *stochastic chemical kinetics* (SCK) considers the reaction events between the molecules and the receptors and can implement the variable threshold-based detection approach at the RN. The performance of these receivers have been investigated in detail.

The application of simple channel codes in CEMC have been extensively investigated in this research. Results show that simple convolutional codes can increase the effective

communication ranges between a pair of nanomachines in CEMC when compared to an uncoded CEMC system. An increase in communication range can alternatively mean an improved signal strength at the RN and can be considered as a potential benefit of applying simple channel codes in CEMC.

Finally, an investigative study of CEMC based on anomalous subdiffusion has also been presented in this thesis. The characteristics of the CEMC channel based on anomalous subdiffusion has been illustrated in detail and a corresponding analysis on the strength-based detection of CEMC signals in anomalous subdiffusion is presented.

9.2 Future Research

The results presented in this thesis show that CEMC has a high potential to be used as a possible information encoding technique and can be adopted as one of the promising techniques of communication at the nanoscale. However, the field of CEMC is very new, which still demands a sufficient amount of fundamental research to be performed from various points of view, as described in this section.

- While Chapters 4, 5, and 8 investigated into the detection performances of impulse-based modulation scheme only, the structures of the optimum receivers presented in Chapters 4 and 5 can also be applied to detect input signals with other modulation formats, e.g. PAM, M-PAM, by properly modifying the signal processing parts. Therefore, sampling-based and strength-based detection schemes for a variety of modulation formats in CEMC can be considered as a future research direction of this work.

- Based on biological relevance to nanomachines with extremely limited capabilities [NAK-11a] [AKY-08], this thesis focused on the sampling-based and strength-based receivers where bionanomachines can sense the signal intensity at regular (i.e. uniform) temporal sampling intervals. To the best of our knowledge, it is not completely known yet whether bionanomachines would be able to sense the concentration intensity efficiently at non-uniform temporal sampling intervals, which would surely require higher complexity in the RN circuitry, given the fact that the nanomachines are in general meant for very limited tasks. However, this can be considered as an open area of research that future works can focus on.

- Although it is already known that bionanomachines, e.g. biological cells, can sense the concentration of molecules continually at their receptors [BER-77] and biological cells can be engineered in order to do required tasks [NAK-11a], the actual implementations of the sampling-based and the strength-based detectors at the cell level still requires a considerable amount of interdisciplinary research at the crossroads of molecular and synthetic biology, information theory, and communication engineering. Based on the prospects of engineered and/or artificial bionanomachines [NAK-11a], researchers can expect that the RN would be able to implement these signal detectors within itself, although this is still an open research question as of today. As shown in Chapter 6, bio-inspired implementation of the strength-based signal detector would be feasible in CEMC. Chapter 6 focused only on the CEMC detection signal processing at the RN to evaluate a strength-based detector that can be built upon the stochastic molecule-receptor binding based on SCK. Designing specific detectors with bionanomachines and/or biochemical processes have not been investigated in this thesis. Therefore, the future work in this direction should include a more detailed analysis of the complexity of the receiver architecture and its feasibility with bionanomachines, for instance, in order to address the challenges of multilevel amplitude modulation-based CEMC system for nanonetworks applications.

- In a similar manner, as shown in Chapter 7, although it should be possible to implement a convolutional encoder and decoder with biological components and computations, a formal evaluation of its feasibility, the effects of component and computation choices on the specific channel-coded scheme under examination, and the complete design of the encoder and the decoder with biochemical reactions can be considered as a future work of this research. Another interesting future work would be to investigate into the performance of a CEMC system based on a code division multiple access (CDMA) technique.

- Experimental verification constitutes another important future direction of this research. In this regard, biological experiments can be set up by using biological cells, e.g. bacteria, as TN and RN and CEMC between them can be studied and verified with the theoretical results. However, experimental setup for CEMC is now in its infancy and so requires a considerable amount of research from interdisciplinary perspectives.

• In this research, several tools from communication theory have been used in CEMC. There exist opportunities in the research of optimized techniques in CEMC using these communication theory tools. Energy expenditure in biological nanomachines should have a role in the performance of the CEMC system, a detailed study of which should be considered as a future direction of this research. Since the detection techniques presented in this thesis are based on temporal sampling of the concentration signal intensity, the CEMC system in this thesis has mainly been analyzed in the time domain. Similar analyses in the frequency domain, especially those of ISI, would also be considered as a future work of this research.

Finally, we strongly believe that CEMC would be a feasible information encoding technique in molecular nanonetworks. However, CEMC is a highly interdisciplinary field that will need more research in the future. Therefore, we strongly believe that the analyses presented in this thesis would help MC engineers to understand a CEMC system in a better way and to evaluate the performance of nanonetworks composed of a huge number of nanomachines based on CEMC.

References

[ABR-64] M. Abramowitz, *Handbook of mathematical functions, with formulas, graphs, and mathematical tables,* Dover Publications, 1964, New York.

[AKY-08] I.F. Akyildiz, F. Brunetti, and C. Blazquez, "Nanonetworks: A New Communication Paradigm," *Computer Networks Journal (Elsevier),* Vol. 52, pp. 2260-2279.

[AKY-10] I.F. Akyildiz, and J.M. Jornet, "The Internet of nano-things," *Wireless Communications, IEEE,* Vol. 17, No. 6, 2010, pp. 58-63.

[AKY-10a] I.F. Akyildiz, "Nanonetworks: A new frontier in communications," in *Proceedings of the 2010 International Conference on Security and Cryptography (SECRYPT),* pp. IS-5., 2010.

[AKY-10b] I.F. Akyildiz, and Jornet, J.M. 2010, "Electromagnetic wireless nanosensor networks," *Nano Communication Networks,* Vol. 1, No. 1, pp. 3-19.

[AKY-10c] I.F. Akyildiz,, J.M. Jornet, and M. Pierobon, "Propagation models for nanocommunication networks," in *Proceedings of the Fourth European Conference on Antennas and Propagation (EuCAP),* pp. 1-5, 12-16 April, 2010.

[AKY-11] I.F. Akyildiz,, J.M. Jornet, and M. Pierobon, "Nanonetworks," *Communications of the ACM,* Vol. 54, No. 11, 2011, pp. 84-89.

[ALB-08] B. Alberts, A. Johnson, J. Lewis, M. Raff, K. Roberts, and P. Walter, *Molecular biology of the cell,* Garland Science, 2008, New York.

[ALE-97] S.B. Alexander, *Optical Communication Receiver Design,* 1st Ed., 1997, SPIE.

[ALF-06] G. Alfano, and D. Miorandi, "On Information Transmission Among Nanomachines," in *Proceedings of 1st International Conference on Nano-Networks and Workshops (NanoNet '06)*, pp. 1-5, September, 2006.

[AND-05] M. F. de Andrade, E. K. Lenzi, L. R. Evangelista, R. S. Mendes and L. C. Malacarne, "Anomalous diffusion and fractional diffusion equation: anisotropic media and external forces," *Physics Letters A*, Vol. 347, pp. 160-169, 2005.

[ANS-12] I. S. Ansari, F. Yilmaz, M. S. Alouini and O. Kucur, "New Results on the Sum of Gamma Random Variates With Application to the Performance of

Wireless Communication Systems over Nakagami-m Fading Channels," ArXiv:1202. 2576 [Cs. IT], pp. 1-10, 2012.

[ATA-07] B. Atakan, and O.B. Akan, "An information theoretical approach for molecular communication," in *Proc. International Conference on Bio-Inspired Models of Network, Information and Computing Systems (BIONETICS 2007),* Hungary, 10-13 December, 2007.

[ATA-08] B. Atakan, and O.B. Akan, "On Channel Capacity and Error Compensation in Molecular Communication," *Springer Transactions on Computational Systems Biology,* C. Priami et al. (Eds.), 2008, pp. 59-80.

[ATA-08a] B. Atakan, and O.B. Akan, "On molecular multiple-access, broadcast, and relay channels in nanonetworks.," in *Proc. the 3rd International Conference on Bio-Inspired Models of Network, Information and Computing Systems (BIONETICS '08),* November, 2008.

[ATA-10] B. Atakan, and O.B. Akan, "Deterministic capacity of information flow in molecular nanonetworks," *Nano Communication Networks,* Vol. 1, No. 1, 2010, pp. 31-42, Elsevier.

[ATA-12] B. Atakan, S. Galmes, and O. Akan, "Nanoscale Communication With Molecular Arrays in Nanonetworks," *IEEE Transactions on NanoBioscience,* Vol. 11, No. 2, pp. 149-160.

[ATA-14] B. Atakan, *Molecular Communications and Nanonetworks: From Nature to Practical Systems*, New York: Springer, 2014.

[BAN-05] D. S. Banks and C. Fradin, "Anomalous diffusion of proteins due to molecular crowding," *Biophys. J.*, Vol. 89, pp. 2960-2971, 2005.

[BEN-04] M. Di Benedetto, *Understanding Ultra Wide Band Radio Fundamentals*, Upper Saddle River, N.J.: Prentice Hall PTR, 2004.

[BER-77] H.C. Berg, and E.M. Purcell, "Physics of chemoreception," *Biophysical Journal,* Vol. 20, No. 2, 1977, pp. 193-219.

[BER-93] H.C. Berg, *Random Walks in Biology,* 1993, Princeton University Press, NJ, USA.

[BHA-05] K. Bhattacharya, and R.D. James, "The Material Is the Machine," *Science,* Vol. 307, No. 5706, 2005, pp. 53-54.

[BHU-04] B. Bhushan, (Ed.) *Springer Handbook of Nanotechnology*, 2004, Springer-Verlag, Berlin; New York.

[BOO-07] J. Boon and J. Lutsko, "Nonlinear diffusion from Einstein's master equation," *EPL (Europhysics Letters)*, Vol. 80, pp. 60006, 2007.

[BOS-63] W. H. Bossert, and E.O. Wilson, "The analysis of olfactory communication among animals," *Journal of theoretical biology,* Vol. 5, No. 3, 1963, pp. 443-469.

[BOX-78] G. E. Box, *Statistics for Experimenters: An Introduction to Design, Data Analysis, and Model Building*, New York; Toronto: Wiley, 1978.

[BRO-28] R. Brown, "A brief account of microscopical observations," *Phil. Mag.*, Vol. 4, pp. 161-173, 1828.

[BUS-09] S.F. Bush, "Wireless ad hoc nanoscale networking," *IEEE Wireless Communications,* Vol. 16, No. 5, 2009, pp. 6-7.

[BUS-10] S.F. Bush, *Nanoscale Communication Networks,* 2010, Artech House, MA.

[BUS-11] S.F. Bush, "Toward in vivo nanoscale communication networks: utilizing an active network architecture," *Frontiers of Computer Science in China,* Vol. 5, No. 3, 2011, pp. 316-326.

[CAV-06] A. Cavalcanti, T. Hogg, B. Shirinzadeh, and H.C. Liaw, "Nanorobot Communication Techniques: A Comprehensive Tutorial," in *Proc. 9th International Conference on Control, Automation, Robotics and Vision (ICARCV '06)*, 2006, p. 1.

[CHA-01] M.-.F. Chang, V.P. Roychowdhury, Z. Liyang, S. Hyunchol, and Q. Yongxi, "RF/wireless interconnect for inter- and intra-chip communications," *Proceedings of the IEEE,* Vol. 89, No. 4, 2001, pp. 456-466.

[CHE-05] S.-T. Cheng, C.-Y. Wang, and M.-H. Tao, "Quantum communication for wireless wide-area networks," *IEEE Journal on Selected Areas in Communications,* Vol. 23, No. 7, pp. 1424-1432, 2005.

[CRA-75] J. Crank, *The mathematics of diffusion,* Clarendon Press, Oxford, UK, 1975.

[DOC-08] N. DoCoMo, "NTT DoCoMo Demonstrates Molecular Delivery System for Molecular Communication,"
Website: http://www.nttdocomo.com/pr/2008/001391.html, last accessed on 24 April 2013.

[DUR-10] R. Durrett, *Probability: Theory and Examples,* Fourth Edition, 2010, Cambridge University Press.

[ECK-07] A.W. Eckford, “Achievable information rates for molecular communication with distinct molecules,” in *Proc. International Conference on Bio-Inspired Models of Network, Information and Computing Systems (BIONETICS 2007),* Hungary, 10-13 December, p. 313, 2007.

[ECK-07a] A.W. Eckford, “Nanoscale Communication with Brownian Motion,” in *Proc. 41st Annual Conference on Information Sciences and Systems (CISS '07)*, Baltimore, MD, pp. 160-165, 2007.

[EIN-05] A. Einstein, “On the movement of small particles suspended in stationary liquids required by the molecular-kinetic theory of heat,” *Annalen der Physik,* Vol. 17, pp. 549-560, 1905.

[EIN-11] A. Einolghozati, M. Sardari, A. Beirami, and F. Fekri, “Capacity of discrete molecular diffusion channels,” in *Proc. IEEE International Symposium on Information Theory (ISIT),* pp. 723-727, 2011.

[EIN-11a] A. Einolghozati, M. Sardari, M. and F. Fekri, “Capacity of diffusion-based molecular communication with ligand receptors,” in *IEEE Information Theory Workshop (ITW),* pp. 85-89, 2011.

[END-08] R.G. Endres and N. S. Wingreen, "Accuracy of direct gradient sensing by single cells," *Proc. Nat. Acad. Sci.*, U. S. A., vol. 105, pp. 15749-15754, 2008.

[FAR-11] N. Farsad, A.W. Eckford, S. Hiyama, and Y. Moritani, “A simple mathematical model for information rate of active transport molecular communication,” in *Proc. IEEE Conference on Computer Communications Workshops (INFOCOM WKSHPS),* pp. 1-6, 2011.

[FEY-60] R.P. Feynman, “There's Plenty of Room at the Bottom,” *Engineering and Science, Caltech, USA,* February, pp. 22-36, 1960.

[FRE-05] R.A. Freitas, “Nanotechnology, nanomedicine and nanosurgery,” *International Journal of Surgery,* Vol. 3, No. 4, pp. 243-246, 2005.

[FRE-99] R.A. Freitas, *Nanomedicine, Vol. 1: Basic Capabilities,* Landes Bioscience, TX, USA, 1999.

[FRI-06] H.B. Frieboes, J.P. Sinek, O. Nalcioglu, J.P. Fruehauf, and V. Cristini, “Nanotechnology in Cancer Drug Therapy: A Biocomputational Approach,” *BioMEMS and Biomedical Nanotechnology*, M. Ferrari, A.P. Lee and L.J. Lee (Eds.), 1st Edition, Springer, NY, USA, pp. 435-460, 2006.

[GAR-11] N. Garralda, I. Llatser, A. Cabellos-Aparicio, E. Alarcón, and M. Pierobon, “Diffusion-based physical channel identification in molecular

nanonetworks," *Nano Communication Networks,* Vol. 2, No. 4, pp. 196-204, Elsevier, 2011.

[GAR-11a] N. Garralda, I. Llatser, A. Cabellos-Aparicio and M. Pierobon, "Simulation-based evaluation of the diffusion-based physical channel in molecular nanonetworks," in Computer Communications Workshops (INFOCOM WKSHPS), IEEE Conference on, pp. 443-448, 2011.

[GIL-00] D.T. Gillespie, "The chemical Langevin equation," *J. Chem. Phys.,* Vol. 113, No. 1, pp. 297-306, 2000.

[GIL-07] D.T. Gillespie, "Stochastic Simulation of Chemical Kinetics," *Annu. Rev. Phys. Chem.*, vol. 58, pp. 35-55, 05/01; 2013/07, 2007.

[GUI-08] G. Guigas and M. Weiss, "Sampling the Cell with Anomalous Diffusion—The Discovery of Slowness," *Biophys. J.*, Vol. 94, pp. 90-94, 2008.

[GUL-10] E. Gul, B. Atakan, and O.B. Akan, "NanoNS: A nanoscale network simulator framework for molecular communications," *Nano Communication Networks,* Vol. 1, No. 2, pp. 138-156, 2010.

[HAY-00] S. Haykin, *Communication Systems,* 4th Edition, John Wiley and Sons, 2000.

[HAY-02] Haykin, S., *Signals and Systems*, Wiley, New York, 2002.

[HIL-00] R. Hilfer, "Fractional diffusion based on Riemann-Liouville fractional derivatives," *The Journal of Physical Chemistry B*, Vol. 104, pp. 3914-3917, 2000.

[HIY-05] S. Hiyama, Y. Moritani, T. Suda, R. Egashira, A. Enomoto, M. Moore, and T. Nakano, "Molecular Communication," in *Proc. of the 2005 NSTI Nanotechnology Conference,* 2005.

[HIY-09] S. Hiyama, R. Gojo, T. Shima, S. Takeuchi, and K. Sutoh, "Biomolecular-Motor-Based Nano- or Microscale Particle Translocations on DNA Microarrays," *Nano Letters,* Vol. 9, No. 6, pp. 2407-2413, 2009.

[HIY-10] S. Hiyama, Y. Moritani, R. Gojo, S. Takeuchi, and K. Sutoh, "Biomolecular-motor-based autonomous delivery of lipid vesicles as nano- or microscale reactors on a chip," *Lab on a Chip,* Vol. 10, No. 20, pp. 2741-2748, 2010.

[HÖF-13] F. Höfling, and T. Franosch, "Anomalous transport in the crowded world of biological cells," *Reports on Progress in Physics*, 76(4), 046602, 2013.

[HOR-10] M. R. Horton, F. Höfling, J. O. Rädler and T. Franosch, "Development of anomalous diffusion among crowding proteins," *Soft Matter*, Vol. 6, pp. 2648-2656, 2010.

[HRA-05] S. Hranilovic, *Wireless optical communication systems,* Springer, New York, 2005.

[JER-00] M. C. Jeruchim, P. Balaban, K. S. Shanmugan, *Simulation of Communication Systems: Modeling, Methodology, and Techniques*, Kluwer Academic/Plenum Publishers, New York, 2000.

[JIA-10] Y. Jiang, *A Practical Guide to Error Control Coding using Matlab*, Artech House, 2010.

[JOH-05] R. A. Johnson, *Miller & Freund's Probability and Statistics for Engineers*, Upper Saddle River, NJ: Pearson Prentice Hall, 2005.

[JOR-10] J.M. Jornet, and I.F. Akyildiz, "Channel Capacity of Electromagnetic Nanonetworks in the Terahertz Band," in *Proc. IEEE International Conference on Communications (ICC),* pp. 1, 2010.

[JOR-11] J.M. Jornet, and I.F. Akyildiz, "Channel Modeling and Capacity Analysis for Electromagnetic Wireless Nanonetworks in the Terahertz Band," *IEEE Transactions on Wireless Communications,* Vol. 10, No. 10, pp. 3211-3221, 2011.

[JOR-11a] J.M. Jornet, and I.F. Akyildiz, "Information capacity of pulse-based Wireless Nanosensor Networks," in *Proc. 8th Annual IEEE Communications Society Conference on Sensor, Mesh and Ad Hoc Communications and Networks (SECON),* pp. 80-88, 2011.

[JOR-12] J.M. Jornet, and I.F. Akyildiz, "The internet of multimedia nano-things in the Terahertz band," in *Proc. 18th European Wireless Conference*, pp. 1, 2012.

[JOS-12] K. Joseph, *Fractional Dynamics: Recent Advances*, World Scientific, 2012.

[JOV-11] T. Jovanovic-Talisman, and A. Zilman, "Nanobiotechnology: building a basic nanomachine," *Nature Nanotechnology,* Vol. 6, No. 7, pp. 397-398, 2011.

[KAD-09] S. Kadloor, and R. Adve, "A Framework to Study the Molecular Communication System," in *Proc. 18th International Conference on Computer Communications and Networks (ICCCN 2009)*, pp. 1, 2009.

[KAD-12] S. Kadloor, R.S. Adve, and A.W. Eckford, “Molecular Communication Using Brownian Motion With Drift,” *IEEE Transactions on NanoBioscience,* Vol. 11, No. 2, pp. 89-99, 2012.

[KAY-93] S. M. Kay, *Fundamentals of Statistical Signal Processing, Vol. 2 Detection Theory*. Englewood Cliffs, NJ: PTR Prentice-Hall, 1993.

[KHO-11] M.N. Khormuji, “On the capacity of molecular communication over the AIGN channel,” in *Proc. 45th Annual Conference on Information Sciences and Systems (CISS),* pp. 1-4, Baltimore, MD, 23-25 March, 2011.

[KIL-13] D. Kilinc and O. B. Akan, "Receiver Design for Molecular Communication," *Selected Areas in Communications, IEEE Journal on*, vol. 31, pp. 705-714, 2013.

[KRI-02] V. Krivan, P. Lánský, and J.P. Rospars, “Coding of periodic pulse stimulation in chemoreceptors,” *Biosystems,* Vol. 67, No. 1-3, pp. 121-128, 2002.

[KRO-11] K.L. Kroeker, “The rise of molecular machines,” *Communications of the ACM,* Vol. 54, No. 12, pp. 11-13, 2011.

[KUR-10] M.S. Kuran, H.B. Yilmaz, T Tugcu, B. Özerman, “Energy model for communication via diffusion in nanonetworks,” *Elsevier Nano Communication Networks*, 1 (2), 86–95, 2010.

[KUR-11] M.S. Kuran, H.B. Yilmaz, T. Tugcu, and I.F. Akyildiz, “Modulation Techniques for Communication via Diffusion in Nanonetworks,” in *Proc. IEEE International Conference on Communications (ICC),* pp. 1-5, 5-9 June, 2011.

[LAC-09] N.R. Lacasa, *Modeling the Molecular Communication Nanonetworks,* M.Sc. thesis, The Universitat Politècnica de Catalunya (UPC), Spain, 2009.

[LEO-94] A. Leon-Garcia, *Probability and Random Processes for Electrical Engineering*, Reading, Mass.: Addison-Wesley, 1994.

[LEE-12] M. S. Leeson and M. D. Higgins, "Error correction coding for molecular communications," in *IEEE MoNaCom 2012 Workshop*, ICC-2012, Ottawa, Canada, 2012.

[LEE-12a] M. S. Leeson and M. D. Higgins. “Forward error correction for molecular communications,” *Nano Communication Networks* Vol. 3, No. 3, pp. 161-167, 2012.

[LEE-94] E. A. Lee and D. G. Messerschmitt, *Digital Communication*, 2nd Ed., Kluwer Academic Publishers, USA, 1994.

[LIN-12] W. Lin, Y. Lee, P. Yeh and C. Lee, "Signal detection and ISI cancellation for quantity-based amplitude modulation in diffusion-based molecular communications," in *Proc. GLOBECOM 2012*, December 2012, pp. 4362-4367.

[LIN-83] S. Lin, *Error control coding: fundamentals and applications*, Englewood Cliffs: Prentice-Hall, 1983.

[LIU-07] J. Liu, and T. Nakano, "An information theoretic model of molecular communication based on cellular signaling," in *Proc. International Conference on Bio-Inspired Models of Network, Information and Computing Systems (BIONETICS 2007),* pp. 316-321, 10-12 December, 2007.

[LIU-11] J. Liu and F. Peper, "Signal transduction in biological systems and its possible uses in computation and communication systems," in *Biol. Func. for Info. and Comm. Tech.*, H. Sawai (Ed.), NY: Springer, 2011, pp. 163-191.

[LIU-12] J. Liu, and T. Nakano, "Principles and Methods for Nanomechatronics: Signaling, Structure, and Functions Toward Nanorobots," *IEEE Transactions on Systems, Man, and Cybernetics, Part C: Applications and Reviews,* Vol. 42, No. 3, pp. 357-366, 2012.

[LIU-12a] Q. Liu, N. Hu, F. Zhang, D. Zhang, K. Hsia and P. Wang, "Olfactory epithelium biosensor: odor discrimination of receptor neurons from a bio-hybrid sensing system," *Biomed. Microdevices,* vol. 14, pp. 1055-1061, 2012.

[LLA-11] I. Llatser, I. Pascual, N. Garralda, A. Cabellos-Aparicio, M. Pierobon, E. Alarcon and J. Sole-Pareta, "Exploring the physical channel of diffusion-based molecular communication by simulation," in Global Telecommunications Conference (GLOBECOM 2011), IEEE, pp. 1-5, 2011.

[LLA-13] I. Llatser, A. Cabellos-Aparicio, M. Pierobon and E. Alarcon, "Detection Techniques for Diffusion-based Molecular Communication," *Selected Areas in Communications, IEEE Journal on*, vol. 31, pp. 726-734, 2013.

[LUT-08] J. F. Lutsko and J. P. Boon, "Generalized diffusion: A microscopic approach," *Physical Review E*, Vol. 77, pp. 051103, 2008.

[LUT-13] J. F. Lutsko and J. P. Boon, "Microscopic theory of anomalous diffusion based on particle interactions," *Physical Review E*, Vol. 88, pp. 022108-1-022108-8, 2013.

[LUT-13a] J. F. Lutsko and J. P. Boon, "Molecular theory of anomalous diffusion," ArXiv Preprint arXiv:1302.5574, 2013.

[MAH-10] M.U. Mahfuz, D. Makrakis, and H. Mouftah, "Spatiotemporal distribution and modulation schemes for concentration-encoded medium-to-long range molecular communication," in Proc. *25th Biennial Symposium on Communications (QBSC),* pp. 100-105, 12-14 May, 2010.

[MAH-10a] M.U. Mahfuz, D. Makrakis, and H.T. Mouftah, "Characterization of Molecular Communication Channel for Nanoscale Networks," in *Proc. 3rd International Conference on Bio-inspired Systems and Signal Processing (BIOSIGNALS-2010)*, pp. 327-332, Valencia, Spain, 20-23 January, 2010.

[MAH-10b] M.U. Mahfuz, D. Makrakis, and H.T. Mouftah, "On the characterization of binary concentration-encoded molecular communication in nanonetworks," *Nano Communication Networks,* Vol. 1, No. 4, pp. 289-300, Elsevier, 2010.

[MAH-11] M.U. Mahfuz, D. Makrakis, and H.T. Mouftah, "A comprehensive study of concentration-encoded unicast molecular communication with binary pulse transmission," in Proc. *11th IEEE Conference on Nanotechnology (IEEE-NANO),* pp. 227-232, Oregon, USA, 15-18 August, 2011.

[MAH-11a] M.U. Mahfuz, D. Makrakis, and H.T. Mouftah, "On the characteristics of concentration-encoded multi-level amplitude modulated unicast molecular communication," in *Proc. 24th Canadian Conference on Electrical and Computer Engineering (CCECE),* pp. 312-316, Niagara Falls, ON, 8-11 May, 2011.

[MAH-11b] M.U. Mahfuz, D. Makrakis, and H.T. Mouftah, "On the Detection of Binary Concentration-Encoded Unicast Molecular Communication in Nanonetworks," in *Proc. 4th International Conference on Bio-inspired Systems and Signal Processing (BIOSIGNALS-2011),* pp. 446-449, Rome, Italy, 26-29 January, 2011.

[MAH-11c] M.U. Mahfuz, D. Makrakis, and H.T. Mouftah, "Transient characterization of concentration-encoded molecular communication with sinusoidal stimulation," in Proc. *4th International Symposium on Applied Sciences in Biomedical and Communication Technologies (ISABEL '11),* Article No. 14, pp. 1-6, Barcelona, Spain, 26-29 October 2011.

[MAH-11d] Mahfuz, M.U., Makrakis, D. & Mouftah, H.T., "Characterization of intersymbol interference in concentration-encoded unicast molecular communication," in *Proc. 24th Canadian Conference on Electrical and Computer Engineering (CCECE)*, Niagara Falls, ON, May 2011, pp. 164-168.

[MAH-12] M.U. Mahfuz, *Nanoscale Communication Systems and Their Role in an Emerging Society,* Mini-course lecture slides, University of Ottawa, 2012.

[MAH-12a] M.U. Mahfuz, D. Makrakis, and H.T. Mouftah, "Strength Based Receiver Architecture and Communication Range and Rate Dependent Signal Detection Characteristics of Concentration Encoded Molecular Communication," in *Proc. Seventh International Conference on Broadband and Wireless Computing, Communication and Applications (BWCCA-2012)*, pp. 28-35, Victoria, BC, Canada, 12-14 November, 2012.

[MAH-13] M.U. Mahfuz, D. Makrakis, and H.T. Mouftah, "Sampling Based Optimum Signal Detection in Concentration-Encoded Molecular Communication Receiver Architecture and Performance," in *Proc. 6th International Conference on Bio-inspired Systems and Signal Processing (BIOSIGNALS-2013),* pp. 372-376, Barcelona, Spain, 11-14 February, 2013.

[MAH-13a] M.U. Mahfuz, D. Makrakis, and H.T. Mouftah, "Concentration Encoded Molecular Communication: Prospects and Challenges Towards Nanoscale Networks," in *Proc. International Conference on Engineering, Research, Innovation and Education (ICERIE-2013)*, Sylhet, Bangladesh, 11-13 January, 2013, pp. 508-513.

[MAH-13b] M.U. Mahfuz, D. Makrakis, and H.T. Mouftah, "A Generalized Strength-Based Signal Detection Model for Concentration-Encoded Molecular Communication," in *Proc. 8th International Conference on Body Area Networks (BodyNets 2013)*, Track: Nano-scale Communications and Networking, 30 Sept.–02 Oct. 2013, Boston, MA, USA, pp. 461-467, DOI: 10.4108/icst.bodynets.2013.253560.

[MAH-13c] M. U. Mahfuz, D. Makrakis, and H. T. Mouftah, "Strength-Based Optimum Signal Detection in Concentration-Encoded Pulse-Transmitted OOK Molecular Communication with Stochastic Ligand-Receptor Binding," *Simulation Modelling Practice and Theory* (Elsevier), Vol. 42, Special Issue: Molecular Communications, March 2014, pp. 189-209, http://dx.doi.org/10.1016/j.simpat.2013.11.005.

[MAH-13d] M. U. Mahfuz, D. Makrakis, and H.T. Mouftah, "Performance Analysis of Convolutional Coding Techniques in Diffusion-Based Concentration-Encoded PAM Molecular Communication Systems", *BioNanoScience* (Springer), vol. 3, no. 3, pp. 270-284, 2013.

[MAH-14] M. U. Mahfuz, D. Makrakis, and H.T. Mouftah, "A Comprehensive Analysis of Strength-Based Optimum Signal Detection in Concentration-Encoded Molecular Communication with Spike Transmission," under revision to *IEEE Transactions on Nanobioscience*, September, 2014.

[MAH-14a] M. U. Mahfuz, D. Makrakis, and H.T. Mouftah, “A Comprehensive Study of Sampling-Based Optimum Signal Detection in Concentration-Encoded Molecular Communication,” *IEEE Transactions on Nanobioscience*, Vol. 13, No. 3, pp. 208-222, September, 2014, DOI: 10.1109/TNB.2014.2341693.

[MAH-14b] M.U. Mahfuz, D. Makrakis, and H.T. Mouftah, “An Investigative Analysis on Concentration-Encoded Subdiffusive Molecular Communication in Nanonetworks,” to appear in *Proc. 14th IEEE International Conference on Nanotechnology (IEEE NANO-2014)*, 18-21 August, 2014, Toronto, Canada.

[MAL-12] D. Malak, and O.B. Akan, “Molecular communication nanonetworks inside human body,” *Nano Communication Networks,* Vol. 3, No. 1, pp. 19-35, Elsevier, 2012.

[MAN-02] M. Mano, *Digital Design*, Prentice-Hall, Upper Saddle River, NJ, 2002.

[MAS-63] J. L. Massey, Threshold Decoding. The MIT Press, Cambridge, MA, 1963.

[MAZ-11] B. Mazzeo and M. Rice, "On monte carlo simulation of the bit error rate," in *Proc. IEEE International Conference on Communications (ICC-2011)*, pp. 1-5.

[MEN-12] L. Meng, P. Yeh, K. Chen and I. F. Akyildiz, "Optimal detection for diffusion-based communications in the presence of ISI," in *Proc. GLOBECOM 2012*, December, 2012, pp. 3819-3824.

[MEN-12a] L. Meng, P. Yeh, K. Chen and I. F. Akyildiz, "A diffusion-based binary digital communication system," in *Proc. Communications (ICC), 2012 IEEE International Conference on*, 2012, pp. 4985-4989.

[MET-00] R. Metzler, and J. Klafter, “The random walk's guide to anomalous diffusion: a fractional dynamics approach,” *Physics Reports,* Vol. 339, No. 1, pp. 1-77, 2000.

[MEY-06] M. Meyyappan, J. Li, J. Li, and A. Cassell, “Nanotechnology: An Overview and Integration with MEMS,” in *Proc. 19th IEEE International Conference on Micro Electro Mechanical Systems (MEMS 2006),* pp. 1-3, Istanbul, Turkey, 22-26 January, 2006.

[MIO-11] D. Miorandi, “A stochastic model for molecular communications,” *Nano Communication Networks,* Vol. 2, No. 4, pp. 205-212, Elsevier, 2011.

[MOO-06] M. Moore, A. Enomoto, T. Nakano, R. Egashira, T. Suda, A. Kayasuga, H. Kojima, H. Sakakibara, and K. Oiwa, “A design of a molecular communication system for nanomachines using molecular motors,” in *Proc.*

Fourth Annual IEEE International Conference on Pervasive Computing and Communications Workshops, 6 pages, 2006.

[MOO-06a] M. Moore, A. Enomoto, T. Nakano, T. Suda, A. Kayasuga, H. Kojima, H. Sakakibara, and K. Oiwa, "Simulation of a Molecular Motor Based Communication Network," in *Proc. International Conference on Bio-Inspired Models of Network, Information and Computing Systems (BIONETICS 2006),* pp. 1, 11-13 December, 2006.

[MOO-07] M.J. Moore, A. Enomoto, T. Suda, T. Nakano, and Y. Okaie, "Molecular Communication: New Paradigm for Communication Among Nano-Scale Biological Machines" in *The Handbook of Computer Networks*, H. Bidgoli (Ed.), John Wiley and Sons Inc., 2007.

[MOO-07a] M. Moore, A. Enomoto, T. Nakano, Y. Okaie, and T. Suda, "Interfacing with nanomachines through molecular communication," in Proc. *IEEE International Conference on Systems, Man and Cybernetics (ISIC 2007),* pp. 18-23, 2007.

[MOO-08] M.J. Moore, A. Enomoto, T. Suda, A. Kayasuga, and K. Oiwa, "Molecular communication: Uni-cast communication on a microtubule topology," in *Proc. IEEE International Conference on Systems, Man and Cybernetics (SMC 2008),* 12-15 October, 2008.

[MOO-09] M.J. Moore, A. Enomoto, T. Nakano, A. Kayasuga, H. Kojima, H. Sakakibara, K. Oiwa, and T. Suda, "Molecular Communication: Simulation of Microtubule Topology," in *Natural Computing, Proceedings in Information and Communications Technology,* Vol. 1, pp. 134-144. 2009.

[MOO-09a] M. Moore, T. Suda and K. Oiwa, "Molecular Communication: Modeling Noise Effects on Information Rate," *IEEE Transactions on NanoBioscience,* Vol. 8, No. 2, pp. 169-180, 2009.

[MOO-11] M.J. Moore, and T. Nakano, "Synchronization of Inhibitory Molecular Spike Oscillators," in *Proc. 6th International Conference on Bio-Inspired Models of Network, Information and Computing Systems (BIONETICS '11),* York, UK, 05-06 December, 2011.

[MOO-11a] M.J. Moore, and T. Nakano, "Addressing by beacon coordinates using molecular communication," in *Proc. IEEE Conference on Computer Communications Workshops (INFOCOM WKSHPS),* pp. 455-460, 10-15 April, 2011.

[MOO-12] M.J. Moore, and T. Nakano, "Comparing Transmission, Propagation, and Receiving Options for Nanomachines to Measure Distance by Molecular

Communication," in *Proc. IEEE International Conference on Communications (ICC),* pp. 6132-6136, Ottawa, Canada, 10-15 June, 2012.

[MOO-12a] M.J. Moore, and T. Nakano, "Multiplexing over molecular communication channels from nanomachines to a micro-scale sensor device," in *Proc. IEEE Global Communications Conference (GLOBECOM 2012),* pp. 4302-4307, 3-7 December, 2012.

[MOO-12b] M.J. Moore, T. Nakano, A. Enomoto and T. Suda "Measuring Distance from Single Spike Feedback Signals in Molecular Communication," *IEEE Transactions on Signal Processing,* Vol. 60, Issue. 7, pp. 3576-3587, 2012.

[MOO-13] M. J. Moore and T. Nakano, "Oscillation and Synchronization of Molecular Machines by the Diffusion of Inhibitory Molecules," *IEEE Transactions on Nanotechnology*, vol. 12, pp. 601-608, 2013.

[MOO-14] M. J. Moore, Y. Okaie and T. Nakano, "Diffusion-Based Multiple Access by Nano-Transmitters to a Micro-Receiver," *IEEE Communications Letters*, vol. 18, pp. 385-388, 2014.

[MOR-06] Y. Moritani, S. Hiyama and T. Suda, "Molecular communication for health care applications," in *Proc. Fourth Annual IEEE International Conference on Pervasive Computing and Communications Workshops,* 5 pages, 13-17 March, 2006.

[MOR-06a] Y. Moritani, S.M. Nomura, S. Hiyama, K. Akiyoshi, and T. Suda, "A Molecular Communication Interface Using Liposomes with Gap Junction Proteins," in *Proc. International Conference on Bio-Inspired Models of Network, Information and Computing Systems,* 1 page, 11-13 December, 2006.

[MOR-07] Y. Moritani, S. S. Hiyama, Nomura, S.M., Akiyoshi, K. and T. Suda 2007, "A Communication interface using vesicles embedded with channel forming proteins in molecular communication," in *Proc. Bio-Inspired Models of Network, Information and Computing Systems (Bionetics 2007)*, 3 pages, Budapest, Hungary, 10-13 December, 2007.

[MOR-07a] Y. Moritani, S. Hiyama and T. Suda 2007, "Molecular Communication A Biochemically-Engineered Communication System," in *Proc. International Conference Frontiers in the Convergence of Bioscience and Information Technologies (FBIT 2007)*, pp. 839-844, Korea, 11-13 December, 2007.

[MOR-10] Y. Moritani, S. Hiyama and T. Suda, "A Molecular Communication System," in *Proc. IWNC 2009, PICT 2,* F. Peper et al. (Eds.), pp. 82-89, 2010.

[MOS-05] E.V. Mosharov, and D. Sulzer, "Analysis of exocytotic events recorded by amperometry," *Nature Methods,* Vol. 2, pp. 651-658, 2005.

[NAK-05] T. Nakano, T. Suda, M. Moore, R. Egashira, A. Enomoto, and K. Arima, "Molecular communication for nanomachines using intercellular calcium signaling," in *Proc. 5th IEEE Conference on Nanotechnology,* pp. 478-481, 2005.

[NAK-06] T. Nakano, M. Moore, A. Enomoto, T. Suda, T. Koujin, T. Haraguchi, and Y. Hiraoka, "A Cell-based Molecular Communication Network," in *Proc. International Conference on Bio-Inspired Models of Network, Information and Computing Systems (BIONETICS 2006),* 1 page, 11-13 December, 2006.

[NAK-07] T. Nakano, T. Suda, T. Koujin, Tokuko Haraguchi and Hiraoka, Y. 2007, "Molecular communication through gap junction channels: System design, experiments and modeling," in *Proc. International Conference on Bio-Inspired Models of Network, Information and Computing Systems (BIONETICS 2007),* pp. 139-146, 10-12 December, 2007.

[NAK-10] T. Nakano, "Biological Computing Based on Living Cells and Cell Communication," in *Proc.13th International Conference on Network-Based Information Systems (NBiS),* pp. 42-47, 2010.

[NAK-10a] T. Nakano, and J. Liu, "Design and Analysis of Molecular Relay Channels: An Information Theoretic Approach," *IEEE Transactions on NanoBioscience,* Vol. 9, No. 3, pp. 213-221, 2010.

[NAK-10b] T. Nakano, and M. Moore, "In-sequence molecule delivery over an aqueous medium," *Nano Communication Networks,* Vol. 1, No. 3, pp. 181-188, Elsevier, 2010.

[NAK-10c] T. Nakano, J. Shuai, T. Koujin, T. Suda, Y. Hiraoka, and T. Haraguchi, "Biological excitable media based on non-excitable cells and calcium signaling," *Nano Communication Networks,* Vol. 1, No. 1, pp. 43-49, Elsevier, 2010.

[NAK-11] T. Nakano, and M. Moore, "Molecular Communication Paradigm Overview," *Journal of Next Generation Information Technology,* Vol. 2, No. 1, pp. 9-16.

[NAK-11a] T. Nakano, M. Moore, A. Enomoto and T. Suda, "Molecular Communication Technology as a Biological ICT," *Biological Functions for Information and Communication Technologies*, H. Sawai (Ed.), Springer-Verlag, Berlin Heidelberg, pp. 49-86. 2011.

[NAK-11b] T. Nakano, "Biologically Inspired Network Systems: A Review and Future Prospects," *IEEE Transactions on Systems, Man, and Cybernetics, Part C: Applications and Reviews,* Vol. 41, No. 5, pp. 630-643.

[NAK-11c] T. Nakano, and J. Shuai, "Repeater design and modeling for molecular communication networks," in *Proc. IEEE Conference on Computer Communications Workshops (INFOCOM WKSHPS),* pp. 501-506, 2011.

[NAK-12] T. Nakano, M.J. Moore, F. Wei, A.V. Vasilakos, and J. Shuai, "Molecular Communication and Networking: Opportunities and Challenges," *IEEE Transactions on NanoBioscience,* Vol. 11, No. 2, pp. 135-148, 2012.

[NAK-12a] T. Nakano, Y. Okaie, and J.-Q. Liu, "Channel Model and Capacity Analysis of Molecular Communication with Brownian Motion," *IEEE Communications Letters,* Vol. 16, No. 6, pp. 797-800, 2012.

[NAK-12b] T. Nakano, Y. Okaie, and A.V. Vasilakos, "Throughput and efficiency of molecular communication between nanomachines," in *Proc. IEEE Wireless Communications and Networking Conference (WCNC),* pp. 704-708, 1-4 April, 2012.

[NAK-13] T. Nakano, T. Haraguchi, and A. W. Eckford. *Molecular Communication*, Cambridge University Press, 2013.

[NOE-13] A. Noel, K. C. Cheung and R. Schober, "Improving Receiver Performance of Diffusive Molecular Communication with Enzymes," ArXiv:1305.1926, pp. 1-12, 2013.

[OKA-12] Y. Okaie, and T. Nakano, "Nanomachine placement strategies for detecting Brownian molecules in nanonetworks," in *Proc. IEEE Wireless Communications and Networking Conference (WCNC), 2012 IEEE*, pp. 1755-1759, 1-4 April, 2012.

[OLV-10] F. W. J. Olver, Ed., *NIST Handbook of Mathematical Functions*, Ed. Frank W.J. Olver Et Al., Cambridge University Press: NIST, 2010.

[OZI-05] G. Ozin, I. Manners, S. Fournier-Bidoz, and A. Arsenault, "Dream Nanomachines," *Advanced Materials,* Vol. 17, No. 24, pp. 3011-3018, 2005.

[PAR-09] L. Parcerisa Giné, and I.F. Akyildiz, "Molecular communication options for long range nanonetworks," *Computer Networks,* Vol. 53, No. 16, pp. 2753-2766, 2009.

[PAR-97] H. Park, *Coded Modulation and Equalization for Wireless Infrared Communications,* Ph.D. thesis, Georgia Institute of Technology, USA, 1997.

[PHI-06] J. Philibert, “One and a Half Century of Diffusion: Fick, Einstein, Before and Beyond,” *Diffusion Fundamentals,* Vol. 4 (2006), pp. 6.1-6.19, 2006.

[PIE-10] M. Pierobon and I.F. Akyildiz, “A physical end-to-end model for molecular communication in nanonetworks,” *IEEE Journal on Selected Areas in Communications,* Vol. 28, No. 4, pp. 602-611, 2010.

[PIE-11] M. Pierobon and I.F. Akyildiz, “Diffusion-Based Noise Analysis for Molecular Communication in Nanonetworks,” *IEEE Transactions on Signal Processing,* Vol. 59, No. 6, pp. 2532-2547, 2011.

[PIE-11a] M. Pierobon and I.F. Akyildiz, “Information capacity of diffusion-based molecular communication in nanonetworks,” in *Proc. IEEE INFOCOM,* pp. 506-510, 10-15 April, 2011.

[PIE-11b] M. Pierobon and I.F. Akyildiz, “Noise Analysis in Ligand-Binding Reception for Molecular Communication in Nanonetworks,” *IEEE Transactions on Signal Processing,* Vol. 59, No. 9, pp. 4168-4182, 2011.

[PRA-00] K. Prank, F. Gabbiani, and G. Brabant, “Coding efficiency and information rates in transmembrane signaling,” *Biosystems,* Vol. 55, No. 1-3, pp. 15-22, 2000.

[QIN-12] D. Qin and B. A. Riggs, "Nanotechnology: A Top–Down Approach," *Encyclopedia of Supramolecular Chemistry*, DOI: 10.1081/E-ESMC-120047104, Taylor & Francis, 2012.

[RAP-02] T. S. Rappaport, *Wireless communications: Principles and Practice*, Prentice Hall PTR, Upper Saddle River, N.J., 2002.

[RAV-09] R. Ravichandran, “Nanotechnology-Based Drug Delivery Systems,” *Nanobiotechnol.,* Vol. 5, pp. 17-33, 2009.

[ROB-23] O.F.T. Roberts, “The Theoretical Scattering of Smoke in a Turbulent Atmosphere,” in *Proc. Royal Society of London. Series A, Containing Papers of a Mathematical and Physical Character,* Vol. 104, No. 728, pp. 640-654, 1923.

[ROS-00] J. Rospars, V. Křivan, and P. Lánský, “Perireceptor and Receptor Events in Olfaction. Comparison of Concentration and Flux Detectors: a Modeling Study,” *Chemical senses,* Vol. 25, No. 3, pp. 293-311, 2000.

[ROS-04] J. P. Rospars and P. Lánský, “Stochastic pulse stimulation in chemoreceptors and its properties,” *Math. Biosci.*, vol. 188, pp. 133-145, 2004.

[RYA-03] Y. E. Ryabov, "Behavior of fractional diffusion at the origin," *Physical Review E*, Vol. 68, pp. 1-4, 2003.

[SAS-06] Y. Sasaki, M. Hashizume, K. Maruo, N. Yamasaki, J. Kikuchi, Y. Moritani, S. Hiyama and T. Suda, "Controlled Propagation in Molecular Communication Using Tagged Liposome Containers," in *Proc. International Conference on Bio-Inspired Models of Network, Information and Computing Systems (BIONETICS 2006),* 1 page, 2006.

[SCH-02] S. Schuster, M. Marhl and T. Höfer, "Modelling of simple and complex calcium oscillations," *European Journal of Biochemistry*, vol. 269, pp. 1333-1355, 2002.

[SCH-03] M. Schliwa, and G. Woehlke, "Molecular motors," *Nature,* Vol. 422, No. 6933, pp. 759-765, 2003.

[SCH-75] H. Scher and E. W. Montroll, "Anomalous transit-time dispersion in amorphous solids," *Physical Review B*, Vol. 12, pp. 2455, 1975.

[SCH-93] C. Schofl, G. Brabant, R.D. Hesch, A. von zur Muhlen, P.H. Cobbold, and K.S. Cuthbertson, "Temporal patterns of alpha 1-receptor stimulation regulate amplitude and frequency of calcium transients," *Am. J. Physiol. Cell Physiol.,* Vol. 265, No. 4, pp. C1030-C1036, 1993.

[SHA-12] H. ShahMohammadian, G.G. Messier and S. Magierowski, "Optimum receiver for molecule shift keying modulation in diffusion-based molecular communication channels," *Nano Communication Networks*, vol. 3, pp. 183-195, Elsevier, 2012.

[SHA-13] H. ShahMohammadian, G.G. Messier and S. Magierowski, "Nano-machine molecular communication over a moving propagation medium," *Nano Communication Networks*, vol. 1 July, pp. 1-12, 2013.

[SHI-12] P.-J. Shih, C.-H. Lee, and P.-C. Yeh. "Channel codes for mitigating intersymbol interference in diffusion-based molecular communications," in *Proc. Global Communications Conference (GLOBECOM)*, pp. 4228-4232, 2012.

[SHI-13] P.-J. Shih, C.-H. Lee, P.-C. Yeh, and K.-C. Chen. "Channel Codes for Reliability Enhancement in Molecular Communication." *Selected Areas in Communications, IEEE Journal on*, Vol. 31, No. 12 , pp. 857-867, 2013.

[SMI-00] J.M. Smith, "The Concept of Information in Biology," *Philosophy of Science,* Vol. 67, No. 2, pp. 177-194, 2000.

[SOK-12] I. M. Sokolov, "Models of anomalous diffusion in crowded environments," *Soft Matter*, Vol. 8, pp. 9043-9052, 2012.

[SRI-12] K. Srinivas, R. Adve, A. Eckford, "Molecular Communication in Fluid Media: The Additive Inverse Gaussian Noise Channel," *IEEE Transactions on Information Theory,* Vol. 58, No. 7, pp. 4678-4692, 2012.

[SUD-05] T. Suda, M. Moore, T. Nakano, R. Egashira, and A. Enomoto, "Exploratory Research on Molecular Communication between Nanomachines," in *Proc. Genetic and Evolutionary Computation Conference (GECCO),* Late Breaking Papers, 25-29 June, 2005.

[SUN-10] H. Sun, W. Chen, C. Li and Y. Chen, "Fractional differential models for anomalous diffusion," *Physica A: Statistical Mechanics and its Applications*, Vol. 389, pp. 2719-2724, 2010.

[TAN-74] N. Taniguchi, "On the basic concept of nanotechnology," in Proc. International Conference of Production Engineering, Part II, Tokyo, Japan Society of Precision Engineering, 1974, pp. 18-23.

[TAY-21] G. I. Taylor, "Diffusion by continuous movements," in *Proceedings of the London Mathematical Society*, Vol. 20, pp. 196-211, 1921.

[THO-04] P.J. Thomas, D.J. Spencer, S.K. Hampton, P. Park, and J.P. Zurkus, "The diffusion mediated biochemical signal relay channel," *Adv. Neural Inform. Process. Syst.,* Vol. 16, pp. 1263-1270, 2004.

[TRA-04] W. H. Tranter, K. S. Shanmugan, T. S. Rappaport, *Principles of Communication Systems Simulation with Wireless Applications*, Upper Saddle River, N.J.: Prentice Hall, 2004.

[TSE-03] A.A. Tseng, K. Chen, C. D. Chen and K. J. Ma, "Electron beam lithography in nanoscale fabrication: recent development," *Electronics Packaging Manufacturing, IEEE Transactions on,* vol. 26, pp. 141-149, 2003.

[URS-11] T.S. Ursell, *The Diffusion Equation A Multi-dimensional Tutorial*, Department of Applied Physics, California Institute of Technology, Pasadena; CA 91125, 2011.

[VAN-05] B.P. van Milligen, P.D. Bons, B.A. Carreras, and R. Sánchez, "On the applicability of Fick's law to diffusion in inhomogeneous systems," *European Journal of Physics,* Vol. 26, No. 5, pp. 913-925, 2005.

[VAN-68] H.L. Van Trees, *Detection, Estimation, and Modulation Theory*, Part-1, New York: Wiley, 1968.

[VIT-67] A. Viterbi, "Error bounds for convolutional codes and an asymptotically optimum decoding algorithm," *IEEE Transactions on Information Theory*, vol. 13, pp. 260-269, 1967.

[VLA-08] L. Vlahos, H. Isliker, Y. Kominis and K. Hizanidis, "Normal and anomalous diffusion: A tutorial." ArXiv e-Prints, 2008.

[WAL-07] F. Walsh, S. Balasubramaniam, D. Botvich, and W. Donnelly, "Review of communication mechanisms for biological Nano and MEMS devices," in *Proc. International Conference on Bio-Inspired Models of Network, Information and Computing Systems (BIONETICS 2007),* pp. 307-312, 2007.

[WEI-04] M. Weiss, M. Elsner, F. Kartberg and T. Nilsson, "Anomalous Subdiffusion Is a Measure for Cytoplasmic Crowding in Living Cells," *Biophys. J.*, Vol. 87, pp. 3518-3524, 200411, 2004.

[WIL-96] J. L. Wilbur, A. Kumar, H. A. Biebuyck, E. Kim and G. M. Whitesides, "Microcontact printing of self-assembled monolayers: applications in microfabrication," *Nanotechnology,* vol. 7, pp. 452-457, 1996-12-01, 1996.

[WOZ-57] J. M. Wozencraft, "Sequential Decoding for Reliable Communications," IRE Nat. Conv. Rec., vol. 5, pp. 11-25, 1957.

[XIA-03] Y. Xia, P. Yang, Y. Sun, Y. Wu, B. Mayers, B. Gates, Y. Yin, F. Kim, and H. Yan, "One-Dimensional Nanostructures: Synthesis, Characterization, and Applications," *Advanced Materials,* Vol. 15, No. 5, pp. 353-389, 2003.

[YUN-07] Y. J. Yun, C. S. Ah, S. Kim, W. S. Yun, B. C. Park and D. H. Ha, "Manipulation of freestanding Au nanogears using an atomic force microscope," Nanotechnology, vol. 18, pp. 505304, 2007.

Appendix A: Convolutional Coded Schemes in the Context of MC

In the case of channel coding without combined modulation and coding (also known as *trellis-coding*) [LEE-94], the added bit redundancy reduces the spectral efficiency of the communication systems, thus when comparing the uncoded and the coded system by holding the occupied frequency band equal, the effective information bit rate of the coded system is lower. Figure A.1 shows a typical channel encoding and channel decoding sections of a digital communication system where the functionality of the channel encoder is located at the TN and that of the channel decoder is located at the RN. The source of information transforms the information content to a sequence of bits that acts as input to the convolutional encoder (CE). The output of the channel encoder is the coded bit sequence. As shown in Fig. A.2, the CE adds redundant bits generated by applying *modulo-2* algebraic operations to the input bit sequence with the addition of delay elements denoted as the blocks marked as "Delay" [LIN-83]. In fact, a CE is a finite memory system, meaning that a CE process depends on the current and previous message inputs (in this case, bits).

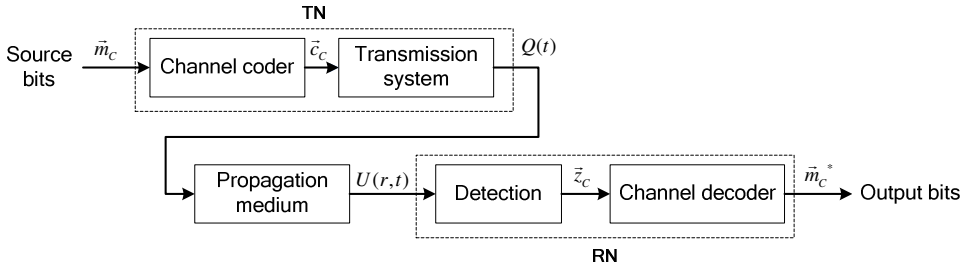

Figure A.1 Channel coding and decoding portions of a digital communication system.

A CE is represented by three parameters: the codeword length n_C, the message[28] length k_C, and the constraint length υ. Here υ is defined as the memory length V (i.e. the number of previous messages involved) of the CE, plus 1, that is, $\upsilon = V + 1$. For each message of length k_C bits, the CE generates a coded sequence of length n_C bits. The coding rate of the CE is k_C/n_C. In most systems that use CE, k_C and n_C are small integers; however, V can

[28] The term *message* refers to a block of k_C bits that is formed and treated as an "entity" by all units of the system.

be large in order to achieve better performance. Since CEMC is a slow communication process, for each bit (i.e. $k_C = 1$) we prefer to test the performance of the CEMC system for a CE system with $n_C = 2$ (i.e. rate ½). In addition, considering the fact that a TN is capable of doing simple tasks only, we would prefer to use small values of υ, e.g. $\upsilon = 2$, 3, and 4 only. For example, for $\upsilon = 4$, the CE at the TN has $V = 3$ memory units in it, containing the 3 earlier input messages before the present one. An (n_C,k_C, υ) convolutional code outputs a sequence for transmission that is determined by the present information symbol and the previous ($\upsilon - 1$) symbols. For instance, for an (n_C,1, υ) binary convolutional code, the binary information sequence $\vec{m}_C = \left[m_{C,1}, m_{C,2}, \ldots \ldots, m_{C,t_{\text{int}}-1}, m_{C,t_{\text{int}}}, m_{C,t_{\text{int}}+1}, \ldots\ldots, m_{C,N_{in}} \right]$, where t_{int} is integer and $\vec{m}_C$ is a binary sequence; when the CE system receives an input bit at time t_{int} as shown in Fig. A.2(a) it produces an n_C-bit (output) codeword $\vec{c}_{C,t_{\text{int}}} = \left(c_{C,t_{\text{int}}}^{(1)} c_{C,t_{\text{int}}}^{(2)} \ldots\ldots c_{C,t_{\text{int}}}^{(n_C)} \right)$ as follows:

$$c_{C,t_{\text{int}}}^{(j)} = gm_0^{(j)} m_{C,t_{\text{int}}} \oplus gm_1^{(j)} m_{C,t_{\text{int}}-1} \oplus gm_2^{(j)} m_{C,t_{\text{int}}-2} \oplus \ldots. \oplus gm_{\upsilon-1}^{(j)} m_{C,t_{\text{int}}-\upsilon+1} \tag{A.1}$$

with $1 \le j \le n_C$ and $gm_i^{(j)} \in \{0,1\}$ where $0 \le i \le \upsilon - 1$. The CE logic block is fully defined by the code generator matrix

$$GM = \begin{bmatrix} gm_0^1 & gm_1^1 & \ldots\ldots & gm_{\upsilon-2}^1 & gm_{\upsilon-1}^1 \\ gm_0^2 & gm_1^2 & \ldots\ldots & gm_{\upsilon-2}^2 & gm_{\upsilon-1}^2 \\ . & . & . & . & . \\ . & . & . & . & . \\ gm_0^{n_C-1} & gm_1^{n_C-1} & \ldots\ldots & gm_{\upsilon-2}^{n_C-1} & gm_{\upsilon-1}^{n_C-1} \\ gm_0^{n_C} & gm_1^{n_C} & \ldots\ldots & gm_{\upsilon-2}^{n_C} & gm_{\upsilon-1}^{n_C} \end{bmatrix} \tag{A.2}$$

with $0 \le i \le \upsilon - 1, 1 \le j \le n_C$. For example, a simple (2,1,3) CE with $GM = \begin{bmatrix} 1 & 1 & 1 \\ 1 & 0 & 1 \end{bmatrix}$ gives the following:

$$\begin{aligned} c_{C,t_{\text{int}}}^{(1)} &= m_{C,t_{\text{int}}} \oplus m_{C,(t_{\text{int}}-1)} \oplus m_{C,(t_{\text{int}}-2)} \\ c_{C,t_{\text{int}}}^{(2)} &= m_{C,t_{\text{int}}} \oplus m_{C,(t_{\text{int}}-2)} \end{aligned} \tag{A.3}$$

The above representation of the code generators is very useful in describing the CE system [JIA-10] and will be useful in understanding Fig. 7.1 in Chapter 7.

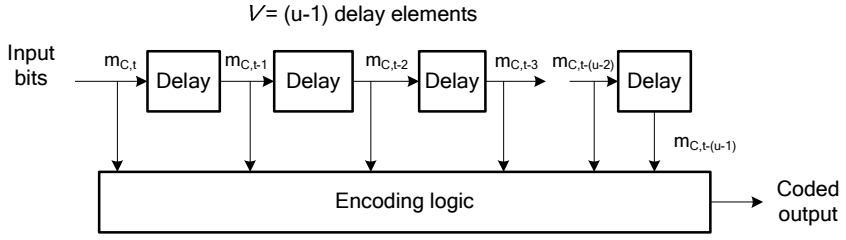

(a) CE: (n,1,υ)

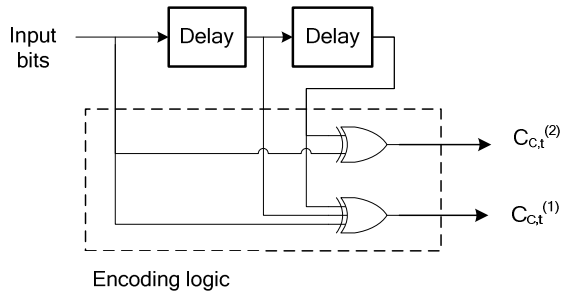

(b) CE: (2,1,3)

Figure A.2 Structure of a binary convolutional encoder: a generalized structure of $(n,1,\upsilon)$ CE in (a), and a typical structure of (2,1,3) CE in (b). For ease in writing the symbols in this figure, the subscript "$_{\text{int}}$" in t_{int} is dropped and hence t_{int} is written as t only.

The performance of the coded system can be improved by increasing the code length [JIA-10]. However, since decoding complexity at the receiver increases exponentially as the code length increases, considering the complexity limitations of the RN, we should be careful of how we use the idea of increasing the code length in order to improve performance, as we could easily end up with a decoder structure that is impractical for implementation in the RN.

The most popular methods for the decoding of convolutional coded bits are *sequential decoding*, *Viterbi decoding*, and *majority logic decoding*, the former two being more popular than the last one. *Sequential decoding,* introduced in [WOZ-57], is the first practical decoding technique developed for CE [JIA-10]. *Majority logic decoding* is a threshold-based approach [JIA-10] [MAS-63] and appeared before *Viterbi decoding*. In 1967 Viterbi published a new decoding method, widely known as *Viterbi decoding,* that is optimum in

the maximum-likelihood (ML) sense (thus under full complexity achieves the highest probability possible to have selected the correct sequence) and requires considerably lower computational complexity compared to *sequential decoding* and *majority logic decoding* [JIA-10] [VIT-67]. Due to their vast popularity and wide-spread use we briefly introduce the ML-based *sequential decoding* and *Viterbi decoding* of convolutional codes in this appendix.

We define $\vec{m}_C = \left[m_{C,1}, m_{C,2}, \ldots\ldots, m_{C,t_{\text{int}}-1}, m_{C,t_{\text{int}}}, m_{C,t_{\text{int}}+1}, \ldots\ldots, m_{C,N_{in}} \right]$ as the *transmitted information sequence (TIS)* entering the CE, where N_{in} is the length of the TIS $\vec{m}_C$. We constrain that the CE generates a unique encoded bit sequence $\vec{c}_{C,\mu_C}$ when $\vec{m}_{C,\mu_C}$ is the TIS, different from any other encoded sequence the encoder can generate for N_{in}-bit long TIS and the property is bidirectional, i.e. when $\vec{m}_{C,\mu_C} \neq \vec{m}_{C,\gamma_C} \Leftrightarrow \vec{c}_{C,\mu_C} \neq \vec{c}_{C,\gamma_C}$. Here μ_C and γ_C denote the corresponding sequence numbers. This is a necessary condition in every practical channel coding system. As shown in Fig. A.1, the PAM transmitted signal at the output of the transmission system block is denoted as $Q(t)$. The signal after passing through the propagation channel can be given by the time domain convolution of the transmitted signal and the energy-normalized impulse response of the propagation channel and can be denoted as $U(r,t)$ as shown in Chapter 3. The selection of the *received information sequence (RIS)* is made by using bit sequence selection rule of the ML-based sequential decoding of convolutional codes expressed as

$$p\left(\vec{m}_C^{\,*} \mid \vec{z}_C\right) = \max_{\{\vec{m}_C\}} p\left(\vec{m}_C \mid \vec{z}_C\right) \Leftrightarrow p\left(\vec{c}_C^{\,*} \mid \vec{z}_C\right) = \max_{\{\vec{c}_C\}} p\left(\vec{c}_C \mid \vec{z}_C\right) \tag{A.4}$$

where $\vec{z}_C = [z_{C,1}, z_{C,2}, ..., z_{C,N_Z}]$ is the sequence of samples $z_{C,j}$ collected at the output of the demodulator-detector $\left(j \in \{1,2,3,...,N_Z-1,N_Z\}\right)$, N_Z is the length of $\vec{z}_C$, and $\vec{m}_C^{\,*}$ is N_{in}–bit TIS selected as RIS and *p* denotes probability of an event. Eq. (A.4) indicates that having received $\vec{z}_C$, among all possible $\vec{m}_C$, $\vec{m}_C^{\,*}$ is the most likely TIS. Equivalently, having received $\vec{z}_C$, among all possible encoded sequences $\vec{c}_C$, $\vec{c}_C^{\,*}(\text{having} \Leftrightarrow \vec{m}_C^{\,*})$ is the most likely coded sequence decided as having been sent. When $p\left(\vec{m}_{C,\mu_C}\right) = p\left(\vec{m}_{C,\gamma_C}\right) \forall\ \vec{m}_{C,\mu_C} \neq \vec{m}_{C,\gamma_C}$, the decision law expressed in Eq. (A.4) is deduced to the following:

$$p\left(\vec{z}_C \mid \vec{m}_C{}^*\right) = \max_{\{\vec{m}_C\}} p\left(\vec{z}_C \mid \vec{m}_C\right) \Leftrightarrow p\left(\vec{z}_C \mid \vec{c}_C{}^*\right) = \max_{\{\vec{c}_C\}} p\left(\vec{z}_C \mid \vec{c}_C\right) \tag{A.5}$$

For a memoryless binary symmetric channel (BSC) this can be written as

$$p\left(\vec{z}_C \mid \vec{m}_{C,\lambda_C} \Leftrightarrow \vec{c}_{C,\lambda_C}\right) = \prod_{i=1}^{n_C} p\left(z_{C,i} \mid c_{C,i}^{\lambda_C}\right) \tag{A.6}$$

where $\vec{m}_{C,\lambda_C} = \left[m_{C,1}^{\lambda_C}, m_{C,2}^{\lambda_C}, ..., m_{C,N_{in}-1}^{\lambda_C}, m_{C,N_{in}}^{\lambda_C}\right] \Leftrightarrow \vec{c}_{C,\lambda_C} = \left[c_{C,1}^{\lambda_C}, c_{C,2}^{\lambda_C}, ..., c_{C,n_C-1}^{\lambda_C}, c_{C,n_C}^{\lambda_C}\right]$, λ_C is the sequence number, and n_C is the length of generated codewords. In the case of BSC, $z_{C,i}$ are binary symbols and

$$p\left(z_{C,i} \mid c_{C,i}^{\lambda_C}\right) = \begin{cases} 1 - p_X & \text{if } z_{C,i} = c_{C,i}^{\lambda_C} \\ p_X & \text{if } z_{C,i} \neq c_{C,i}^{\lambda_C} \end{cases} \tag{A.7}$$

with p_X being the *crossover probability* of the BSC. From Eqs. (A.6) and (A.7) we get the likelihood function of the BSC as [JIA-10]

$$p\left(\vec{z}_C \mid \vec{m}_{C,\lambda_C} \Leftrightarrow \vec{c}_{C,\lambda_C}\right) = p_X{}^{d_H\left(\vec{z}_C;\vec{c}_{C,\lambda_C}\right)} \left(1 - p_X\right)^{\left[n_C - d_H\left(\vec{z}_C;\vec{c}_{C,\lambda_C}\right)\right]} \tag{A.8}$$

where $d_H\left(\vec{z}_C;\vec{c}_{C,\lambda_C}\right)$ is the *Hamming distance* between the received sequence and the coded sequence, i.e. the number of locations the binary sequences $\vec{z}_C$ and $\vec{c}_{C,\lambda_C}$ differ, $d_H\left(\vec{z}_C;\vec{c}_{C,\lambda_C}\right) = \sum_{i=1}^{n_C} (z_{C,i} \oplus c_{C,i}^{\lambda_C})$ and $\oplus$ is modulo-2 addition. As seen from Eq. (A.8), $p\left(\vec{z}_C \mid \vec{c}_{C,\lambda_C}\right)$ is a monotonically decreasing function of $d_H\left(\vec{z}_C;\vec{c}_{C,\lambda_C}\right)$, and therefore, maximizing $p\left(\vec{z}_C \mid \vec{c}_{C,\lambda_C}\right)$ results in selecting the code sequence with the minimum Hamming distance in respect to $\vec{z}_C$. Thus, from Eq. (A.8) we deduce:

$$\vec{m}_C{}^* \Leftrightarrow \vec{c}_C{}^* = \min_{\{\vec{m}_C \Leftrightarrow \vec{c}_C\}} \left[d_H(\vec{z}_C;\vec{c}_C)\right] \tag{A.9}$$

The complexity and decoding time of ML sequential decoder increases exponentially with the length of bit sequence, which makes sequential decoding non-scalable when TIS is long. Performance wise, the *Viterbi decoder* provides exactly the same output as that of the ML sequential decoder, however, with reduced complexity in decoder structure by virtue of performing the decoding process more intelligently. The Viterbi decoding is based on the minimum distance path between the received sequence and the coded sequence. Viterbi

decoding relies on the calculation of two metrics: a branch metric (BM) and a path metric (PM) [JIA-10].

Assuming that $\vec{c}_C$ and $\vec{z}_C$ denote the transmitted codeword and received vector (corresponding to the transmitted codeword) respectively, the BM and the PM can be expressed as in Eq. (A.10) for a BSC channel [JIA-10]. The BM measures the distance between the received vector and the transmitted codeword in terms of $d_H\left(\vec{z}_C, \vec{c}_C\right)$, whereas the PM of a given state Ω_S at any time t_{Ω_S} in the trellis is the accumulation of all the branch metrics on the path, as shown below.

$$
\begin{aligned}
&BM\left(\vec{z}_C, \vec{c}_C\right) = d_H\left(\vec{z}_C, \vec{c}_C\right) \\
&PM_{\left(\Omega_S, t_{\Omega_S}\right)} = \sum_{\{\text{branch}\}} BM\left(\vec{z}_C, \vec{c}_C\right) \\
&PM_{\left(\Omega_S, t_{\Omega_S}+1\right)} = PM_{\left(\Omega_S', t_{\Omega_S}\right)} + BM_{\left(\Omega_S', t_{\Omega_S}\right)\rightarrow\left(\Omega_S, t_{\Omega_S}+1\right)}
\end{aligned}
\tag{A.10}
$$

The PM of the next node is also the summation of the PM of the current node and the BM of the branch from current node to the next node. Viterbi decoding decodes the output bits according to the minimum PM.

As mentioned before, convolutional coding scheme adds redundancy in the bit sequence transmitted by the TN in the propagation medium, implying that information data rate needs to be sacrificed for the sake of reliability of communication, unless there is any available technique that restores the original data rate of the system. An uncoded bit sequence does not have redundant bits and the bit rate of the uncoded system is $B_{Sys} = f_u \log_2 M_u$ where f_u and M_u denote the symbol rate and the alphabet size of the uncoded system respectively. There are two possible ways to introduce redundancy into the transmitted signal, either or both of which can be adopted simultaneously [LEE-94]. The first method introduces a higher symbol rate $f > f_u$ by inserting extra symbols into the bit stream, which increases B_{Sys}. In this case, the coded symbols are of less time duration compared to the uncoded symbols, i.e. $\left(1/f\right) < \left(1/f_u\right)$. The second method uses a larger alphabet size $M > M_u$, i.e. it increases B_{Sys} by increasing the number of symbols in the alphabet. Applying both methods simultaneously is also possible; however, in this research, as shown in Chapter 7, we have explored the first two approaches only and examined their implication in the design of CEMC system.

Appendix B: Additional Results on Strength-based Detection

B.1 Strength-based Generalized ASK Detection in CEMC

While Chapter 5 presented strength-based optimum signal detection in CEMC in detail, here we present a suboptimum version of the strength-based receiver that relies only on computing the strength observation z_{ED} and comparing it with a threshold. The results on generalized strength-based receiver presented here have been published in one of our earlier works reported in [MAH-13b].

Using Eq. (5.4a) in Chapter 5 the ROC curves have been analytically found for the generalized ASK-modulated signal detection scheme with diffusion noise and ISI as shown below

$$P_{\text{FA}} = \Pr\left\{z_{\text{ED}} > \tilde{\gamma}_{\text{ED}}; \text{H}_0\right\} = \mathcal{Q}\left(\frac{\tilde{\gamma}_{\text{ED}} - s_{\text{ED}}^{(0)} - \mu_{\text{ISI (ED)}}}{\sqrt{\sigma_{\text{S (ED)}}^{2(0)} + \sigma_{\text{ISI (ED)}}^2}}\right) \tag{B.1}$$
$$P_{\text{D}} = \Pr\left\{z_{\text{ED}} > \tilde{\gamma}_{\text{ED}}; \text{H}_1\right\} = \mathcal{Q}\left(\frac{\tilde{\gamma}_{\text{ED}} - s_{\text{ED}}^{(1)} - \mu_{\text{ISI (ED)}}}{\sqrt{\sigma_{\text{S (ED)}}^{2(1)} + \sigma_{\text{ISI (ED)}}^2}}\right)$$

where $\tilde{\gamma}_{\text{ED}}$ is the threshold for strength-based generalized ASK detection and the other symbols have been as described in Chapter 5. Expressing the threshold $\tilde{\gamma}_{\text{ED}}$ in terms of P_{FA} yields the P_{D} as shown below.

$$P_{\text{D}} = \mathcal{Q}\left(\frac{\sqrt{\sigma_{\text{S (ED)}}^{2(0)} + \sigma_{\text{ISI (ED)}}^2}}{\sqrt{\sigma_{\text{S (ED)}}^{2(1)} + \sigma_{\text{ISI (ED)}}^2}}\mathcal{Q}^{-1}(P_{\text{FA}}) - \frac{\left(s_{\text{ED}}^{(1)} - s_{\text{ED}}^{(0)}\right)}{\sqrt{\sigma_{\text{S (ED)}}^{2(1)} + \sigma_{\text{ISI (ED)}}^2}}\right) \tag{B.2}$$

Here $s_{\text{ED}}^{(1)} > s_{\text{ED}}^{(0)}$ and $\mathcal{Q}(\cdot)$ is the *right tail probability* expressed as $\mathcal{Q}(x_{\mathcal{Q}}) = \int_{x_{\mathcal{Q}}}^{\infty} \frac{1}{\sqrt{2\pi}} \exp\left(-\frac{1}{2}q^2\right) dq$ [KAY-93]. For equiprobable bits transmitted by the TN, $\Pr(\text{H}_0) = \Pr(\text{H}_1) = 1/2$, and so BER can be expressed as the following.

$$\text{BER} = \frac{(1 - P_{\text{D}}) + P_{\text{FA}}}{2} \tag{B.3}$$

For a given P_{FA}, BER decreases as P_{D} increases and vice versa. Therefore, keeping P_{FA} unchanged a detector that maximizes P_{D} would be desired. The most noteworthy feature of the detection performance of the generalized ASK receiver (Eq. (B.2)) is that the terms

$\sqrt{\left(\sigma^{2(0)}_{\mathrm{S\,(ED)}}+\sigma^{2}_{\mathrm{ISI\,(ED)}}\right)\Big/\left(\sigma^{2(1)}_{\mathrm{S\,(ED)}}+\sigma^{2}_{\mathrm{ISI\,(ED)}}\right)}$ and $\left(s^{(1)}_{\mathrm{ED}}-s^{(0)}_{\mathrm{ED}}\right)\Big/\sqrt{\sigma^{2(1)}_{\mathrm{S\,(ED)}}+\sigma^{2}_{\mathrm{ISI\,(ED)}}}$ impact the detection performance, which is different from the detection performance found in many traditional AWGN-affected communication signals, e.g. see [KAY-93]. In addition, it is important to note that the variances of the diffusion noise in both H_1 and H_0 hypotheses are functions of the signal values themselves respectively (see Eq. (5.1)), which ultimately yield the complicated structure of the detection performance shown in Eq. (B.2).

B.2 A Simple Receiver for ASK Detection

Using Eq. (B.2) the performance of any detector that detects ASK-modulated CEMC signals can be obtained. However, in this appendix, the detection performance of a generalized binary CEMC receiver is investigated, where the TN transmitted Q_0 and Q_1 molecules respectively, and $Q_1 = 2Q_0$. As a result, the mean and the variance of z_{ED} can be expressed as below.

$$\begin{aligned} & s_1(t)=Q_1 p(t),\ s_0(t)=Q_0 p(t),\ \text{where } Q_1=2Q_0 \\ \Rightarrow\ & s_1(t)=2s_0(t) \text{ which gives } s^{(1)}_{\mathrm{ED}}=2s^{(0)}_{\mathrm{ED}} \text{ and } \sigma^{2(1)}_{\mathrm{S\,(ED)}}=2\sigma^{2(0)}_{\mathrm{S\,(ED)}} \end{aligned} \tag{B.4}$$

In this particular and simple detection model, the receiver is not capable of estimating the exact number of ISI-producing molecules in the current symbol and assumes that a minimum ISI is present in the system. Under this scenario the receiver is simple in terms of functional complexity required to detect the information symbols. This can be considered acceptable in view of the extremely limited tasks and capabilities of a nanomachine [AKY-08] such that the RN may not have the ability to compute the ISI-producing molecules at all. In this particular scenario, the RN assumes that there occurs minimum one ISI-producing molecule on average such that $n^{\mathrm{ISI}}_{\mathrm{ED}} \sim \mathcal{N}\left(\mu_{\mathrm{ISI\,(ED)}},\sigma^2_{\mathrm{ISI\,(ED)}}\right)=\mathcal{N}(1,1)$. From the system designer's point of view, it would be possible to design a CEMC transmitted signal such that T_{sym} is much greater than the RMS delay spread [RAP-02] of the CEMC channel, which would ensure that minimum or no ISI-producing molecules are present in the current symbol. As a result, $\sigma^{2(0)}_{\mathrm{S\,(ED)}} \gg \sigma^{2}_{\mathrm{ISI\,(ED)}}$ and $\sigma^{2(1)}_{\mathrm{S\,(ED)}} \gg \sigma^{2}_{\mathrm{ISI\,(ED)}}$. Correspondingly, using Eq. (B.2) the detection performance of the detector based on Eq. (B.4) can be derived as below.

$$P_{\mathrm{D}} = \mathcal{Q}\left(\frac{\mathcal{Q}^{-1}\left(P_{\mathrm{FA}}\right)}{\sqrt{2}} - \frac{1}{2}\left(\frac{s_{\mathrm{ED}}^{(1)}}{\sigma_{\mathrm{S\,(ED)}}^{(1)}} \right) \right) \tag{B.5}$$

The analytical detection performance and the ROC of the detector based on Eqs. (B.4) and (B.5) are shown in Figs. B.1 and B.2 respectively. Note that the term $\left(s_{\mathrm{ED}}^{(1)}/\sigma_{\mathrm{S\,(ED)}}^{(1)}\right)$ can be thought of as the *signal to noise ratio* (SNR) when H_1 is true, where $\left(\sigma_{\mathrm{S\,(ED)}}^{(1)}/s_{\mathrm{ED}}^{(1)}\right)$ is known as the *coefficient of variation* (c_{V}) of z_{ED} when H_1 is true.

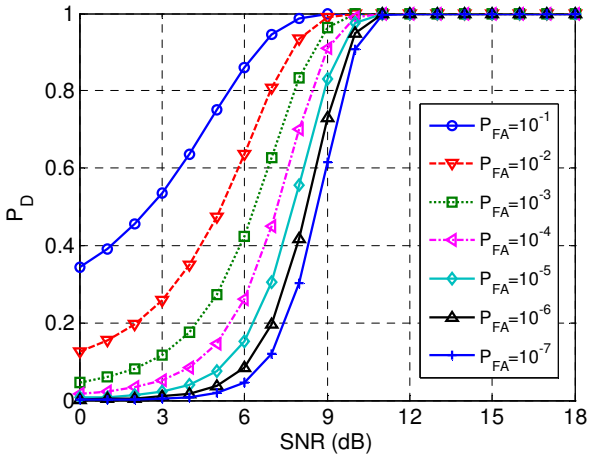

Fig. B.1 Detection performance of the simple ASK receiver shown in Eq. (B.5).

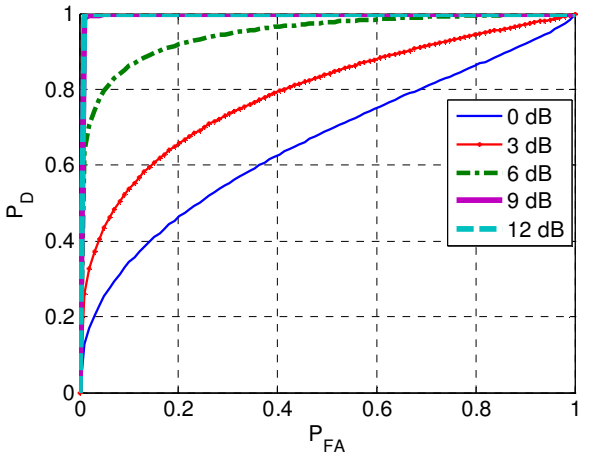

Fig. B.2 ROC of the simple ASK receiver shown in Eq. (B.5)

As shown in Fig. B.1, when SNR is kept unchanged, P_{D} can be increased by choosing a higher P_{FA}. Alternatively, for a chosen P_{FA} increasing the SNR gives a higher P_{D}. As shown in Fig. B.2, for this particular detector, a family of ROCs can be obtained when SNR varies. When SNR is 9 dB, an ideal ROC can be achieved meaning that the particular detector

would provide $P_D = 1$ for any P_{FA}. When SNR is unchanged each point on the ROC represents a value of (P_{FA}, P_D) for a given threshold $\tilde{\gamma}_{ED}$. As expected when $\tilde{\gamma}_{ED}$ increases, both P_{FA} and P_D decrease and vice versa. By adjusting the threshold the system designer can obtain any point on the ROC. However, it is possible to adjust the system settings in order to obtain an operating point close to the ideal detector point (0,1) located at the upper left-hand corner in Fig. B.2. Note also that using the same approach shown above, the detection performance and the ROC for $Q_1 = \xi Q_0$, $\xi > 1$, can be obtained, which would allow the system designer to choose the value of ξ and thereby adjust the difference between the transmitted numbers of molecules in H_1 and H_0 hypotheses based on the particular CEMC system under examination. It should be noted that, unlike this particular scenario, a detailed analysis of the impact of ISI-producing molecules at the RN is given in Chapter 5 for strength-based optimum signal detection in CEMC.

B.3 Properties of Mean and Variance of Test Statistic

Proposition 1: At both H_0 and H_1 respectively, $\mu_{T^*(H_0)} \gg 1$, $\sigma^2_{T^*(H_0)} \gg 2$ and $\mu_{T^*(H_1)} \gg 1$ and $\sigma^2_{T^*(H_1)} \gg 2$.

Proof: When $t_s \leq 1\text{s}$, using Eq. (5.1), since $p(nt_s) \geq 0$, it can be shown that $s^{(1)}_{ED} \geq \sigma^{2(1)}_{S(ED)}$, $s^{(0)}_{ED} \geq \sigma^{2(0)}_{S(ED)}$, and $\mu_{ISI(ED)} \geq \sigma^2_{ISI(ED)}$. Hence, considering the above inequalities in Eqs. (5.10) and (5.11), the following can be found for ASK and OOK systems respectively.

$$\text{ASK}\begin{cases} \mu_{T^*(H_0)} \geq \left(s^{(0)}_{ED} + \mu_{ISI(ED)}\right) \gg 1 & \sigma^2_{T^*(H_0)} \geq 4\left(s^{(0)}_{ED} + \mu_{ISI(ED)}\right) \gg 2 \\ \mu_{T^*(H_1)} \geq \left(s^{(1)}_{ED} + \mu_{ISI(ED)}\right) \gg 1 & \sigma^2_{T^*(H_1)} \geq 4\left(s^{(1)}_{ED} + \mu_{ISI(ED)}\right) \gg 2 \end{cases} \qquad \text{(B.6)}$$

$$\text{OOK}\begin{cases} \mu_{T^*(H_0)} \geq \mu_{ISI(ED)} \gg 1 & \sigma^2_{T^*(H_0)} \geq 4\mu_{ISI(ED)} \gg 2 \\ \mu_{T^*(H_1)} \geq \left(s^{(1)}_{ED} + \mu_{ISI(ED)}\right) \gg 1 & \sigma^2_{T^*(H_1)} \geq 4\left(s^{(1)}_{ED} + \mu_{ISI(ED)}\right) \gg 2 \end{cases}$$

For instance, in Eq. (5.10), $\mu_{T^*(H_0)}$ will be minimum when $s^{(0)}_{ED} = \sigma^{2(0)}_{S(ED)}$, $\mu_{ISI(ED)} = \sigma^2_{ISI(ED)}$, and $c_{ED} = 0$, and so $\min[\mu_{T^*(H_0)}] = s^{(0)}_{ED} + \mu_{ISI(ED)}$. As shown in the simulation setup, in CEMC, the number of transmitted molecules is generally large, and so, as shown in Eq. (5.1), $s^{(0)}_{ED}$, $s^{(1)}_{ED}$, and $\mu_{ISI(ED)}$ are reasonably large numbers, which yields $s^{(0)}_{ED} + \mu_{ISI(ED)} \gg 1$. Since χ^2_1 has mean 1 and variance 2, the means and the variances of the test statistics above have been compared with 1 and 2 respectively.

When $t_s > 1\text{s}$, since $p(nt_s) \geq 0$ is still valid, as shown in Eq. (5.1), the relationships between $s_{\text{ED}}^{(i)}$ and $\sigma_{\text{S (ED)}}^{2(i)}$ and $\mu_{\text{ISI (ED)}}$ and $\sigma_{\text{ISI (ED)}}^2$ depend on the factor $t_s^2\left(1-p(nt_s)\right)$ and its relationship with t_s. When $t_s \gg 1\text{ s}$, $t_s^2\left(1-p(nt_s)\right) > t_s$, and yields $s_{\text{ED}}^{(1)} < \sigma_{\text{S (ED)}}^{2(1)}$, $s_{\text{ED}}^{(0)} < \sigma_{\text{S (ED)}}^{2(0)}$, and $\mu_{\text{ISI (ED)}} < \sigma_{\text{ISI (ED)}}^2$. In addition, it can be understood that when *r* is small, $s_{\text{ED}}^{(i)} > \mu_{\text{ISI (ED)}}$ and $\sigma_{\text{S (ED)}}^{2(i)} > \sigma_{\text{ISI (ED)}}^2$, whereas at large *r*, $s_{\text{ED}}^{(i)} < \mu_{\text{ISI (ED)}}$ and $\sigma_{\text{S (ED)}}^{2(i)} < \sigma_{\text{ISI (ED)}}^2$, $i \in \{0,1\}$. Hence, for instance, when *r* is small and large respectively, considering the above inequalities when $t_s > 1\text{s}$, using Eqs. (5.1), (5.10) and (5.11), and applying algebraic simplifications, it can be shown that

$$\text{ASK}\begin{cases} \left.\begin{aligned} &\mu_{T''(\text{H}_i)} \geq \mathcal{K}_{\mu:\,(\text{Small } r)}^{(i)} s_{\text{ED}}^{2(i)} / \sigma_{\text{S (ED)}}^{2(i)} \gg 1 \\ &\sigma_{T''(\text{H}_i)}^2 \geq 4\mathcal{K}_{\sigma:(\text{Small } r)}^{(i)} s_{\text{ED}}^{2(i)} / \sigma_{\text{S (ED)}}^{2(i)} \gg 2 \end{aligned}\right\} & \text{(Small } r\text{)} \\ \left.\begin{aligned} &\mu_{T''(\text{H}_i)} \geq \mathcal{K}_{\mu:\,(\text{Large } r)}^{(i)} \mu_{\text{ISI (ED)}}^2 / \sigma_{\text{ISI (ED)}}^2 \gg 1 \\ &\sigma_{T''(\text{H}_i)}^2 \geq 4\mathcal{K}_{\sigma:(\text{Large } r)}^{(i)} \mu_{\text{ISI (ED)}}^2 / \sigma_{\text{ISI (ED)}}^2 \gg 2 \end{aligned}\right\} & \text{(Large } r\text{)} \end{cases} \tag{B.7}$$

where $\mathcal{K}_{\mu:\,(\text{Small } r)}^{(i)}$, $\mathcal{K}_{\sigma:(\text{Small } r)}^{(i)}$, $\mathcal{K}_{\mu:\,(\text{Large } r)}^{(i)}$, and $\mathcal{K}_{\sigma:(\text{Large } r)}^{(i)}$ are constants related to mean and variance of $T''(\text{H}_i)$ when *r* is small and large respectively. The proposition above offers an opportunity to simplify the test statistic as shown in Section 5.4.2.

B.4 Suboptimum ASK Receiver (Scenario 2)

When transmission data rates are in the range from *f* = 0.01 bps to 0.1 bps as shown in Chapter 5, in general, the symbol intervals T_{sym} can be much larger than the r.m.s. delay spread τ_{DS} [RAP-02] of the channel. Hence, such cases may arise when long ranges or long temporal instants may cause $p(t) \approx 0$. As a result, the value of $p(t)$ can be considered as an indicative factor to possible detection scenarios. For instance, when $p(t) \approx 0$, it may refer to long-range CEMC with reduced complexity in the design of RN possible. When $p(t) \approx 0$, from Eqs. (4.5) and (4.6), at any time instant *t* the intensity of molecular concentration can be expressed as $\mathcal{N}\left(s(t), s(t)\right)$. Since in most realistic scenarios, when sampling intervals vary between 1 s and 50 s, as shown in Fig. B.3, $0 \leq p(t) \leq 0.5$, $p(t) \to 0$ as $t \to \infty$, and symbol duration can be considered long enough, e.g. $T_{\text{sym}} \gg \tau_{\text{DS}}$, which results in $p(t) \approx 0$ at long temporal instants, this would overestimate the variance of signal intensity at the

temporal samples in the earlier part of the symbol interval, where in reality the variance of signal intensity is smaller than its mean. However, as $t \to \infty$, the variance of signal intensity approaches its mean. Considering $p(t) \approx 0$ yields $s_{\text{ED}}^{(0)} \approx \sigma_{\text{S (ED)}}^{2(0)}$, $s_{\text{ED}}^{(1)} \approx \sigma_{\text{S (ED)}}^{2(1)}$, and $\mu_{\text{ISI (ED)}} \approx \sigma_{\text{ISI (ED)}}^{2}$, which as a result provides that $c_{\text{ED}} \approx 0$ (since $b_{\text{ED}} \approx 0$ and $a_{\text{ED}} \neq 0$). The importance of $T_{\text{sym}} \gg \tau_{\text{DS}}$ is that it determines the severity of ISI in the system. The quantity $p(t)$ is important in the sense that MC system designers have the option to consider approximations in the system based on $p(t)$.

As a result, applying $c_{\text{ED}} \approx 0$ in Eq. (5.9), we find that the suboptimum detector in this case becomes a threshold detector [MAH-13b] as follows.

$$T'(z_{\text{ED}}) = z_{\text{ED}} \underset{\text{Select H}_0}{\overset{\text{Select H}_1}{\gtrless}} \gamma_{\text{ED}}^{\text{(Threshold)}} \text{ where } \gamma_{\text{ED}}^{\text{(Threshold)}} = \sqrt{\gamma'_{\text{ED}}} \tag{B.8}$$

As reported in one of our previous works in [MAH-13b], the detection performance of a threshold detector in CEMC can be expressed as shown in Eq. (B.2) mentioned earlier. In addition, Eq. (B.2) can be used to express the detection performance in terms of the ISI-related quantities as the following.

$$P_{\text{D}} = \mathcal{Q}\left(\mathcal{Q}^{-1}(P_{\text{FA}}) \sqrt{\frac{1+\left(R_{\sigma}^{(0)}\right)^2}{\xi+\left(R_{\sigma}^{(0)}\right)^2}} - \Lambda^{(0)} \frac{(\xi-1)}{\sqrt{\xi+\left(R_{\sigma}^{(0)}\right)^2}} \right) \tag{B.9}$$

$$\text{where } s_{\text{ED}}^{(1)} = \xi s_{\text{ED}}^{(0)},\ \sigma_{\text{S (ED)}}^{2(1)} = \xi \sigma_{\text{S (ED)}}^{2(0)} \text{ and } R_{\sigma}^{(0)} = \frac{\sigma_{\text{ISI (ED)}}}{\sigma_{\text{S (ED)}}^{(0)}}.$$

However, note that in this scenario $\Lambda^{(0)} = s_{\text{ED}}^{(0)} / \sigma_{\text{S}}^{(0)} \approx \sqrt{s_{\text{ED}}^{(0)}}$. Note that Eq. (B.9) differs from Eq. (5.18) in that it does not have $R_{\mu}^{(i)}$ terms because in the suboptimum threshold detector [MAH-13b] the RN simply compares the strength z_{ED} of the symbol with the threshold without further processing it to derive the test statistic of the optimum receiver or the suboptimum version of the receiver in Scenario 1, see. Eq. (5.7), and hence the mean of ISI gets eliminated in the detection performance [MAH-13b].

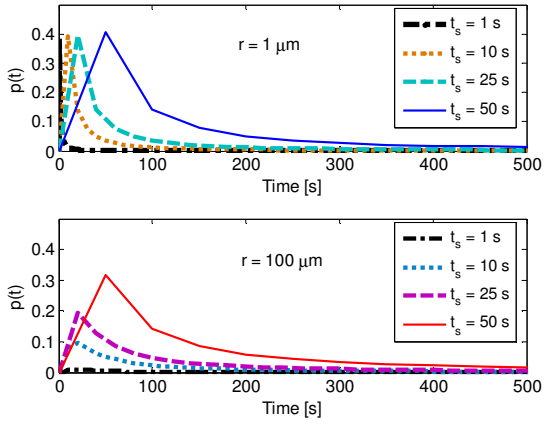

Fig. B.3 Variation of $p(t)$ as a function of time for different t_s when r = 1 μm (top) and r = 100 μm (bottom) respectively.

In OOK, since $s_{\mathrm{ED}}^{(0)} = 0$ and $\sigma_{\mathrm{S\,(ED)}}^{2(0)} = 0$, in a scenario just above, following a similar approach yields the detection performance as shown below.

$$P_{\mathrm{D}} = \mathcal{Q}\left(\mathcal{Q}^{-1}(P_{\mathrm{FA}}) \frac{R_{\sigma}^{(1)}}{\sqrt{1+\left(R_{\sigma}^{(1)}\right)^2}} - \frac{\Lambda^{(1)}}{\sqrt{1+\left(R_{\sigma}^{(1)}\right)^2}} \right) \tag{B.10}$$

where $\Lambda^{(1)} = s_{\mathrm{ED}}^{(1)} / \sigma_{\mathrm{S\,(ED)}}^{(1)}$ and $R_{\sigma}^{(1)} = \sigma_{\mathrm{ISI\,(ED)}} / \sigma_{\mathrm{S\,(ED)}}^{(1)}$.

Here, the signal strength to noise strength ratio can be given as $\Lambda^{(1)} = s_{\mathrm{ED}}^{(1)} / \sigma_{\mathrm{S}}^{(1)} \approx \sqrt{s_{\mathrm{ED}}^{(1)}}$.

Appendix C: Measurement of Bit Error Rate

C.1 Measurement of Bit Error Rate

In digital communications, bit error rate (BER) is the most common and widely used figure of merit for analyzing the performance of a communication system. For CEMC, we also use BER in evaluating its performance. The Monte Carlo method has been very popular and thus widely used in estimating the BER of a digital communication system [JER-00] [TRA-04]. In order to find the estimate of the BER of a digital communication system, $N_{\text{bit seq}}$ randomly-generated bits are passed through the system model and the number of errors is counted. Let us assume that when $N_{\text{bit seq}}$ data bits are passed through the simulation model it results in N_{error} bit errors. Therefore, the estimate of the BER can be given as below [TRA-04].

$$\widehat{\text{BER}} = \frac{N_{\text{error}}}{N_{\text{bit seq}}} \tag{C.1}$$

It is understood that the $\widehat{\text{BER}}$ is a random variable and its accurate estimation requires that the estimator shown in Eq. (C.1) be unbiased and have small variance. Requiring $\widehat{\text{BER}}$ to have small variance in turn requires that $N_{\text{bit seq}}$ be large. In simulating a digital communication system, in order to ensure that the variance of the estimator is suitably small, the value of $N_{\text{bit seq}}$ is chosen such that a sufficient number of bit errors occurs [TRA-04], p. 380. Here $N_{\text{bit seq}}$ can be expressed as $N_{\text{bit seq}} = K_{\text{bit seq}} / p_{\text{true}}$, where p_{true} is the true symbol error probability (or "a good guess" [MAZ-11] of the symbol error probability) and $K_{\text{bit seq}}$ is a constant that determines the reliability of the estimate. Typically $K_{\text{bit seq}}$ is in the range from 10 to 100 [JER-00], p. 682. BER is most often reported in the form of a single point estimate [MAZ-11], as shown in Eq. (C.1), that is a single number and provides with a useful figure of merit in the performance analyses. In digital communication systems, this single point estimate of the BER is most often presented without additional statistical analysis [MAZ-11].

Based on available literature on the error probability of CEMC systems, it is found that in reality true error probability p_{true} is a function of signal to noise ratio. For MC, it is also

found that the value of p_{true} can be ≥ 10^{-3} depending on the signal to noise ratio and the related experimental settings, e.g. modulation scheme under investigation and the receiver's capability to compute the ISI-producing molecules correctly. It is also found in the literature that the BER in MC can be as high as in the range from 0.1 to 0.5 [MOO-14]. Chapters 4 and 5 showed high values of P_{D} close to unity. To decide on the chosen value of $N_{\text{bit seq}}$, let us consider minimum theoretical BER scenario, which will ensure maximum number of bits to be generated in the Monte Carlo method. Since $\text{BER}=\left\{\left(1-P_{D}\right)+P_{\text{FA}}\right\}/2$, minimum BER will occur when P_{FA} is minimum and P_{D} is maximum. Considering $P_{\text{FA}} = 0$ and $P_{\text{D}} = 0.999$, theoretical BER can be found as 0.0005. Considering p_{true} as 0.0005 yields $N_{\text{bit seq}} = 20000$ when $K_{\text{bit seq}} = 10$ is assumed. Similarly, considering $P_{\text{FA}} = 0$ when $P_{\text{D}} = 0.998$, theoretical minimum BER can be obtained as 0.001, which yields $N_{\text{bit seq}} = 10000$ and $N_{\text{bit seq}} = 100{,}000$ when $K_{\text{bit seq}} = 10$ and $K_{\text{bit seq}} = 100$ are assumed respectively.

In this thesis work, in order to provide a point estimate of the average BER at all experimental scenarios presented, we have used 100,000 randomly-generated bits to measure the BER. In addition, as mentioned in Chapters 4 and 5, each bit in the transmitted bit sequence is tested by using at least 30 different randomly generated CIR realizations. This ensures that the probability that the sample mean of the CIR at the RN differs from the true mean by less than one standard deviation is 0.96 [LEO-94]. Therefore, we strongly believe that the simulation model using such a large number of 100,000 randomly generated bits and testing each bit with 30 randomly generated CIR realizations is capable of providing a reliable estimate of the BER of the CEMC system.

C.2 Confidence Interval Calculation

Although as shown in the previous section we used a large number of 100,000 randomly generated bits in the Monte Carlo simulations at each scenario in order to get the point estimate of the BER, in the following we investigate into the interval estimate, often known as the confidence interval (CI), of the BER results obtained in this work. Simulated quantities such as BER have been measured by taking the mean of a successive of N_{run} runs. Each run uses a randomly generated bit sequence with length N_{b}. For example, in order to find the BER results of 100,000 randomly generated bits, we use $N_{\text{run}} = 1000$ runs each

using $N_b = 100$ randomly generated bits. For any experimental setup, all of the N_{run} runs are independent of one another, which ensures that there is no correlation in the presented results from all the simulation runs.

As an example, if the BER results from N_{run} independent runs are denoted as BER_1, BER_2, BER_3,……, $BER_{(N_{run}-1)}$, $BER_{N_{run}}$, the mean BER obtained from all the simulation runs can be expressed as $\overline{BER} = \frac{1}{N_{run}} \sum_{i=1}^{N_{run}} BER_i$. The mean BER found from all the independent simulation runs provides a single point estimate of the expected value $E[BER] = \mu_{BER}$. The variance of BER expressed as $\sigma_{BER}^2 = \frac{1}{N_{run}-1} \sum_{i=1}^{N_{run}} \left(BER_i - \overline{BER}\right)^2$ from N_{run} independent runs shows how good the $\overline{BER}$ is. A small σ_{BER}^2 means that the BER results are tightly clustered around $\overline{BER}$, while a large σ_{BER}^2 indicates that the results are widely dispersed around $\overline{BER}$. We can specify an interval of values that is highly likely to contain the true value of the BER. We specify a high probability $(1-\beta_{CI})$ in order to find an interval $[BER_{LOW}, BER_{HIGH}]$ such that the probability $[BER_{LOW} \le \mu_{BER} \le BER_{HIGH}] = 1-\beta_{CI}$. This interval contains the true value of the BER with a probability $(1-\beta_{CI})$, and therefore, such an interval is known as $(1-\beta_{CI})\times 100\%$ CI. The BER_{LOW} and the BER_{HIGH} for 95% confidence interval can respectively be found as the following, where $\mathcal{T}^{DIST}_{\left[\frac{0.05}{2};N_{run}-1\right]}$ is the value from *t*-distribution and σ_{BER} is the standard deviation of the measurements.

$$BER_{LOW} = \overline{BER} - \frac{\mathcal{T}^{DIST}_{\left[\frac{0.05}{2};N_{run}-1\right]} \times \sigma_{BER}}{\sqrt{N_{run}}}$$

$$BER_{HIGH} = \overline{BER} + \frac{\mathcal{T}^{DIST}_{\left[\frac{0.05}{2};N_{run}-1\right]} \times \sigma_{BER}}{\sqrt{N_{run}}} \qquad \text{(C.2)}$$

As shown in Eq. (C.2), 95% of the simulation results fall within the interval. Simulation results have been obtained based on 1000 independent runs, each run using 100 randomly generated bits. From *t*-distribution, $\mathcal{T}^{DIST}_{\left[\frac{0.05}{2};999\right]}$ can be found as 1.96, which can be used in the expresssion above to get the upper and the lower values of the CI. However, since we used a large number of randomly generated bits through a large number of independent runs, our

CIs have been found too small to report. In other words, small CIs indicate that the single point estimate of the BER as shown earlier can be considered as a reliable measure of the BER in such cases. However, in the following we show the computation of CIs for the BER results shown in Fig. 4.7(b). We found that more than 95% of the simulation results were within the calculated values of the CIs in all of the simulation experiments.

■ Referring to Fig. 4.7 for binary system with $N = 10$				
			Confidence Interval	
r	$\overline{\text{BER}}$	σ_{BER}	BER_{LOW}	BER_{HIGH}
400 nm	0	0	0	0
800 nm	0	0	0	0
1 μm	0	0	0	0
5 μm	0	0	0	0
10 μm	0	0	0	0
50 μm	0.0081	0.0081	0.0076	0.0086
100 μm	0.4697	0.0493	0.4666	0.4727

■ Referring to Fig. 4.7 for quaternary system with $N = 10$				
			Confidence Interval	
r	$\overline{\text{BER}}$	σ_{BER}	BER_{LOW}	BER_{HIGH}
400 nm	0.0035	0.0056	0.0031	0.0038
800 nm	0.0031	0.0054	0.0028	0.0034
1 μm	0.0031	0.0052	0.0027	0.0034
5 μm	0.0036	0.0061	0.0032	0.0040
10 μm	0.0044	0.0067	0.0040	0.0048
50 μm	0.2322	0.0552	0.2288	0.2356
100 μm	0.4424	0.0556	0.4389	0.4458

■ Referring to Fig. 4.7 for binary system with $N = 4$				
			Confidence Interval	
r	$\overline{\text{BER}}$	σ_{BER}	BER_{LOW}	BER_{HIGH}
400 nm	0.0535	0.0251	0.0519	0.0550
800 nm	0.0527	0.0240	0.0512	0.0542
1 μm	0.0530	0.0248	0.0514	0.0545
5 μm	0.0536	0.0242	0.0521	0.0551
10 μm	0.0602	0.0248	0.0587	0.0617
50 μm	0.2882	0.0351	0.2861	0.2904

100 μm	0.4727	0.0502	0.4696	0.4759

■ Referring to Fig. 4.7 for quaternary system with $N = 4$				
			Confidence Interval	
r	$\overline{\text{BER}}$	σ_{BER}	BER_{LOW}	BER_{HIGH}
400 nm	0.3355	0.0542	0.3321	0.3388
800 nm	0.3356	0.0539	0.3323	0.3390
1 μm	0.3357	0.0532	0.3324	0.3390
5 μm	0.3356	0.0526	0.3323	0.3388
10 μm	0.3408	0.0544	0.3374	0.3442
50 μm	0.4129	0.0493	0.4099	0.4160
100 μm	0.4486	0.0539	0.4453	0.4520